



Université  
de Toulouse

# THÈSE

En vue de l'obtention du

## DOCTORAT DE L'UNIVERSITÉ DE TOULOUSE

**Délivré par:**

Université Toulouse 3 Paul Sabatier (UT3 Paul Sabatier)

**Cotutelle internationale avec:**

TERI University, New Delhi, India

---

**Présentée et soutenue par  
DESHMUKH Chandrashekhar**

Le jeudi 28 mars 2013

**Titre:**

Greenhouse gases (CH<sub>4</sub>, CO<sub>2</sub> and N<sub>2</sub>O) emissions from a newly flooded hydroelectric reservoir in subtropical South Asia: case of Nam Theun 2 Reservoir, Lao PDR

---

ED SDU2E : Océan, Atmosphère et Surfaces Continentales

**Unité de recherche:**

Laboratoire d'Aérodologie- Geoscience Environnement Toulouse

**Directeur(s) de Thèse:**

Dominique Serça, Laboratoire d'Aérodologie  
Frédéric Guérin, IRD-Geoscience Environnement Toulouse  
Arun Kansal, TERI University, India

**Rapporteurs:**

David Bastviken, Linköping University, Sweden  
Yves Prairie, Université du Québec à Montréal, Canada  
Bernhard Wehrli, ETH Zurich, Switzerland

**Autre(s) member(s) du jury:**

Stéphane Descloux, Electricité de France (EDF)  
Suneel Pandey, TERI University



## Acknowledgements

---

I feel great pleasure and privilege to express my deep sense of gratitude and thankfulness towards Dr. Dominique Serça and Dr. Frédéric Guérin for their invaluable guidance, constant supervision, and continuous encouragement throughout the thesis work. Their humanity and helping personally during my entire stay in Toulouse made them the dearest people for the accomplishment of this work.

I would like to thank Dr. Arun Kansal for his continuous support and encouragement throughout the thesis work. I would also like to thank Dr. Nandani Kumar, Dr. Suneel Pandey and Dr. Suresh Jain from TERI University, India for their support during this work.

I thank Electricité de France (EDF) for providing financial support to this research. I would like to express my deep sense of gratitude to Laurent Bellet, Stephane Descloux and Vincent Chanudet from EDF.

I express gratitude to the Nam Theun 2 Power Company (NTPC) for providing on site support for field measurements. I am grateful to the members of the Aquatic Environmental Laboratory (AEL) of the Nam Theun 2 project, Pierre, Arnaud, Sylvie, Fabien, Maud, Joanna, Axay, Souk, Sith, Souliphone, Sython, Tick, Sadavee, Peun, and all other members for the help given during field trips and for the monitoring data. This work would not have been achievable without a successful collaboration with Stephane Audry, Priscia Oliva, Claire Delon, Corinne Galy-Lacaux, Maud Demarty and Cyril Zouiten, thanks everyone !

I would like to express my deepest appreciation to administrative and technical staff at Laboratoire d'Aérologie (LA) and Géosciences Environnement Toulouse (GET) for their helpful hands and noble cooperation.

The friends that made me forget about work and focus on the other fun things in life. I deeply value the time, encouragement, love and care I had from the lab mates at LA... Florian, Romain, Yvan, Thierno, Simon, Alan, Heloise, Vincent, Albon...merci beaucoup for skiing, hiking, climbing, rafting and paragliding lessons! Without a single thought, they have never been less than my biological brother and sister. I am also thankful to all those who were around me directly or indirectly during this work, specially, *Darbaris*, Vikas, Sat and Guru.

The most amazing officemates without which last months would not be so easy and whom were honestly a total pleasure to share the office....Merci Emilie and Pinky!!

Finally, I want to thank my parents for their unending support. They have always stood behind me even when none of us were sure about outcomes. And I have no doubt that they will always be there for me no matter what!



# Table of contents

---

<b>Introduction</b>	1
<b>Chapter 1. State of the art</b>	
1.1. Climate system and greenhouse gas effect	5
1.1.1. Climate change/global warming	6
1.1.2. Major greenhouse gases and their abundances in the atmosphere	7
1.1.2.1. Carbon dioxide (CO <sub>2</sub> )	7
1.1.2.2. Methane (CH <sub>4</sub> )	8
1.1.2.3. Nitrous oxide (N <sub>2</sub> O)	9
1.2. Processes behind GHG emissions from a watershed	9
1.2.1. Carbon and nitrogen cycle in a natural watershed	9
1.2.2. Carbon cycling in an aquatic ecosystem	11
1.2.3. Methane cycling in an aquatic ecosystem	12
1.2.3.1. Aerobic methane oxidation	13
1.2.4. Nitrous oxide (N <sub>2</sub> O) cycling in an aquatic ecosystem	14
1.2.5. Emissions pathways	15
1.2.5.1. Diffusive emissions	15
1.2.5.2. Bubbling/ebullition	16
1.2.5.3. Plant mediated emissions	17
1.3. Carbon cycling in a reservoir	17
1.3.1. Key processes influencing emission of GHGs to the atmosphere from hydroelectric reservoirs	19
1.3.2. GHGs emitted by hydroelectric reservoirs	20
1.3.3. Global distribution of hydroelectric reservoirs and GHG emissions	20
1.3.4. Important scientific advances	23
1.3.5. Emissions from reservoirs at the global scale	24
1.3.6. The importance of considering net emissions	24
<b>Chapter 2. Site description, sampling strategy and methodology</b>	
2.1. Site description	27
2.2. Sampling stations and sampling strategy	30
2.2.1. Pre-impoundment GHG exchange	30
2.2.2. Post-impoundment GHG exchange	30
2.3. Methodology	34
2.3.1. Soil sampling	34
2.3.2. Determination of kinetics of potential CH <sub>4</sub> and CO <sub>2</sub> production rates	35
2.3.3. Determination of CH <sub>4</sub> concentrations in sediment layer	36
2.3.4. Determination of GHG concentrations in the water	36
2.3.5. Determination of kinetics of potential aerobic CH <sub>4</sub> oxidation rates	37
2.3.6. Diffusive GHG fluxes	38

2.3.6.1. Eddy covariance measurements	38
2.3.6.1.1. Basic principle	38
2.3.6.1.2. Instrumentations	39
2.3.6.1.3. Ancillary measurements	41
2.3.6.1.4. Data processing	41
2.3.6.2. Floating chamber measurements	42
2.3.6.3. Estimation of diffusive gas fluxes from surface GHG concentrations	42
2.3.7. Ebullition of GHG	43
2.3.8. Diffusive GHG flux from the drawdown area	44
2.3.9. Gas chromatography	44
2.3.10. Determination of physico-chemical parameters	45
2.3.11. Estimation of degassing	45
2.3.12. Dissolved CH <sub>4</sub> storage within the reservoir	46
2.3.13. Statistical analysis	46
2.3.14. Extrapolation of fluxes for the estimation of NT2 total GHG emissions	46
2.3.15. General Approaches	48
2.3.15.1. Estimates of annual GHG gross emissions	48
2.3.15.2. Carbon import through the rivers and export from the reservoir	48

### **Chapter 3. Physical controls on CH<sub>4</sub> and CO<sub>2</sub> emissions from a newly flooded subtropical hydroelectric reservoir: Nam Theun 2**

Abstract	51
3.1. Introduction	52
3.2. Material and methodology	54
3.2.1. Site Description	54
3.2.2. Methodology	56
3.2.2.1. Diffusive CH <sub>4</sub> fluxes measured by floating chamber	56
3.2.2.2. Ebullition of CH <sub>4</sub> flux	56
3.2.2.3. Gas chromatography	56
3.2.2.4. Instrumentation of eddy covariance system	57
3.2.2.4.1. Ancillary measurements	58
3.2.2.4.2. Data processing	58
3.2.2.4.3. EC data quality control	59
3.2.2.4.4. Footprint analysis	59
3.2.2.5. Statistical analysis and artificial neuronal network	60
3.2.2.6. Other calculations	61
3.3. Result	
3.3.1. <i>In situ</i> parameters and, dissolved CO <sub>2</sub> and CH <sub>4</sub> in the water column	61
3.3.2. Meteorological and physical conditions during the study periods	63

3.3.3. Quantitative estimates of the CH <sub>4</sub> fluxes	66
3.3.4. Bubbling CH <sub>4</sub> fluxes from the reservoir surface	69
3.3.5. Quantitative Estimates of the CO <sub>2</sub> fluxes	71
3.3.6. Footprint analysis and inter-comparison of EC fluxes with other techniques	73
3.4. Discussion	
3.4.1. Physical controls on CH <sub>4</sub> emissions	74
3.4.1.1. Semidiurnal cycle of CH <sub>4</sub> emissions	75
3.4.1.2. Water depth and water level fluctuation	76
3.4.1.3. Dependency on other environmental variables	77
3.4.1.4. Bubbling CH <sub>4</sub> fluxes from the reservoir surface	77
3.4.2. Physical controls on CO <sub>2</sub> fluxes	78
3.4.3. Inter-comparison of EC fluxes with independent floating chamber and submerged funnel measurements	82
3.5. Conclusion	83
Appendix	85

## **Chapter 4. Methane dynamics and gross emissions from a newly impounded hydroelectric reservoir in subtropical south-east Asia: the Nam Theun 2 Reservoir (Lao PDR)**

Abstract	89
4.1. Introduction	89
4.2. Material and methods	91
4.2.1. Study area	91
4.2.2. Sampling strategy	93
4.2.3. Experimental methods	
4.2.3.1. In situ water quality parameter	95
4.2.3.2. Methane concentration in water	95
4.2.3.3. Methane concentration in the pore water of the flooded soils	95
4.2.3.4. Diffusive fluxes measured by floating chamber	95
4.2.3.5. Ebullition of CH <sub>4</sub>	96
4.2.3.6. Diffusive fluxes from the soils surrounding the reservoir and the drawdown area	96
4.2.3.7. Potential CH <sub>4</sub> production in flooded soils	96
4.2.3.8. Aerobic CH <sub>4</sub> oxidation in the water column	97
4.2.3.9. Gas chromatography	97
4.2.4. Calculation	
4.2.4.1. Methane storage in the reservoir water column	97
4.2.4.2. Estimation of diffusive fluxes from surface concentrations	98
4.2.4.3. Degassing	99
4.2.4.4. Artificial neural network	99
4.2.4.5. Extrapolation of fluxes for the estimation of the NT2 total emissions	99

4.2.4.6. Statistical analysis	100
4.3. Results	
4.3.1. Temperature, O <sub>2</sub> and CH <sub>4</sub> concentrations and CH <sub>4</sub> storage in the reservoir water column	100
4.3.2. Methane concentration in the reservoir surface water	103
4.3.2.1. CH <sub>4</sub> and O <sub>2</sub> concentrations in the Nam Theun River and the downstream channel	104
4.3.3. Methane the pore water of flooded soils	105
4.3.4. Diffusive CH <sub>4</sub> fluxes from the reservoir	106
4.3.5. CH <sub>4</sub> ebullition	109
4.3.6. Diffusive fluxes from the drawdown area	110
4.3.7. Downstream emissions	112
4.5.7.1. Degassing and diffusive fluxes from downstream of the turbines	112
4.5.7.2. Degassing and diffusive CH <sub>4</sub> fluxes from downstream of the Nakai Dam	113
4.3.8. Potential CH <sub>4</sub> production in flooded soils	113
4.3.9. Aerobic CH <sub>4</sub> oxidation in the NT2 Reservoir, downstream channel and Nam Theun River	115
4.4. Discussion	
4.4.1. CH <sub>4</sub> dynamic in the reservoir water column	117
4.4.2. Diffusive fluxes from the reservoir surface	117
4.4.2.1. At the monitoring stations RES1, 2, 4, 5, 6, 7 and 8	117
4.4.2.2. At the monitoring station RES3 (flooded forest)	118
4.4.2.3. At the monitoring station RES9 (water intake)	118
4.4.2.4. Estimation of total diffusive fluxes from the reservoir	119
4.4.3. Ebullition of CH <sub>4</sub>	119
4.4.4. Diffusive fluxes from the drawdown area	120
4.4.5. Downstream emissions	120
4.4.6. Total gross emissions and comparison with other tropical reservoirs	121
4.4.7. CH <sub>4</sub> mass balance in the NT2 Reservoir	123
4.4.7. 1. Estimation of the CH <sub>4</sub> production during the mineralization of the flooded soils	123
4.4.7.2. Estimation of the aerobic CH <sub>4</sub> oxidation (AMO) in NT2 waters	125
4.4.7.3. Comparison of the total CH <sub>4</sub> source and sinks in the NT2 system	126
4.5. Conclusion	128
 <b>Chapter 5: Gross carbon dioxide (CO<sub>2</sub>) emissions and carbon budget for a subtropical hydroelectric reservoir: case of Nam Theun 2, Lao PDR</b>	
Abstract	129
5.1. Introduction	129
5.2. Results	131
5.2.1. CO <sub>2</sub> concentrations along with physico-chemical parameters in the reservoir	131
5.2.2. CO <sub>2</sub> concentrations in the downstream of the	



powerhouse and downstream of the Nakai Dam	134
5.2.3. The kinetics of potential CO <sub>2</sub> production rate at the bottom of the reservoir	136
5.2.4. Bubbling flux from the reservoir water surface	137
5.2.5. Diffusive flux from the reservoir water surface	137
5.2.6. Fluxes from drawdown area	139
5.2.7. Emissions from downstream	141
5.2.7.1. Degassing	141
5.2.7.2. Diffusive fluxes	142
5.3. Discussion	
5.3.1. Dissolved CO <sub>2</sub> and physico-chemical parameters	143
5.3.2. Estimates of all components of gross CO <sub>2</sub> emissions	144
5.3.3. Tentative carbon budget for year 2010 and 2011	146
5.4. Conclusions	149

## **Chapter 6: Nitrous oxide (N<sub>2</sub>O) dynamics and gross atmospheric emissions**

Abstract	151
6.1. Introduction	151
6.2. Study area and methodology	153
6.2.1. The Nam Theun 2 Hydroelectric Reservoir	153
6.2.2. Strategies (stations design)	154
6.2.3. Methodology	154
6.2.4. Gas chromatography	154
6.2.5. Statistical analysis	155
6.3. Result and discussions	
6.3.1. N <sub>2</sub> O concentrations in water column along with physico-chemical parameters	155
6.3.2. N <sub>2</sub> O concentrations in the downstream of powerhouse and the downstream of the Nakai Dam	160
6.3.3. Emissions from upstream	162
6.3.3.1. Bubbling flux	162
6.3.3.2. Diffusive flux from reservoir surface	162
6.3.3.3. N <sub>2</sub> O fluxes from the drawdown area	164
6.3.4. Emissions from downstream	167
6.3.4.1. Degassing	167
6.3.4.2. Diffusive fluxes from downstream of the power house and downstream of the Nakai Dam	167
6.4. Estimates of different components of gross N <sub>2</sub> O emissions	169
6.5. Conclusions	170

## **Chapter 7: Net GHG footprint of a newly impounded subtropical hydroelectric reservoir: Nam Theun 2 case study**

Abstract	171
7.1. Introduction	171
7.2. Site description and methodology	173
7.2.1. Site Description	173
7.2.2. General Approach	174

7.2.3.	Pre-impoundment GHG exchange	175
7.2.3.1.	CO <sub>2</sub> exchange	176
7.2.3.2.	CH <sub>4</sub> exchange	176
7.2.3.3.	N <sub>2</sub> O exchange	177
7.3.	Results	
7.3.1.	Pre-impoundment GHG exchange	177
7.3.1.1.	CO <sub>2</sub> exchanges	178
7.3.1.2.	CH <sub>4</sub> exchange	178
7.3.1.3.	N <sub>2</sub> O exchanges	179
7.3.1.4.	Spatial and temporal integration of fluxes and estimation	180
7.3.1.4.1.	CO <sub>2</sub> budget	180
7.3.1.4.2.	CH <sub>4</sub> budget	181
7.3.1.4.3.	N <sub>2</sub> O budget	181
7.3.1.5.	Assessment of GHG exchange in CO <sub>2</sub> equivalent	184
7.3.2.	Post-impoundment GHG exchange	185
7.4.	Net GHG Emissions	187
7.5.	Net GHG emissions and energy generation	188

## **Chapter 8: Conclusion and outlook**

8.1.	Methane (CH <sub>4</sub> )	191
8.1.1.	CH <sub>4</sub> dynamics	191
8.1.2.	Techniques for assessing CH <sub>4</sub> emissions	191
8.1.3.	Environmental drivers of CH <sub>4</sub> flux variability	192
8.1.4.	Gross CH <sub>4</sub> emissions	193
8.2.	Carbon dioxide (CO <sub>2</sub> )	193
8.2.1.	Techniques for assessing CO <sub>2</sub> emissions	183
8.2.2.	Environmental drivers of CO <sub>2</sub> flux variability	194
8.2.3.	Gross CO <sub>2</sub> emissions and carbon budget	194
8.3.	Nitrous oxide (N <sub>2</sub> O) dynamics and gross emissions	194
8.4.	Net GHG footprint	195
8.5.	Outlook and implications for future GHG emission research	196
	<b>References</b>	<b>199</b>

*Knowledge shall always be the ultimate goal of all mankind. I salute such Gurus who not only craft knowledge but also share it.*



## Introduction

---

The identification and accurate quantification of sinks or sources of GHG has become a key challenge for scientists and policy makers groups working on climate change or global warming. The creation of a hydro-reservoir while damming a river for power generation converts the terrestrial ecosystems into aquatic ecosystem and subsequently decomposition of flooded terrestrial soil organic matter stimulates GHG production and thereby emissions to the atmosphere from the reservoir water surface and downstream of powerhouse (St. Louis et al., 2000; Tremblay et al., 2005). The major GHGs related to hydroelectric reservoir creation are carbon dioxide (CO<sub>2</sub>), methane (CH<sub>4</sub>) and nitrous oxide (N<sub>2</sub>O) (Eggleton et al., 2006). The contribution of hydroelectric reservoirs to the increase of the atmospheric GHGs concentrations is of rising concern. Recently, a meta-analysis on 85 published data on emissions from reservoirs show that tropical or subtropical hydroelectric reservoirs are more significant sources of GHG than boreal or temperate one (Barros et al., 2011). Around 25% of the existing 45000 large dams are used for electricity production. The number of hydroelectric reservoirs continues to increase at fast pace specially in the tropical or sub-tropical regions which still hold significant amount of hydropower resources to be exploited (Kumar et al., 2011).

In addition to reliable estimates of reservoir gross GHG emissions taken over space and time, a realistic assessment of the GHG footprint of hydroelectric reservoir requires, robust estimates of the GHG budget from the terrestrial and natural aquatic ecosystems existing in the pre-impoundment landscape, and which disappear due to flooding (Teodoru et al., 2012; Tremblay et al., 2010). For the governing bodies (e.g. IPCC, UNESCO, etc.) and the energy sector (International Hydropower Association, International Energy Agency, etc.), the evaluation of net GHG emissions (post impoundment emissions - pre impoundment emission) from hydroelectric reservoirs is becoming more and more relevant to ensure that methods of energy production are adequately compared. This is a necessary step for assessing carbon credits.

In spite of the increasing awareness from the scientific community, international agencies and the energy sector of the significance of reservoir GHG emissions for these two last decades, only one pre-and-post impoundment GHG balance has ever been carried out (Eastmain 1 Reservoir, Quebec; Teodoru et al., 2012; Tremblay et al., 2010). The study at Eastmain 1 Reservoir suggests that net GHG emissions (mostly CO<sub>2</sub> and negligible amount of CH<sub>4</sub>) are substantial in the first years after flooding and decrease rapidly, stabilizing after about 10 years. Notably, no study dedicated to “net emissions” has ever been conducted in tropical or subtropical regions which is believed to be the “hot spot” for CH<sub>4</sub> emissions (Barros et al, 2011; DelSontro et al, 2011; Demarty and Bastien, 2011; Kemenes et al, 2011; St. Louis et al., 2000).

In this context, we studied the subtropical hydroelectric Nam Theun 2 (NT2) Reservoir, a complex-structural-designed, created on the Nam Theun River in Laos PDR. This reservoir has a 1070 MW installed capacity, and an annual production of 6 TWh. The overall

aim of our study was to: (1) Study the GHG dynamics ( $\text{CH}_4$ ,  $\text{N}_2\text{O}$  and  $\text{CO}_2$ ) in the reservoir and in the whole area of influence (downstream and drawdown areas), (2) determine the environmental controls on the different emission terms; (3) attempt to determine the first net GHG budget of a subtropical hydroelectric reservoir. This study implied the implementation of a wide range of techniques and calculations to assess the different emission terms from laboratory and in situ measurements. A detailed description of the spatial and temporal variability of these different terms has been achieved during six field campaigns and an fortnightly sampling of about thirty four stations distributed all over the reservoir and its impacted zone.

Considering the above objectives, the whole thesis is divided into seven chapters. A brief overview of each manuscript chapter is given below

- ***Chapter 1: State of the art***

*This chapter gives a brief review of climate system and role of greenhouse gas, fundamental processes and scientific understandings behind GHG emissions from natural terrestrial and aquatic ecosystems. It also presents the advancements in the field of GHG emissions from hydroelectric reservoirs.*

- ***Chapter 2: Site description, sampling strategy and methodology***

*This chapter first details the main features of the studied site and the sampling strategy. Then, the chapter describes the different field measurements, laboratory experiments and data processing activities performed during the whole study.*

- ***Chapter 3: Physical controls on methane ( $\text{CH}_4$ ) and carbon dioxide ( $\text{CO}_2$ ) emissions from a newly impounded hydroelectric reservoir in subtropical south-east Asia: the Nam Theun 2 Reservoir (Lao PDR)***

In this chapter, we investigate the physical controls on  $\text{CH}_4$  and  $\text{CO}_2$  emissions using the eddy covariance (EC) technique. Additionally, we explore the effectiveness of the EC technique via a cross-comparison of EC fluxes with fluxes those measured with traditional techniques (i.e. floating chamber and submerged funnel). We study the temporal variations in  $\text{CH}_4$  emissions at different scales i.e. from daily to seasonal, and link these variations to environmental controlling factors. Further, a comprehensive dataset on ebullition allowed constructing a predictive artificial neuron network (ANN) model for ebullition using water depth, change in water level, atmospheric pressure, change in atmospheric pressure and bottom water as inputs.

We explore the influence of heating and cooling of the water column on the process of gas exchange at the air-water interface. Further, the influence of wind speed on the diffusive  $\text{CO}_2$  fluxes was evaluated during different physical conditions (i.e. heating versus cooling, and stratification versus non-stratification in the water column).

- ***Chapter -4: Methane (CH<sub>4</sub>) dynamics and gross atmospheric emissions from a newly impounded hydroelectric reservoir in subtropical south-east Asia: the Nam Theun 2 Reservoir (Lao PDR)***

This chapter describes the seasonal pattern of CH<sub>4</sub> concentrations and discusses the major determinants of CH<sub>4</sub> in the water column. Results from laboratory work in controlled conditions are used to assess production rates of CH<sub>4</sub> and pelagic aerobic CH<sub>4</sub> oxidation rates. Around three years of measurements of the different pathways revealed that ebullition dominates in this relatively shallow subtropical reservoir. Physical dynamics and structural design of the reservoir explain lower downstream CH<sub>4</sub> emissions than other previously studied reservoirs. It includes also the CH<sub>4</sub> mass balance for years 2010 and 2011 based on storage in the water column, production, inflow, pelagic oxidation, emissions and export of CH<sub>4</sub> to downstream.

- ***Chapter 5: Gross carbon dioxide (CO<sub>2</sub>) emissions and carbon budget for a subtropical hydroelectric reservoir: case of Nam Theun 2, Lao PDR***

In this chapter, we assess the gross CO<sub>2</sub> emissions for years 2010 and 2011. Gross CO<sub>2</sub> emissions include all major pathways of emission: diffusion from the reservoir surface, downstream emissions (diffusion and degassing) and emissions from the drawdown area. Vertical profiles of dissolved CO<sub>2</sub>, inorganic carbon (IC) and total organic carbon (TOC) were determined in the reservoir at nine sampling stations, whereas import and export of dissolved CO<sub>2</sub>, IC and TOC were estimated through surface water sampling in the pristine rivers and downstream of power house and Nakai Dam at twenty sampling stations. Additional laboratory work in controlled conditions allowed assessing the benthic production of CO<sub>2</sub> at the bottom of the reservoir. Estimates of primary production in the water column were made using *chlorophyll a* concentrations in the reservoir. Finally, considering CH<sub>4</sub> mass balance (Chapter 4); carbon budgets are presented for years 2010 and 2011.

- ***Chapter 6: - Nitrous oxide (N<sub>2</sub>O) dynamics and gross atmospheric emissions***

This chapter deals with the dynamics of nitrous oxide (N<sub>2</sub>O) along with inorganic nitrogen compounds i.e. ammonium (NH<sub>4</sub><sup>+</sup>), nitrate (NO<sub>3</sub><sup>-</sup>) and nitrite (NO<sub>2</sub><sup>-</sup>) in NT2 reservoir. We found that seasonal variation in the N<sub>2</sub>O emissions was stronger than the spatial one, with much higher N<sub>2</sub>O emissions observed from reservoir water surface and downstream during the wet season. This could be due to an enhanced nitrification process during hydrodynamical mixing of NH<sub>4</sub><sup>+</sup>-rich hypolimnetic water and oxygenated epilimnetic water. Further, we show that the drawdown area is the major source of N<sub>2</sub>O emissions at NT2 Reservoir.

- ***Chapter 7: - The net GHG footprint of a newly impounded subtropical hydroelectric reservoir: Nam Theun 2***

In this chapter, we present the comprehensive assessment of greenhouse gas (GHG) footprint associated with the creation of NT2 reservoir. Pre-impoundment GHG exchanges were assessed in year 2008. Considering gross CH<sub>4</sub> emissions (*Chapter 4*), gross CO<sub>2</sub> emissions (*Chapter 5*) and gross N<sub>2</sub>O emissions (*Chapter 6*), we deduced gross post-impoundment GHG exchanges as the sum of the three. Net GHG emission (difference between post and pre-impoundment emissions), which is the actual anthropogenic disturbance related to the NT2 reservoir creation, was estimated for the years 2010 and 2011.



# Chapter 1

## State of the art

### 1.1. Climate system and greenhouse gas effect

As described in IPCC (2007), “the climate system is a complex, interactive system consisting of the atmosphere, land surface, snow and ice, oceans and other water bodies, and living things”. The climate system changes with time because of the influence of its own internal dynamics and due to changes in external factors that affect climate (called ‘forcings’). External forcings include natural phenomena such as volcanic eruptions and solar variations, as well as human-induced changes in atmospheric composition (IPCC, 2007). Solar radiation controls the climate system. There are three primary ways to modify the radiation balance of the Earth: 1) by changing the incoming solar radiation (e.g., by changes in Earth’s orbit or in the Sun itself); 2) by changing the fraction of solar radiation that is reflected (called ‘albedo’; e.g., by changes in cloud cover, atmospheric particles or vegetation); and 3) by altering the long wave radiation emitted from the Earth surface backwards space (e.g. by changing greenhouse gas concentrations, term equal to  $40 \text{ W.m}^{-2}$  in Figure 1.1).

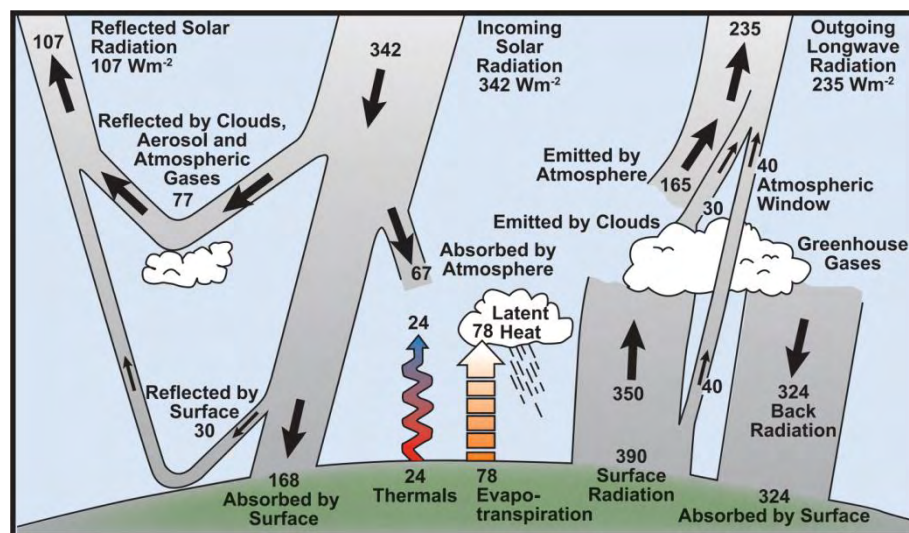


Figure 1.1: Estimate of the Earth’s annual and global mean energy balance.

Over the long term, the amount of incoming solar radiation absorbed by the Earth and atmosphere is balanced by the Earth and atmosphere releasing the same amount of outgoing long wave radiation. About half of the incoming solar radiation is absorbed by the Earth’s surface. This energy is transferred to the atmosphere by warming the air in contact with the surface (thermals), by evapotranspiration and by long wave radiation that is absorbed by clouds and greenhouse gases. The atmosphere in turn radiates long wave energy back to the Earth as well as out to space. Source: Kiehl and Trenberth (1997).

The top of the Earth’s atmosphere receives  $1,370 \text{ Watts}$  each second on a surface area of one square meter facing the Sun. The amount of energy per square meter per second averaged over the entire planet is  $342 \text{ W.m}^{-2}$  (one-quarter). About one-third of the sunlight

reaching the top of the atmosphere is jointly reflected back to space by earth surface ( $30 \text{ W.m}^{-2}$ ) and by clouds, aerosol and atmospheric gases ( $77 \text{ W.m}^{-2}$ ). The energy that is not reflected back to space is absorbed by the Earth's surface ( $168 \text{ W.m}^{-2}$ ) and the atmosphere ( $67 \text{ W.m}^{-2}$ ) (Figure 1.1). To balance the absorbed incoming energy, the Earth must, on average, radiate the same amount of energy back to space. Because the Earth is much colder than the Sun, it radiates at much longer wavelengths, primarily in the infrared part of the spectrum. To emit the equal amount of energy absorbed by the surface-atmosphere system ( $241 \text{ W.m}^{-2}$ ), a surface would have to have a temperature of around  $-18^\circ\text{C}$ . This is  $33^\circ\text{C}$  colder than the conditions that actually exist at the Earth's surface (global mean surface temperature is about  $15^\circ\text{C}$ ). The difference between the radiative temperature ( $-18^\circ\text{C}$ ) and the actual mean temperature at the Earth surface ( $15^\circ\text{C}$ ) is due to the presence of greenhouse gases in the atmosphere. Much of the thermal radiation emitted by the land and ocean is absorbed by the atmosphere, including clouds, and reradiated back to Earth. This is the so-called greenhouse effect (Figure 1.2).

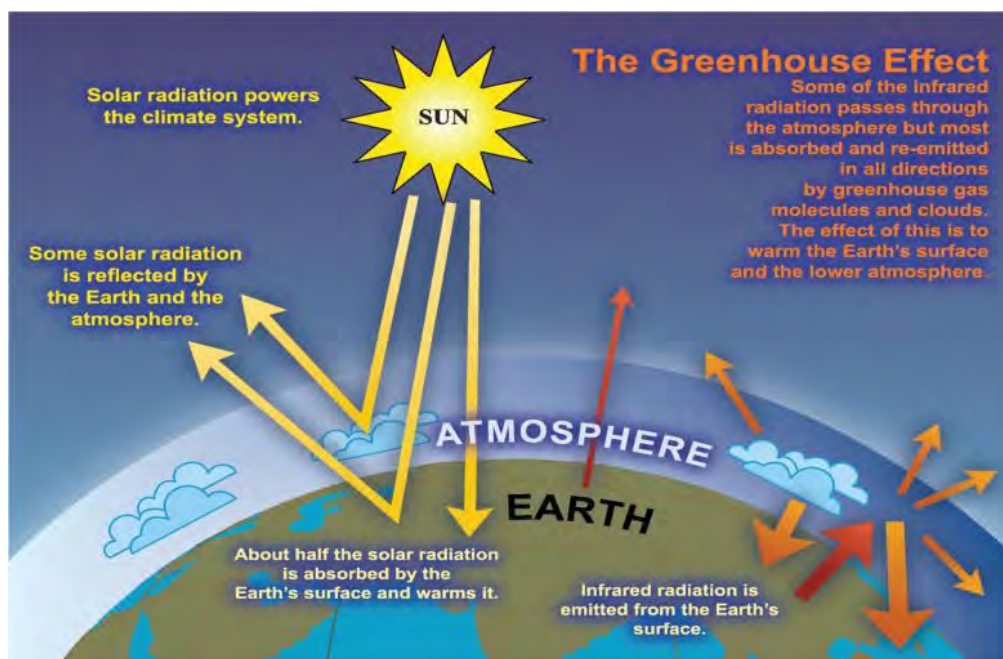


Figure 1.2: An idealized model of the natural greenhouse effect (IPCC, 2007).

The greenhouse effect comes from molecules that absorb the terrestrial infrared radiation in the range from 5 to 25  $\mu\text{m}$ . Water vapor is the most important greenhouse gas, carbon dioxide ( $\text{CO}_2$ ), methane ( $\text{CH}_4$ ), and nitrous oxide ( $\text{N}_2\text{O}$ ) being the three next ones by decreasing importance of additional radiative forcing since pre-industrial times.

### 1.1.1. Climate change/global warming

As discussed in previous sections, greenhouse gases are naturally present in the Earth's atmosphere, causing the natural greenhouse gas effect. Increasing concentration of GHGs (including water vapor, carbon dioxide, methane, nitrous oxide, and others) in the atmosphere strengthen the green house effect, this is the so-called additional green house effect. This led to an increase of global surface and atmospheric temperatures; it is referred as

the global warming. Global warming causes different changes such as increase in extreme weather events, rising sea levels, ecosystem migrations. Further more generally, interactions between the atmosphere, the biosphere and the oceans are disturbed by the global warming.

Demographic expansion and industrialization are responsible for changes in land use pattern, mainly to produce food and energy (Figure 1.3), occurring since the beginning of the industrial era. The changes in land use pattern have been the main causes of modifications in sources and sinks of greenhouse gases. According IPCC (2007), however, there is a net increase in atmospheric GHG concentrations. High atmospheric GHG concentrations are responsible for high strength of green house effect which causes global warming /climate change. Since the early 20<sup>th</sup> century, the Earth mean surface temperature has increased by about 0.8°C, with about two third of the increase occurring since 1980. Consequently, identification and quantification of sources and sinks of greenhouse gases have become an important environmental/political/public issue

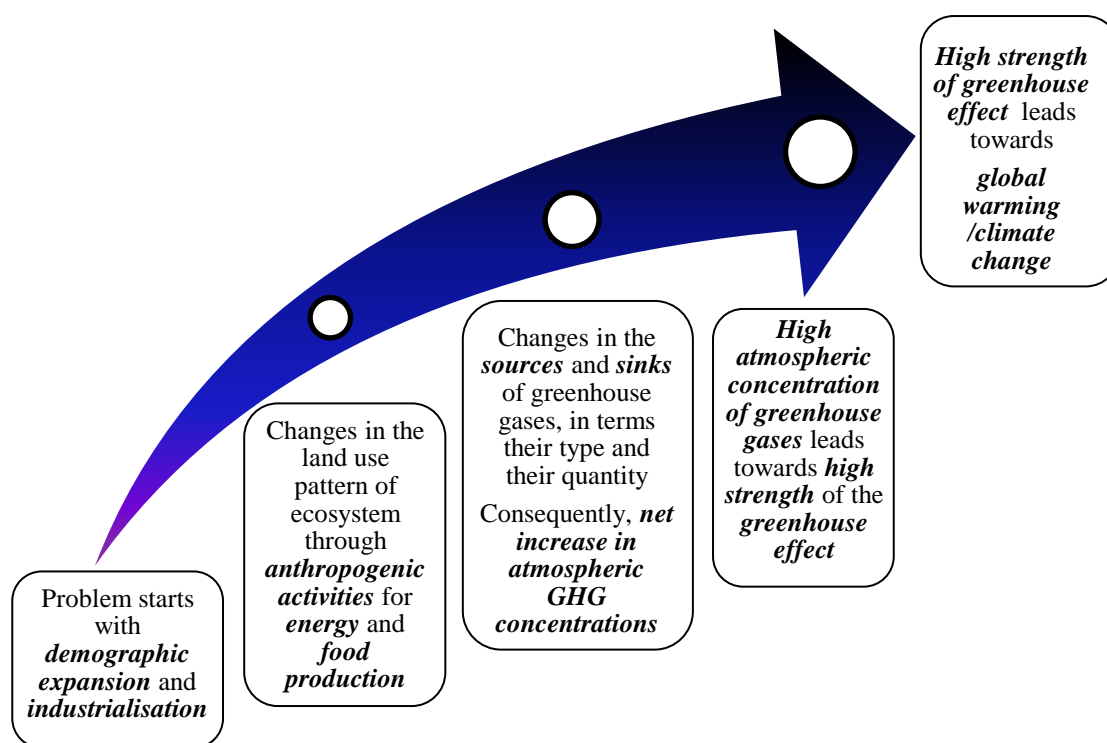


Figure 1.3: Effect of demographic expansion and industrialization on global warming/climate change.

## 1.1.2. Major greenhouse gases and their abundances in the atmosphere

### 1.1.2.1. Carbon dioxide (CO<sub>2</sub>)

The atmospheric carbon dioxide concentrations were reasonably stable (typically quoted as 278 ppm) before industrialization. Since beginning of the 20<sup>th</sup> century, carbon dioxide concentrations have increased by about 40 per cent, up to 390 ppmv (Figure 1.4). The growth rate of the atmospheric carbon dioxide has averaged about 1.68 ppm per year over the past 31 years (1979-2010), averaging about 1.43 ppmv per year before 1995, and 1.94 ppm per year thereafter. Carbon dioxide increase from pre-industrial mixing ratio has induced a

radiative forcing of  $+1.66 (\pm 0.17) \text{ W.m}^{-2}$ . Past emissions of fossil fuels and cement production have likely contributed about three-quarters of the current radiative forcing, with the remainder caused by land use changes (IPCC, 2007).

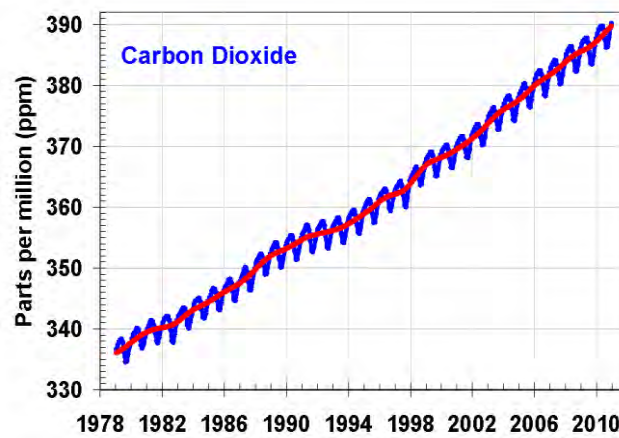


Figure 1.4: Atmospheric carbon dioxide mixing ratio since 1978.

#### 1.1.2.2. Methane ( $\text{CH}_4$ )

Like carbon dioxide, the atmospheric methane concentrations were reasonably stable before industrialization (typically quoted as 700 ppb). Since industrialization, the atmospheric methane concentrations have increased by more than 150 % to present day values ( $\sim 1790$  ppb in 2009) (Figure 1.5).

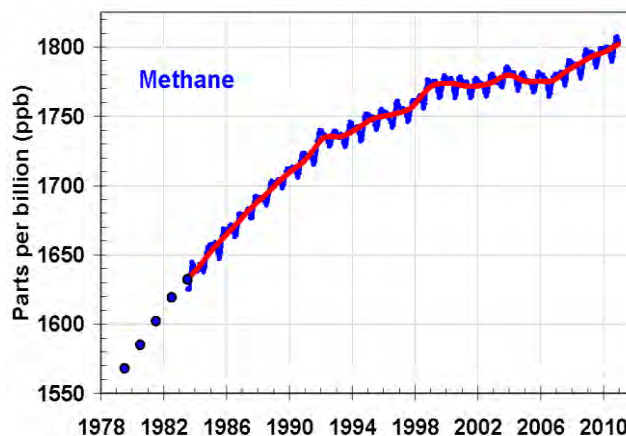


Figure 1.5: Atmospheric methane mixing ratio since 1978.

The growth rate of methane declined from 1983 until 1999, consistent with an approach to steady state for concentration. Superimposed on this decline is significant interannual variability in growth rates (Dlugokencky et al., 1998, 2003). The approach to steady state may have been accelerated by the economic collapse of the former Soviet Union and decreased emissions from the fossil fuel sector in that region. From the year 1999 to 2006, the atmospheric  $\text{CH}_4$  concentration was about constant.

However, this decrease and the negligible long-term change in its main sink (the hydroxyl radical, OH) imply that total CH<sub>4</sub> emissions were not increasing during that period. Since 2007, globally averaged CH<sub>4</sub> has begun increasing again. Causes for the recent increases are warm temperatures in the Arctic in 2007 and increased precipitation in the tropics in 2007 and 2008 (Dlugokencky et al., 2009). Methane increase from pre-industrial mixing ratio has induced a radiative forcing of +0.48 (±0.05) W.m<sup>-2</sup>.

### 1.1.2.3. Nitrous oxide (N<sub>2</sub>O)

Similar to CO<sub>2</sub> and CH<sub>4</sub>, The atmospheric concentrations of nitrous oxide were reasonably stable before industrialization (typically quoted as 270 ppb). Since industrialization, nitrous oxide concentrations have increased by about 20 % (Figure 1.6) due to agricultural/land-use practices (for example the use of nitrogenous fertilizers). It continues to rise approximately linearly (0.26% yr<sup>-1</sup>, Montzka et al., 2011) to reach the present day values (~323 ppb in 2009)

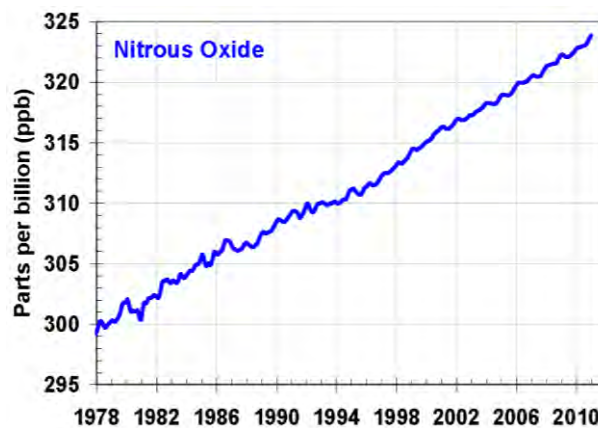


Figure 1.6: Atmospheric nitrous oxide mixing ratio since 1978.

N<sub>2</sub>O increase from pre-industrial mixing ratio has induced a radiative forcing of +0.16 (±0.02) W.m<sup>-2</sup>. Recent studies reinforce the large role of emissions from tropical regions in influencing the observed spatial concentration gradients.

## 1.2. Processes behind GHG emissions from a natural watershed

### 1.2.1. Carbon and nitrogen cycle in a natural watershed

A natural catchment is depicted in Figure 1.7. In a natural catchment, the main source of carbon is atmospheric CO<sub>2</sub>. Atmospheric CO<sub>2</sub> is fixed by plants during photosynthesis leading to primary production (PP) of organic matter (OM). Part of the produced OM is either directly incorporated into the soil organic matter (SOM) via processes occurring in the rhizosphere or stored in the living biomass until the plant decays. Carbon can be released from soil as CO<sub>2</sub> through respiration. Soils are also the place of CH<sub>4</sub> production (methanogenesis in anoxic conditions). CH<sub>4</sub> can be oxidized by methanotrophic bacteria when diffusing from the production zone to the oxic part. In well-drained 'upland' soils, aerobic CH<sub>4</sub> oxidation usually

dominates (Conrad, 1989). In ‘lowland’ or flood-plain soils, anoxic conditions may prevail and CH<sub>4</sub> production is higher than CH<sub>4</sub> oxidation leading to CH<sub>4</sub> emission.

Organic and inorganic carbon is transported within the aquatic system of the river basin (river, lakes and wetlands) by surface or subsurface runoff (Figure 1.7). CO<sub>2</sub> and dissolved inorganic carbon are either consumed for aquatic primary production or follow the pathways. CH<sub>4</sub> is either oxidized in the soil and water column or emitted to the atmosphere. The fraction that is not emitted is either stored in the aquatic system or exported downstream (Cole et al., 2007).

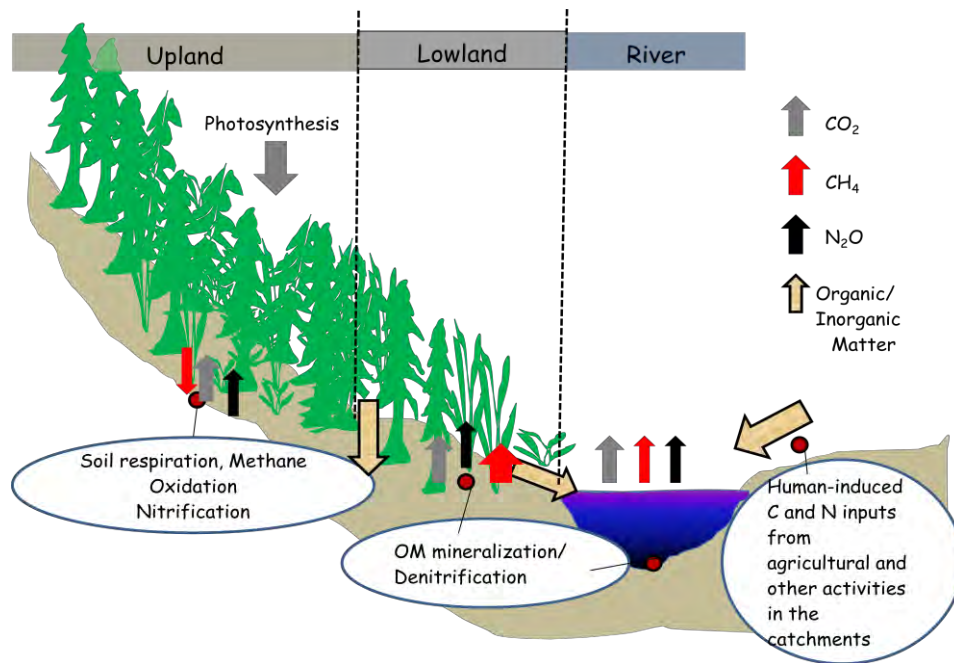


Figure 1.7: GHG cycling from a natural catchment adapted from concepts in Conrad 1989 and Cole et al. 2007 (UNESCO/IHA, 2008).

N<sub>2</sub>O can be produced during both nitrification and denitrification processes. Nitrification is an aerobic microbial process that converts ammonium (NH<sub>4</sub><sup>+</sup>) to nitrate (NO<sub>3</sub><sup>-</sup>) in the presence of oxygen. During denitrification, nitrates are transformed into nitrogen (N<sub>2</sub>). Denitrification requires anoxic conditions, but denitrifying bacteria are facultative anaerobes (Schlesinger, 1997; Hahn et al., 2000). Higher N<sub>2</sub>O emissions observed in tropical conditions could reflect the influence of temperature on nitrification and denitrification processes, as well as nitrogen availability, which is greater in tropical than in boreal and temperate forests (Sitaula and Bakken, 1993; Stange et al., 2000; Clein et al., 2002). Production of N<sub>2</sub>O through nitrification or denitrification will depend on the presence of ammonium or nitrate, and on the soil moisture content. Agricultural and other human activities can increase nitrogen availability in the contributing area leading to significantly higher N<sub>2</sub>O emissions from agricultural soils. Intense rainfall can contribute to increase labile carbon and nutrients and subsequent N<sub>2</sub>O emissions.

### 1.2.2. Carbon cycling in an aquatic ecosystem

The aquatic carbon cycle is depicted in Figure 1.8. The pool of OM in an ecosystem is defined as the sum of the biomass of the living or dead autotrophs and heterotrophs (autochthonous OM), and of the whole OM coming from other ecosystems in the surroundings (allochthonous OM). The quantity of autochthonous OM can be highly influenced by the trophic status of the water body. Photosynthesis in the water occurs in the presence of light (euphotic zone) and nutrients (nitrogen, phosphate, silica) leading to production of OM (which contains about 40-45% of carbon) and oxygen ( $O_2$ ). The carbon from  $CO_2$  assimilated in OM is called organic carbon (OrgC). Organisms responsible for the PP are called primary producers or autotrophs. They are basically constituted algae (macroalgae and phytoplankton) in aquatic ecosystems. In aquatic ecosystems, autotrophs use dissolved  $CO_2$ , that is dissolved Inorganic Carbon (DIC:  $HCO_3^-/CO_3^{2-}$ ). The quantity of allochthonous carbon can be highly influenced by anthropogenic activities in the watershed.

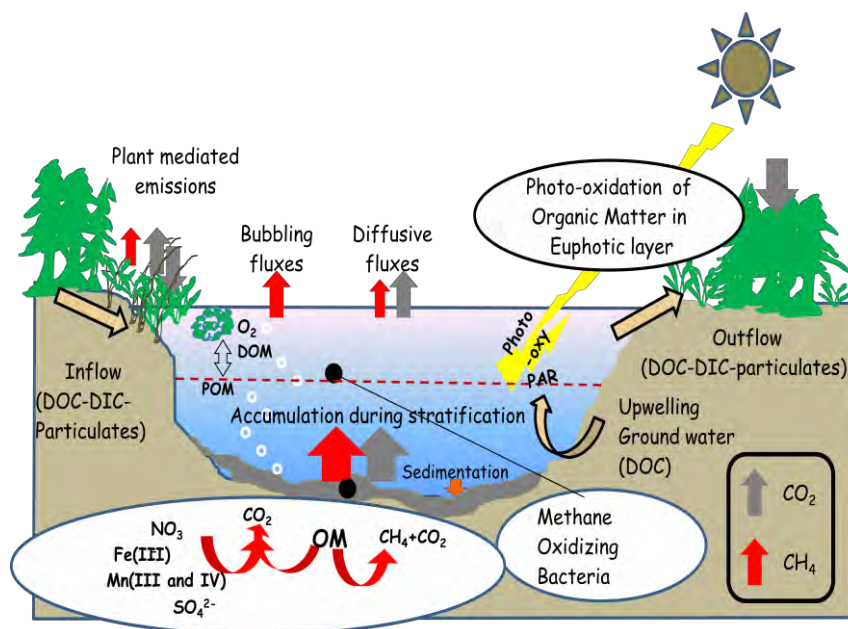


Figure 1.8: Carbon cycling in an aquatic ecosystem. It mainly includes photosynthesis activity, OM loading from surrounding and ground water, soil and plant respiration, mineralization of OM, emissions of gaseous products via diffusion, ebullition or plant mediated emission.

OM from allochthonous and autochthonous sources is decomposed in the water column and in the sediments, the most refractory part being buried in the sediments. During the process of decomposition of OM (oxidation of OM), there is a sequence of oxidation-reduction reactions mediated by microbial community which results in the production, consumption and accumulation of a wide spectrum of intermediate or end product (Froelich et al., 1979) (Figure 1.9). Oxidants (electron acceptors) are consumed in order to decrease energy production per mole of organic carbon oxidized. As oxygen produces maximum energy per mole of organic carbon oxidized, consumption of oxygen occurs first. Consumption of  $O_2$  during decomposition promotes an anoxia at the bottom. Then

consumption of electron acceptors follows the following order:  $O_2$  > nitrate~ manganese oxides > iron oxides > sulfate.  $CO_2$  is produced during the transformation/consumption of OM by bacteria. Decomposition of OM contributes to the pool of dissolved  $CO_2$  + DIC in the water and is either consumed by primary producers or diffuses to the atmosphere. In the euphotic zone of the water column, UVs are able to chemically break down recalcitrant terrigenous DOM into  $CO_2$  (Bertilsson and Allard, 1996). It is believed that photomineralization could play a significant role in the carbon balance of aquatic ecosystem (Soumis et al., 2007).

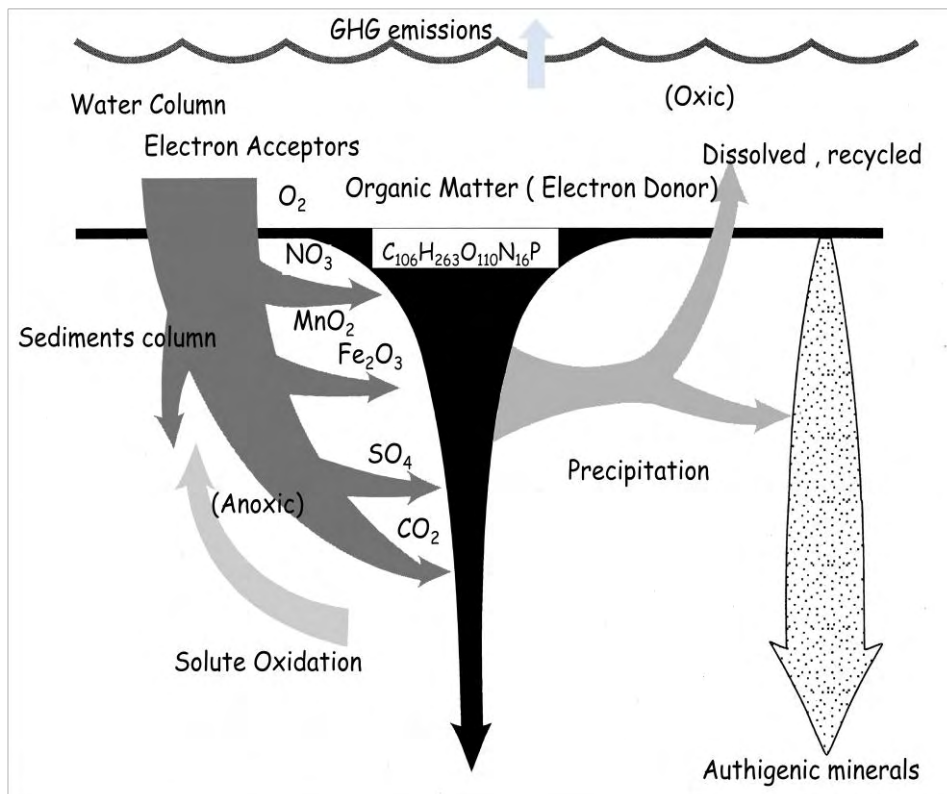


Figure 1.9: Oxidation of organic matters in sediments (modified from Aller, 2004).

### 1.2.3. Methane cycling in an aquatic ecosystem

Methane formation occurs in strictly anaerobic condition as the result of microorganism Achaea known as methanogens, and this process is known as methanogenesis (Zinder, 1993). Methanogenesis occurs when organic matter in the sediment is undergoing anaerobic microbial degradation in the absence of significant quantities of alternative terminal electron. It takes place in a diverse range of anaerobic habitats, e.g. marine and freshwater sediments, marshes, swamps, flooded soils, bogs.

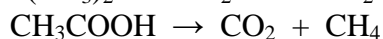
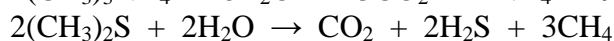
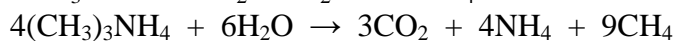
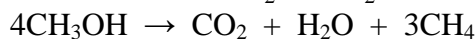
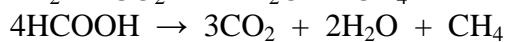
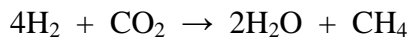
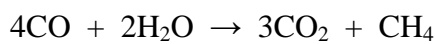
Methanogenesis processes are accomplished in a chain where products excreted by one bacterium are utilized by another one until the organic matter is finally broken down to substrates which then can be used by methanogens to form  $CH_4$  as an end product (Zehnder, 1978, Conrad, 1989, Table 1.1). Stimulation in the production of  $CH_4$  is due to enhanced fermentative production of  $CH_4$  precursors. In principle,  $CH_4$  production would be expected to



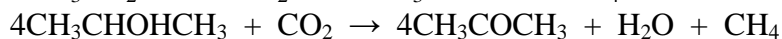
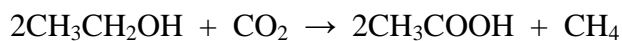
be more or less proportional to the input of organic carbon. High temperature provides favorable condition of CH<sub>4</sub> production. Limitation of methanogenesis by temperature results from: - direct effects: in situ temperature is generally below the growth optimum required by methanogens (according to cultivable methanogenic species). - indirect effects: low temperatures limit the activities of H<sub>2</sub>- producing syntrophs (Chin and Conrad, 1995; Schulz and Conrad, 1996) and then limit the rate of production of methanogenic substrates, particularly those for hydrogenotrophic methanogens. Louis et al. (2005) observed higher methane production at 25°C, than 5 and 10°C. Most isolates of methanogenic bacteria are mesophilic ones, i.e. they have temperature optimum between 30 and 40°C (Vogels et al., 1988). The pH is another controlling factor of the methanogenesis activity, with an optimum value around 6–8 (Conrad, 1989).

Table 1.1: Methanogenesis processes as described in Conrad, 1989

#### Complete degradation



#### Incomplete degradation



In aquatic ecosystems, consumption of methane is done by specific groups of microorganisms, known as methanotrophs or methanotrophic bacteria. Generally, methanotrophs are considered to consume more than 80% of the CH<sub>4</sub> produced in aquatic ecosystems (Cicerone and Oremland, 1988; Reeburgh et al., 1993).

#### **1.2.3.1. Aerobic methane oxidation**

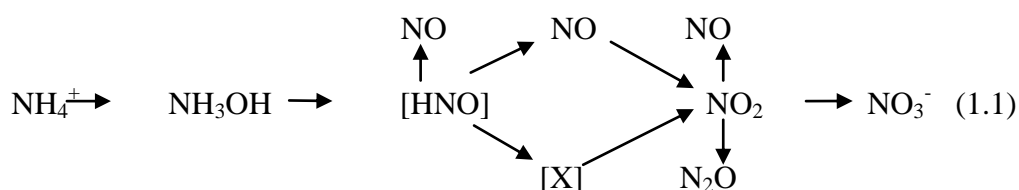
The aerobic methane oxidation is a microbial metabolic process for energy generation and carbon assimilation from methane that is carried by the methanotrophs. Methane (CH<sub>4</sub>) is oxidized using molecular oxygen (O<sub>2</sub>) into carbon dioxide (CO<sub>2</sub>).

In a stratified aquatic ecosystem, the aerobic oxidation process is carried out in the oxycline zone and in the oxic layers, whereas in well-mixed water bodies with oxygenated water column this happens in the sediments itself. Galchenko et al. (1989) named this the "bacterial filter" for reducing methane emission from the aquatic ecosystem. Methane oxidation rate is governed by methane concentration since methanotrophs use it as source of energy and their activity depends on the availability of their main substrates, namely CH<sub>4</sub> and O<sub>2</sub> (Rudd et al., 1975; Guerin and Abril, 2007), temperature (Wuebbles and Hayhoe, 2002),

light intensity (Murase and Sugimoto, 2005), and nutrient availability, particularly nitrogen (Bodelier et al., 2000). In anaerobic environments, methane is oxidized by consortia of methanogens and sulfate reducers. The methanogens are thought to oxidize methane anaerobically by reversing the methanogenic reaction involving CO<sub>2</sub> and H<sub>2</sub> (Ehrlich and Dianne, 2009).

#### 1.2.4. Nitrous oxide (N<sub>2</sub>O) cycling in an aquatic ecosystem

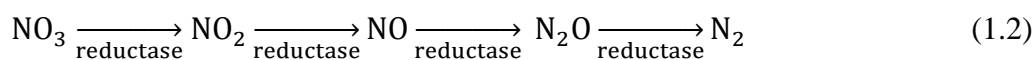
Nitrogen is incorporated in organic matter during photosynthesis by assimilation of nitrate (NO<sub>3</sub><sup>-</sup>) and ammonium (NH<sub>4</sub><sup>+</sup>) by primary producers. During mineralization of OM, NH<sub>4</sub><sup>+</sup> is produced and it diffuses from the anoxic to the oxic zone. NO<sub>3</sub><sup>-</sup> is produced from NH<sub>4</sub><sup>+</sup> during the nitrification in aerobic conditions. This process produces N<sub>2</sub>O as a by-product. The simplest scheme of nitrification can be shown as



Square brackets indicate incompletely known processes and intermediates.

The relative importance of either ammonium produced by the mineralization of OM is consumed by bacteria of the genus *Nitrosomonas* to produce nitrite (NO<sub>2</sub><sup>-</sup>), and *Nitrobacter* oxidize nitrite to nitrate. This is during that second step that N<sub>2</sub>O is produced.

During OM mineralization, NO<sub>3</sub><sup>-</sup> is used as electron acceptors. This is denitrification during which nitrates are transformed into nitrogen (N<sub>2</sub>) producing N<sub>2</sub>O as a by-product. Denitrification requires anoxic conditions, but denitrifying bacteria are facultative anaerobes (Schlesinger 1997). In anoxic environments, heterotrophic bacteria such as *Pseudomonas denitrificans* can use NO<sub>3</sub><sup>-</sup> as the terminal electron acceptor, with N<sub>2</sub> and N<sub>2</sub>O being the gaseous nitrogen products. The simplest scheme of denitrification can be shown as



Denitrification in soils also consumes N<sub>2</sub>O through the reduction of N<sub>2</sub>O to N<sub>2</sub>. Hence, this bacterial process may serve either as a source or as a sink of N<sub>2</sub>O.

Aquatic systems are considered to be significant, but not the dominant sources of atmospheric N<sub>2</sub>O (IPCC, 2007). According to Mengis et al. (1997), N<sub>2</sub>O concentrations seem to be strongly correlated with O<sub>2</sub> concentrations in lakes. In oxic waters below the mixed surface layer, N<sub>2</sub>O concentrations usually increase with decreasing O<sub>2</sub> concentrations. N<sub>2</sub>O is produced in oxic epilimnia, in anoxic hypolimnia and at oxic-anoxic boundaries, either in the water or at the sediment-water interface. It is consumed, however, in completely anoxic layers. Anoxic water layers are therefore most of the time N<sub>2</sub>O undersaturated. All studied lakes were sources for atmospheric N<sub>2</sub>O, including those with anoxic N<sub>2</sub>O undersaturated

hypolimnion. However, compared to agriculture, lakes seem not to contribute significantly to the atmospheric N<sub>2</sub>O emissions (Mengis et al., 1997).

### 1.2.5. Emission pathways

Greenhouse gases, which are produced at bottom of water body or in the water column during the decomposition of organic material, are either consumed within the aquatic system (photosynthesis, methane oxidation., etc.), or emitted to the atmosphere through diffusion from water surface, ebullition (bubbling), and advection through rooted water plants. In very simple terms, flux can be described as how much of a chemical compound moves (either out or into the system) through a unit area per unit time.

#### 1.2.5.1. Diffusive emissions

Diffusion is a net transport of molecules from a region of higher concentration to one of lower concentration by random molecular motion. Equation-1.3 indicates that a diffusive flux (F) depends on the concentration difference between water and air ( $\Delta P$ ), solubility coefficient of gas ( $\alpha$ ), and gas transfer velocity  $k_{g,T}$ .

$$F = \alpha k_{g,T} \Delta P \quad (1.3)$$

Gas transfer velocity is governed by turbulence at the air-water interface. Many studies have shown that various factors will affect gas transfer velocity, such as wind (Wanninkhof 1992; Wanninkhof and McGillis 1999) wind fetch (Frost and Upstill-Goddard 2002; Borges et al. 2004; Guerin et al. 2007), tidal currents (Borges et al. 2004; Zappa et al. 2007), rainfall (Ho et al. 1997, 2007), microscale breaking waves (Zappa et al. 2004), thermal convection (Schladow et al. 2002; Eugster et al. 2003), organic matter or suspended matter (Abril et al. 2009; Calleja et al. 2009), and surfactants (Frew et al. 1990; McKenna and McGillis 2004). The gas transfer velocity, however, depends upon the turbulence at the air-water interface (Banerjee and MacIntyre, 2004; McGillis et al., 2004) which does not depend upon wind alone. For instance, the turbulence from heat loss that occurs when buoyancy fluxes are negative often exceeds that from wind mixing in tropical lakes and is the dominant cause of mixing in many small lakes world-wide (MacIntyre et al., 2002; MacIntyre and Melack, 2009). The concentration in the surface water is driven by the consumption and production in the surface layer of water, also by the exchange of the gas from the subsurface water layer to the surface layer during diffusion and thermal convection.

There are many methods by which diffusive GHG fluxes from the aquatic ecosystem can be measured. There are some direct fluxes measurements techniques: the floating chambers (Guerin et al., 2007), the eddy correlation (McGillis et al., 2001) and the gradient flux techniques (Zappa et al., 2003), and some indirect methods which consist in measuring the gas concentration air-water gradient and determining  $k$  by using inert tracers such as SF<sub>6</sub> (Wanninkhof et al., 1985) or SF<sub>6</sub><sup>3</sup>He (Clark et al., 1994). Eddy covariance technique can be considered as the reference one since flux is directly measured with not interferences with the surface (non intrusive method).

### 1.2.5.2. Bubbling/Ebullition

When  $\text{CH}_4$  accumulate in the flooded soils,  $\text{CH}_4$  bubbles can develop if  $\text{CH}_4$  concentration in the interstitial water becomes higher than the maximum solubility of this gas in water. Once bubbles are present in the sediment, a variety of environmental factors can favor their release if they have not yet overcome the sediment forces holding them back. Bubble release from the sediment and its movement through the water column, however, are controlled mostly by physical mechanisms. The strongest factors are those that reduce the overlying hydrostatic pressure, such as tides in coastal regions (Martens and Val Klump, 1980) or water level drop in reservoirs (Ostrovsky, 2003). Bubbling fluxes correspond to the direct transfer of  $\text{CH}_4$  from the sediment to the atmosphere with little interactions with processes occurring within the water column. This means that  $\text{CH}_4$  experiences very little oxidation along the bubble ascent in the water column. Bubbling fluxes mainly occur in shallow part of lakes and reservoirs (Keller and Stallard, 1994; Galy-Lacaux et al., 1997; Abril et al., 2005) where the hydrostatic pressure is not high enough to increase the solubility of  $\text{CH}_4$ .

Algar and Boudreau (2010) proposed a mechanism by which the reduction in hydrostatic pressure in a region where bubble growth has been halted would allow the bubble pressure to overcome the sediment pressure, preventing fractionation and upward movement. Increased ebullition is also observed in relation to decreased air pressure (Mattson and Likens, 1990) and as a response to strong winds (Keller and Stallard, 1994), both presumably due to a mechanism similar to what Algar and Boudreau (2010) described. Joyce and Jewel (2003) concluded that near-bottom current acceleration (shear stress at the sediment surface) often demonstrated a better correlation with ebullition events than with wind speed or current velocity alone. It has been shown that bubbles can also be formed for water depth higher than 10m, but those bubbles dissolve into the water column during their transport before reaching the surface (McGinnis et al., 2006). To sum up, the release of the bubbles can be triggered by atmospheric pressure variations (e.g., Casper et al., 2000), variations in water current velocity due or not to tide (Martens and Val Klump, 1980; Chanton et al., 1989; Scranton et al., 1993), shear stress at the sediment surface (Joyce and Jewell, 2003), variation of hydrostatic pressure associated with rapid changes of the water level above the sediment (e.g., Smith et al., 2000), increase of temperature making the  $\text{CH}_4$  solubility to decrease (Chanton and Martens, 1989) and strong wind events (Keller and Stallard, 1994).

One should note that due to the higher solubility of  $\text{CO}_2$  and  $\text{N}_2\text{O}$  in the water, their concentrations in the bubbles are low (Huttunen et al., 2002), when  $\text{CH}_4$  concentration make up to 80% of the bubble air composition (Stadmark et al., 2008). Ultimately, the spatial and temporal heterogeneity of ebullition caused by variability of various physical and chemical parameters make the phenomenon sporadic and difficult to accurately quantify. For this reason, bubbling fluxes have probably always been underestimated in the past studies (e.g., Glaser et al., 2004).

### 1.2.5.3. Plant mediated emissions

Uptake and advective transport of gases through aquatic, submerged and plant that grows in shallow littoral zones is another mechanism of emission. It may transport significant quantities of GHG to the atmosphere (Chanton et al., 1989; Sorrell and Boon, 1992; Hamilton et al., 1995; Boon, 2000; Chen et al., 2009). This flux component depends on gases production and consumption in the rizosphere. The vascular system of the plant allows the diffusion of CH<sub>4</sub> from sediments into the atmosphere (Sebacher et al., 1985). The same vascular system is also able to oxidize the CH<sub>4</sub> via diffusing the O<sub>2</sub> into the roots and from there, eventually into the sediments. The mechanism and efficiency of vascular transport seems to be specific to plant species (Conrad, 1989).

### 1.3. Carbon cycling in a reservoir

The creation of reservoirs floods both terrestrial and aquatic ecosystems, leading to anthropogenic aquatic ecosystems. In the reservoirs, degradation and primary production processes are similar to the processes described for natural aquatic ecosystems, but with an additional source of OM from the flooded soils and vegetation (Figure 1.10). The mineralization of the huge amount of OM at the bottom of the man-made lake causes the release of carbon (in OM form and CO<sub>2</sub> form) as well as nutrients (particularly, N, P, and K) to the water column (Schetagne 1994; Chartrand et al., 1994). The release of nutrients enhances the primary production in reservoir during the first years after flooding. This phenomenon, known as the "trophic upsurge", can be responsible for the production of significant amount of autochthonous OM. The chemical and biological oxygen demand in the water column and the flooded soil and biomass are high and causes anoxia in the former soils and, under certain circumstances, in the water column. Anoxia in the flooded soils allows the establishment of methanogenesis. Figure 1.10 depicts the different processes behind the GHG emissions and also shows the different emission pathway of GHG from a typical hydroelectric reservoir. The production of GHGs occurs from the OM coming from watershed and OM flooded in the soils and vegetations. CO<sub>2</sub> is produced during benthic and pelagic respirations. CH<sub>4</sub> is produced in the anoxic soil or sediment layers. N<sub>2</sub>O can be produced either in the oxic or the anoxic environment through nitrification and denitrification processes respectively.

GHGs, which are produced at the bottom of reservoir or in the water column during the decomposition of organic material, are either consumed within the reservoir (photosynthesis and methane oxidation), or emitted to the atmosphere through different pathways: (1) bubble fluxes (ebullition) from shallow waters, mainly methane; (2) diffusive fluxes from the water surface of the reservoir; (3) diffusion through plant stems; (4) degassing downstream of the reservoir outlet(s); and (5) diffusive fluxes all along the river course downstream of the outlet(s). GHG emissions from the river downstream of the dam, just below the turbines and other outlets, make reservoir emissions necessarily different from the ones observed in natural aquatic ecosystems (Delmas et al., 2004; Abril et al., 2005, Guérin et al., 2006, Roehm and Tremblay, 2006, Kemenes et al., 2007, 2011).

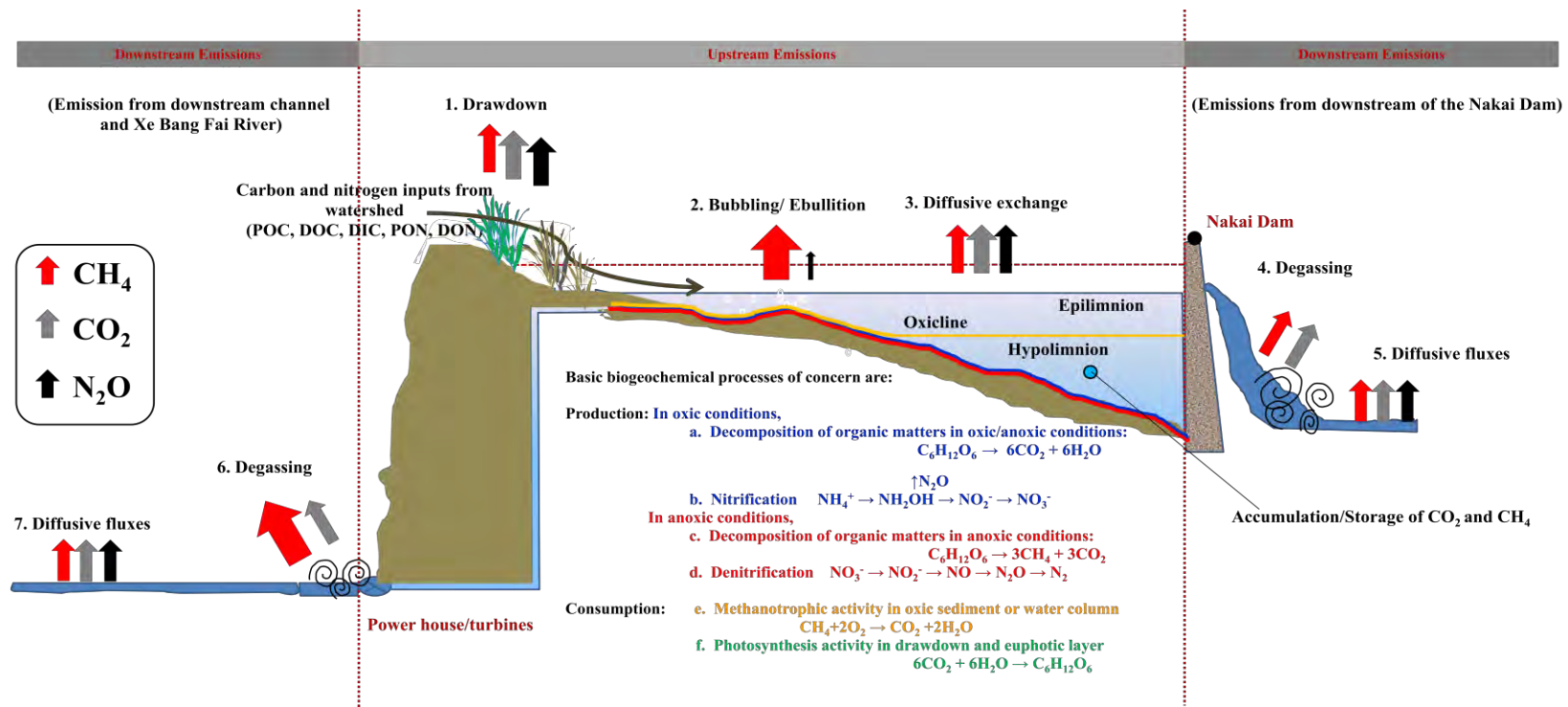


Figure 1.10: Methane, Carbon dioxide and Nitrous oxide dynamics in a hydroelectric reservoir: case of Nam Theun 2, Lao PDR (Abril et al., 2005; Chen et al., 2011; Guérin et al., 2006, 2008a, 2008b; Guérin and Abril et al., 2007; Kemenes et al., 2007, 2011).

When water from below the surface of the reservoir is released from the turbines or from the spillway, the pressure acting upon water suddenly drops and - according to the chemical principle of Henry's Law - gases are less soluble. Due to the decline in pressure, the solubility of CH<sub>4</sub> and CO<sub>2</sub> decreases, resulting in degassing to the atmosphere. Compared with the other emission mechanisms, gas emission from water degassing only depends on the average dissolved methane concentration in the water column and on the water discharge. Therefore, the location of the water intake to turbine is very important (Roehm and Tremblay, 2006). The degassing term could be dominant in the total CH<sub>4</sub> or CO<sub>2</sub> emissions if CH<sub>4</sub> and CO<sub>2</sub>-rich hypolimnetic waters are released (Delmas et al., 2004, Abril et al., 2005, Kemenes et al., 2007, 2011). Part of dissolved GHGs in reservoir water that are not released at the spillway and turbine may be emitted to the atmosphere further downstream as reported for tropical reservoirs and this emission could contribute a significant amount (Abril et al., 2005; Guerin et al., 2006; Kemenes et al., 2007, 2011). It has been reported that total emissions from downstream, including degassing and diffusive emission, could be significant in term of CH<sub>4</sub> emissions. For example, it has been reported that 55 and 57% of all methane released from the Balbina hydroelectric reservoir (Kemenes et al., 2007) and Petit Saut reservoir in French Guyana (calculated from Abril et al. (2005), respectively come from downstream emissions. Lima et al., 2007 claims that downstream methane emissions could be in between 92 and 98% of the total CH<sub>4</sub> emissions in the tropical hydroelectric reservoirs.

Depending on reservoir operation planning, water level fluctuations in many reservoirs are higher than for natural lakes. Water level fluctuation allows a significant drawdown zone where soil respirations can contribute significantly to the CO<sub>2</sub> emissions. During low water level period, vegetation can grow in the littoral zone, and later be decomposed in OM when littoral zone is flooded during the high water level period. In addition, emissions can occur from standing vegetation. A study shows that this pathway contributed significantly to the total CH<sub>4</sub> emissions from the Three Gorge Dam (Chen et al., 2009, Yang et al., 2012).

### **1.3.1. Key processes influencing emission of GHGs to the atmosphere from hydroelectric reservoirs:**

#### **1. Processes supplying organic carbon to the reservoir or its sediments:**

- a. Inputs of OM through groundwater, streams, transfer channels, tunnels rivers (controlled by the discharge rate and the concentrations of OM in the catchment);
- b. Net primary productivity of aquatic macrophytes, periphyton and phytoplankton growing in or on the water or in the drawdown zone around the reservoir, depending on the supply of nutrients and light;
- c. Entrainment of terrestrial OM in living plants, litter and soils during impoundment;
- d. Erosion of soil in the reservoir shore zone (adding OM to the reservoir).

#### **2. Processes producing conditions conducive to the production of GHGs:**

- a. Decomposition of flooded OM and the various types of OM entering the system, depending on the organisms present, temperature, dissolved oxygen and nutrients;

- b. Photo-oxidation of dissolved organic carbon (DOC);
- c. Aerobic oxidation of CH<sub>4</sub>;
- d. Nitrification and denitrification processes.

### **3. Processes influencing the distribution of GHGs within the reservoir:**

- a. Mixing and transport processes in the water column;
- b. Withdrawal through spillways and outlets;
- c. CH<sub>4</sub> oxidation within the water or sediments, depending on the physical stratification, dissolved oxygen, inhibition by light, nutrient levels and temperature;
- d. Primary production in the euphotic zone of the reservoir water column consuming CO<sub>2</sub> and depending mainly on light and nutrient availability.

### **4. Pathways for the GHGs from the reservoir/downstream river to the atmosphere:**

- a. Ebullition (bubbling);
- b. Diffusive gas exchange from the reservoir/downstream river to the atmosphere
- c. Degassing after turbines and spillways;
- d. Transport via aquatic plant stems.
- e. Emissions from the drawdown area

#### **1.3.2. GHGs emitted by hydroelectric reservoirs**

The three main GHGs that scientists are looking at are: carbon dioxide, methane and nitrous oxide. These gases are both emitted and absorbed by natural aquatic and terrestrial ecosystems. According to UNESCO/IHA (2009), CO<sub>2</sub> is a natural component of the carbon cycle, often accounting for more than 80% of the GHG emissions. Although these emissions may be influenced in time and space by the creation of a reservoir, CO<sub>2</sub> emissions are potentially similar at the basin level, in pre- and post-impoundment conditions. On the opposite, CH<sub>4</sub> are favored in post-impoundment conditions (anoxia) not present under the previous land use. There is little knowledge on N<sub>2</sub>O emissions in freshwater reservoirs, when terrestrial ecosystems are known sources of this compound. The few published studies report very low N<sub>2</sub>O emissions in boreal aquatic ecosystems, but there are no conclusive results for tropical reservoirs (UNESCO/IHA, 2009).

#### **1.3.3. Global distribution of hydroelectric reservoirs and GHG emissions**

The availability of technical hydropower throughout the Globe is highlighted in the Figure 1.11. The installed capacity of hydropower by the end of 2008 contributed 16% of worldwide electricity supply, and hydropower remains the largest source of renewable energy in the electricity sector (IPCC, 2011).

The total worldwide technical potential for hydropower generation is 14,576 TWh/yr (52.47 EJ/yr) with a corresponding installed capacity of 3,721 GW, roughly four times the current installed capacity.



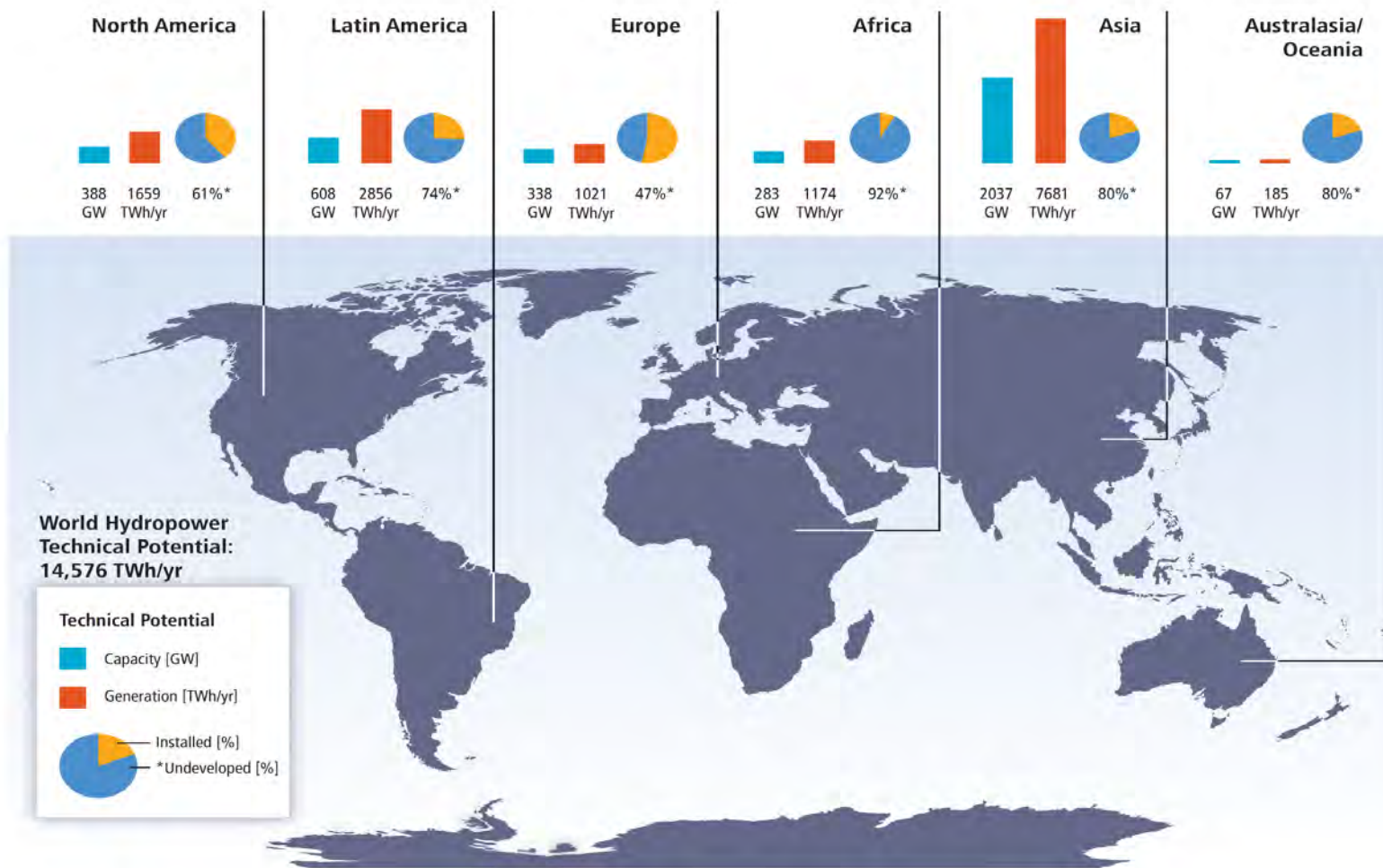


Figure 1.11: Regional hydropower technical potentials in terms of annual generation and installed capacity, and percentage of undeveloped technical potential in 2009 (Source: IJHD, 2010).

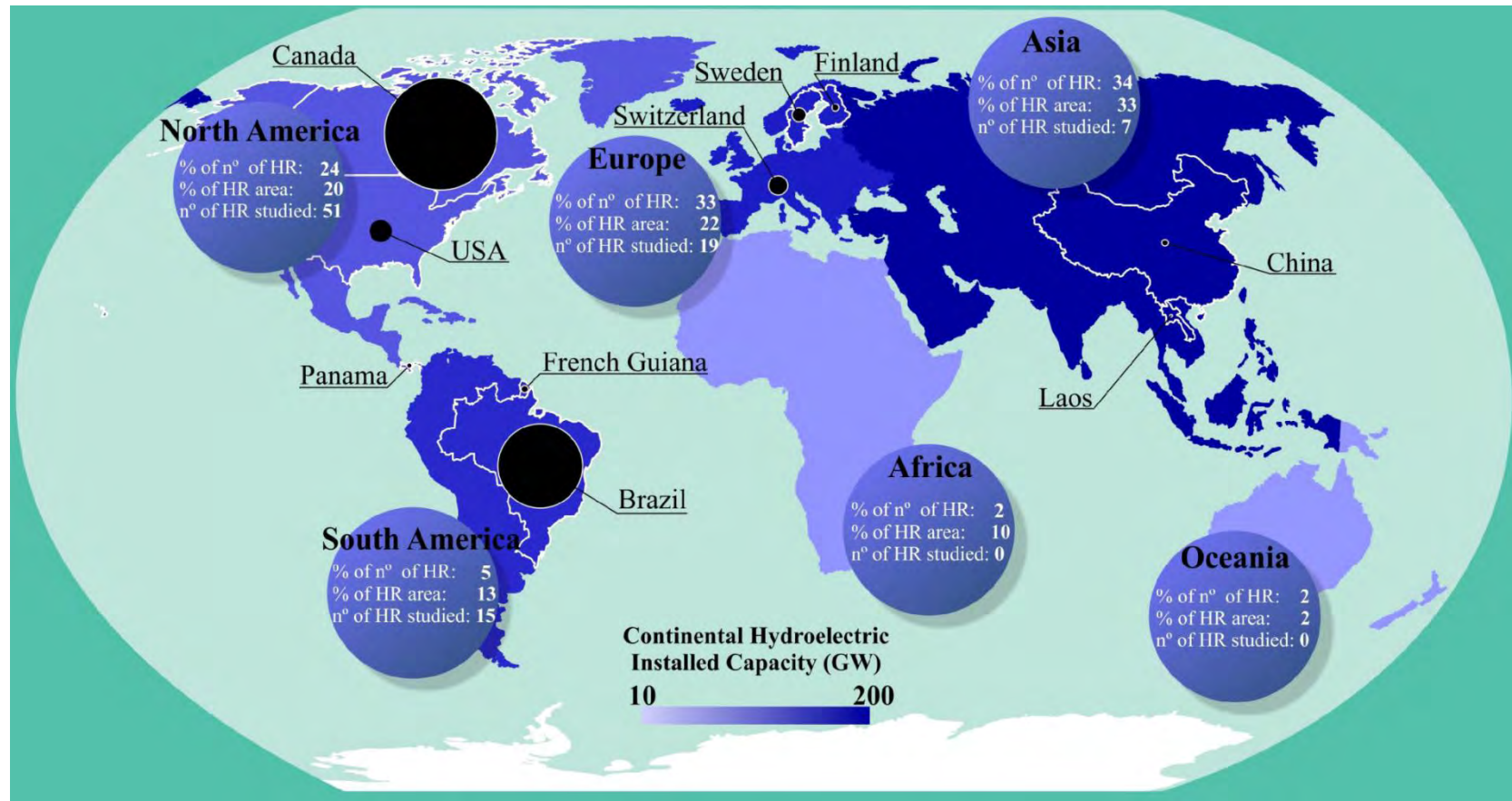


Figure 1.12: Global distribution of hydroelectric reservoirs (HR), expressed as the proportion of the total number of reservoirs globally constructed on each continent, the proportion of the global HR area on each continent and the number of HR studied on each continent. The blue gradient indicates the hydroelectric installed capacity per continent. The black circle sizes are proportional to the number of papers published dealing with GHG emissions from reservoirs located in each country. The percentages of total number and total area of hydroelectric reservoirs were calculated based on ICOLD (2007). The numbers of papers published approaching GHG emissions from hydroelectric reservoirs are extracted from Barros et al., 2011, Chanudet et al., 2011, Wang et al., 2011, and Zheng et al., 2011. (from Mendonça et al., 2011).

Of the total technical potential for hydropower, undeveloped capacity ranges from about 47% in Europe and North America to 92% in Africa. This indicates large opportunities for continued hydropower development worldwide, with the largest growth potential in Africa, Asia and Latin America. Figure 1.12 clearly reveals that most of the studies on GHGs emissions from reservoirs are located in Canada and South America. Interestingly, there is very few information from reservoirs in Asia. Our previous section claims that this region holds a large undeveloped hydropower potential. It means there are many hydroelectric reservoirs to be built in order to fulfill the energy requirement in fast growing economies (e.g. China, India, etc.). All these make this region of particular interest to study impact of hydroelectric reservoirs on the total GHGs emissions.

#### **1.3.4. Important scientific advances**

Since the early 90's, the role of man-made reservoirs as sources or sinks of GHG has rapidly become a global topic of investigation. At least 85 globally distributed hydroelectric reservoirs have so far been studied with focus on GHG fluxes (Barros et al., 2011). The first scientific papers focused on reservoirs located in Canada (e.g. Rudd et al., 1993; Duchemin et al., 1995), Brazil (e.g. Rosa and Schaeffer, 1994; Fearnside, 1995, 1997), Panama (Keller & Stallard, 1994) and French Guyana (e.g. Galy-Lacaux et al., 1997; Galy-Lacaux et al., 1999). Later, reservoirs in Finland (e.g. Huttunen et al., 2002), USA (e.g. Soumis et al., 2004), Sweden (e.g. Aberg et al., 2004; Bergstrom et al., 2004) and Switzerland (e.g. Diem et al., 2007) were studied. GHG emissions have been measured from South American reservoirs including four Amazonian sites (Balbina, Curuá-Una, Samuel, Tucuruí), and additional sites in central and southern Brazil (Barra Bonita, Carvalho, Corumbá, Funil, Furnas, Itaipu, Itumbira, Manso, Mascarenhas de Moraes, Miranda, Ribeirão das Lajes, Serra da Mesa, Segredo, Três Marias, Xingó). Until very recently, no measurements were available from reservoirs in other regions of the tropics or subtropics excepted for Gatum, Panama and Petit-Saut, French Guyana. These last four years, those measurements were completed by the very first studies conducted in tropical Asian countries: Chen et al., 2009, 2010; Chanudet et al., 2011; Wang et al., 2011; Zheng et al., 2011, Yang et al., 2012.

Measurements in boreal/temperate regions are available from Canada, Finland, Iceland, Norway, Sweden, Switzerland and USA (UNESCO/IHA, 2009). As a conclusion, most of the studies on the GHG emissions from reservoirs were conducted in the Americas and Northern Europe, with much fewer in tropical Asia and Africa (IPCC, 2011). As mentioned before, these regions will experience a major growth with hundreds of planned reservoirs in the coming years, especially on India and China.

For most of the studied reservoirs, diffusion from the reservoir water surface has been investigated. The sporadic nature of the ebullitions makes it difficult to accurately quantification, for this reason, bubbling fluxes have probably always been well explored in the past studies (e.g., Glaser et al., 2004). Studies at the Petit-Saut, Samuel and Balbina reservoirs have investigated GHG emissions from the downstream of the dam. But, similar to bubbling, in most of the previous studies, downstream emissions have not been studied well.

### **1.3.5. Emissions from reservoirs at the global scale**

There are many estimates of GHG emissions from reservoirs providing with a wide range of total emission, from 4 to 321 Tg C.y<sup>-1</sup> (Barros et al., 2011, St. Louis et al., 2000). This large range of the estimates mainly originates from the extrapolation/interpolation of spatially and temporally variable measurements. As discussed in Mendonça et al. (2011), GHG emissions from hydroelectric reservoirs vary at the spatial scale (inter-reservoir as function of latitude, activities in the watershed, allochthonous/autochthonous inputs, initial flooded organic matter, etc.; and intra-reservoir as function of longitudinal gradients from the tributaries to the dam, from littoral to deep zone, upstream and downstream of the dam, etc.). GHG emissions also varies at temporal scale (with age of the reservoir, seasonally, daily, with changes in anthropogenic activities in the watershed, and with reservoir operation planning).

Many of the reported studies are not comprehensive since they do not include all of the major pathways like downstream emissions, which are not well documented at the global scale. Degassing data are also missing to estimate the importance of the degassing pathway relative to the diffusion and bubbling ones. Published estimates of degassing from two tropical dams (Balbina, Brazil; and Petit Saut, French Guyana) are many-fold higher than the diffusive and bubbling fluxes. It is almost impossible to extrapolate the ratio of bubbling to diffusive flux based on the data presented in their study to the reservoir where one of the two terms is missing. Finally, there are some uncertainties in these emissions because of the lack of data from different geographical regions, and high spatial and temporal variability in the emissions from one reservoir to another (Barros et al., 2011). Transferring results from one reservoir to another is difficult because there are many site-specific factors influencing the potential for a reservoir to emit GHGs.

These uncertainty also arises from multiplicative error from the uncertainty in the global surface area of hydroelectric reservoirs, and its spatial and temporal variations. The global reservoir area varies from 0.26 to 1.5 M km<sup>2</sup>, but a conservative global reservoir area seems to be around 0.5 M km<sup>2</sup> on the basis of high-resolution mapping of Global Reservoir and Dam database (Lehner et al. 2011). The extremely large area obtained by St. Louis et al. (reference in Downing et al. 2006) was mainly due to the vague distinctions between impounded natural lakes and man-made reservoirs. Yet, this largest data were adopted by Barros et al. (2011). While the percentage of hydroelectric reservoirs (i.e., 25 %) before 1998 adopted by Barros et al. (2011) is much lower than Varis et al. (2012), hydropower reservoirs account for around 62 % of the total surface area of the world's reservoirs.

### **1.3.6. The importance of considering net emissions**

To validly assess the climate impacts of dams, net emissions estimates are needed. Considering only gross from reservoirs will most likely lead to attribute excess values to GHG emissions by hydroelectricity and reservoirs. The great majority of the currently available data deals with gross emissions. Data that only looks at gross emission can be misleading. A challenge for the scientific community is to calculate net emissions, rather than simply gross

emissions. Net emission considers only the incremental GHG emission due to the creation of reservoirs (WCD, 2000).

$$\text{Net emissions} = \text{gross emission} - \text{emission before reservoir} \quad (1.4)$$

In an ideal case, GHG emissions from the reservoir area pre-impoundment are known. Then these emissions can be subtracted from the emissions measured after impoundment (gross emissions) to calculate the net emissions. If the pre-impoundment site would be a source of emissions, then the net emissions would decrease. If it would be a sink (as often the case for tropical forests), the net emissions would actually rise, since this sink would have been lost due to flooding.

Despite the scarcity of data in the scientific literature on net GHG assessments from freshwater reservoirs, the results presented on the Petit Saut reservoir by Delmas et al. (2001), and estimates made using stable isotope data for the Robert-Bourassa reservoir (Tremblay et al., 2005), suggest that, on a 100 year basis, net GHG emissions can be about 25% to 50% less than gross GHG emissions.

Based on the previous sections, considering the need to study GHG emissions from a reservoir, we started this work on newly flooded sub-tropical reservoir to attempt the following objectives:

- 1). Quantification of CO<sub>2</sub>, CH<sub>4</sub>, also N<sub>2</sub>O from all the major known pathways (including both downstream and drawdown area) while taking into account the spatial and temporal variability.
- 2). Extrapolation of the emissions at the reservoir scale through the characterization of biogeochemical processes and physical controls regulating the GHG emissions.
- 3). Assessment of the net GHG footprint of the reservoir that is difference between post-flooding emissions and pre-flooding emissions.



## Chapter 2

### Site description, sampling strategy and methodology

---

#### 2.1. Site description

The Nam Theun 2 (NT2) hydroelectric reservoir was built on the Nam Theun River by Électricité de France (EDF) and now operated by Nam Theun 2 Power Company (NTPC) in the subtropical region of Lao People's Democratic Republic (Lao PDR). With an average annual turbine discharge of  $220 \text{ m}^3 \cdot \text{s}^{-1}$ , NT2 hydroelectric plant delivers an annual power production of 6 TWh (with an installed capacity of 1070 MW) and demonstrates a high ratio between the annual power production and inundated area ( $13.3 \text{ GWh} \cdot \text{km}^{-2}$ ).

Being on the northern hemisphere at  $17^\circ 59' 49'' \text{N}$ ,  $104^\circ 57' 10'' \text{E}$ , the project area experiences a sub-tropical monsoon climate with distinct wet and dry (initial cold then warm dry) seasons, i.e. three seasons: a wet (May-September), a dry cold (October-January) and a dry warm season (February-April) (NTPC, 2005). The mean daily temperature is  $24^\circ \text{C}$ , and varies from  $17^\circ \text{C}$  in January to  $26^\circ \text{C}$  in April (NTPC, 2005). Except for rain storms mostly during the monsoon, the wind speeds are generally rather low and  $2.6 \text{ m} \cdot \text{s}^{-1}$  on average. Mean annual rainfall is about 2400 mm, mainly occurs in between May and September (NTPC, 2005). Since the water inputs are directly related to rainfall, filling of the NT2 reservoir typically occurring during the wet season. The maximum and minimum mean monthly inflows are respectively 735 and  $30 \text{ m}^3 \cdot \text{s}^{-1}$ .

The NT2 reservoir receives average annual runoff of 7527 million  $\text{m}^3$  from its major inflowing tributaries (Nam Xot, Nam Mon, Nam Theun, Nam Noy, Nam Yang and Nam On), which is almost double of maximum volume capacity of the NT2 reservoir (3530 million  $\text{m}^3$ ). The NT2 is a trans-basin diversion hydroelectric reservoir that receives water from the Nam Theun watershed and releases it into the Xe Bang Fai River through a 27 km long artificial downstream channel (Figure 2.1). A continuous ecological flow of only  $2 \text{ m}^3 \cdot \text{s}^{-1}$  (and occasionally spillway release) is discharged from the Nakai Dam to the Nam Theun River, the remaining water being diverted to the powerhouse (Figure 2.1). The intake of the turbines is located at the bottom between 506 m and 524 m above sea level (full supply level = 538 m and minimum operating level = 525.5 m). Before being released into the Xe Bang Fai River, turbinated water is stored and the flow controlled in an 8 million  $\text{m}^3$  artificial regulating pond.

The filling of the reservoir started on 15<sup>th</sup> of April 2008. During the flooding, soils and different types of vegetations have gradually disappeared by the end of October 2009 when the maximum of the reservoir surface was first reached, which resulted of inundations of a dendritically shaped area of  $450.2 \text{ km}^2$ . Until commercial operation of the NT2 hydroelectric power plant started in March 2010, the water level in the reservoir was nearly constant from October 2009 to March 2010.

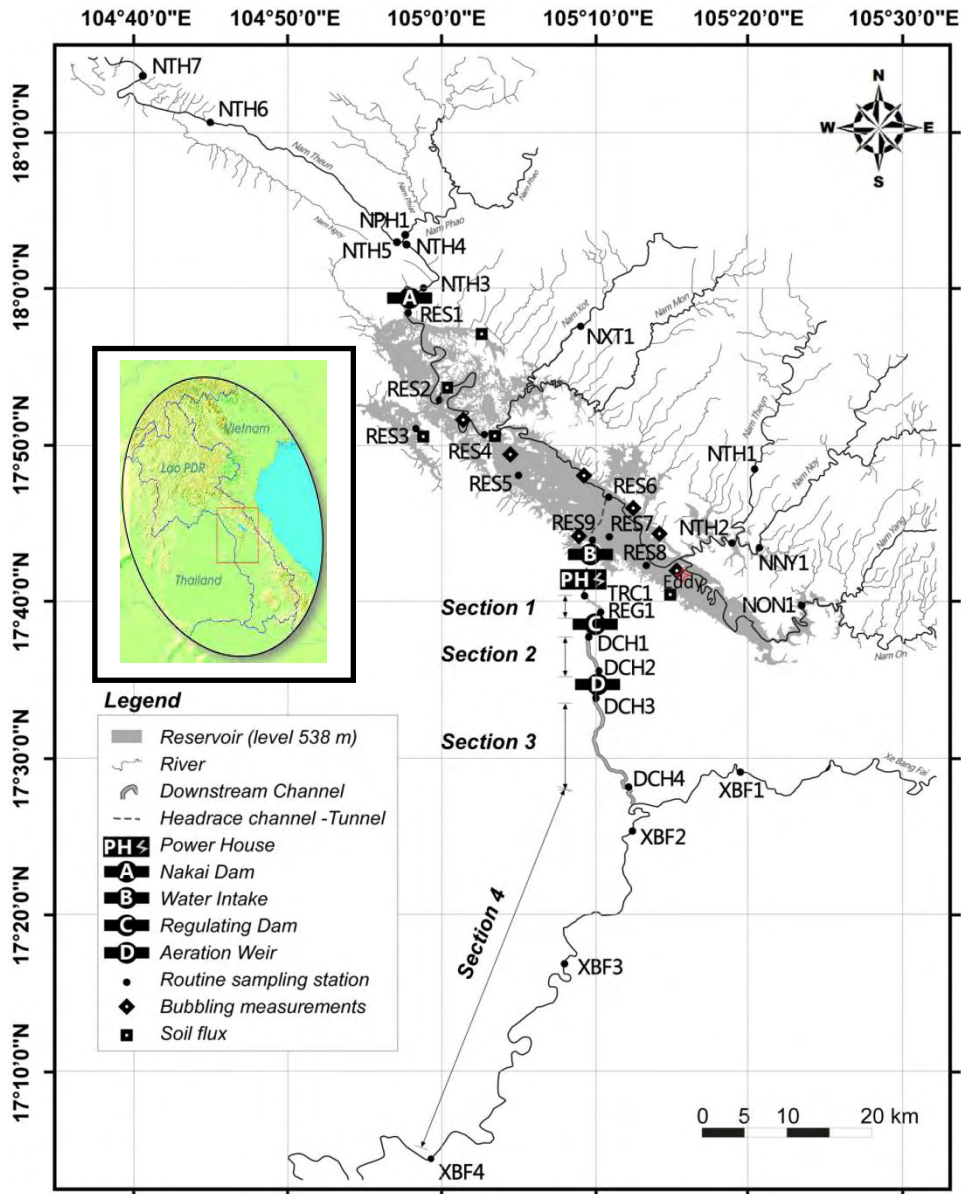


Figure 2.1: Location map showing different components of Nam Theun 2 (NT2) hydroelectric reservoir and location of the sampling stations. The reservoir is shown at its full capacity (538 m above sea level).

The NT2 Reservoir is characterized as a warm monomictic lake i.e. completely mixed from top to bottom once a year during the dry cold season (Chanudet et al., 2012). During the wet season, sudden, short and partial destratification occur irregularly (Chanudet et al., 2012). More physical and meteorological characteristics are summarized in Table 2.1.

Due to sub-tropical conditions the vegetations in the drowned area of the NT2 Reservoir was luxuriant but variable, and a large amount of it has been submerged. Maximum water level corresponds to the flooding of a landscape of dense, medium, light, degraded forest, riparian forest, agricultural soils and swamps (Descloux et al., 2011).



Table 2.1: The main characteristics of the Nam Theun 2 Hydroelectric reservoir, Lao PDR.

<b>General</b>	Country	Lao People's Democratic Republic (Lao, PDR)
	River	Nam Theun
	Latitude	17°59'49"N
	Longitude	104°57'10"E
	Year of impoundment	2008
	Installed capacity	1070 MW
	Annual Power Production	6000 GWh
<b>Meteorological</b>	Wind Speed	2.6 m.s <sup>-1</sup>
	Average relative humidity	63% (Jan) - 89% (Jul)
	Precipitation	2400 mm
	Air temperature	24.7 °C
<b>Lake</b>	Surface at full water level, 538 msl	450 km <sup>2</sup>
	Surface at low water level 525.5 msl	70 km <sup>2</sup>
	Average Depth	7.8 m
	Active storage	3530 million m <sup>3</sup>
	Catchment Area	4013 km <sup>2</sup>
<b>Regulating Pond</b>	Maximum turbined discharge	345 m <sup>3</sup> .s <sup>-1</sup>
	Surface area	0.76 km <sup>2</sup>
<b>Downstream Channel</b>	Length	27 km

Table 2.2: Distribution (area) of cover types in the reservoir area below 538 m (full reservoir water level).

Cover type	Total	
	km <sup>2</sup>	%
Dense forest	154.5	34.6
Medium forest	45.2	10.1
Light forest	110.9	24.8
Degraded forest	51.8	11.6
Riparian forest	4.0	0.9
Agricultural soil	48.7	10.9
Swamps	10.5	2.4
Water	15.3	3.4
"Others"(road, villages)	5.3	1.2
Total	446	100

The distribution of different cover types in the reservoir area below 538 m (full reservoir water level) are summarized in the Table 2.2. The flooded area was mainly covered by dense and light forests (59%), whereas agricultural lands and swamps accounted for 11% and 2% respectively. Even though the vegetation was partially burnt before the impoundment, the total amount of flooded organic carbon was around  $5.1 \pm 0.7$  Tg C (i.e. 2.2 Tg C from above ground biomass, litter and dead wood and 2.9 Tg C from below ground biomass and soil organic carbon) (Descloux et al., 2011).

The maximal depth of the NT2 Reservoir is 39 m and the mean depth is 7.8 m. Owing to hydrological cycle and reservoir operation, the reservoir water surface fluctuates from 70 (at minimum operating level) to 450.2 km<sup>2</sup> (at full water level) respectively during the dry and the wet season. Therefore, since the starting of turbine (March 2010), the reservoir surface varies seasonally and achieves its maxima and minima respectively during the wet and during the warm dry season. The seasonal variation of the water level drop can be up to as large as 12.5 m. Consequently, very large drawdown area runs dry seasonally and stays dry during several months, occurring in the dry season. During the study period reservoir exhibited the maximum drawdown area about 275 km<sup>2</sup> in the late warm dry season.

## **2.2. Sampling stations and sampling strategy**

Our sampling strategy aimed to reduce the uncertainty, which often comes out because of spatial and temporal variability, in all estimates of either measured or calculated variables. For spatial variability, all previous landscape types that flooded during impoundment (Descoux et al., 2011) and physical dynamics of the NT2 reservoir were also taken into account while allocating the sampling stations after post-impoundment. The temporal variability was precisely considered by means of fortnightly sampling, which has been carried out by the AELab at all sampling stations since April 2009 at all sampling stations.

### **2.2.1. Pre-impoundment GHG exchange**

The pre impoundment GHG emissions were based on a field campaign conducted from 11 to 21 May 2008, the beginning of the rainy season. Further, some measurement of N<sub>2</sub>O emissions were also conducted in June 2010, and data related to fluxes of GHG from previously existing rivers were considered from fluxes from sampling station monitored at pristine rivers after flooding. Details about the measurements are given in Chapter 7.

### **2.2.2. Post-impoundment GHG exchange**

A total of 29 routine monitoring stations were selected: nine stations (RES1 to RES9) on the reservoir area, fifteen stations in the downstream rivers and artificial downstream channels, five stations in the pristine inflowing rivers (Figure 2.1). The name of the sampling stations and their locations are given in Table 2.3.

The allochthonous inputs to the NT2 reservoir from the Nam Theun River and other major tributaries were monitored at five stations (NXT1, NTH1, NTH2, NNY1 and NON1, Figure 2.1). At the reservoir, the stations RES1 (close to Nakai Dam), RES2, RES4 and RES6 are located in the upstream of the Nakai Dam on the thalweg of the Nam Theun River. The stations RES5, RES7 and RES8 are respectively located in the flooded degraded forest, flooded swamp area and flooded agricultural land. Station RES3 is located in the flooded primary forest, and station RES9 is located at the upstream of the turbine intake.

Table 2.3: Name of the sampling stations at NT2 hydroelectric system

Components	Sampling Station	Remarks
Upstream pristine rivers	NXT1	Nam Xot River
	NTH1	Nam Theun River
	NTH2	Nam Theun River
	NNY1	Nam Noy River
	NON1	Nam On River
Reservoir	RES1	~100m upstream of the Nakai Dam
	RES2	Thalweg of the Nam Theun River
	RES3	Flooded primary forest
	RES4	Thalweg of the Nam Theun River
	RES5	Flooded degraded forest
	RES6	Thalweg of the Nam Theun River
	RES7	Flooded swamp area
	RES8	Flooded agricultural area
	RES9	~100m upstream of the turbine intake
Downstream of the Nakai Dam	NTH3 to NTH7	Nam Theun River, below the Nakai Dam
Downstream of the powerhouse	TRC1	Exit of the turbines, in the tail race channel
	REG1	Regulating Pond (~4 km from turbine outlet)
	DCH1	Artificial downstream channel just below regulating pond (~5 km from turbine outlet)
	DCH2	Artificial downstream channel before Aeration Weir (~12 km from turbine outlet)
	DCH3	Artificial downstream channel after Aeration Weir (~13 km from turbine outlet)
	DCH4	Artificial downstream channel before confluence with Xe Bang Fai River (~27 km from turbine outlet)
	XBF1	Xe Bang Fai River before confluence with Artificial Downstream Channel
	XBF2 to XBF4	Xe Bang Fai River after confluence with Artificial Downstream Channel

Four sections were defined in the downstream of turbine: Section 1 (length = ~4 km, area = ~0.76 km<sup>2</sup>) - area between tailrace channel (TRC1) and regulating pond area (REG1); Section 2 (length = ~8.5 km, width = ~30m) - area between DCH1 and DCH2 (from the regulating pond to the aerating weir); Section 3 (length = ~18.5 km, width = ~70 m) - area between DCH3 and DCH4; Section 4 (length = ~80 km, width = ~70m) - area between DCH4 and XBF4. The site XBF1 is located in the pristine Xe Bang Fai River and is used as a reference site. The downstream river below Nakai dam till NTH7 is defined as section 5.

Since April 2009, water samples were collected on a fortnightly basis at the 29 previously described monitoring stations located in the upstream pristine rivers, in the reservoir and in the downstream of the power house and the Nakai Dam. The vertical profiles of water samples were collected at the sampling stations located on the reservoir. At the

sampling stations located in the pristine inflowing rivers and downstream of the Nakai Dam and the powerhouse, only surface water sampling was performed as described in Abril et al., (2007). Surface and deep water samples were taken with a surface water sampler (Abril et al., 2007) and a peristaltic pump, respectively. Sometimes, deep water samples were also collected using Niskin bottle. Water samples were analyzed for GHG concentrations, carbon and nitrogen species, cations and anions, and Fe-form. The sampling stations located in the reservoir, vertical profiles of O<sub>2</sub>, O<sub>2</sub> saturation level, temperature, pH and conductivity were measured, whereas only surface observations were made at stations located in the pristine inflowing rivers and downstream of the Nakai Dam and the powerhouse.

During all field campaigns, the diffusive fluxes of CH<sub>4</sub> across the water-air interface were measured with the floating chamber in stations RES1 to RES8. Diffusive fluxes of CO<sub>2</sub> and N<sub>2</sub>O fluxes were also measured with the floating chamber during the March 2011 and June 2011 field campaigns respectively. Additionally, diffusive GHG fluxes were calculated from the fortnightly monitoring of surface GHG concentrations using thin boundary layer equation. The database of measured and calculated fluxes includes flux data from open waters, flooded agricultural, flooded forest sites.

During the dry season, when the water level was usually at its minimum level, sediments (flooded soils + recently sedimented OM) were collected from the shallow zone (depth <6m). Three sediment cores with length ranging from 13 to 21-cm were retrieved from flooded forest (near RES3) and flooded agricultural area (near RES8).

During a low water periods dry season (June 2010), 19 vertical profiles of soil were collected from the same 5 sampling sites monitored for diffusive fluxes of GHG from soils. Each vertical profile were divided into surface (upper 20 cm soil layer) and subsurface (below 20 cm to 120 cm) soil and collected separately. The total 22 samples (13 surface soils and 9 subsurface soils) were incubated for GHG production experiment over a year (November 2010 to October 2011). Soil samples were categorized in FS1 (soils from the primary dense and medium forest), FS2 (soils from light, degraded forest and riparian forest) and AG (soils from agricultural land). Soil incubation experiment could not be performed on flooded swamps area and AG subsurface soils. The soils located in the upland zone were characterized as acrisol, ferralisol and planosol whereas all flooded soils were reductisols.

During field campaigns in May 2009 and March 2010, the eddy covariance system was deployed in an open water area offering a smooth fetch. This site corresponds very precisely to the site used in the former Nam Theun floodplain (pre-impoundment study in May 2008, 17°41.56'N, 105°15.36'E). For practical reasons, the EC system was deployed on a tree stump around 500 meters South-East of the former EC site during the field campaigns in March 2011 and June 2011.

The ebullitions of GHGs (bubbling) were measured at 7 sites with different depths during five field campaigns and a weekly monitoring during the period from March to December 2012 by AELab. The choice of the different sampling sites was determined by the

water depth and the type of flooded ecosystem. The bubbling fluxes were measured with the submerged funnel technique (Keller & Stallard, 1994).

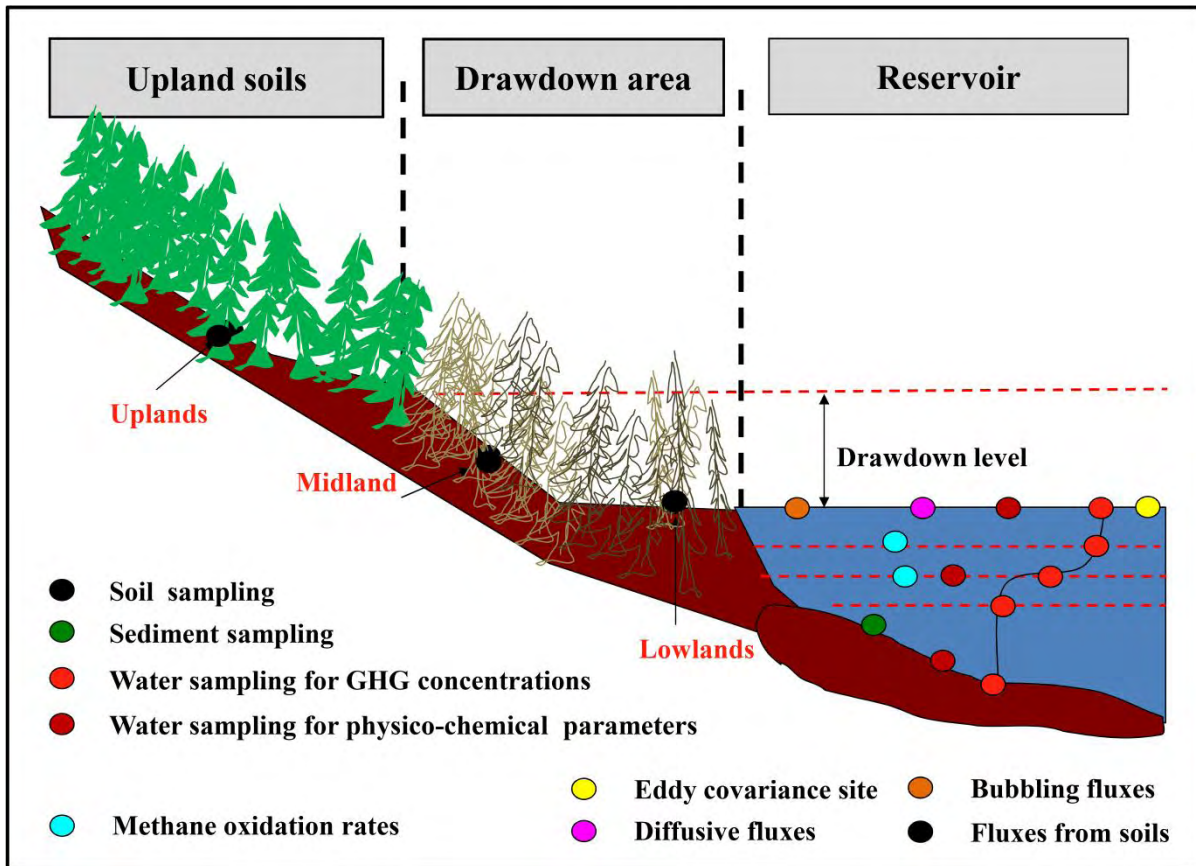


Figure 2.2: Schematic sketch of sampling strategies at the Nam Theun 2 hydroelectric reservoir.

During two low water periods (June 2010 and June 2011), diffusive fluxes of GHG were measured at five stations from the soils surrounding NT2 Reservoir (never flooded soils) and soils located in the drawdown area (Figure 2.2). Soil moisture content and temperature were measured at each site. Sampling sites were chosen based on the representativeness of each flooded ecosystems. At each stations, four zones were defined: the upland zone located in a zone which was never flooded (soil moisture ~20%); the midland zone 1 which was flooded during high water level ( $20\% \leq \text{soil moisture} \leq 30\%$ ); the midland zone 2 which was flooded during moderate water level ( $30\% < \text{soil moisture} < 40\%$ ); and the lowland zone which was close to the shoreline and water saturated (soil moisture ~40%. The upland zone has been disappeared after first full-impoundment in October 2009.

Experiments on aerobic  $\text{CH}_4$  oxidation (AMO) in the pelagic waters were performed on the water samples collected from three sites in the lake (RES1, RES3 and RES7) and one site in the downstream of the Nakai Dam (i.e. NTH3) and one site in the downstream of powerhouse (i.e. DCH1). Water samples were taken from two depths in the lake (at mid-epilimnion, depth ranging from 1.5 to 4 m and from the metalimnion, depth ranging from 3 to 8 m, depending on the season). While, only surface waters were taken from the downstream.

Details of all performed activities during routine monitoring, field campaigns and lab work are summarized in Table 2.4.

Table 2.4: Details about routine monitoring, different field campaigns and laboratory experiments

	Campaign	Period	Performed Activities*
Pre-impoundment activities	First	May, 2008	3, 9
Post impoundment activities	Routine monitoring	January 2009- till date	1, 2, 4
	Second	May, 2009	1, 2, 3, 4, 5
	Third	March, 2010	1, 2, 3, 4, 5, 6
	Fourth	May-June, 2010	1, 2, 4, 5, 6, 7, 8, 9
	Fifth	February-March 2011	1, 2, 3, 4, 5, 6, 10
	Sixth	May-June, 2011	1, 2, 3, 4, 5, 6,7,9
	Experiments on GHG production	November 2010 - October 2011	11

\*Note:

1. Measurements of vertical profiles of GHG concentrations and water chemistry parameters (in situ)
2. Measurements of diffusive fluxes using floating chamber (FC) (in situ)
3. Measurements of diffusive fluxes using eddy covariance (EC) (in situ)
4. Measurements of bubbling fluxes using submerged funnel technique, (SF) (in situ)
5. Determination of aerobic methane oxidation rates (lab work)
6. Quantification of degassing component of emission (calculation)
7. Measurements of vertical profile of GHG concentration in sediment layer using sediment corer
8. Sampling of vertical profile of soils (in situ)
9. Measurements of diffusive fluxes from soils including drawdown area using static chamber (SC) (in situ)
10. Measurements of concentrations and diffusive fluxes of CH<sub>4</sub> and CO<sub>2</sub> using automated systems (in situ)
11. Determination of kinetics of GHG production and analysis of anions, cations, Fe and Mn (lab work).

At NT2, degassing occurs at five sites. At four of them, degassing occurs continuously: at the outlet of the Nakai Dam where  $2 \text{ m}^3 \cdot \text{s}^{-1}$  of water is released for ecological purposes, below the turbines, below the regulating pond dam, and at the aeration weir. In addition, degassing occurs occasionally during spillway release at the Nakai Dam for water level regulation purpose. To quantify the degassing emissions, water samples for GHG concentrations were collected at inflow and outflow of the degassing structures.

In order to monitor exports of GHG and other variables with the water release from the reservoir, measurements were performed at NTH3 and TRC1 located respectively in the downstream of the Nakai Dam and the downstream of the powerhouse.

## 2.3. Methodology

### 2.3.1. Soil sampling

The vertical profiles of soils were collected using a soil auger. Each vertical profile were divided into surface (upper 20 cm soil layer) and subsurface (below 20 cm to 120 cm)

soil and collected separately in zipped plastic bags. Soils samples were dried in the laminar flow dryer at 30°C.

### 2.3.2. Determination of kinetics of potential CH<sub>4</sub> and CO<sub>2</sub> production rates

After drying, soil samples were ground, sieved with 2-mm sieve and homogenized. 750 g of homogenized samples of each type of soil were then redistributed to three replicate serum vials (570 ml), i.e. 250 g of soil in each vial. After adding 250 ml de-ionized water in each vial (i.e. soil/water ratio = 1), vials were closed with butyl stoppers and aluminum crimps. Vials were covered with aluminum foil to avoid effect of light on any bacterial activity. The vials were flushed with N<sub>2</sub> for 30 minutes to create an anaerobic environment. The flushed vials were stored in the dark at 20°C (this temperature corresponds to the average bottom water temperature of the NT2 reservoir). Incubations were performed without agitation to avoid the destruction of symbiotic microbial associations involved in methanogenesis (Dannenberg et al., 1997). Two days before the determination of the GHG production rates, the vials were flushed with N<sub>2</sub> for 30 minutes to eliminate accumulated CO<sub>2</sub> which can increase the methanogenesis (Das and Adhya, 2011, cited therein) and any volatile compounds inhibiting methanogenesis (Williams and Crawford, 1984). Incubated soils samples were analyzed at a frequency of 1 week to 2 months over a year from November 2010 to October 2011.

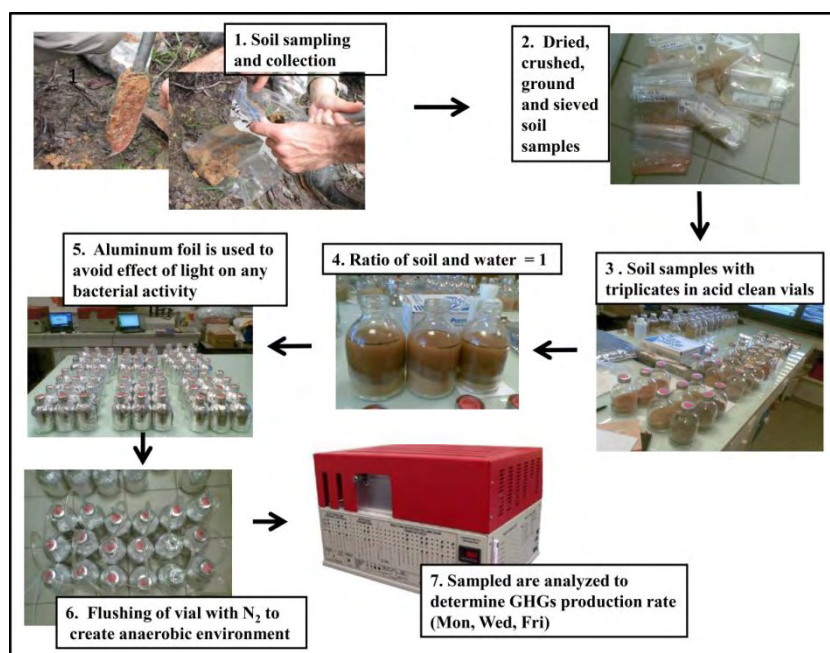


Photo 2.1: Experiment on the determination of GHG production rates in the incubated soil samples collected from the surrounding of the NT2 hydroelectric reservoir and its drawdown area.

After six months of experiments, when no measurements were performed for more than one month, the vials were flushed monthly with N<sub>2</sub>. Before each GC analysis, vials were vigorously shaken for about 30 seconds to ensure equilibration between the liquid and the gas

phase. Total GHG concentrations in the vials were measured in the headspace of the vials 3-times a week to calculate the production rate, as the slope of the concentration versus time. The concentrations of GHG were determined using GC.

### 2.3.3. Determination of CH<sub>4</sub> concentrations in sediment layer

The sediment cores, retrieved from littoral zone of the reservoir, were cut in 1 cm slices within around 15 minutes of sampling. Two replicates were sampled for each depth. Each slice of these cores was transferred into pre-weighed glass vials containing 20 ml of NaOH that were quickly closed with rubber stoppers, vigorously shaken to break up the sediment and to ensure equilibration between gas and slurry phase before analysis (Guérin et al., 2008a). A sub-sample of each slice was immediately sealed in a pre-weighed vial for determination of water content and porosity. The CH<sub>4</sub> concentrations were determined using GC.

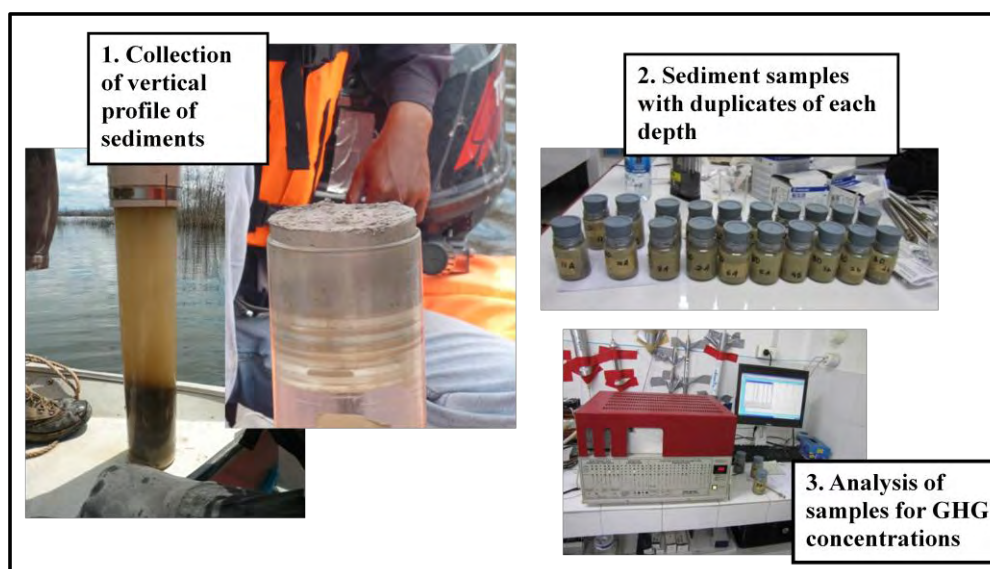


Photo 2.2: Sediment sampling for the determination of GHG concentrations in the flooded soils/sediments.

### 2.3.4. Determination of the GHG concentrations in the water

Water samples were collected at each sampling depth and stored in 27 ml or 60 ml glass vials, capped with butyl stoppers, sealed with aluminum crimps and poisoned until analysis (Guérin and Abril, 2007). Before GC analysis for GHG concentrations, a N<sub>2</sub> headspace was created and vials were vigorously shaken to ensure an equilibration between the liquid and gas phases.



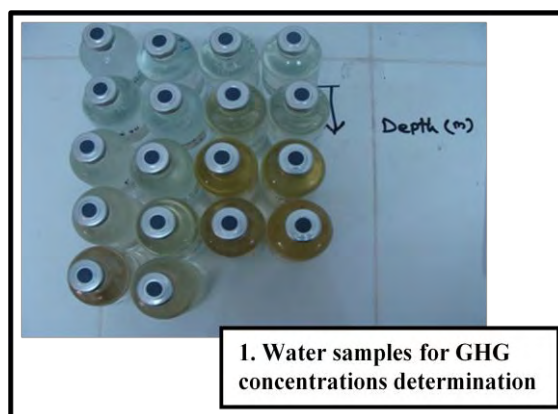


Photo 2.3: Water samples for the determination of GHG concentrations in the water.

### 2.3.5. Determination of kinetics of potential aerobic CH<sub>4</sub> oxidation rates

The water samples for the aerobic CH<sub>4</sub> oxidation rates measurements were collected in 1.5L HDPE bottle, with additional water sampling of 60 ml- vial dedicated to CH<sub>4</sub> concentrations. Water sample for CH<sub>4</sub> concentrations were immediately poisoned and subsequently analyzed for CH<sub>4</sub> concentration within 2 hours using GC. The water samples for CH<sub>4</sub> oxidation rates determinations were homogenized. The water was then redistributed to three replicate serum vials (160-ml) for the preparation of different concentrations (i.e. in-situ concentration, 2 times of in-situ concentration; 3 times of in-situ concentration; 4 times of in-situ concentration).

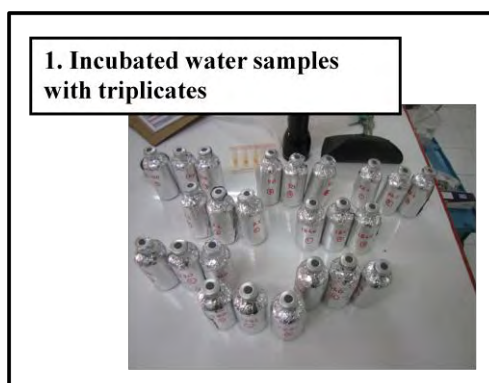


Photo 2.4: Incubated water samples for determination of the aerobic methane oxidation.

Samples were capped using butyl stoppers and sealed with aluminum crimps. Subsequently, according to in-situ concentration of CH<sub>4</sub> in the water, different amounts of pure CH<sub>4</sub> were added by syringe at the same time withdrawal of an equal volume of air from the headspace. Vials were covered with aluminum foil to avoid effect of light on any bacterial activity (Dumestre et al., 1999, Murase and Sugimoto, 2005). Methanotrophic experiments were performed at in-situ water temperature (changing from 20°C to 30°C, depending on seasons). Incubations were performed with agitation to ensure continuous equilibrium between gas and water phases; therefore total CH<sub>4</sub> was available for methanotrophy activity. Total CH<sub>4</sub> concentrations in the vials were measured 5-times in a row at a 12 hours interval and oxidation rates were calculated as the total loss of CH<sub>4</sub> in the vial. All sets of

concentrations were prepared in triplicates; therefore the oxidation rate for each concentration was averaged value of the three replicates with standard deviation ( $\pm$ SD).

### 2.3.6. Diffusive GHG fluxes

#### 2.3.6.1. Eddy covariance measurements

##### 2.3.6.1.1. Basic Principle

Eddy covariance (EC) is one of the most direct techniques to measure fluxes. This method is widely used to measure heat, water, carbon dioxide (CO<sub>2</sub>) and trace gases i.e. methane (CH<sub>4</sub>), nitrous oxide (N<sub>2</sub>O) fluxes from the surface. The essence of method is that the vertical flux can be presented as the covariance (measure of how much two variables change together) between the vertical velocity and the concentration of the scalar of interest. For example, the vertical flux ( $F_c$ ) of an atmospheric property ( $c$ ) is directly determined by the covariance of that property and the vertical velocity (equation 2.1). This can be obtained by calculating the time averaged product (over the period  $t_1$  to  $t_2$ ) of the deviation ( $c'$ ) of atmospheric property ( $c$ ), from  $c = \bar{c} + c'$ , and the deviation ( $w'$ ) of the vertical wind velocity ( $w$ ) from  $w = \bar{w} + w'$

$$F_c = w'c' = \frac{1}{t_2 - t_1} \int_{t_1}^{t_2} w'(t) c'(t) dt \quad (2.1)$$

The EC technique requires an instrument with high precision, accuracy and system stability as well as high sampling rates and short instrument response time (typically 10 Hz). With some assumptions and instrumental errors, eddy covariance measurements can be erroneous. Consequently, removal of errors needs to be done by applying corrections and a set of quality controls. The main corrections to eliminate the errors are the following: frequency response correction is needed to remove the errors due to instrumental time response, sensor separation, tube attenuation, high and low pass filtering, sensor response mismatch. Frequency response correction has a multiplicative effect on the calculated fluxes. Webb-Pearman-Leuning term, (often referred to as WPL or density term), is used to compensate for the fluctuations of temperature and water vapor that affect the measured fluctuations in CO<sub>2</sub> and H<sub>2</sub>O and other gases. WPL has an additive effect on the calculated fluxes.

The gas analyzers used to measure gas concentrations in the ambient air are separated into two main categories: closed-path analyzer (CH<sub>4</sub> analyzer in our study) and open-path analyzer (CO<sub>2</sub>/H<sub>2</sub>O analyzer in our study). The main difference between the two types of analyzer is that the air sampling location and the optical cell are coincident for open-path and separated for a closed-path analyzer. This difference is not just a formal aspect, but leads to a series of implications in the experimental design and data processing (Haslwanter et al., 2009). For example, a closed-path system requires the use of a power-hungry pump to draw the air through the sampling tube into the optical cell. The pump size is based on the volume and operating pressure of the cell, which needs to be flushed at a frequency determined by the spectra to avoid excessive and undesirable loss of signal.

### 2.3.6.1.2. Instrumentations

The different EC instruments were mounted on the mast/tree stump (photo 2.5) in a large open water area. The basic EC instrumentation included a 3D sonic anemometer (Windmaster Pro, Gill Instruments, Lymington Hampshire, UK, during the field campaigns in May 2008, May 2009 and in March 2010 and a CSAT-3, Campbell Scientific, Logan, UT, USA, during the field campaigns in March 2011 and June 2011), an open-path CO<sub>2</sub>/H<sub>2</sub>O infrared gas analyzer (LI-7500, LI-COR Biogeosciences, Lincoln, NE, USA) and a closed-path fast methane sensor (DLT-100 FMA, Los Gatos Research, CA, USA). Data acquisition was carried out with a Campbell datalogger (CR3000 Micrologger®, Campbell Scientific).

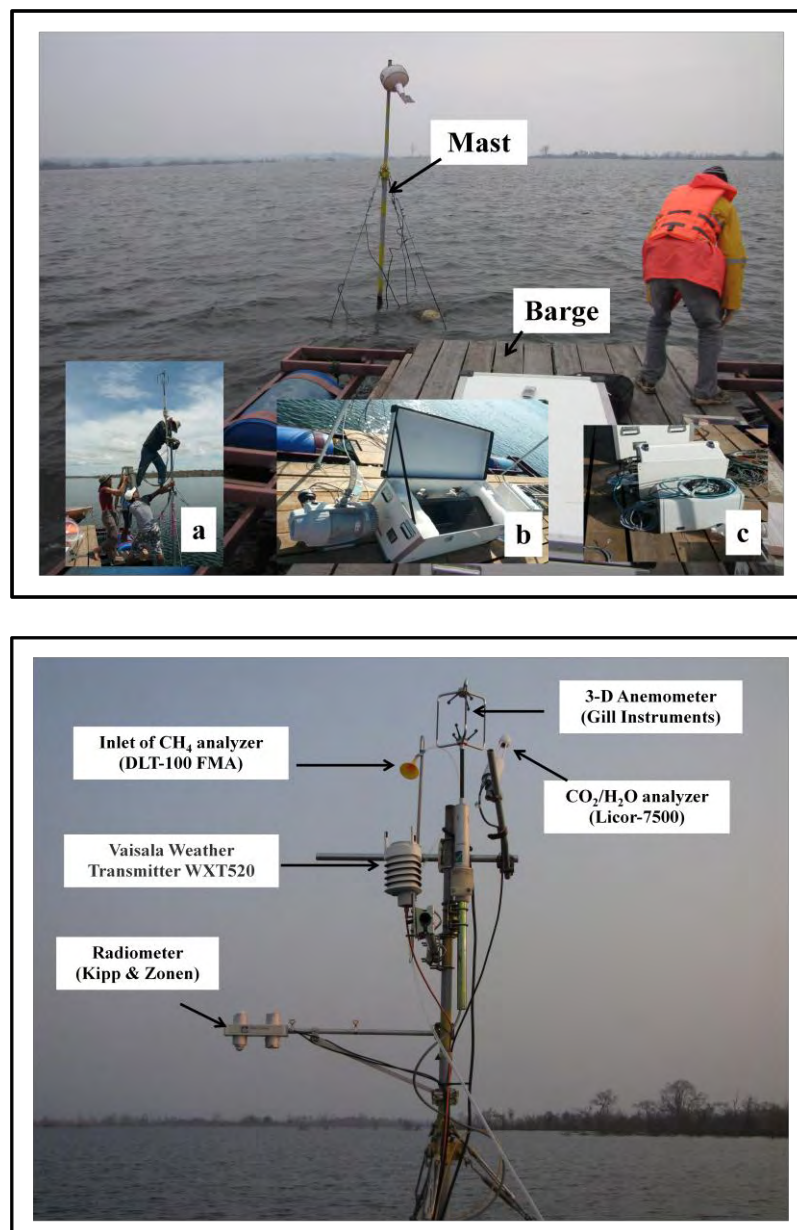


Photo 2.5: A collection of photographs of the eddy covariance instrumental set-up in a large open and smooth fetch. The upper panel shows (a) mounting of the sensors on mast, and

(b) CH<sub>4</sub> analyzer with vacuum pump and (c) datalogger unit on the barge. The lower shows mounted sensors on the mast.

The eddy covariance system was deployed in the NT2 reservoir for different deployment periods (5 to 14 days) during four field campaigns conducted between May 2009 to June 2011 after impoundment of the NT2 reservoir and one field campaign devoted to CO<sub>2</sub> exchange before impoundment (May 2008).

The DLT-100 fast methane analyzer is an off-axis integrated cavity output spectrometer (ICOS) (Baer et al., 2002). More details can be found in Hendriks et al., (2008) and Eugster and Pluss et al., (2010). Hendriks et al., (2008) demonstrated that the time constant of the fast CH<sub>4</sub> analyzer is about 0.1 s, that is a sample frequency of 10 Hz which is far enough for the EC technique.

The DLT-100 was operated in a closed path EC set-up that carried sampled air through a 6 m long tube Synflex-1300 tubing (Eaton Performance Plastics, Cleveland) with an internal diameter of 8 mm. A standard plastic funnel was used to protect the inlet against rain. An internal 2µm Swagelok filter to protect the sampling cell from the dust, aerosols, insects and droplets was already set up in the DLT-100. The tube inlet was mounted 0.20 m behind the sonic anemometer sensors and 0.1m from the LI7500 open path. High CH<sub>4</sub> frequency measurements from the DLT-100 was obtained by the use of a dry vacuum scroll pump (XDS35i, BOC Edwards, Crawly, UK) providing a maximum pumping speed of  $9.72 \times 10^{-3} \text{ m}^3 \cdot \text{s}^{-1}$ . Power was provided by a 5 kVA generator running on gasoline. Possible contaminations of the atmospheric CO<sub>2</sub> and CH<sub>4</sub> concentration measurements from the generator were checked using a footprint model (Kljun et al., 2004).

Pre-impoundment EC measurements (May 2008) were performed at a height of 5m above the ground. After impoundment, the heights of the sensors were approximately 4, 3.2, 2.7 and 2.6 m above the reservoir water surface at the time of the installation respectively during the May 2009, March 2010, March 2011 and June 2011 field campaigns (see Table 2.5 for details on the different EC deployments).

Table 1.5: Summary of eddy covariance deployment, before and after impoundment of Nam Theun 2 (NT2) hydroelectric reservoir

Deployments	Duration	Measured gas species	Remarks
First (May 2008)	10 days	CO <sub>2</sub>	Before impoundment
Second (May 2009)	10 days	CO <sub>2</sub> and CH <sub>4</sub>	After impoundment
Third (March 2010)	14 days	CO <sub>2</sub> and CH <sub>4</sub>	After impoundment
Fourth (March 2011)	5 days	CO <sub>2</sub> and CH <sub>4</sub>	After impoundment
Fifth (June 2011)	5 days	CH <sub>4</sub>	After impoundment

### 2.3.6.1.3. Ancillary measurements

During each EC deployments, temperature (0.2 m depth of water after impoundment, soil temperature at 0.2 m deep before impoundment), atmospheric temperature, rainfall, solar radiation (short wave and long wave), humidity, atmospheric pressure, wind direction and wind speed were recorded as 1 min averages with the CR3000 Micrologger®, Campbell Scientific datalogger. Meteorological data were measured using a meteorological data sensor (Weather Transmitter Model WXT510, Helsinki, Finland) and a radiometer (CNR-1, Kipp & Zonen, Delft, The Netherlands).

### 2.3.6.1.4. Data Processing

10 Hz raw data from all field campaigns were recorded on the CR3000 Micrologger® Campbell Scientific datalogger, and transfer on a laptop. Raw data were then divided into daily blocks, resulting in files containing 864,000 data points (from midnight to midnight) per variable. Different processing steps were made from the raw 10 Hz data using the EdiRe software (R. Clement, 2004; University of Edinburgh).

These processing steps include: 1/ spike detection using a standard de-spiking algorithm whereby wind vector and scalars values outside given limits are removed, 2/ lag correction and tube attenuation relevant to the closed path DLT-100 gas analyzer, 3/ coordinate rotation using the planar fit method, 4/ high frequency correction factors to take into account the loss at high frequency due to insufficient sampling rate, 5/ Webb-Pearman-Leuning density correction (WPL; Webb et al., 1980). Differences among the deployments specific variables i.e. sensor separation distance and instrument placement height in case of different instruments were also considered while processing the data. Averages were computed for intervals of 5 and 30 min to see the influence of specific averaging interval on the CH<sub>4</sub> flux computations and to quantify the quality control parameters.

For CH<sub>4</sub>, fluxes over a hydroelectric reservoir can also result in highly sporadic processes such as ebullition (Chapter 3). Therefore, it is much more problematic to deal with cases of unrealistic CH<sub>4</sub> fluxes measured over such aquatic ecosystem than the terrestrial one. Therefore, neither CarboEurope quality flags nor  $u^*$  criterion can be used for quality control on fluxes (Eugster et al., 2011).

The flux footprint area was computed with the Kljun et al. (2004) model. This simple parametric model estimates the cross-wind integrated flux footprint area in the upwind direction from the flux tower. The governing variables for flux footprint calculations are the upwind distance  $x$  (m), the measurement height above the surface  $z_m$  (m), the height of the atmospheric boundary layer  $h$  (m), the friction velocity for mechanical turbulence  $u_*$  ( $\text{m}\cdot\text{s}^{-1}$ ), and the square-root of the variance of the vertical wind speed component  $\sigma_w$  ( $\text{m}\cdot\text{s}^{-1}$ ). The roughness length  $z_0$  value is not known therefore we considered 0.0002 m as reported for no obstacle terrain (WMO Guide to Meteorological Instruments and Methods of Observation WMO-No. 8 page I.5-12, 2008).

### 2.3.6.2. Floating chamber measurements

The direct flux measurements were performed with two circular chambers, (surface area = 0.15 m<sup>2</sup>; volume = 24.6 L) following the same design as Guérin et al. (2007). The floating chambers were covered with a reflective surface to limit the warming of inside air during measurements. The floating chambers were deployed simultaneously from a boat that was left drifting during measurement to avoid creation of artificial turbulence (Frankignoulle et al., 1998).

Within 45 minutes, four air samples were collected with a syringe from the chambers (duplicates) at 15 minutes interval. Air samples for CH<sub>4</sub> and N<sub>2</sub>O were collected in 10-ml glass vials which contained 6M NaCl solution capped with high density butyl stoppers and aluminum seals, whereas air samples for CO<sub>2</sub> were collected in vials flushed with N<sub>2</sub>. All samples were analyzed within 48 hours by GC. GHG fluxes were calculated from the slope of the linear regression of gas concentration in the chamber versus time.

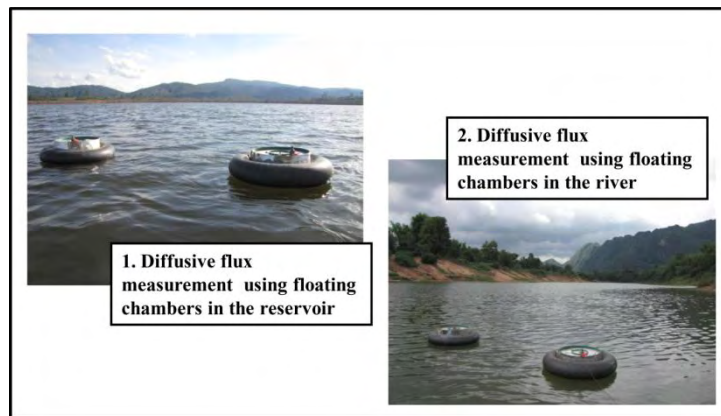


Photo 2.6: Floating chamber measurements in the reservoir and river using floating chamber technique.

The fluxes were accepted when the correlation coefficient ( $r^2$ ) of the linear regression is higher than 0.80. Each direct flux measurement was done together with a determination of the GHG concentration in surface water.

### 2.3.6.3. Estimation of diffusive gas fluxes from surface GHG concentrations

The fluxes measured using floating chambers and concomitant water and air CH<sub>4</sub> concentrations were applied on equation (2.2) to calculate gas transfer velocity:

$$F = k_T \times \Delta C \quad (2.2)$$

where F, the diffusive flux at water-air interface;  $k_T$ , the gas transfer velocity (or piston velocity) for at a measured in-situ temperature (T);  $\Delta C = C_w - C_a$ , the concentration gradient between the water ( $C_w$ ) and the overlying atmosphere ( $C_a$ ).

Afterward, the  $k_{600}$  were computed from  $k_T$  with the following equation:

$$k_{600} = k_{g,T} \times (600/S_{cT})^{-n} \quad (2.3)$$

with  $S_{cT}$ , the Schmidt number of GHG at a measured in-situ temperature (T) (Wanninkhof, 1992);  $n$ , a number that is either  $2/3$  for low wind speed ( $< 3.7 \text{ m s}^{-1}$ ) or 0.5 for higher wind speed and turbulent water (Liss and Merlivat, 1986; Jahne et al., 1987).

Since many of the diffusive  $\text{CH}_4$  fluxes measured by floating chamber were contaminated by ebullition of  $\text{CH}_4$  and few fluxes for the  $\text{CO}_2$  and  $\text{N}_2\text{O}$ , no relationship between  $k_{600}$  and wind speed was found in the database of accepted fluxes measured using floating chamber. The formulation of  $k_{600}$  from MacIntyre et al. (2010) was used which consider the influence of heating and cooling of water column. MacIntyre et al's relationship was compared with the  $k_{600}$  obtained from the measured  $k_{600}$  dataset and with values from the literature: Guérin et al. (2007) obtained in a tropical hydroelectric reservoir, Crucius and Wanninkhof (2003) and Frost and Upstill-Goddard (2002) from temperate reservoirs and with the relationship of Cole and Caraco (1998) which encompasses all type of natural aquatic ecosystems. For the calculation purpose, wind speed (at 10 m height) and rainfall from two adjacent meteorological stations located at Nakai and at the Ban Thalang Bridge (close to RES4 station, Figure 2.1) were used.

Owing to the morphometric configuration of the reservoir, horizontal water movements, especially in area influenced by the turbine water intake are high (Chanudet et al., 2012). Hence, after beginning of turbines, turbulence driven by high horizontal water current dominates over wind driven turbulence, we considered a constant value of  $k_{600}$  ( $10 \text{ cm.hr}^{-1}$ ) at the sampling station located in this region i.e. RES9. Since the  $k_{600}$  value is not known in downstream of NT2 reservoir, we used  $10 \text{ cm.hr}^{-1}$ . This assumed  $k_{600}$  value seems to be conservative for such riverine systems, where turbulence is high due to water currents (Borges et al., 2004; Guérin et al., 2007; Zappa et al., 2003).

During the estimation of diffusive fluxes using thin boundary layer equations, we used an average value of atmospheric concentrations obtained during the floating chamber measurements, i.e. 2 ppmv, 400 ppmv, 0.327 ppmv respectively for  $\text{CH}_4$ ,  $\text{CO}_2$  and  $\text{N}_2\text{O}$ .

### 2.3.7. Ebullition of GHG

Several sets of 5 to 10 funnels were positioned at the surface of the water, and attached one to each other at 1 m distance. The sets of funnels were placed above particular water depths, ranging from 0.5 to 15 m.

The funnels remained on site for 24 or 48 hours. After this period, the captured gas sample was collected from the funnel and stored in 10-ml glass vials which contained 6M NaCl solution capped with high density butyl stoppers and aluminum seals. The collected gas samples were taken to the laboratory to be analyzed by GC.

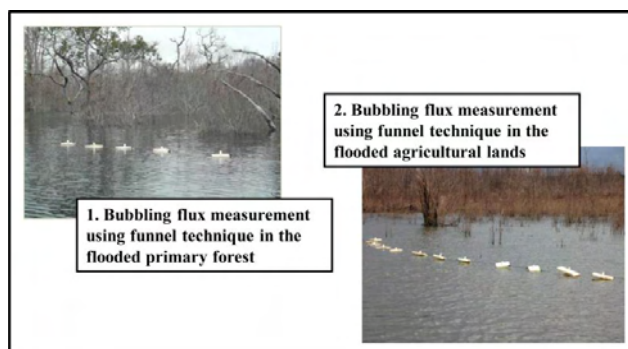


Photo 2.7: Ebullition measurement in the flooded primary forest and flooded agricultural lands using funnel technique.

### 2.3.8. Diffusive GHG flux from the drawdown area

The diffusive soil-air exchanges were measured using rectangular metallic static chamber with metallic collar (Serça et al., 1994).

At each zone, 2 chambers (surface area = 0.08 m<sup>2</sup>) were deployed on the collars installed in the soil around one hour before the measurements, since installation of collar was not possible before due to constraints concerning UXO (Unexploded Ordnance) detection. The samples collection, storage and analysis were performed in the similar approach as described for floating chamber technique.

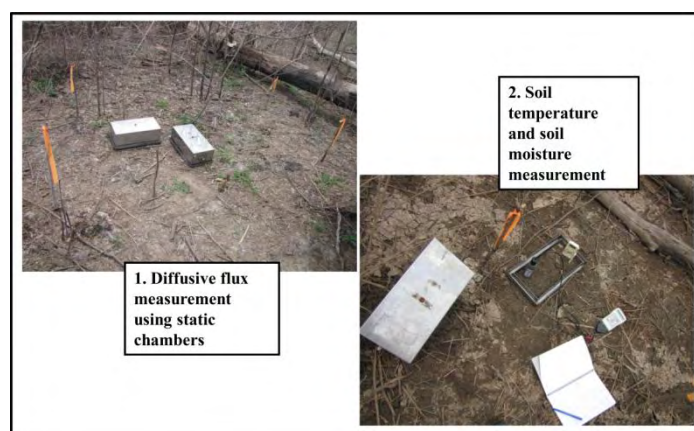


Photo 2.8: Diffusive flux measurements from the soils using static chambers.

### 2.3.9. Gas Chromatography

Analysis of GHG concentrations were performed by gas chromatography on a SRI 8610C gas chromatograph (SRI, Torrance, CA, USA) equipped with a *flame ionization detector* (FID) with a methanizer for CH<sub>4</sub> and CO<sub>2</sub>, and an *electron capture detector* (ECD) for N<sub>2</sub>O. A subsample of 0.5 ml from the headspace of water sample vials and 1 ml of air from flux sample vials were injected. Simultaneous integration of peaks is made using the Peak Simple 3.54 software (SRI, Torrance, CA, USA). Gas standards (400, 1000, and 1010 ppmv, Air Liquid "crystal" standards, uncertainties less than 2% for CO<sub>2</sub>; 2, 10, 100, 1000 ppmv, Air Liquid "crystal" standards, uncertainties less than 2% for CH<sub>4</sub>; 347 and 1020 ppbv



for N<sub>2</sub>O Air Liquid "crystal" standards, uncertainties less than 10%) were injected after every 10 samples of analysis to calibrate the GC. Duplicate injection of samples showed reproducibility better than 5%. The specific gas solubility for CH<sub>4</sub> (Yamamoto et al., 1976), CO<sub>2</sub> (Weiss, 1974) and N<sub>2</sub>O (Weiss and Price, 1980) were used respectively for calculation of total CH<sub>4</sub>, CO<sub>2</sub> and N<sub>2</sub>O concentrations dissolved in water.

### 2.3.10. Determination of physico-chemical parameters

A multi-parameter water quality instrument Quanta<sup>®</sup> (Hydrolab, Austin, TX, USA) capable of simultaneously monitoring of temperature, oxygen (concentration and saturation level), conductivity, pH and depth was used with a 0.5 m resolution above the oxic-anoxic limit and 1 m below the oxic–anoxic limit. Oxygen was measured with a calibration performed on the field at 100% saturation in water-saturated air. Water samples for different carbon species, major cations and anions, total nitrogen (N<sub>tot</sub>) and total phosphorus (P<sub>tot</sub>) were sampled separately in HDPE bottles at 3 to 5 depths including surface, middle and bottom at the sampling sites located in the reservoir, whereas only surface waters were sampled in the pristine rivers and the downstream of the power house and the Nakai Dam. A high performance liquid chromatography (HPLC; Metrohm IC 861 Advanced Compact) combined with an auto-sampler (Metrohm IC 863 Compact Autosampler) was used to determine anions (nitrite, nitrate, phosphate and sulfate) and cations (ammonium, among others not used in this study). Limits of detection for ions were between 0.01 – 0.50 mg.L<sup>-1</sup>. Total carbon (TC), total organic carbon (TOC) and dissolved organic carbon (DOC) analysis were performed by IR spectrophotometry using an Automated Carbon Analyzer (Shimadzu TOC-V CSH) combined with a magnetic stirring capability auto-sampler (Shimadzu ASI-V). Inorganic carbon (IC) excluding CO<sub>2</sub> and CH<sub>4</sub> (mainly HCO<sub>3</sub><sup>-</sup>), and particulate organic carbon (POC) were calculated from these measurements, as follow: IC (mg.L<sup>-1</sup>) = TC (mg.L<sup>-1</sup>) -TOC (mg.L<sup>-1</sup>); POC (mg.L<sup>-1</sup>) = TOC (mg.L<sup>-1</sup>) – DOC (mg.L<sup>-1</sup>). The limit of detection was 0.50 mg.L<sup>-1</sup> for different carbon forms. N<sub>tot</sub> and P<sub>tot</sub> were determined using a spectrophotometer (WTW S12) with detection limits of 0.5 mg.L<sup>-1</sup> and 0.03 mg.L<sup>-1</sup>, respectively. In the carbon analysis, Milli-Q water was used as blank. *Chlorophyll a* was analyzed spectrophotometrically following filtration and hydrochloric acid (0.1 N) extraction.

### 2.3.11. Estimation of degassing

Degassing was calculated using the difference between concentrations upstream and downstream of the structures and the difference was multiplied by the discharge (Galy-Lacaux et al., 1997) as shown in equation (2.4):

$$\text{Degassing} = (C_{\text{upstream}} - C_{\text{downstream}}) \times \text{discharge rate} \quad (2.4)$$

At the Nakai Dam and the aeration weir, we considered surface concentrations at RES1 and DCH2 as upstream concentrations ( $C_{\text{upstream}}$ ), respectively. The  $C_{\text{upstream}}$  was the average of the vertical profile of concentrations at RES9 and REG1 for the degassing below the turbines (TRC1) and below the regulating pond (DCH1), respectively. When necessary, the degassing due to spillway release was computed at the Nakai Dam. For this latter case, the

degassing was calculated using the average CH<sub>4</sub> concentration in the epilimnion at RES1 (from surface to 10 m depth) and the surface concentration at NTH3. For the outflows (C<sub>downstream</sub>), CH<sub>4</sub> surface concentrations at TRC1, DCH1, DCH3 and NTH3 were considered for the calculations. Degassing efficiencies were also estimated using following equation:

$$\text{Degassing efficiency} = (C_{\text{upstream}} - C_{\text{downstream}}) / C_{\text{upstream}} \quad (2.5)$$

### **2.3.12. Dissolved GHG storage within the reservoir**

The measurements of the vertical profiles of methane concentrations were performed at 9 sampling stations in the reservoir. GHG concentrations between two sampling depth of profiles were assumed to change linearly. The volume of each layers were calculated using the volume-capacity curve (Chanudet, personal communication, EDF). Dissolved GHG was determined for each 1 m layer of water by multiplying the weighted-area average GHG concentrations by the volume of the layer. Horizontal mixing was assumed. The total GHG storage was the sums of the GHG stored at all depth intervals (Bastviken et al, 2004).

### **2.3.13. Statistical analysis**

The Kolmogorv-Sminrov test indicated the non-normal behavior of GHG concentrations and thereby diffusive fluxes, and water chemistry variables at different sampling stations in the reservoir. Hence, non-parametric Spearman rank correlation coefficients were calculated between GHG concentrations, and water chemistry and physical parameters. Similarly, the differences in GHG concentrations and diffusive fluxes at different sampling stations in the reservoir were statistically examined using non-parametric Kruskal-Wallis test with GraphPad Prism (GraphPad Software, Inc., v5.04).

### **2.3.14. Extrapolation of fluxes for the estimation of NT2 total GHG emissions**

Based on statistical analysis, GHG diffusive fluxes clustered in three groups: RES1, RES2, RES4, RES5, RES6, RES7 and RES8 behaved similarly whereas RES3 (located in a small embayment) and RES9 (close to the water intake) had their own seasonal pattern. Based on physical modeling (Chanudet et al., 2012) it was found that RES9 is representative of an area of around 2 km<sup>2</sup> before the water intake, whatever the season. Therefore, we extrapolated diffusive fluxes from RES9 to an area of 2 km<sup>2</sup> whatever the season. The embayment where RES3 is located has a surface area of 6% of the total surface area of the reservoir whatever the season (maximum 26 km<sup>2</sup>) to which were attributed the specific fluxes from RES3. The average diffusive fluxes calculated for the stations RES1, RES2, RES4, RES5, RES6, RES7 and RES8 were attributed to the rest of the reservoir surface, taking into account the seasonal variation of the reservoir surface using the area-capacity curve (Figure 2.3a).

Ebullition, mainly CH<sub>4</sub>, occurred only in area shallower than 13 m and depends, among other parameters, on depth (see chapter 3). The surface area corresponding to a particular water level in the reservoir was estimated using the area-capacity curve and bubbling corresponding to the same particular level was estimated from the equations given

by the Artificial Neuronal Network. The surface area below 13 m depth varied between 171 km<sup>2</sup> to 386 km<sup>2</sup> and followed the same pattern as the reservoir surface.

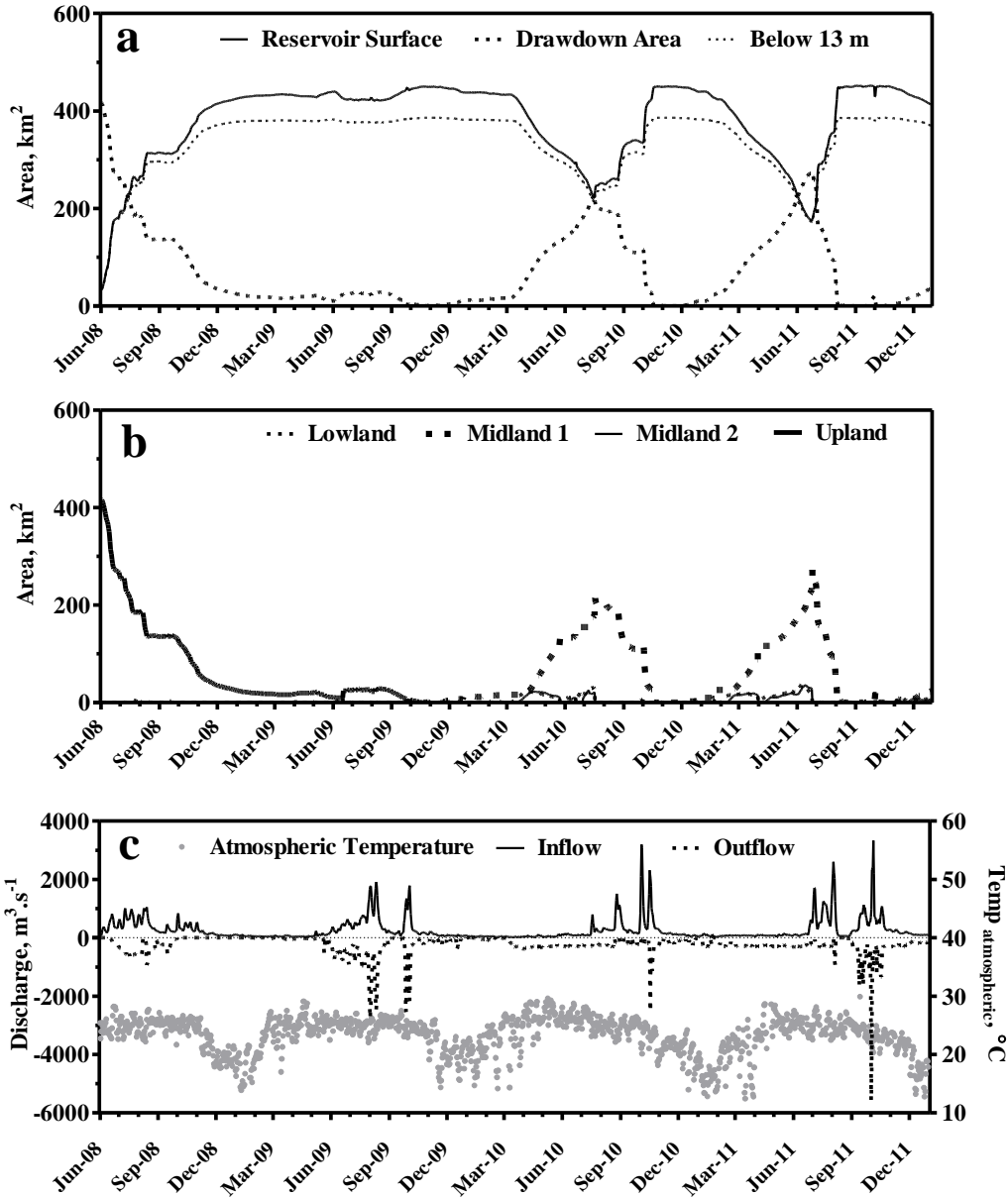


Figure 2.3: (a) variation in the surface area of reservoir, drawdown area, area below 13 m depth of water level, (b) variation in the surface area of upland, midland 1, midland 2 and lowland, (c) input and output ( release from the Nakai Dam and turbines) discharges with atmospheric temperature.

The diffusive GHG fluxes from the drawdown area depended on the soil moisture content. The extrapolation of these fluxes required the use of the area-capacity curves and the determination of the time of exposure of the soils to air in order to attribute the emission corresponding to the moisture content of the soils. We attributed, based on field observations, the average flux observed for soils having a moisture content of 20 to 30% to soils exposed to

air for more than 20 days (midland 1), the average flux observed for soils having a moisture content 30 to 40% for soils exposed to air between 10 to 20 days (midland 2) and the average flux observed for soils having a moisture content between 40 to 45% for soils exposed to air between 1 to 10 days (lowland). The diffusive fluxes obtained from soils located outside the influence of the reservoir (upland soils) were used to calculate emission from the drawdown area before the first full-impoundment of the reservoir.

Figure 2.3b depicts the temporal evolution of the surface of each individual sub-zone of the drawdown area. The upland area disappeared after first full-impoundment of the reservoir in October 2009 (Figure 2.3b). The drawdown area consisted mostly of midland 1 after the full impoundment (up to 200 km<sup>2</sup>). The surface areas of midland 2 (0-50 km<sup>2</sup>) and lowland (0-20 km<sup>2</sup>) represented a small portion of the drawdown area.

### **2.3.15. General Approaches**

#### **2.3.15.1. Estimates of annual GHG gross emissions**

For diffusive GHG emissions from the reservoir, the area-weighted monthly average fluxes were estimated using fluxes from three different clusters. Afterwards, the area-weighted monthly average fluxes were multiplied by the water surface area of that given month. The area-weighted bubbling fluxes were obtained at daily basis using ANN equations and thereby these fluxes were multiplied with the reservoir water surface of given day to calculate the total CH<sub>4</sub> emitted through ebullition. For diffusive fluxes from the drawdown, the diffusive fluxes for an individual sub-zone (i.e. lowland, midland 1, midland 2 and upland) was multiplied by the area covered by that sub-zone for that day. Average monthly degassing emissions at different sites were summed to obtain total degassing emission. For diffusive fluxes from downstream, the monthly diffusive GHG flux for a given section of the downstream was multiplied by the area of that section. Total diffusive GHG emissions from the downstream were obtained by summing up emissions from all sections of the downstream of the Nakai Dam and the downstream of the powerhouse.

The annual estimates were calculated by summing up the monthly estimates for diffusion from the reservoir, degassing and diffusion from the downstream, whereas daily estimates were summed up for the drawdown area and for the ebullition.

#### **2.3.15.2. Carbon import through the water inputs and export from the releases**

The monthly averages of the concentrations of CH<sub>4</sub>, CO<sub>2</sub>, total organic carbon (TOC) and inorganic carbon (IC) were calculated in the upstream pristine tributaries and thereby multiplied by monthly average water input from different tributaries. The annual total carbon import was estimated by summing up all species of carbon for all months of the year. The monthly averages of concentrations of CH<sub>4</sub>, CO<sub>2</sub>, TOC and IC were calculated in water releasing to the downstream of the Nakai Dam and the downstream of powerhouse. Thereby, these monthly averages of the concentrations of CH<sub>4</sub>, CO<sub>2</sub>, TOC and IC were multiplied with their respective water discharges. Annual total carbon export was calculated by summing up all carbon species for all months of the year.

The area-capacity, volume-capacity curves and daily values of reservoir water level, water input, water release from spillway or turbine discharge, rainfall and wind speed were provided by Nam Theun 2 Power Company (NTPC) and Électricité de France (EDF).



## Chapter 3

# Physical controls on CH<sub>4</sub> and CO<sub>2</sub> emissions from a newly flooded subtropical hydroelectric reservoir: Nam Theun 2

**Abstract:** Hydroelectric reservoirs have globally been identified as a significant source of methane (CH<sub>4</sub>) and carbon dioxide (CO<sub>2</sub>) to the atmosphere. The assessments of these emissions and their variations at small and large time scale represent important scientific challenges. The measurement of CH<sub>4</sub> and CO<sub>2</sub> fluxes along with sensible and latent heat were performed over a recently impounded (in 2008) subtropical hydroelectric reservoir, Nam Theun 2 (NT2), in Lao PDR, Asia, using the direct micrometeorological eddy covariance (EC) technique. The measurements were performed in the different meteorological and physical conditions at the reservoir during intensive field campaigns (three for CO<sub>2</sub> and four for CH<sub>4</sub>) in between May 2009 and June 2011. Independent measurements of diffusive and bubbling fluxes were performed using respectively floating chamber (based both on *in-situ* and gas chromatography concentration determinations) and submerged funnel techniques around the mast, i.e. within the footprint of the EC. Additional measurements of bubbling fluxes were performed on a weekly basis from March to December 2012.

After applying a set of quality control criteria on EC fluxes, we obtained reservoir-representative flux. Results from the four field campaigns show individual 30min EC fluxes of CH<sub>4</sub> varying over 4 orders of magnitude (from 0.02 to 103 mmol.m<sup>-2</sup>.day<sup>-1</sup>). Individual diffusive fluxes measured by floating chambers ranged between 0.2 and 5 mmol.m<sup>-2</sup>.day<sup>-1</sup>. Bubbling fluxes were found to be highly sporadic, with individual flux values varying from 0 to 102 mmol.m<sup>-2</sup>.day<sup>-1</sup>. The EC fluxes were very consistent with the sum of the two terms measured independently (diffusive fluxes + bubbling fluxes = EC fluxes,  $p = 0.49$ ), indicating that the EC system picked-up both diffusive and bubbling fluxes from the reservoir, which is a very new and encouraging result for further studies. The CO<sub>2</sub> EC fluxes ranged from 11 to 616 mmol.m<sup>-2</sup>.day<sup>-1</sup>, and well compared with the floating chamber measurements at the same time performed in the footprint area ( $p = 0.90$ ). To our knowledge, this is the first example of an inter-comparison for CH<sub>4</sub> and CO<sub>2</sub> flux measurement in a sub-tropical hydroelectric reservoir where EC flux data were used to compare/validate the fluxes measured with traditional methodologies (i.e. floating chamber and submerged funnel measurements).

A semidiurnal variation of the EC fluxes of CH<sub>4</sub> was observed during the four campaigns with two peaks per day - one in early morning and one in the afternoon- linked to the semi-diurnal atmospheric pressure variation. Our results suggest that the significant seasonal variation in CH<sub>4</sub> fluxes was strongly correlated with associated changes in water depth. From the bubbling measurements, we developed an artificial neuron network model which can explain up to 50% of variability of bubbling fluxes using total static pressure, variations in the water level and atmospheric pressure, and bottom temperature as inputs. Application of the EC method revealed the importance to consider the water-air heat exchange along with thermal and CO<sub>2</sub> gradient in the water column in the process of CO<sub>2</sub> exchange to the atmosphere. Our result suggest that when reservoir was thermally and chemically stratified, higher value of CO<sub>2</sub> fluxes occurred at low to moderate wind speeds with surface cooling ( $T_{\text{water}} > T_{\text{air}}$ ). Whereas CO<sub>2</sub> fluxes were significantly lower during non-stratified period than found during the stratified period ( $p < 0.0001$ ). Our result confirmed that buoyancy controls the influence of wind on CO<sub>2</sub> fluxes. When buoyancy  $< 0$ , during low wind condition CO<sub>2</sub> fluxes are mainly controlled by the physical processes occurring in the water column rather than by wind speed and CO<sub>2</sub> fluxes increased exponentially at high speed. Whereas, CO<sub>2</sub> fluxes increased linearly with the wind speed when buoyancy  $> 0$ .

Our results suggest that CH<sub>4</sub> and CO<sub>2</sub> emissions are not only site-specific, but also time-specific as they are governed by physical processes occurring within the water column and above water surface at the time of measurement.

### 3.1. Introduction

Significant amounts of terrestrial and flooded carbon are processed in the hydroelectric reservoirs and emitted to the atmosphere as carbon dioxide (CO<sub>2</sub>) and methane (CH<sub>4</sub>) (St. Louis et al., 2000; Barros et al., 2011). Over the last decade, there have been increasing efforts to understand the complex interplay between biogeochemical and physical processes responsible for elevated levels of CH<sub>4</sub> and CO<sub>2</sub> emissions that have been recorded following hydroelectric reservoir creation. Most of the studies based on in situ measurements have reported large spatial and temporal variations in CH<sub>4</sub> and CO<sub>2</sub> emissions (Barros et al., 2011; Bastviken et al., 2011). In view to assess temporal and spatial variability, comparative measurements on CO<sub>2</sub> and CH<sub>4</sub> fluxes are needed for better understanding of the physical controls regulating water-air gas transfer in natural conditions, and to parameterize the exchange of these gases.

The equatorial hydroelectric reservoirs are generally characterized by high flooded organic carbon, significant exchange of heat, thermal and chemical stratifications and an anoxic bottom (Barros et al., 2011, St. Louis et al., 2000). All these conditions jointly make a favorable environ for significant production of CH<sub>4</sub> and CO<sub>2</sub> in the sediment layers. From the reservoir surface, CO<sub>2</sub> is mainly emitted via diffusion, whereas in recent times, ebullition has been reported as a major pathway of CH<sub>4</sub> emission (DelSontro et al., 2010, 2011). Studies suggest that large variability in the CH<sub>4</sub> emissions occurs because of the complexity in the controlling processes (DelSontro et al., 2011). Owing to stochastic behavior, ebullition process has been poorly understood and very few previous studies based on CH<sub>4</sub> emissions from hydroelectric reservoir have given much consideration on this phenomenon. This has resulted in a need of comprehensive dataset for process-based understanding of the main environmental drivers influencing ebullition from hydroelectric reservoirs.

The diffusive exchange of CO<sub>2</sub> and CH<sub>4</sub> across the air-water interface is regulated by turbulence. The magnitude of turbulence is defined by the rate of dissipation of turbulent kinetic energy in the water near the interface (Vachon et al., 2010). The rate of the dissipation of turbulent kinetic energy is mainly a function of buoyancy flux and wind shear (Burchard, 2002). At high wind speed, rates of energy dissipation can be dominated by shear term. At matter of fact, during low wind speed event and during heat loss, rates of energy dissipation are considered to be controlled by buoyancy term (MacIntyre et al., 2002, 2010; MacIntyre and Melack, 2009). Particularly, tropical hydroelectric reservoirs receive a significant amount of solar energy. These reservoirs exhibit higher temperature of surface water than air not only in the night throughout the year, but also during the day time especially in warm seasons (Anis and Singhal, 2006). Such conditions constructs free convection above the water surface, and trigger turbulent conditions even, at low wind speed. Thus, energy budget analyses indicate that current parameterizations will likely underestimate gas fluxes by a factor of two in tropical environments (MacIntyre et al., 2001). Further, thermal stratification seal the hypolimnion from the exchange of gases with the epilimnion thereby with the atmosphere, therefore trapping significant amount of CH<sub>4</sub> and CO<sub>2</sub>. Convective mixing due to heat loss could break such thermal and chemical gradients, allowing for the trapped CH<sub>4</sub> and CO<sub>2</sub> to



reach the surface water. Despite having a significant importance on physical processes in the water column, the consideration of heat loss has rarely been applied to describe the gas fluxes from the hydroelectric reservoirs. Therefore, it is important to understand the influence of the thermal and chemical stratification along with heat exchange on gas exchange processes.

The natural variability of surface water CO<sub>2</sub> and CH<sub>4</sub> fluxes on small and large time scale from tropical hydroelectric reservoirs is still somewhat unknown, and even annual flux estimates are often based on sporadic and scanty samples (Kemenes et al., 2007, 2011; Abril et al., 2005; Guerin et al., 2007). The understanding of large variability in the CH<sub>4</sub> and CO<sub>2</sub> emission rates and their temporal variability requires continuous and long-term field measurements of these fluxes in different physical and meteorological conditions at representative sites. Previous studies on CH<sub>4</sub> and CO<sub>2</sub> emissions from hydroelectric reservoirs have mostly been based on measurements performed with floating chamber (FC) or thin boundary layer (TBL) estimates and submerged funnel (SF) for ebullition. These measurements are often discrete and might not capture the dynamics of CH<sub>4</sub> and CO<sub>2</sub> fluxes on the different time scales. Moreover FC and TBL techniques estimate fluxes from very small surface areas that are necessarily not representative of the whole ecosystem. Particularly, ebullition represents a significant part of CH<sub>4</sub> emission, which is a sporadic process (DelSontro et al., 2011). Therefore, discrete measurements of such sporadic process can mislead the estimation. Further, CH<sub>4</sub> and CO<sub>2</sub> emission studies are often focusing on only one single type of methodology (e.g. FC, TBL, or SF). It is therefore rather challenging to validate the obtained fluxes.

Alternatively, direct micrometeorological methods like eddy covariance (EC) offer measurements over large areas (typically hectares), that is a spatial representativeness and can be comparable to the ecosystem scale. Short and continuous integration intervals (e.g. 30 min), typical for the EC technique are useful to capture the temporal variability related to biological and physical processes underlying CH<sub>4</sub> and CO<sub>2</sub> emissions (Eugster et al., 2003; 2011, Long et al., 2010; MacIntyre et al., 2010). The EC technique relies on fast response (10 Hz), field deployable and high-sensitivity instruments, able to rapidly resolve small concentration changes in CH<sub>4</sub> and CO<sub>2</sub> concentration at ambient level. The EC is a direct method, i.e. the net flux across the water-air interface is calculated directly from the covariance of the vertical wind speed and scalar fluctuations. No parameterization such as the relationship between flux and gas transfer velocity as used in the TBL technique is needed.

The EC technique has already been used in previous measurements done over freshwaters for CO<sub>2</sub> flux measurements (Anderson et al., 1999; Morison et al., 2000; Eugster et al., 2003; Vesala et al., 2006; Guerin et al., 2007; Jonsson et al., 2008; Huotari et al., 2011). Most of those studies were conducted in boreal regions (except Guerin et al., 2007) and measurement periods were often short. For CH<sub>4</sub>, several studies have already been carried out with EC technique in terrestrial ecosystems. But, up to now, only fewer studies have been made on CH<sub>4</sub> using eddy covariance system in freshwaters or hydroelectric reservoirs (e.g. Eugster et al., 2011).

This work deals with the CH<sub>4</sub> and CO<sub>2</sub> emission measurements at the Nam Theun 2 (NT2) reservoir in Lao PDR, Asia. The measurement of CO<sub>2</sub> and CH<sub>4</sub> fluxes were performed during different meteorological conditions. The main aims here were to reveal (1) the natural course of the CH<sub>4</sub>, and CO<sub>2</sub> fluxes from a newly flooded subtropical hydroelectric reservoir, (2) the physical controls on CH<sub>4</sub> and CO<sub>2</sub> emissions from the reservoir water surface (3) the applicability of EC technique for CO<sub>2</sub> and CH<sub>4</sub> fluxes in such a subtropical environment. Accurate determination of gas exchange between water and the atmosphere is moreover a vital point. So, we performed cross-validation experiment, where submerged funnel (SF) technique, floating chamber (FC<sub>GC</sub>, followed by GC analysis for concentration determination), and floating chamber (FC<sub>insitu</sub>, in situ concentration determination) and the EC flux measurement were simultaneously performed. This study compares and validates for the very first time fluxes obtained on a subtropical hydroelectric reservoir from the most common methodologies used worldwide together with the EC technique.

## **3.2. Material and methodology**

### **3.2.1. Site Description**

The Nam Theun 2 (NT2) hydroelectric reservoir (17°59'49"N, 104°57'08"E) is constructed on the Nam Theun River located in the subtropical region of Lao People's Democratic Republic (Lao PDR). Six turbines deliver an annual production of 6 TWh (with an installed capacity of 1070 Megawatts). The classical meteorological years can be separated in three seasons: a wet (May-September), a dry cold (October-January) and a dry warm season (February-April) (NTPC, 2005). Daily average air temperature varies between 14°C (winter) to 30°C (summer). The mean annual rainfall is about 2400 mm, mainly occurs in the wet season between May and September (NTPC, 2005).

The filling of the reservoir began in April 2008, and first time full water level of the reservoir was reached in October 2009. The normal operation of NT2 hydroelectric power plant began in March 2010. The NT2 Reservoir is characterized as a warm monomictic nature, i.e. completely mixed from top to bottom once a year (Chanudet et al., 2012). The NT2 Reservoir exhibits strong thermal and chemical stratifications in the end of the warm dry period (April-May). In the most parts of the reservoir, the stratification (both thermal and chemical) disappears with the high water inflow during the wet season (June-September), and restarts to build up during the cold dry season (October-November) (Chanudet et al., 2012). Mixing in the whole water column can last until the beginning of the cold dry season, and then thermocline is deepening towards the end of the cold season.

Two EC deployments (May 2009 and June 2011) were performed during the period between the end of the warm dry season and the beginning of the wet season. These two campaigns differ in terms of average water depth during the EC deployment i.e. ~10 m and ~2 m in May 2009 and June 2011 respectively. The two other field campaigns (March 2010 and March 2011) were made between the end of the cold dry season and the beginning of the warm dry season. The water depths were ~10.5 m and ~6.5 m respectively in March 2010 and March 2011. In May 2009, water was stored since impoundment (April 2008) and not

released from the turbines. As a result, the water level remained more or less constant during the EC deployment periods. For the three other campaigns, the water level in the reservoir was always decreasing, indicating a water inputs from the watershed were lower than the water releases.

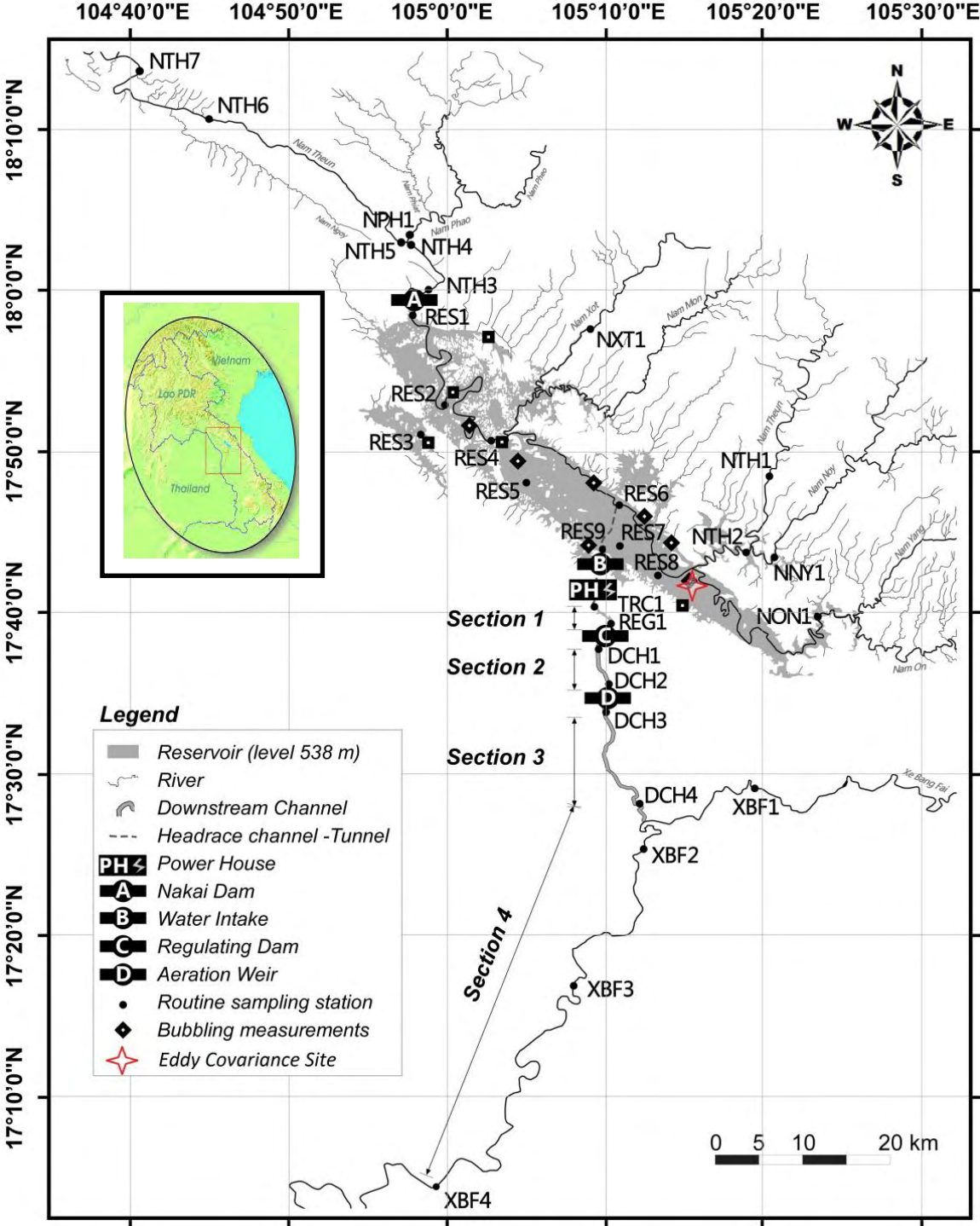


Figure 3.1. Location map showing different components of Nam Theun 2 (NT2) hydroelectric reservoir and location of the sampling stations. The reservoir is shown at its full capacity (538 m above sea level).

### 3.2.2. Methodology

#### 3.2.2.1. Diffusive CH<sub>4</sub> fluxes measured by floating chamber (FC<sub>GC</sub> and FC<sub>insitu</sub>)

Diffusive fluxes measurements were performed with two circular floating chambers, (surface area = 0.15 m<sup>2</sup>; volume = 24.6 L) following the same design as in Guérin et al. (2007) around the EC site. Floating chambers were covered with a reflective surface to limit warming inside the chamber during measurements. To avoid any artificial increase of turbulence in the FC, FCs was left drifting all along the measurements (Marino and Howarth, 1993; Frankignoulle et al., 1998; Raymond and Cole, 2001). For the same reason, the walls of FCs extended few centimeters below the water surface to avoid artifacts at low wind speed (Matthews et al., 2003). Within 45 min, four air samples were collected with a syringe from the chambers (duplicates) at 15 min interval. Air samples For CH<sub>4</sub> were collected in 10-ml glass vials which contained NaCl 6M solution capped with butyl stoppers and aluminum seals, whereas air samples for CO<sub>2</sub> were collected in the vials flushed with N<sub>2</sub>. All samples were analyzed within 48 hours by gas-chromatography.

In March 2011, a floating chamber connected to a Picarro analyzer for the direct measurement of CO<sub>2</sub> and CH<sub>4</sub> concentrations (*in situ*) inside the FC<sub>insitu</sub>. CO<sub>2</sub> and CH<sub>4</sub> fluxes were calculated from the slope of the linear regression of gas concentration in the chamber versus time. The fluxes were accepted when the determination coefficient ( $r^2$ ) of the linear regression was higher than 0.80 (n = 8).

#### 3.2.2.2. Ebullition of CH<sub>4</sub>

The ebullitions (bubbling) of CH<sub>4</sub> were measured at various sites with different depths during 5 field campaigns and on a daily basis monitoring from March to December 2012. The selection of the sampling sites was determined by the water depth and the type of flooded ecosystems. The bubbling fluxes were measured with the funnel technique (Keller and Stallard, 1994). Several sets of 5 to 10 funnels (diameter = 26 cm) were positioned at the surface of the water, and attached one to each other at 1 m distance. The sets of funnels were placed above particular water depths, ranging from 0.5 to 15 m and remained on sites for 24 to 48 hours. The samples were collected and stored in glass vials which contained NaCl 6M solution, before being analyzed by GC.

The bubbling fluxes were also determined from the FC<sub>insitu</sub> measurement in March 2011. From the concentration monitoring in the FC<sub>insitu</sub>, sudden increases in the concentrations of CH<sub>4</sub> were attributed to bubbles, and subsequent bubbling fluxes calculated.

#### 3.2.2.3. Gas chromatography

Analysis of CH<sub>4</sub> and CO<sub>2</sub> concentrations were performed by gas chromatography (SRI 8610C gas chromatograph, Torrance, CA, USA) equipped with a flame ionization detector with a methanizer. A subsample of 0.5 ml from the headspace of water sample vials and 1 ml of air from flux sample vials were injected. Commercial gas standards (2, 10 and 100 ppmv,

Air Liquid "crystal" standards and mixture of N<sub>2</sub> with 100% CH<sub>4</sub> for CH<sub>4</sub>, and 402 and 1000 ppmv, Air Liquid "crystal" standards for CO<sub>2</sub>) were injected after analysis of every 10 samples for calibration. Duplicate injection of samples showed reproducibility better than 5%. The specific gas solubility for CH<sub>4</sub> (Yamamoto et al., 1976) and CO<sub>2</sub> (Weiss, 1974) as a function of temperature were used for calculation of CH<sub>4</sub> and CO<sub>2</sub> concentrations dissolved in water.

#### **3.2.2.4. Instrumentation of EC system**

The EC system was deployed in the NT2 reservoir for different deployment periods (5 to 14 days) during four field campaigns conducted in between May 2009 to June 2011. The different EC instruments were mounted on a mast/tree stump in a large open water area. The heights of the sensors were approximately 4, 3.2, 2.7 and 2.6 m above the reservoir water level at the time of the installation respectively during the May 2009, March 2010, March 2011 and June 2011 field campaigns.

The basic EC instrumentation included a 3D sonic anemometer (Windmaster Pro, Gill Instruments, Lymington Hampshire, UK, during field campaigns in May 2009 and March 2010 and a CSAT-3, Campbell Scientific, Logan, UT, USA, during field campaigns in March 2011 and June 2011), an open-path CO<sub>2</sub>/H<sub>2</sub>O infrared gas analyzer (LI-7500, LI-COR Biogeosciences, Lincoln, NE, USA) and a closed-path fast methane sensor (DLT-100 FMA, Los Gatos Research, CA, USA). Data acquisition was carried out with a Campbell datalogger (CR3000 Micrologger®, Campbell Scientific).

The DLT-100 fast methane analyzer is an off-axis integrated cavity output spectrometer (ICOS) (Baer et al., 2002). More details can be found in Hendriks et al., (2008) and Eugster and Pluss et al., (2010). Hendriks et al., (2008) demonstrated that the time constant of the fast CH<sub>4</sub> analyzer is about 0.1 s, that is a sample frequency of 10 Hz, high enough for the EC technique. The DLT-100 was operated in a closed-path EC set-up that carried sampled air through a 6 m long tube Synflex-1300 tubing (Eaton Performance Plastics, Cleveland) with an internal diameter of 8 mm. A standard plastic funnel was used to protect the inlet against rain. An internal 2 µm Swagelok filter to protect the sampling cell from the dust, aerosols, insects and droplets is part of the default set up of the DLT-100. The tube inlet was mounted 0.20 m behind the sonic anemometer sensors and 0.1 m from the LI-7500 open path. High frequency CH<sub>4</sub> measurements from the DLT-100 is obtained by the use of a dry vacuum scroll pump (XDS35i, BOC Edwards, Crawly, UK) providing a maximum pumping speed of  $9.72 \times 10^{-3} \text{ m}^3 \cdot \text{s}^{-1}$ . Power was provided by a 5 kVA generator running on the gasoline. The possible contaminations of the atmospheric CO<sub>2</sub> and CH<sub>4</sub> concentration measurements from the generator were checked using the wind direction and a footprint model (Kljun et al., 2004), see sections 3.2.2.4.3 and 3.2.2.4.4.

#### **3.2.2.4.1. Ancillary measurements**

During each field campaigns, water temperature (0.2 m depth of water), rainfall, solar radiation, relative humidity, atmospheric pressure, wind direction and wind speed were recorded at 1 min averages with the CR3000 Campbell Scientific datalogger. Meteorological data were measured using a meteorological data sensor (Weather Transmitter Model WXT510, Helsinki, Finland), and a radiometer (CNR-1, Kipp & Zonen, Delft, The Netherlands).

#### **3.2.2.4.2. Data processing**

10 Hz raw data from all field campaigns were recorded on the CR3000 Campbell Scientific datalogger, and transfer on a laptop. Raw data were then divided into daily blocks, resulting in files containing 864,000 data points (from midnight to midnight) per variable. Different processing steps were made from the raw 10 Hz data using the EdiRe software (R. Clement, 2004; University of Edinburgh). These processing steps include: 1/ spike detection using a standard de-spiking algorithm whereby wind vector and scalars values outside given limits are removed, 2/ lag correction and tube attenuation relevant to the closed path DLT-100 gas analyzer, 3/ coordinate rotation using the planar fit method, 4/ high frequency correction factors to take into account the loss at high frequency due to insufficient sampling rate, 5/ Webb-Pearman-Leuning density correction (WPL; Webb et al., 1980).

Differences among the deployments specific variables i.e. sensor separation distance and instrument placement were considered while processing the data. Averages were computed for intervals of 5 and 30 min to see the influence of specific averaging interval on the CH<sub>4</sub> flux computation and to check the stationarity and intermittency of the 30 min flux calculation (see section 3.2.2.4.3). The micrometeorological fluxes of heat, momentum, CO<sub>2</sub> and CH<sub>4</sub> were calculated as covariance between the scalars and vertical wind speed fluctuations according to commonly accepted procedures (Aubinet et al., 2001). We use the micrometeorological sign convection with positive values for vertical fluxes if they are directed away from the surface toward the atmosphere, and negative values if the direction is toward the surface.

Spectral and co-spectral analyses have been conducted for each of the 30 min calculated flux. The overall performance of the EC equipment was similarly satisfactory along the four field campaigns. Spectral and co-spectral analyses done by Hendriks et al., (2008) and Eugster and Pluss (2010) also confirmed that the quality of the DLT-100 FMA measurements was good enough for EC flux calculation. During experiments at NT2, a mean time lag between CH<sub>4</sub> concentration and wind speed of about 0.8 s has been calculated. This time lag has been accounted for in the data processing and flux calculation. No time lag was noticed between CO<sub>2</sub> signal and wind speed. We did not perform field calibration, but DLT-100 calibration and stability has already been checked and certified. Tests performed by Detto et al., (2011) with a standard calibration gas produced 10 Hz concentration measurements with a precision of  $\pm 4$  ppb out of a background of 1900 ppb at ambient temperature of 25 °C.

That same study reported a very small instrumental drift of  $1.5 (\pm 2)$  ppb.day<sup>-1</sup>. These different tests showed that drifts could be negligible in the context of EC applications.

#### **3.2.2.4.3. EC data quality control**

We used following quality control criteria to ensure that the pre-conditions of the EC measurements are fulfilled. First, nonstationarity according to a definition given by Foken and Wichura (1996). In nonstationarity calculation, the time interval (30 minutes) used for a calculation of a single flux value is divided into six intervals (5 min subrecords). If there is a difference of less than 30% between the mean covariance of subrecords and the covariance of the full period, the measurement is considered stationary. Second, a flux was considered intermittent if its intermittency (standard deviation of six 5 min averaged covariance divided by 30-mins covariance) rose above unity (Mahrt et al., 1998). Third, for CO<sub>2</sub> concentration and vertical wind component, the skewness (SK; third statistical moment describing a degree of asymmetry of distribution) and kurtosis (KU; fourth statistical moment describing a flatness) were used to stay within the range of (-2,2) and (1,8), respectively (Vickers and Mahrt, 1997). Fourth, the momentum flux,  $\overline{u'w'}$ , was required to be negative implying a downward directed momentum flux. In addition, the fluxes were rejected when wind was coming from the power generator unit.

Owing to stochastic nature of CH<sub>4</sub> fluxes, therefore, we did not use Vickers and Mahrt's criteria on CH<sub>4</sub> concentration over such aquatic ecosystem (Eugster et al., 2011). During the heat loss from the water column, turbulence at the air-water interface can be higher due to convection in the water column (MacIntyre et al., 2002). Therefore during the cooling, a minimum threshold of friction velocity cannot be considered as a good criterion to reject records, whereas it is often considered as an indicator for data quality over terrestrial ecosystem.

Quality control criteria applied all together resulted in the acceptance of 51% of the flux data. The acceptance rates were more or less similar for daytime (53%) and nighttime (49%) periods. This percentage is in the upper range of acceptance rate found in earlier study made over water bodies (10% in Huotari et al., 2011; and 46% in Jonsson et al., 2008).

#### **3.2.2.4.4. Footprint analysis**

The flux footprint area was computed with the Kljun et al. (2004) model. This simple parametric model estimates the cross-wind integrated flux footprint area in the upwind direction from the flux tower. The governing variables for flux footprint calculations are the upwind distance, the measurement height above the water surface, the height of the atmospheric boundary layer, the friction velocity for mechanical turbulence, and the square-root of the variance of the vertical wind speed component. The roughness length value is not known therefore we considered 0.0002 m as reported for no obstacle terrain (WMO, 2008).

### 3.2.2.5. Statistical analysis, multi linear regression and artificial neuronal network

Statistical tests were performed to assess the methodological variation in the CH<sub>4</sub> and CO<sub>2</sub> fluxes measured with different methods. The differences in fluxes were statistically examined using non-parametric Kruskal-Wallis test and Wilcoxon matched-pairs signed rank test with GraphPad Prism (GraphPad Software, Inc., v5.04).

A multi linear regression (MLR) was used to find the linear relationship between CH<sub>4</sub> bubbling fluxes (output) and three environmental variables averaged at the daily scale (inputs): total static pressure (water depth plus atmospheric pressure), change in the total static pressure (sum of change water level and change in atmospheric pressure) and temperature at the bottom of the reservoir. The MLR used in this study is based on the SPSS 15.0 for Windows.

An artificial neural network (ANN) was used to find the best non-linear regression between CH<sub>4</sub> bubbling fluxes (output) and three environmental variables averaged at the daily scale (inputs): total static pressure (water depth plus atmospheric pressure), change in the total static pressure (sum of change water level and change in atmospheric pressure) and temperature at the bottom of the reservoir. The choice of these parameters is detailed in the result and discussion section. The ANN used in this study is the multi layer perceptron (MLP). The database of raw data was composed of 1489 individual bubbling fluxes. The fluxes from a given station measured the same day and at the same depth were averaged. Finally, the database for ANN was composed of 394 lines and 4 columns (1 output and 3 inputs). The dataset used by the MLP is separated in two pools, the training set (244 lines) and the validation set (150 lines). During the training process, a set of optimal weights is determined and applied on the validation set.

The neural network used in this study is based on a commercial version of the Neuro One 5.0 © software, (Netral, Issy les Moulineaux, France), and the whole methodology was described in Delon et al. (2007). The architecture of the MPL (deduced from the Vapnik–Chervenenkis theory; Vapnik, 1995) is composed of 3 hidden neurons. All inputs and output are normalized and centered in order to avoid artifact in the training process. After normalization, the data have the same order of magnitude. The network is used in a static version where examples of the database are independent of each other

Weight values associated to each input are modified a 100 times (optimization process). Ten initializations (10 series of different sets of weights) are tested for each model. This configuration (100 modifications of weights, 10 models) is tested several times, in order to avoid a local minimum solution. The transfer (activation function), is the hyperbolic tangent.

The best algorithm within the 10 launched is chosen, by assessing the following criteria: (1) The lowest generalization cost is chosen, (2) Root Mean Square Error (RMSE) of the training set has to be close to the RMSE of the validation set (21 and 29 in our case), and



(3) results giving negative fluxes are discarded. Learning (training) cost is 6.56, validation cost is 7.63, generalization cost is 9.41, and homogeneity is 0.95, which are considered as good enough criteria for choosing the equation.

### 3.2.2.6. Other calculations

Calculations of the sensible heat (H) and the latent heat (LE) fluxes were made using EdiRe software. The incoming and the outgoing shortwave and longwave radiations from the CNR1 sensor were used to determine the net short wave, the net long wave and thereby the net radiation. Finally, the net surface heat flux (G,  $W.m^{-2}$ ) calculated as following:

$$\text{Net surface heat flux (G, } W.m^{-2}) = SW_{in} - SW_{out} + LW_{in} - LW_{out} - LE - H$$

where G is the net surface heat flux,  $SW_{in}$  is the incoming shortwave radiation,  $SW_{out}$  is the outgoing shortwave radiation;  $LW_{in}$  is the incoming long wave radiation;  $LW_{out}$  is the outgoing long wave radiation; LE is the latent heat flux, H is the sensible heat flux, all terms in  $W.m^{-2}$ .

Due to shallow secchi disk depths (~1.5 m) in the water column during all deployment, more than 90% of the solar radiation was absorbed in the upper meter of the surface boundary layer (Idso and Gilbert, 1974). Therefore, the surface buoyancy flux, B, was calculated from the net surface heat flux G, as (Dorrenstein, 1979).

$$\text{Buoyancy flux, B (m}^2.s^{-3}), = (g/\rho_w) \times (\alpha/C_p) \times G$$

Where g is the gravitational acceleration ( $9.81 \text{ m.s}^{-2}$ );

$\rho_w$  is the density of water and was calculated as a function of temperature,

$$\rho_w = 1000 (1 - (T+288.9414) / (508929.2 \times (T+68.12963))) \times (T-3.9863)^2,$$

where T is in  $^{\circ}C$  (McCutcheon et al., 1993);

$\alpha$  is the thermal expansion co-efficient,  $\alpha$  in the range  $20\text{-}30^{\circ}C$  can be estimated from

$$\alpha = 1.6 \times 10^{-5} + 9.6 \times 10^{-6} T, \text{ where T is in } ^{\circ}C;$$

$C_p$  is the specific heat of water ( $4148 \text{ J.kg}^{-1}.^{\circ}C^{-1}$ ).

## 3.3. Results

### 3.3.1. Temperature, $O_2$ , $CO_2$ and $CH_4$ in the water column

During the EC deployment in May 2009, five in situ vertical profiles of temperature,  $O_2$ ,  $O_2$  saturation, pH and conductivity were measured near the EC site. No such in situ vertical profiles are available at the EC site for the other field campaigns. However, around

two km from the EC site (Figure 3.1), a sampling station (RES 8) has been monitoring for vertical profiles of in situ parameters along with dissolved  $\text{CO}_2$  and  $\text{CH}_4$  in the water column. The shape of vertical profiles of temperature and  $\text{O}_2$  at EC site and RES8 from May 2009 confirmed that both stations behaved similar in term of thermal and chemical properties in the water column (Figure 3.2). Therefore we used in situ and dissolved  $\text{CO}_2$  and  $\text{CH}_4$  concentrations from RES8 to describe the thermal and chemical conditions at the EC site during other field campaigns.

The NT2 reservoir experienced a warm dry season before field campaigns in May 2009 and June 2011, therefore water column showed a strong thermal and chemical stratification (Figure 3.2). The surface water temperatures were highest in May 2009 and June 2011. In May 2009 and June 2011 surface temperature rose up to  $\sim 30^\circ\text{C}$ , whereas the bottom temperature was approximately  $20^\circ\text{C}$ , giving a temperature difference of  $\sim 10^\circ\text{C}$  between the epilimnion and the hypolimnion.

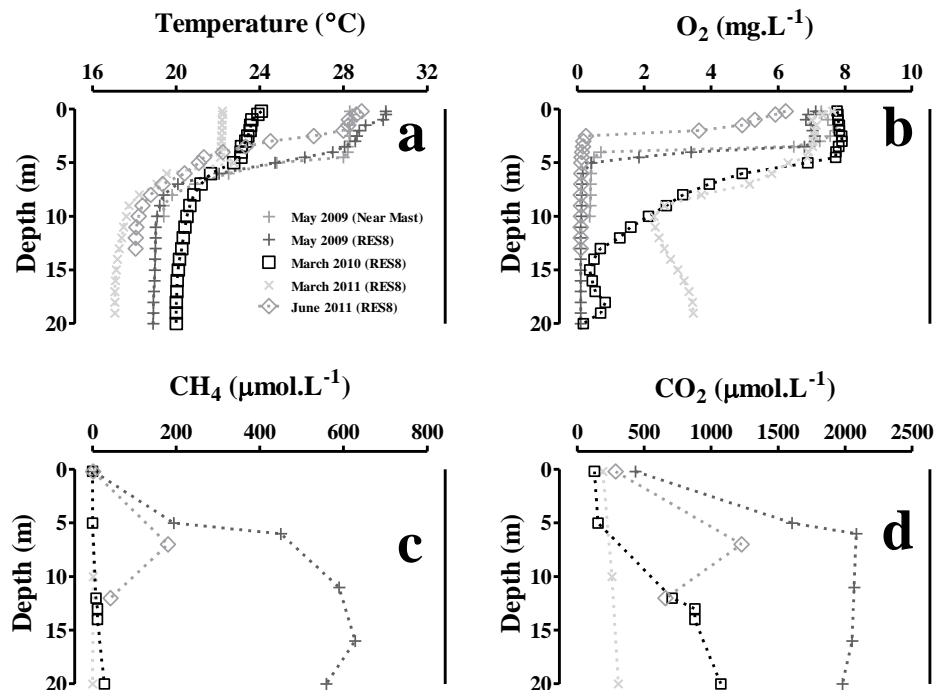


Figure 3.2: Vertical profiles of temperature (a),  $\text{O}_2$  (b),  $\text{CH}_4$  (c) and  $\text{CO}_2$  (d) at the EC site and at the sampling station (RES8) during the four different EC deployments.

The field campaigns in March 2010 and March 2011 followed a cold dry period, leading to a lower temperature difference between the epilimnion and the hypolimnion, i.e.  $\sim 5^\circ\text{C}$ . Thermal stratification was weaker during these two last campaigns (Figure 3.2). In May 2009 and June 2011, epilimnion was oxic ( $\sim 6.5 \text{ mg.L}^{-1}$ ) and  $\text{O}_2$  level abruptly dropped to anoxic level in the metalimnion and in the hypolimnion. In March 2010, epilimnion was oxic ( $\sim 7 \text{ mg.L}^{-1}$ ) and  $\text{O}_2$  level gradually fall in the metalimnion and dropped to anoxic level in the hypolimnion. In March 2011, whole water column was oxic. Water column exhibited a sharp

CO<sub>2</sub> gradient in May 2009, March 2010 and June 2011 (Figure 3.2), while no CO<sub>2</sub> gradient was observed in March 2011.

### 3.3.2. Meteorological and physical conditions in the water column

Like physical conditions in the water column, weather conditions also differed considerably between one deployment to another. During all the deployments, obvious diel patterns were observed in air temperature, surface water temperature, wind speed, atmospheric pressure, relative humidity, shortwave and longwave radiations, net surface heat flux and buoyancy fluxes as shown in Figure 3.3 for March 2011. Statistical details of these parameters during all the deployments are summarized in Table 3.1.

Table 3.1: Details of the meteorological and physical conditions at the EC site during the four different deployments. SD: standard deviation, na: not available.

Average $\pm$ SD (range)	March 2009	March 2010	March 2011	June 2011
Wind speed (m.s <sup>-1</sup> )	2.4 $\pm$ 1.1 (0.3–6.7)	2.9 $\pm$ 2.3 (0.2–10)	3.0 $\pm$ 1.9 (0.2–7.3)	1.4 $\pm$ 0.9 (0.2–4.3)
Friction velocity, u <sub>*</sub> (m.s <sup>-1</sup> )	0.25 $\pm$ 0.11 (0.07–0.7)	0.21 $\pm$ 0.11 (0.03–0.59)	0.19 $\pm$ 0.12 (0.02–0.47)	0.15 $\pm$ 0.08 (0.02–0.39)
Atmospheric pressure (hPa)	947 $\pm$ 2 (943–950)	953 $\pm$ 3 (948–960)	951 $\pm$ 2 (947–955)	949 $\pm$ 1 (946–951)
Relative humidity (%)	77 $\pm$ 9 (47–91)	66 $\pm$ 14 (35–86)	72 $\pm$ 11 (45–87)	73 $\pm$ 15 (20–93)
Air temperature, T <sub>air</sub> (°C)	25 $\pm$ 2 (23–30)	23 $\pm$ 4 (16–33)	22 $\pm$ 3 (17–30)	26 $\pm$ 2 (24–30)
Water temperature, T <sub>water</sub> (°C)	29 $\pm$ 1 (28–31)	24 $\pm$ 2 (21–30)	23 $\pm$ 1 (21–27)	29 $\pm$ 2 (25–32)
T <sub>water</sub> -T <sub>air</sub> (°C)	3.6 $\pm$ 1.2 (0.2–6.2)	1.0 $\pm$ 2.6 (-5.7–5.2)	1.5 $\pm$ 1.9 (-3.1–3.9)	2.9 $\pm$ 1.5 (0.2–5.3)
Net shortwave radiation (W.m <sup>-2</sup> )	141 $\pm$ 200 (-3–634)	114 $\pm$ 169 (-4–551)	219 $\pm$ 314 (-6–880)	149 $\pm$ 253 (-5–1018)
Net longwave radiation (W.m <sup>-2</sup> )	-28 $\pm$ 11 (-49–(-6))	-43 $\pm$ 9 (-63–(-10))	-75 $\pm$ 8 (-88–(-48))	-38 $\pm$ 15 (-61–(-6))
Net radiation (W.m <sup>-2</sup> )	90 $\pm$ 188 (-51–596)	67 $\pm$ 171 (-60–497)	117 $\pm$ 307 (-94–777)	110 $\pm$ 251 (-66–1011)
Latent heat flux (W.m <sup>-2</sup> )	123 $\pm$ 57 (11–414)	90 $\pm$ 60 (6–305)	85 $\pm$ 52 (4–219)	na
Sensible heat flux (W.m <sup>-2</sup> )	35 $\pm$ 16 (9–102)	16 $\pm$ 20 (-32–95)	13 $\pm$ 13 (-27–43)	na
Net heat loss (W.m <sup>-2</sup> )	201 $\pm$ 67 (70–406)	195 $\pm$ 87 (23–443)	200 $\pm$ 53 (112–311)	na
Net surface heat flux, G (W.m <sup>-2</sup> )	-80 $\pm$ 194 (-399–435)	-84 $\pm$ 201 (-445–404)	-7 $\pm$ 322 (-296–721)	na
Buoyancy flux (10 <sup>7</sup> $\times$ m <sup>2</sup> .s <sup>-3</sup> )	-0.5 $\pm$ 1.3 (-2.7–3.1)	-0.4 $\pm$ 1.1 (-2.4–2.6)	0.003 $\pm$ 1.8 (-1.6–4.4)	na

T<sub>water</sub> was comparatively higher in May 2009 (29 $\pm$ 1°C) and June 2011 (29 $\pm$ 2°C) and was never below than T<sub>air</sub> (25 $\pm$ 2°C) (Table 3.1). In March 2010 and March 2011, T<sub>water</sub> was higher than T<sub>air</sub> during the night but opposite during the day due to the solar heating. The average difference between T<sub>water</sub> and T<sub>air</sub> were 1.0 $\pm$ 2.6°C and 1.5 $\pm$ 1.9°C respectively for March 2010 and March 2011.

In May 2009, wind speed was lower ( $2.4 \pm 1.1 \text{ m.s}^{-1}$ ) than for the other field deployments, but had mean turbulent friction velocity ( $u_*$ ) of  $0.25 \pm 0.11 \text{ m.s}^{-1}$ , which was comparable to other field campaigns. In the beginning of field campaign in March 2010, wind speeds were lower ( $\sim 2 \text{ m.s}^{-1}$ ) but in the middle of the field campaign during stormy weather, wind speed went up to  $10 \text{ m.s}^{-1}$ . In March 2011, wind speeds were higher in the beginning and the end of the field campaign (up to  $7 \text{ m.s}^{-1}$ ), but always low ( $> 2 \text{ m.s}^{-1}$ ) in the middle of the field campaign. In June 2011, winds were weak all along the campaign with an average of  $1.4 \pm 0.9 \text{ m.s}^{-1}$ .

The sensible heat flux was always positive in May 2009, that is heat was released from reservoir water to the atmosphere with 30 min means ranging from 9 to  $102 \text{ W.m}^{-2}$ . Whereas during March 2010 and March 2011, sensible heat flux was  $> 0 \text{ W.m}^{-2}$  at night and  $< 0 \text{ W.m}^{-2}$  in daytime and 30 min mean sensible heat fluxes ranged from -32 to  $95 \text{ W.m}^{-2}$  and -27 to  $43 \text{ W.m}^{-2}$  in March 2010 and March 2011, respectively. The latent heat flux was always positive during all the field campaigns and ranged from 11 to  $414 \text{ W.m}^{-2}$ . The net shortwave and net longwave radiation ranged respectively from -6 to 1018 and -88 to  $(-6) \text{ W.m}^{-2}$ . The net radiation (sum of net shortwave radiation and net longwave radiation) was maximum in March 2011 with an average value of  $117 \pm 307 \text{ W.m}^{-2}$ .

The calculated net surface heat fluxes indicated that water column received heat during the day time, whereas heat losses occurred at other times. All EC deployment taken together, the net heat surface heat ranged from -445 to  $721 \text{ W.m}^{-2}$ . On average, maximum buoyancy loss occurred in May 2009 ( $-2.7 \times 10^{-7}$  to  $3.1 \times 10^{-7} \text{ m}^2.\text{s}^{-3}$ ), whereas minimum average value was in March 2011 (Table 3.1). The range of the buoyancy fluxes are very similar as reported for a tropical reservoir ( $-4.7 \times 10^{-7}$  to  $1.5 \times 10^{-7} \text{ m}^2.\text{s}^{-3}$ ; Anis and Singhal 2006) and a boreal lake (MacIntyre et al., 2010).

As an example, data series of the different meteorological parameters obtained in March 2011 are presented in Figure 3.3. Maximum air temperature ( $T_{\text{air}}$ ) and water temperature ( $T_{\text{water}}$ ) occurred in the late morning or early afternoon and gradually decreased, while minimum occurred in the early morning (Figure 3.3a). Winds were often lower during the night when compared to day time, but sometime did not exhibit a clear day-night pattern as shown in Figure 3.3b. Wind-induced turbulent friction velocity ( $u_*$ ) followed the similar pattern of wind speed (Figure 3.3b). Relative humidity was at the lowest in the late morning and during the afternoon (Figure 3.3c), and was always greater than 20%, never reaching to the saturation level during all field campaigns. Atmospheric pressure showed semidiurnal pattern with two peaks on 24 hours time period (Figure 3.3c).

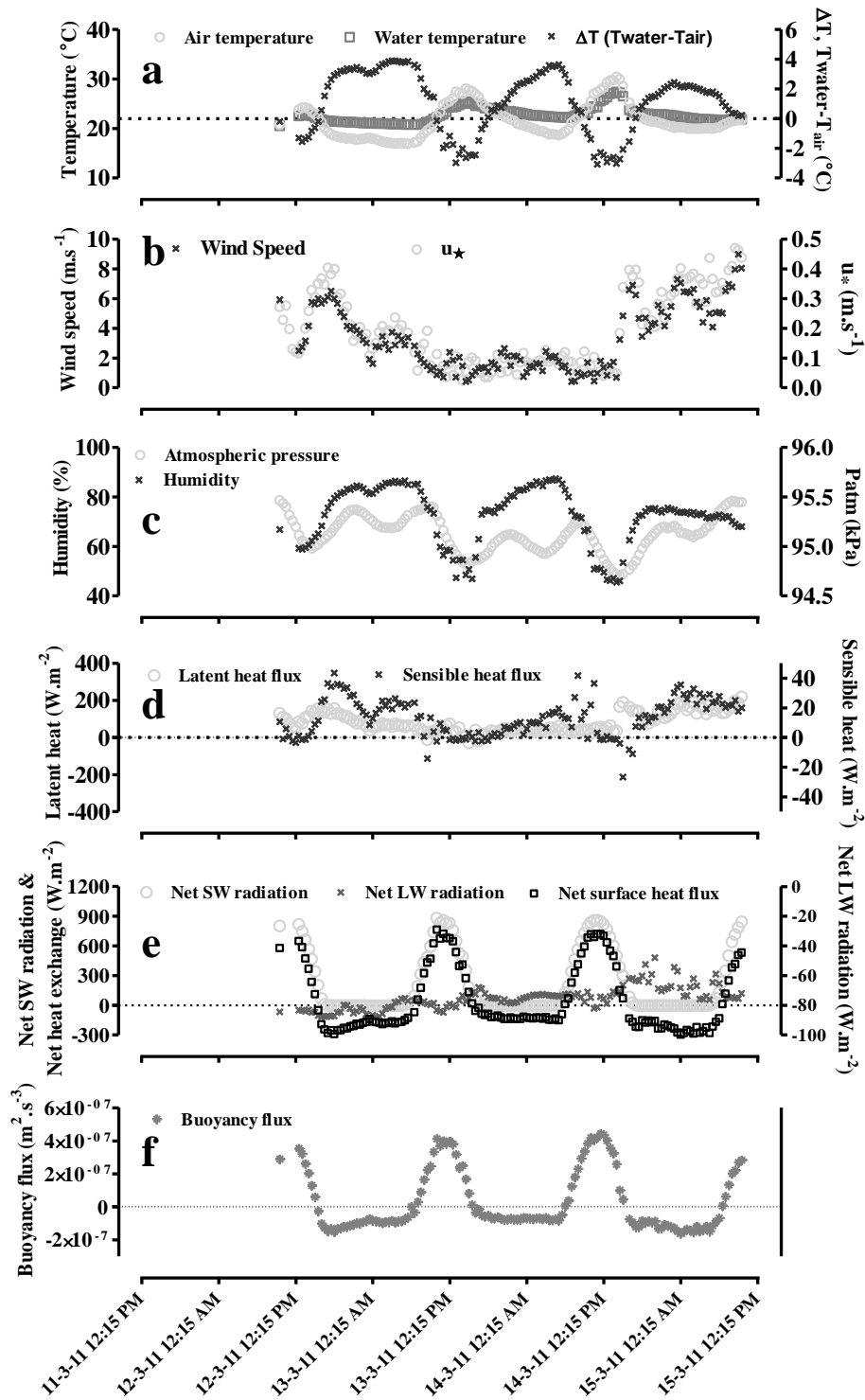


Figure 3.3. Time series (from 11<sup>th</sup>-15<sup>th</sup> March 2011) of (a) water temperature ( $T_{\text{water}}$ ), atmospheric temperature ( $T_{\text{air}}$ ), and  $T_{\text{water}} - T_{\text{air}}$  difference, (b) wind speed measured at 2.7 m height above the water surface and friction velocity ( $u_*$ ), (c) relative humidity and atmospheric pressure, (d) sensible heat ( $H$ ) and latent heat ( $LE$ ) fluxes, (e) net shortwave radiation, net long wave radiation and net surface heat flux, and (f) buoyancy flux.

Measurements of the energy balance components were performed during three EC deployments (May 2009, March 2010 and March 2011). Sensible heat fluxes are mostly driven by water-air temperature difference together with wind speed. High sensible heat fluxes were observed for high wind speed and low water-air temperature difference, and vice versa (Figure 3.3d). Similarly, the variation of latent heat fluxes is driven by changes in the water-air vapor deficit and the wind speed (Figure 3.3d).

The average diurnal course of net surface heat flux and corresponding buoyancy flux is similar to the one of net solar radiation, that is a positive peak at noon (Figure 3.3e & f).

During the four field campaigns, CH<sub>4</sub> concentrations in the ambient air at EC height (about 3m above water level) showed a minimum of 1.800 ppmv. The atmospheric CH<sub>4</sub> concentrations occasionally reached close to 5 ppm, about three times the background CH<sub>4</sub> concentration (1.774 ppmv, Forster et al., 2007). Such large CH<sub>4</sub> concentration may be attributed to pressure drop that could probably trigger ebullitive plumes of CH<sub>4</sub> or build-up of high CH<sub>4</sub> concentrations accumulated after normal or stable conditions. In contrast, during strong wind conditions, CH<sub>4</sub> is flushed away and no accumulation occurs (March 16-18, 2010, data not shown). The CO<sub>2</sub> concentrations in ambient air showed a diurnal pattern with maximum values during nighttime and minimum ones during daytime. Higher peaks of CO<sub>2</sub> concentrations were observed under relatively low wind conditions rather than under high wind conditions. Lower level of the atmospheric CO<sub>2</sub> concentrations were not affected by wind conditions.

### 3.3.3. Quantitative estimates of the CH<sub>4</sub> fluxes

CH<sub>4</sub> EC fluxes were always positive, indicating an emission of CH<sub>4</sub> from the reservoir water surface to the atmosphere. Table 3.2 summarizes statistical details (mean, median and inter quartiles range (IQR)) of 30 min integrated EC CH<sub>4</sub> fluxes measured during the four EC deployments, together with additional measurements performed using floating chamber (FC<sub>GC</sub> and FC<sub>insitu</sub>) and submerged funnel (SF) measurements within the EC footprint area.

The individual 30 min CH<sub>4</sub> EC flux varied by four orders of magnitude during all the EC deployments. On average, CH<sub>4</sub> EC fluxes varied oppositely with the water depth, with the highest mean flux in June 2011 for the shallowest water depth (~2m) (Table 3.2).

In May 2009, CH<sub>4</sub> EC fluxes ranged from 2.1 to 16 mmol.m<sup>-2</sup>.day<sup>-1</sup>, with an average value of  $6.5 \pm 0.5$  mmol.m<sup>-2</sup>.day<sup>-1</sup>. Only 9 measurements of SF<sub>bubb</sub> were performed and ranged from 0 to 3 mmol.m<sup>-2</sup>.day<sup>-1</sup>. Some FC<sub>GC</sub> fluxes were affected with sporadic bubble events. The floating chamber measurements affected with bubbles included bubbling and diffusive fluxes, FC<sub>GC(diff+bubb)</sub>, and had a mean of  $7.3 \pm 0.9$  mmol.m<sup>-2</sup>.day<sup>-1</sup>. Only one floating chamber flux was able to fulfill the criteria ( $r^2 > 0.8$ , see the methodology section) of reasonable diffusive flux and had a value of 1.9 mmol.m<sup>-2</sup>.day<sup>-1</sup>.

With a water depth of 10.5 m in March 2010, CH<sub>4</sub> EC fluxes ranged from 0.2 to 27 mmol.m<sup>-2</sup>.day<sup>-1</sup> and had an average value of 5.8 ± 0.4 mmol.m<sup>-2</sup>.day<sup>-1</sup>. On average FC<sub>GC(diff)</sub> fluxes ranged from 0.2 to 1.8 mmol.m<sup>-2</sup>.day<sup>-1</sup>. No independent measurements of bubbling fluxes were performed within the EC footprint area.

Table 3.2: Details of CH<sub>4</sub> fluxes obtained from different measurement techniques. Avg: average; SE: standard error of the mean (all flux values in mmol.m<sup>-2</sup>.day<sup>-1</sup>)

Measurement technique		May-09	Mar-10	Mar-11	Jun-11
Fluxes (EC) <sup>a</sup>	Avg ± SD	6.5 ± 0.5	5.8 ± 0.4	7.2 ± 0.3	29 ± 1.4
	Range (N)	2.1-16.1 (39)	0.2 -26.8 (138)	2.8-16.8 (105)	6.0 -103 (138)
Fluxes (FC <sub>GC(diff+bubb)</sub> ) <sup>b</sup>	Avg ± SD	7.3 ± 0.9		11.6 ± 2.2	64 ± 12
	Range (N)	6.3 – 8.3 (2)		0.8-49 (30)	31 – 132 (9)
Diffusive (FC <sub>insitu(diff)</sub> ) <sup>c</sup>	Avg ± SD	NA	NA	1.9 ± 2.2	NA
	Range (N)	NA	NA	0.02 - 5.0 (28)	NA
Diffusive (FC <sub>GC(diff)</sub> ) <sup>d</sup>	Avg ± SD	1.9 (1)	1.1 ± 0.5	NA	NA
	Range (N)	NA	0.3 – 1.8 (10)	NA	NA
Bubbling (FC <sub>insitu(bubb)</sub> ) <sup>e</sup>	Avg ± SD	NA	NA	4.6 ± 1.3	NA
	Range (N)	NA	NA	0-24.6 (30)	NA
Bubbling (SF <sub>bubb</sub> ) <sup>f</sup>	Avg ± SD	0.8 ± 0.9		4.5 ± 0.4	28 ± 1.0
	Range (N)	0 – 3 (9)		0.5-22 (80)	10 - 65 (126)

Note: <sup>a</sup>EC; 30 min integrated CH<sub>4</sub> fluxes measured using eddy covariance technique; <sup>b</sup>FC<sub>GC(diff+bubb)</sub>, FC measurements affected by bubbles; <sup>c</sup>FC<sub>insitu (diff)</sub>, diffusive fluxes measured using FC with in situ measurement; <sup>d</sup>FC<sub>GC(diff)</sub>, diffusive fluxes measured using FC with gas chromatography analysis; <sup>e</sup>FC<sub>insitu(bubb)</sub>, bubbling fluxes measured using FC with *in situ* measurement; <sup>f</sup>SF, bubbling fluxes measured using submerged funnel.

The CH<sub>4</sub> fluxes assessed with different methods in March 2011 are shown in the Figure 3.4a. EC fluxes of CH<sub>4</sub> varied from 2.8 to 16.8 mmol.m<sup>-2</sup>.day<sup>-1</sup> and had an average value of 7.2 ± 0.3 mmol.m<sup>-2</sup>.day<sup>-1</sup>. SF<sub>bubb</sub> fluxes ranged from 0 to 22 mmol.m<sup>-2</sup>.day<sup>-1</sup> with an average of 4.5 ± 0.4 mmol.m<sup>-2</sup>.day<sup>-1</sup>, where as independent measurement of bubbling fluxes with FC<sub>insitu(bubb)</sub> ranged from 0 to 24.6 mmol.m<sup>-2</sup>.day<sup>-1</sup>. FC<sub>insitu(diff)</sub> ranged from 0.02 to 5 mmol.m<sup>-2</sup>.day<sup>-1</sup>, whereas there were no qualified diffusive fluxes measured with FC<sub>GC</sub>. Some few very high FC<sub>GC(diff+bubb)</sub> (up to 49 mmol.m<sup>-2</sup>.day<sup>-1</sup>) were observed (Figure 3.4a).

In June 2011, water depth was around ~ 2 m i.e. the lowest among all four EC deployments. CH<sub>4</sub> EC fluxes were highest among all field campaigns and had a mean of 29 ± 1.4 mmol.m<sup>-2</sup>.day<sup>-1</sup>, ranging from 6 to 103 mmol.m<sup>-2</sup>.day<sup>-1</sup>. SF<sub>bubb</sub> fluxes ranged from 10 to 65 mmol.m<sup>-2</sup>.day<sup>-1</sup> with a mean of 28 ± 1.0 mmol.m<sup>-2</sup>.day<sup>-1</sup>. All FC<sub>GC(diff+bubb)</sub> measurements

were affected with sporadic bubble events, with fluxes ranging from 31 to 132  $\text{mmol.m}^{-2}.\text{day}^{-1}$ .

When zooming in the EC  $\text{CH}_4$  flux time series (Figure 3.5), it can be noticed that  $\text{CH}_4$  flux exhibits two peaks per day. During the daytime, EC  $\text{CH}_4$  flux peaks coexist with atmospheric temperature and wind speed peaks (Figure 3.3a & b and Figure 3.4a). In March 2010,  $\text{CH}_4$  EC fluxes were comparatively higher during the high atmospheric temperature than the periods of low atmospheric temperature. EC  $\text{CH}_4$  fluxes were also low during the high wind conditions ( $\sim 10 \text{ m.s}^{-1}$ ). The second diurnal peak in EC  $\text{CH}_4$  flux occurs during the nighttime and did not match up anymore with atmospheric temperature and wind speed in all the field campaigns.  $\text{CH}_4$  fluxes were not influenced by wind direction (data not shown). Hence, there was no consistency among the relationships between  $\text{CH}_4$  fluxes and wind speed or atmospheric temperature during the different field campaigns, suggesting that there must be other factors controlling  $\text{CH}_4$  emissions.

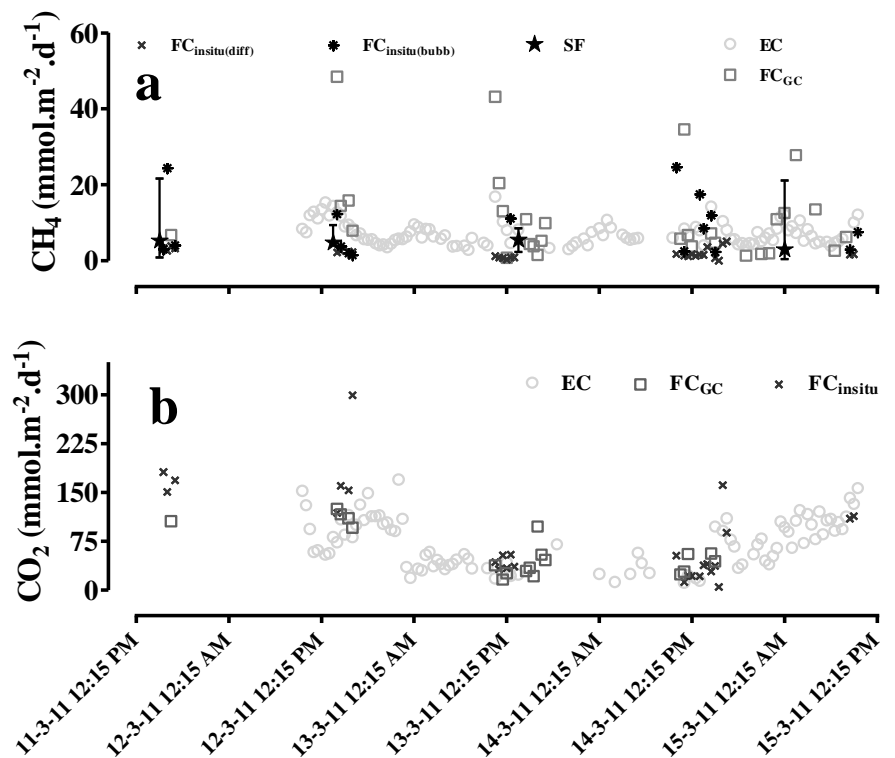


Figure 3.4.  $\text{CH}_4$  and  $\text{CO}_2$  fluxes obtained from EC, floating chambers and submerged funnel during the field campaign in March 2011. EC; 30 min integrated fluxes measured using eddy covariance technique;  $\text{FC}_{\text{insitu}(\text{diff})}$ , diffusive  $\text{CH}_4$  fluxes measured using FC with in situ measurement;  $\text{FC}_{\text{GC}(\text{diff})}$ , diffusive  $\text{CH}_4$  fluxes measured using FC with gas chromatography analysis;  $\text{FC}_{\text{insitu}(\text{bubb})}$ , bubbling  $\text{CH}_4$  fluxes measured using FC with in situ measurement; SF, bubbling  $\text{CH}_4$  fluxes measured using submerged funnel;  $\text{FC}_{\text{GC}}$ , diffusive  $\text{CO}_2$  fluxes measured using FC with gas chromatography analysis;  $\text{FC}_{\text{insitu}}$ , diffusive  $\text{CO}_2$  fluxes measured using FC with in situ measurement.



For analysis purpose, we calculated for each field campaigns the 24 hours standard variation of 30 min integrated EC fluxes. Flux data were binned by time of day and then averaged for all days during the time period (deployment periods differ for each field campaign: i.e. approximately 2 days, 14 days, 4 days and 4 days respectively for May 2009, March 2010, March 2011 and June 2011).

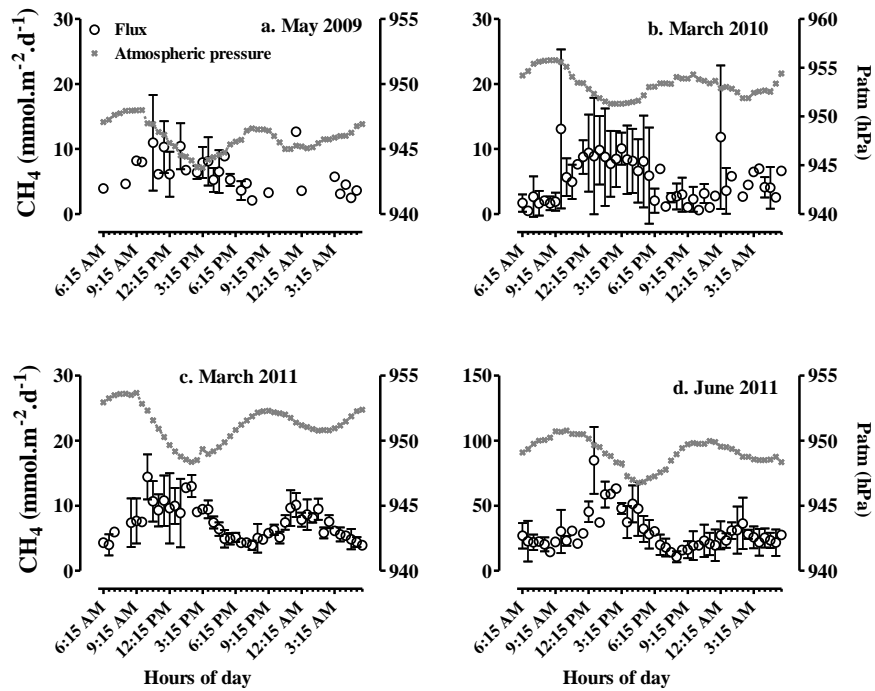


Figure 3.5. 24h standard variation of 30 min integrated  $\text{CH}_4$  fluxes for the four different field campaigns (May 2009, March 2010, March 2011, and June 2011). Note that left y-axis scale differs for June 2011.

Influence of the atmospheric pressure is quite evident with strong changes in the magnitude of  $\text{CH}_4$  fluxes concomitant with the atmospheric pressure drops (Figure 3.5). Comparatively scattered and higher  $\text{CH}_4$  fluxes were observed during a period of low atmospheric pressure (high flux standard deviation in Figure 3.5). On the opposite, much more stable and lower fluxes were observed during a period of high atmospheric pressure.

### 3.3.4. Bubbling $\text{CH}_4$ fluxes from the reservoir surface

Bubbling fluxes were measured at different depths (from 0.5 m to 15 m) at 44 locations spread over 7 stations in various parts of the reservoir including the EC site (Fig. 3.1). Bubble composition ranged from 0.5% up to 61% of  $\text{CH}_4$  and had a mean value of  $20 \pm 12\%$ . The average  $\text{CH}_4$  proportion in the bubbles is lower than commonly found in bubbles from other aquatic environment, which might be because of the higher  $\text{N}_2$  content (Chanton et al., 1989; DelSontro et al., 2011; Keller and Stallard, 1994).

Methane bubbling fluxes decreased from 102 to 0  $\text{mmol.m}^{-2}.\text{d}^{-1}$  for water depth ranging from 0.5 to 15 m and no bubbling was observed for a water depth higher than 13 m. The average ebullition was  $9.5\pm 9.5 \text{ mmol.m}^{-2}.\text{d}^{-1}$  from 1489 measurements. This average bubbling emission was about five times lower than the Petit Saut Reservoir average bubbling emission after 2 year of impoundment ( $50 \text{ mmol.m}^{-2}.\text{d}^{-1}$ ; Galy-Lacaux et al., 1999) and almost one order of magnitude higher than the value found 10 years after impoundment ( $0.7\pm 0.5 \text{ mmol.m}^{-2}.\text{d}^{-1}$ ; Abril et al., 2005). The average ebullition at NT2 was about two times higher than maximum reported for the temperate Lake Wohlen ( $5 \text{ mmol.m}^{-2}.\text{d}^{-1}$ ; DelSontro et al., 2010). Even so, hydroacoustic measurements done by DelSontro et al., (2011) showed that bubbling fluxes could vary over several orders of magnitude (up to  $\approx 6000 \text{ mmol.m}^{-2}.\text{day}^{-1}$ ). It should be noticed that without any idea about physical variable e.g. mean depths of the measurements, such comparisons are not consistent or irrational.

The bubbling  $\text{CH}_4$  fluxes were dependent on various environmental variables (Fig 3.6a and b). Results from the EC measurements suggest the dependency of  $\text{CH}_4$  emissions on atmospheric pressure. While considering the atmospheric pressure, total static pressure at the bottom of the reservoir was estimated, i.e. water depth and atmospheric pressure were summed. When considering the total static pressure, a relationship ( $r^2 = 0.13$ ,  $p = 0.0001$ ) is observed between bubbling fluxes and total static pressure (Fig. 3.6a).

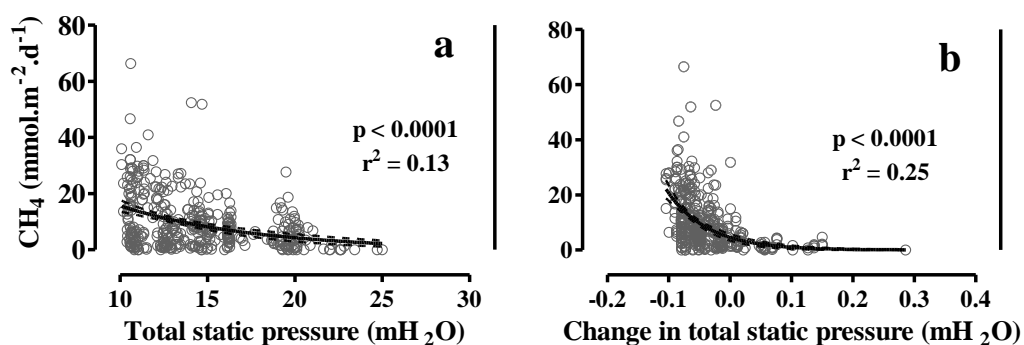


Figure 3.6. Influence of total static pressure (a) and change in the total static pressure (b) on bubbling fluxes.

Bubbling fluxes were higher when water level was decreasing in the reservoir than when the reservoir water level was increasing. Considering the change in atmospheric pressure along with the change in the water level (change in total static pressure), a relationship ( $r^2 = 0.25$ ,  $p < 0.0001$ ) was found between the fluxes and this later parameter (Figure 3.6b).

Based on the results presented in Fig. 3.6, and work by Boon and Sorrel (1995); Casper et al., (2000); DelSontro et al., (2010, 2011); Eugster et al., (2011) and Smith et al., (2000), we chose the following parameters as potential controlling factors for ebullition: water depth, water depth variation, atmospheric pressure, atmospheric pressure variation and

temperature as controlling factors. In order to obtain an equation including the main potential factors controlling ebullition (i.e. total static pressure, change in total static pressure and bottom temperature), we used multi linear regressions (MLR) and artificial neuron network (ANN) approaches. While applying the multi linear (MLR) model on bubbling fluxes (as output), total static pressure, change in the total static pressure and bottom temperature (as inputs), the low explanatory power of equation ( $r^2=0.3$ ) obtained by MLR model is probably an indication of a complex regulation of bubbling fluxes that cannot be fully assessed with simple relationships.

Further, we used an ANN to resolve the flux in a non-linear way on the same dataset. The resulting algorithm leads to an  $r^2$  of 0.50 between calculated and measured flux when all controlling factors are taken into account in the ANN calculation. The ANN equation (Appendix 3.A) derived from these 1489 individual SF measurements will be used for subsequent integrated bubbling calculation (Chapter 4).

### 3.3.5. Quantitative estimates of the CO<sub>2</sub> fluxes

During all field campaigns, NT2 reservoir water surface acted as a source of CO<sub>2</sub> with an efflux rate varying from 5 to ~ 600 mmol.m<sup>-2</sup>.day<sup>-1</sup>. Table 3.3 summarizes statistical details (averages, median and inter quartiles range (IQR)) of 30 min integrated EC CO<sub>2</sub> fluxes measured during the four EC deployments, together with additional measurements performed using floating chamber technique (FC<sub>GC</sub> and FC<sub>insitu</sub>) within the EC site footprint area.

Table 3.3: Details of CO<sub>2</sub> fluxes obtained during different EC deployments with different techniques. Avg: average, SE: standard error of the mean, IQR: inter quartile range, N: number of observations.

Values are in mmol.m <sup>-2</sup> .day <sup>-1</sup>		Avg ± SE	Range	Median (IQR)	N
May-09	EC	140 ± 9	34-493	117 (73)	99
Mar-10	EC	176 ± 10	13-616	130 (164)	175
Mar-11	EC	74 ± 4	11-170	71 (65)	98
	FC <sub>insitu</sub> (diff)	83 ± 13	5 - 299	53 (118)	27
	FCGC(diff)	60 ± 9	16 - 125	46 (70)	19

In May 2009, EC CO<sub>2</sub> fluxes scattered and did not showed clear relationship with any measured environmental variables e.g. wind speed. CO<sub>2</sub> fluxes were higher during night time than during the day time fluxes. Few very high fluxes were observed (up to 493 mmol.m<sup>-2</sup>.day<sup>-1</sup>) in the nighttime, and fluxes were 140±9 mmol.m<sup>-2</sup>.day<sup>-1</sup> on average.

In March 2010, during low wind speed periods ( $< 4 \text{ m.s}^{-1}$ ), EC  $\text{CO}_2$  fluxes ranged from 13 to 200  $\text{mmol.m}^{-2}.\text{day}^{-1}$ . During the nighttime, fluxes went up to 616  $\text{mmol.m}^{-2}.\text{day}^{-1}$  with high wind speed ( $\sim 10 \text{ m.s}^{-1}$ ).

Figure 3.4b presents the daily courses of  $\text{CO}_2$  fluxes measured in March 2011 with different measurement techniques.  $\text{CO}_2$  fluxes followed the pattern of wind (Figure 3.3b and Figure 3.4b). In March 2011, EC  $\text{CO}_2$  fluxes varied from 11 to 170  $\text{mmol.m}^{-2}.\text{day}^{-1}$  and had an average value of  $74 \pm 4 \text{ mmol.m}^{-2}.\text{day}^{-1}$ , a value around 2 times lower than in May 2009 and March 2010. During calm wind conditions, fluxes were lower than the fluxes during high wind speed and high heat loss.  $\text{CO}_2$  fluxes from  $\text{FC}_{\text{insitu}}$  and  $\text{FC}_{\text{GC}}$  were on average equal to  $83 \pm 71$  and  $60 \pm 37 \text{ mmol.m}^{-2}.\text{day}^{-1}$  respectively, values comparable to EC measurements.

This is the first study on  $\text{CO}_2$  flux measured on a sub-tropical reservoir with EC technique. There is only one study in a tropical reservoir, where  $\text{CO}_2$  fluxes were measured in a hydroelectric reservoir (Guerin et al., 2007). EC  $\text{CO}_2$  fluxes at NT2 are larger than  $\text{CO}_2$  EC fluxes measured in boreal and temperate lakes (Eugster et al., 2003; Jonsson et al., 2008; Vesala et al., 2006; Huotari et al., 2011).

### **3.3.6. Footprint analysis and inter-comparison of EC fluxes with other techniques**

When deploying the EC technique, it is important to check whether the measurements are contained within the footprint of the source to be evaluated. In our case, it was critical to see if  $\text{CH}_4$  and  $\text{CO}_2$  fluxes were really contributed from the water surface, and not from the forest surrounding the reservoir. This is particularly critical here where strongly negative photosynthesis flux from the forest would overcome order of magnitude lower positive fluxes from the water surface. Kljun et al, (2004) model was used to calculate the footprint area (see Figure 3.7 for flux footprint in March 2011). It was noticed that flux footprint was different in extension and prevalent wind directions from one campaign to the other one. Footprint area was the smallest during the March 2010 campaign, and the biggest for the June 2011 one. In all the cases, the greatest upwind distance contributing to the flux measurements rarely exceeded 500 m. Given the mast location, open water was found in all the directions for distances higher than 500 m. As a matter of consequence,  $\text{CH}_4$  and  $\text{CO}_2$  fluxes measured on the mast were only contributed by reservoir water surface. No influence of primary forest ecosystems located beyond the footprint area can be suspected in the flux measurement. Note that mast location was chosen to correspond to the floodplain ecosystem existing before the impoundment. By definition, floodplain was a very flat and horizontal terrain. From this, we can guarantee that the mean water depth was constant over the whole footprint area.

The footprint analysis also confirmed that FC and SF measurements were conducted within the EC footprint area.

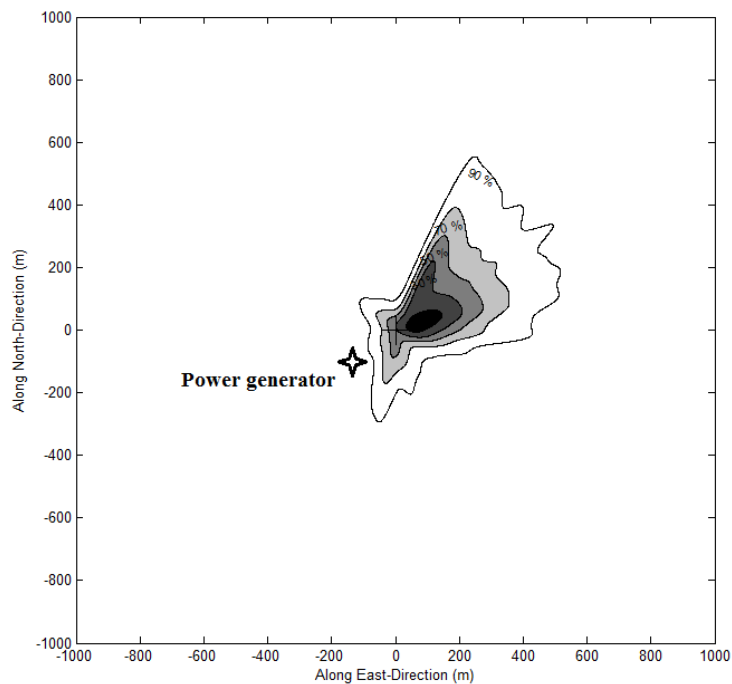


Figure 3.7. Flux footprint for CO<sub>2</sub> fluxes from NT2 reservoir during a EC deployment in March 2011. Isolines (10, 30, 50, 70 and 90 %) show the percentage of flux contributing to the total flux, i.e., the footprint area. Measurement mast is at the center of the figure.

**CH<sub>4</sub>:** In May 2009, the sum of the independent averages of SF<sub>bubb</sub> and FC<sub>GC</sub> fluxes was around 2 times lower than fluxes measured with the EC technique. However, the averages of the FC<sub>GC(diff+bubb)</sub> and EC fluxes are reasonably comparable with each other ( $7.3 \pm 0.9$  vs.  $6.5 \pm 0.5$  mmol.m<sup>-2</sup>.day<sup>-1</sup>). In March 2010, direct comparison was not possible as SF bubbling measurement could not be performed in the EC footprint area.

In March 2011, on average, continuous estimates of the EC fluxes were lower than the discrete estimates of FC<sub>GC(diff+bubb)</sub> fluxes. But, when comparison is made for the same time of measurement, fluxes compare well (Wilcoxon matched-pairs signed rank test,  $p = 0.37$ ). On the daily basis, EC CH<sub>4</sub> fluxes compare very well with the sum of SF<sub>(bubb)</sub> and FC<sub>insitu(diff)</sub> fluxes (Wilcoxon matched-pairs signed rank test,  $p=0.62$ ) and with the sum of FC<sub>insitu(diff)</sub> and FC<sub>insitu(bubb)</sub> (Wilcoxon matched-pairs signed rank test,  $p=0.15$ ), whereas the daily averages of FC<sub>insitu(bubb)</sub> and SF bubbling fluxes poorly compare, (Wilcoxon matched-pairs signed rank test,  $p = 0.06$ ). It should be noticed that more than 50% of the FC<sub>insitu(bubb)</sub> measurement had no bubbles i.e. zero bubbling fluxes during the small time of measurement (e.g. 5-20 min). On the other hand, sudden capturing of even a single bubble could lead to a significantly large flux that might not be a true representation of a daily average as it is measured for that particular small time of measurements.

In June 2011, on average, estimates of the EC fluxes were lower than the estimate of  $FC_{GC(\text{diff+bubb})}$  fluxes. But again, if comparison is made for the same time of measurement, fluxes compare well (Wilcoxon matched-pairs signed rank test,  $p = 0.64$ ).

Often the  $FC_{GC(\text{diff+bubb})}$  fluxes were close to EC fluxes, unless bubbles were captured in FC leading to significantly increased fluxes (as seen in Figure 3.4a). Therefore the average  $FC_{GC(\text{diff+bubb})}$  fluxes were higher than the average EC and the sum of independent measurement of diffusive and bubbling measurement. This suggests that such sporadic measurements of high fluxes due to bubbles in the FC can lead to overestimate of the bubbling fluxes. Further, Owing to short measurement time (5-20 min),  $FC_{\text{insitu}(\text{bubb})}$  bubbling fluxes were very sporadic. Most of the time, no bubbles were captured, but on other hand, sudden capturing of bubble could lead to fluxes up to  $25 \text{ mmol.m}^{-2}.\text{day}^{-1}$ .  $SF_{(\text{bubb})}$  fluxes were performed on a larger time scale (typically 24hr), therefore these fluxes included all the temporal variability over a deployment time. This suggests that since bubbling is a highly random and discontinuous process, estimates of bubbling fluxes should not be done at too short time scale (e.g. 5-20 min).

**CO<sub>2</sub>:** Comparison of EC CO<sub>2</sub> fluxes was only possible for the March 2011 campaigns. A total of 27 and 19 measurements were performed with  $FC_{\text{insitu}}$  and  $FC_{GC}$  respectively within the EC footprint area. Comparing the measurement done at the same time with the three techniques shows a good matched up (Kruskal-Wallis test,  $p = 0.90$ ). EC fluxes are well in agreement with  $FC_{GC}$  fluxes ( $p = 0.69$ ) and  $FC_{\text{insitu}}$  fluxes ( $p = 0.92$ ),  $FC_{\text{insitu}}$  fluxes being also well in agreement with  $FC_{GC}$  fluxes ( $p = 0.70$ ) in the same time.

### **3.4. Discussion**

#### **3.4.1. Physical controls on CH<sub>4</sub> emissions**

With flux time series, our aim now is to describe their temporal behavior, and to identify the mechanism that modulates the natural dynamics of EC CH<sub>4</sub> fluxes. We will first examine the daily variation in 30 min integrated EC fluxes and later, study the seasonal variation in average CH<sub>4</sub> fluxes from the different field campaigns. In our attempt to link temporal variability of CH<sub>4</sub> fluxes to driving forces, different environmental variable were tested i.e. atmospheric pressure and atmospheric pressure fluctuation, water depth and water level fluctuation in the reservoir, surface water temperature, wind speed, atmospheric temperature, relative humidity and wind direction.

In the following, we address first the influence of variation in atmospheric pressure on EC CH<sub>4</sub> fluxes. Then, we discuss the seasonal variations in EC CH<sub>4</sub> fluxes considering the dependency with water level fluctuation and water depth. Next, we discuss the variation in bubbling fluxes considering the dependency with water depth and water level fluctuation, atmospheric pressure and atmospheric pressure fluctuation, and bottom temperature. Finally, comparison between the different methodologies and models to assess the CH<sub>4</sub> fluxes will be discussed.

### 3.4.1.1. Semidiurnal cycle of CH<sub>4</sub> emissions

A clear semidiurnal variation of EC fluxes, with one peak in early morning, and one in the afternoon, can be observed during all four campaigns (Figure 3.5). Atmospheric pressure follows a typical semi-diurnal pattern, which is most likely the cause of semidiurnal variability observed in EC CH<sub>4</sub> fluxes. Anti-correlation between atmospheric pressure and CH<sub>4</sub> fluxes also works in term of intensity. The larger drop in atmospheric pressure in the late morning is associated with the higher daily CH<sub>4</sub> flux peak, when again atmospheric pressure drop and CH<sub>4</sub> flux increase is smaller during the late afternoon.

In addition, we propose a hypothesis to define the amplitude of the peak of CH<sub>4</sub> fluxes, taken example from March 2011 field campaign. D1 and D2 indicate the daily drops/recessions in the atmospheric pressure; these are the time periods when trapped bubbles are released from the sediment and boost the CH<sub>4</sub> release from the water surface. G1 and G2 indicate the daily gains/growths/recoveries in the atmospheric pressure, which slows down the release of CH<sub>4</sub>, allowing for the next build-up of bubbles in the sediment.

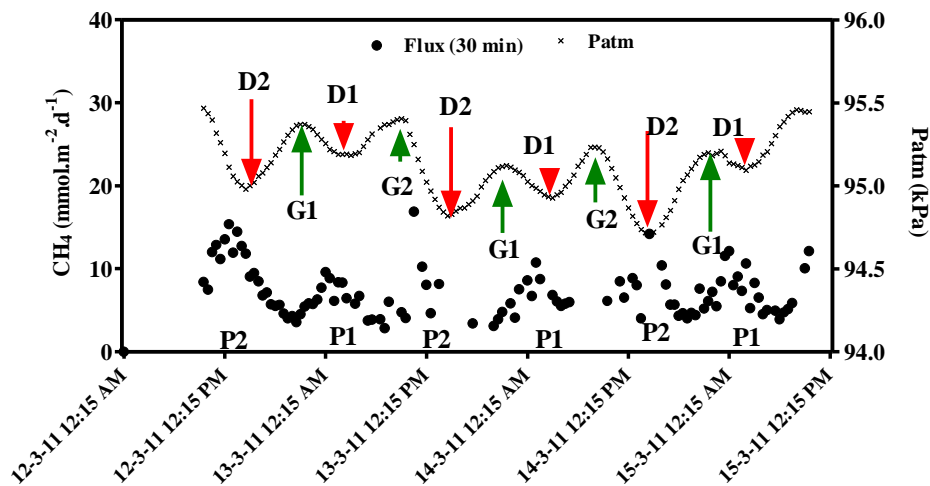


Figure 3.8. Time series of EC CH<sub>4</sub> fluxes with atmospheric pressure obtained from March 2011. D1 and D2 correspond to daily drops/recessions in the atmospheric pressure; G1 and G2 correspond to daily gains/growths/recoveries in the atmospheric pressure; P1 and P2 correspond to daily peaks of CH<sub>4</sub> fluxes.

P1 and P2 indicate the daily peaks of CH<sub>4</sub> fluxes. It is clearly seen that the first drop (D1) is lower than the second drop (D2). Further, the first growth or recovery period (G1) is greater than the second one (G2). Therefore, after a large growth or recovery (G1), even a small decrease in atmospheric pressure (D1) will generate a peak (P1) in the CH<sub>4</sub> fluxes. Second growth or recovery period (G2) is comparatively small than G1, but it is followed by the large drop/recessions (D2) causing peak P2. Therefore the amplitude of P1 could be regulated by the succession of G1 and D1 and similarly for P2 with the succession of G2 and D2. This might explain why a relatively weak correlation coefficient between CH<sub>4</sub> fluxes and

change in atmospheric pressure is found (Figure 3.9), even though CH<sub>4</sub> emissions are very sensitive to fluctuation in the atmospheric pressure. The regression against change in atmospheric pressure was able to explain up to 49% of the variation in the CH<sub>4</sub> fluxes from the reservoir (Figure 3.9). It is noteworthy to point out that the regression coefficients are better for the two campaigns (March and June 2011) with the lower water depth at the EC site (6.5 m and 2 m respectively).

Most of the studies in peat lands, rice paddy fields, submerged ecosystems and hydroelectric reservoirs relate diurnal changes with diurnal variation in the temperature or water level (Suyker et al., 1998; Long et al., 2010; Simpson et al., 1995; Satpathy et al., 1997; Tseng et al., 2010; Eugster et al., 2011). However, this is the first time to our knowledge that, thanks to continuous automated EC flux determination, such a semidiurnal pattern of CH<sub>4</sub> emissions is evidenced.

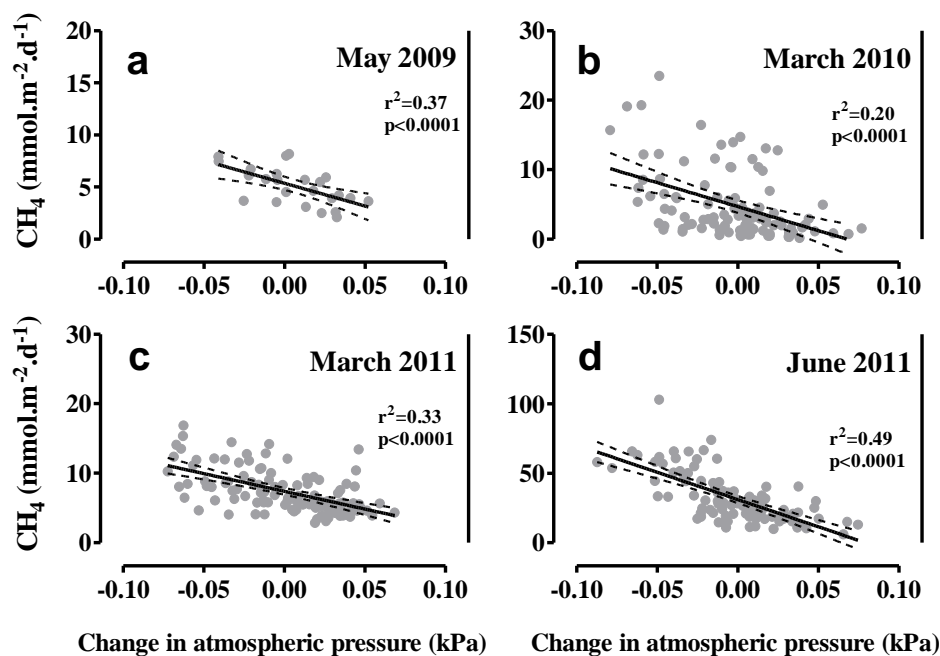


Figure 3.9: Dependence of individual 30-min CH<sub>4</sub> fluxes with changes in the atmospheric pressure. Note that scale of y-axis differs for different field campaigns.

### 3.4.1.2. Water depth and water level fluctuation

A large seasonal variation in averaged CH<sub>4</sub> flux is observed with values from a minimum of  $5.8 \pm 0.4 \text{ mmol.m}^{-2}.\text{day}^{-1}$  in May 2009, to a maximum of  $29 \pm 1.4 \text{ mmol.m}^{-2}.\text{day}^{-1}$  during the late dry season in June 2011. As in most of the tropical reservoirs, water depth in NT2 follows a seasonal pattern with the highest level in the wet season, and the lowest at the end of dry season. This seasonal change in water depth is most likely responsible for the variability observed in the CH<sub>4</sub> fluxes at that time scale. The role of water level changes has also been reported in previous studies (Eugster et al., 2011; Ostrovsky et al., 2008).



We normalize the rate of water level change with average depth of water during the deployment. This provides the specific water level change rates (in units  $\text{d}^{-1}$ ) corresponding to the fraction of the water depth prone to change each day. The specific water level change rates were 0.001, -0.004, -0.01, -0.04  $\text{day}^{-1}$  respectively for deployments in May 2009, March 2010, March 2011 and June 2011. The positive specific water level change rate calculated for the May 2009 indicates that the water level was increasing, which might not have favored  $\text{CH}_4$  emissions during that field campaign (Eugster et al., 2011; Ostrovsky et al., 2008). In contrast, negative specific water level change rate reveals a decrease in the water level during the deployment.  $\text{CH}_4$  emissions are strongly correlated with the specific water level change rate ( $r^2 = 0.98$ ). Highest  $\text{CH}_4$  emissions measured at the end of warm dry period (June 2011), correspond to a combination of the most favorable physical conditions: shallow water depth together with the highest rate of water level decrease, i.e. strong negative specific water level change.

### **3.4.1.3. Dependency on other environmental variables**

We have not observed  $\text{CH}_4$  flux variation with other parameter such as water and air temperature changes. High  $\text{CH}_4$  fluxes in the beginning of the afternoon occur simultaneously with the highest atmospheric temperature of the day. Our results suggest that these high  $\text{CH}_4$  emissions were most likely linked with the drop in the atmospheric pressure, rather than with increase in the atmospheric temperature. Short-term variations in the near-surface water temperature do not directly result in corresponding temperature changes in the deeper methanogenesis sediment layer. As a matter of consequences, on a daily basis, variations in temperature at the bottom of the reservoir are too small for the methanogenesis occurring on the sediment to be significantly affected. At short time-scale (e.g. day),  $\text{CH}_4$  fluxes from the water surface are more related to changes in physical properties rather than to changes in the biological properties. On the opposite, on an annual basis, a clear relationship between water temperature and  $\text{CH}_4$  concentration at the bottom of the reservoir can be observed (Chapter 4).

### **3.4.1.4. Bubbling $\text{CH}_4$ fluxes from the reservoir water surface**

Our results clearly show that  $\text{CH}_4$  ebullition decreases with total static pressure at the bottom of the reservoir (Fig 3.6a). The influence of water depth on ebullition was frequently documented in various environments: lakes (Bastviken et al., 2004), hydroelectric reservoirs (Galy-Lacaux et al., 1999; Keller and Stallard, 1994), estuaries (Chanton et al., 1989) and marine environment (Algar and Boudreau, 2010, Martens and Val Klump, 1980). This depth-dependent behavior could be attributed to two physical processes. First, the deeper the water is, the higher the hydrostatic pressure is preventing the formation of bubbles by increasing  $\text{CH}_4$  solubility in the sediment pore waters. Second, while the  $\text{CH}_4$  bubbles can escape the sediment even in deep aquatic ecosystems, bubbles partly dissolve in the water on their way up to the atmosphere (DelSontro et al., 2010; McGinnis et al., 2006).

A very high scatter in the data presented in Fig. 3.6a suggests that absolute depth is not the only factor controlling bubbling. As shown in Fig. 3.6b, higher bubbling is observed

when the water level is decreasing when compared to the situation where water level is increasing (Smith et al., 2000). It is likely that CH<sub>4</sub> accumulates in the dissolved form in the sediment pore water when the water level is stable, rising, or higher than 15m. When the water level falls, the decrease of the hydrostatic pressure triggers the ebullition of previously accumulated CH<sub>4</sub> in the bottom sediment (Algar and Boudreau, 2010).

As explained previously, water depth, water level variation, atmospheric pressure, change in atmospheric pressure and bottom temperature are relevant parameters to describe CH<sub>4</sub> bubbling fluxes. Water depth and the atmospheric pressure were combined and converted to express the total static pressure (TSP) in meter of water at the bottom of the water column. Similarly, sum the change in water depth and change in atmospheric pressure were converted in TSP change. ANN calculation is finally performed using TSP, TSP change and bottom temperature as inputs parameters. These parameters are easily measurable in the field, and provide an equation that can be used to integrate bubbling at the reservoir scale.

In our study, the independent measurements of bubbling and diffusive fluxes reveal that CH<sub>4</sub> emitted at the water surface can mostly be attributed to the bubbling pathway, more than 95% particularly during warm dry season when reservoir exhibits low water depth.

### **3.4.2. Physical controls on CO<sub>2</sub> fluxes**

The relative role of the different physical processes can be assessed by comparing the diffusive CO<sub>2</sub> fluxes obtained from the EC measurements under different meteorological and physical conditions in the water column. The pattern of CO<sub>2</sub> fluxes is more complex at the NT2 reservoir. This makes it difficult to simply parameterize CO<sub>2</sub> fluxes with wind speed. In the following, we analyze EC CO<sub>2</sub> fluxes from different field campaigns to develop a mechanistic understanding of the processes affecting diffusive CO<sub>2</sub> fluxes. For this, we have calculated the different terms of the surface energy budget. The aim is to determine whether wind forcing or buoyancy forcing due to heat losses could be drivers of the CO<sub>2</sub> fluxes.

Figure 3.10 shows significant differences between EC CO<sub>2</sub> fluxes observed during strong thermal and CO<sub>2</sub>-gradient (May 2009), weak thermal and strong CO<sub>2</sub>-gradient (March 2010), and weak thermal and no CO<sub>2</sub> gradient (March 2011) in the water column. There are clear indications that other factors besides wind speed need to be considered when trying to parameterize CO<sub>2</sub> fluxes.

When the EC CO<sub>2</sub> fluxes are plotted against wind speed, it appears that CO<sub>2</sub> fluxes depends more strongly on wind speed in the cold water periods (March 2010 and 2011) than in the warm water period (May 2009). Indeed, wind speed explained ~ 6, 52 and 68% of the variation in CO<sub>2</sub> fluxes for the May 2009, March 2010 and March 2011 field campaigns respectively. These results suggest that relationship of CO<sub>2</sub> fluxes with wind speed is then not only site-specific, but also strongly time-specific. When the three field campaign datasets are combined, wind speed and friction velocity  $u_*$  explain 36 and 27 % of the variation in CO<sub>2</sub> fluxes ( $p < 0.0001$ ) (Figure 3.10a and b).

Other variables that best explained the variation in CO<sub>2</sub> fluxes were sensible and latent heat fluxes that could explain 26 and 41 % of the variation in CO<sub>2</sub> fluxes ( $p < 0.0001$ ) (Figure 3.10c & d). When we consider fluxes from all field campaigns together, our multiple linear analysis (MLR) model using sensible heat flux, latent heat flux, wind speed and friction velocity  $u_a^*$  as input parameters would explain up to 46% of the variation seen in the EC CO<sub>2</sub> fluxes ( $r^2 = 0.45$ ,  $p < 0.0001$ ). It is important to notice that if we apply the same MLR model on May 2009 EC CO<sub>2</sub> fluxes, it only explains 9% of the variability in CO<sub>2</sub> fluxes. Whereas, the same MLR model explains 63 and 69% of the variability in CO<sub>2</sub> fluxes from March 2010 and March 2011. A considerable fraction of the variation of CO<sub>2</sub>, not related to either the wind speed or the heat loss, remained unexplained in May 2009.

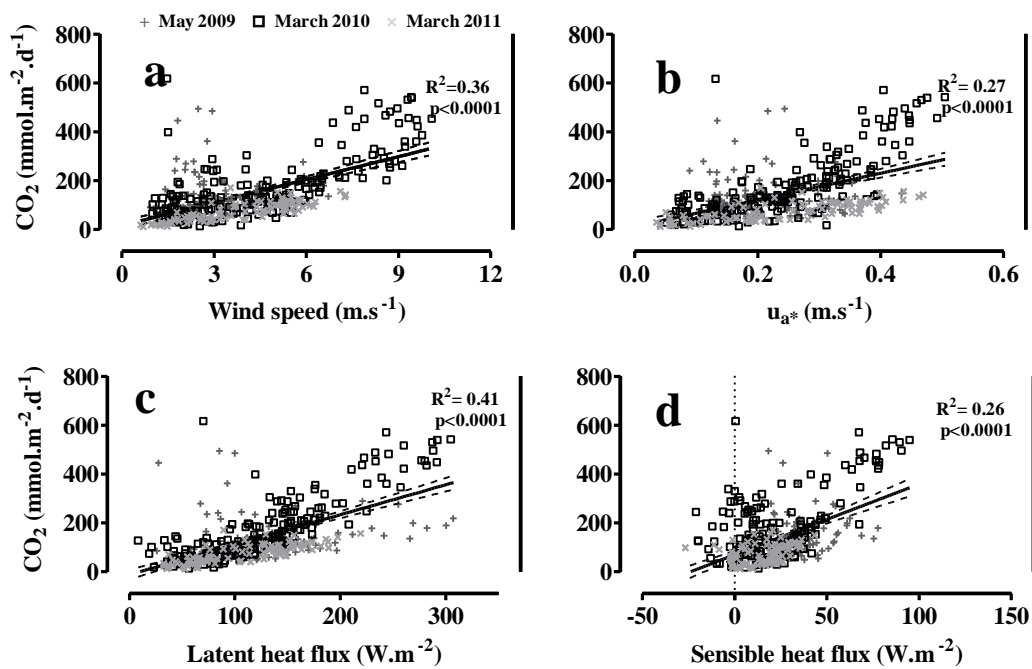


Figure 3.10: Influence of (a) wind speed (b) friction velocity (c) latent heat, and (d) sensible heat on EC CO<sub>2</sub> 30 min fluxes

Figure 3.11a shows the role of buoyancy flux on the process of CO<sub>2</sub> exchange across the water-air interface. During the heat loss from the reservoir water shows negative buoyancy values. During cooling, buoyancy fluxes explained around 24% ( $p < 0.0001$ ) of the variation in CO<sub>2</sub> fluxes, whereas during heating, buoyancy fluxes explained only 8% ( $p < 0.0001$ ) of the variation. MacIntyre et al. (2010) found similar results of gas transfer velocity dependency on buoyancy.

Buoyancy not only explain the variation in CO<sub>2</sub> fluxes, but also it suggests the influence of the wind speed on CO<sub>2</sub> fluxes during cooling and heating of surface water layer. Figure 3.11b and 3.11c showed the dependency of CO<sub>2</sub> fluxes during two different physical conditions i.e. when buoyancy  $> 0$  and buoyancy  $< 0$ . The transition from buoyancy  $> 0$  to

buoyancy flux  $<0$  occurs in the late afternoon and persists until the next morning. Surface heat losses contributed to the surface layer deepening of the time from midafternoon until midmorning.

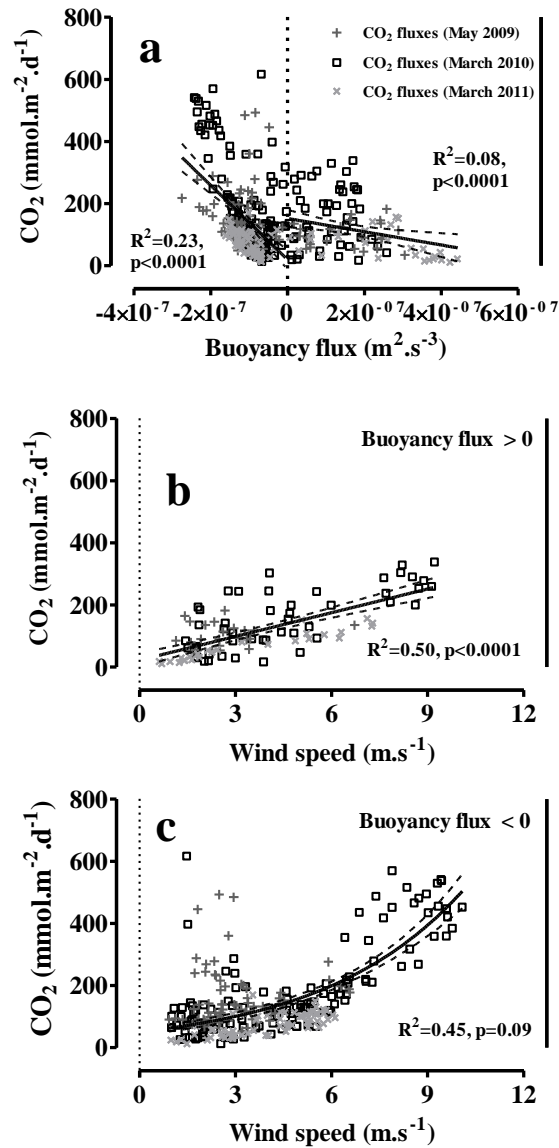


Figure 3.11. (a) buoyancy versus CO<sub>2</sub> fluxes (b) wind speed versus CO<sub>2</sub> fluxes for buoyancy  $> 0$  (c) wind versus CO<sub>2</sub> fluxes for buoyancy  $< 0$ .

Figure 3.11b clearly shows that CO<sub>2</sub> fluxes are less scattered and are strongly dependent on wind speed ( $r^2 = 0.50, p < 0.0001$ ) when buoyancy  $> 0$ . During the day time (buoyancy  $> 0$ ), absorption of solar radiation in the water column diminishes the surface layer and thereby convective velocity (MacIntyre et al., 2001; 2002). This suggests that during such conditions, the physical processes at the water-air interface rely more on meteorological conditions, and associated influence on the water column (MacIntyre et al., 2010). Therefore, when buoyancy is positive, CO<sub>2</sub> fluxes are linearly dependent on wind speed (Figure 3.11b).

Figure 3.11c shows the influence of wind speed on CO<sub>2</sub> fluxes when buoyancy is negative. Convective mixing in the water column occurs when heat losses exceed heat inputs (buoyancy < 0, MacIntyre et al., 2001; 2002). Figure 3.11c clearly shows that there is no clear pattern for low wind speed (<3 m.s<sup>-1</sup>), CO<sub>2</sub> fluxes would have been governed by some other factors. This is particularly the case during free convection conditions above the water surface (May 2009), and also when strong thermal gradient and CO<sub>2</sub> gradient in the water column existed (May 2009 and March 2010). It suggests that during such conditions, the physical processes at the water-air interface are jointly dependent on the physical conditions above water surface and within the water column (MacIntyre et al., 2010). During high wind conditions, CO<sub>2</sub> fluxes increased exponentially with high wind speed ( $r^2 = 0.45$ ,  $p = 0.09$  for buoyancy < 0). This suggests the additive thermal effect of cooling on CO<sub>2</sub> exchange (MacIntyre et al., 2010).

Only 5 temperature profiles were measured in May 2009 during the day time (in between 12 am to 4 pm local time), i.e. the heating period. All vertical profiles of temperature confirmed that the thermocline depth positioned at 4 m. The active surface mixed layer is shallow in the day, and deepening of the mixed layer and entrainment of thermocline waters occurs in the late afternoon when convective velocity scale increases (MacIntyre et al., 2001; 2002). Therefore during the cooling the thickness of active mixed layer must have been greater than 4 m. The penetrative convection velocity  $w^*$  is a function of buoyancy flux (B) and depth of the active surface mixed layer (h), and can be calculated as following:  $w^* = (Bh)^{1/3}$  (Deardoff 1970). During cooling periods we used a constant mixing depth (h) of 4 m to calculate the convective velocity scale ( $w^*$ ). The convective velocity ranged from 0.4 to 1.2 cm.s<sup>-1</sup>, very comparable to values reported for a tropical lake (MacIntyre et al., 2002). Our results clearly show that  $w^*$  values were 2 times higher ( $0.9 \pm 0.1$  cm.s<sup>-1</sup>) than the  $u_{*w}$  ( $0.5 \pm 0.2$  cm.s<sup>-1</sup>) calculated at the same time. These values must be considered as estimates representing relative conditions within the measurement period and thus provide an understanding of the physical processes occurring in the water column. The comparison between  $u_{*w}$  and  $w^*$  clearly suggest that during the cooling, convective velocity scale is comparatively higher than shear velocity scale.

In May 2009, it should be noted that air was cooler than the surface waters throughout the field campaign (sensible heat > 0, Figure 3.11c). Consequently, the boundary layer above the air-water interface was unstable due to free convection condition. We examined the Monin-Obukhov stability parameter  $z.L^{-1}$  in the atmosphere and found that during each downward CO<sub>2</sub> fluxes,  $z.L^{-1}$  was negative, indicating good mixing conditions in the atmosphere, even during low wind conditions. The high temperature gradient (~10°C) between surface water and metalimnion could generate larger convective mixing and thereby turbulence at the surface. Not only penetrative convection does increase gas transfer during periods with low wind speed, but also the associated entrainment of metalimnetic water may lead to increased gas concentrations in surface waters and appreciably enhance CO<sub>2</sub> fluxes. Process of penetrative convection is most important to CO<sub>2</sub> fluxes when it is coupled to strong vertical stratification of CO<sub>2</sub> in the water (May 2009).

Temperature difference between metalimnion and surface water and subsequent sensible heat loss were much higher in May 2009 than March 2010 and March 2011 (Table 3.1). As a matter of consequences, penetrative convection was more likely on May 2009 than March 2010 and March 2011. However, because of the lack of continuous temperature profile data, it is not possible to relate the growth of the convective mixing layer to the efflux pattern observed in the EC flux data.

In March 2010, CO<sub>2</sub> fluxes went up to 570 mmol.m<sup>-2</sup>.day<sup>-1</sup> with wind speed of ~10 m.s<sup>-1</sup> (Figure 3.10a). It suggests that because of the warm surface waters compared to air, the cooling was largely increased due to evaporation (~300 W.m<sup>-2</sup>) and sensible heat loss (100 W.m<sup>-2</sup>) with wind speed. Accordingly, it seems that high wind speed not only increased the turbulent friction velocity above water surface but also increased the convective velocity in the water column through heat loss. Additionally, it can be assumed that CO<sub>2</sub> gradient was eroded by the combination of wind and heat loss.

In March 2011, the variability in CO<sub>2</sub> fluxes is closely coupled with the wind speed variation. CO<sub>2</sub> fluxes were lower in March 2011, even though this field campaigns exhibited high wind speed (up to 8 m.s<sup>-1</sup>). During March 2011, the short wave radiation was maximum among all the field campaigns (up to 880 W.m<sup>-2</sup>, with a mean of 219 ± 314 W.m<sup>-2</sup>), which is almost twice higher than the other two field campaigns. With low surface water temperature and with a weak thermal gradient, it seems than even high wind conditions during the day were not able to overcome with the heating effect (lowest buoyancy fluxes, 0.003±1.8 m<sup>2</sup>.s<sup>-3</sup>, Table 3.1). Therefore without this deepening, gas concentrations quickly equilibrate with those in the atmosphere leading to lower rates of gas flux. As there were no CO<sub>2</sub> trapped in the hypolimnion water, it also suggests that even high wind could have deepened the mixed layer but could not increase the supply of CO<sub>2</sub> concentration in the surface layer and subsequently CO<sub>2</sub> concentrations in the surface water quickly equilibrate with those in the atmosphere leading to lower rates of gas flux. This can be confirmed as there were no sporadic high fluxes observed. Such high sporadic high fluxes (up to 600 mmol.m<sup>-2</sup>.day<sup>-1</sup>) were noticed few times during May 2009 and March 2010, when reservoir exhibited a CO<sub>2</sub> gradient in the water column. Probably such high sporadic CO<sub>2</sub> fluxes were due to erosion of CO<sub>2</sub> gradient during convective mixing in the water column (Eugster et al., 2003; MacIntyre et al., 2002). Such high fluxes indicate the importance of heat loss for mixed layer deepening circulation, and thereby the magnitude of gas fluxes.

### **3.4.3. Inter-comparison of EC CH<sub>4</sub> fluxes with independent floating chamber and submerged funnel measurements**

As mentioned before, floating chamber (FC<sub>GC</sub> and FC<sub>insitu</sub>) and funnel measurements were made in the footprint of the eddy covariance system. When there was not enough direct measurements for a statistical comparison of the different techniques, thin boundary layer (TBL) technique (MacIntyre et al., 2010) and ANN model were used respectively to calculate diffusive and bubbling fluxes.

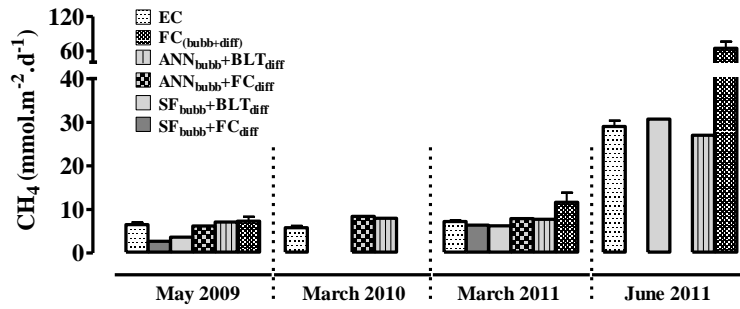


Figure 3.12. Inter-comparison of different methodology to assess CH<sub>4</sub> emissions

EC fluxes were found very consistent with the sum of the two terms measured independently (diffusive fluxes + bubbling fluxes = EC fluxes, see Figure 3.12). Figure 3.12 indicates that the eddy covariance system picked-up both diffusive and bubbling fluxes from the reservoir, which is a very new and encouraging result for further studies. A good agreement ( $p = 0.49$ , one way ANOVA test) among the different assessments confirms and validates the comparison between those different measurement techniques. Owing to stochastic nature of CH<sub>4</sub> emissions, Figure 3.12 clearly cautions that sporadic sampling with floating chambers can also results in erroneous estimates of the daily averages, due to significant variation over a day.

### 3.5. Conclusion

This study presents CO<sub>2</sub> and CH<sub>4</sub> fluxes from a newly flooded hydroelectric reservoir in sub-tropics. Understandings of the physical controls on these emissions were sought from the continuous EC flux and discrete floating chamber and submerged funnels measurements. This study is the first direct EC flux measurements of CH<sub>4</sub> fluxes along with CO<sub>2</sub> and energy fluxes from a sub-tropical hydroelectric reservoir. Our study carefully aimed at matching EC measurements with floating chamber and funnel measurements. The direct comparison between the different techniques used to assess CO<sub>2</sub> and CH<sub>4</sub> emissions from the NT2 hydroelectric reservoir confirmed that the EC methodology is able to capture both emissions for diffusion and ebullition in the same time.

Overall, assessing CO<sub>2</sub> and CH<sub>4</sub> fluxes from a hydroelectric reservoir is a complicated task. An accurate quantification of CO<sub>2</sub> and CH<sub>4</sub> fluxes from a hydroelectric reservoir requires capturing both the spatial and temporal variability in emissions. From the continuous EC measurements at NT2 reservoir, we have showed that the natural course of CH<sub>4</sub> and CO<sub>2</sub> fluxes is so dynamic that it is easy to miss episodic events.

The high resolution flux sampling provided by EC allowed us to examine the influence of changes in the physical mechanisms on CH<sub>4</sub> emissions at shorter timescales. We have evidenced the timing of CH<sub>4</sub> emissions on daily and seasonal time scales. On the short term, it seems that CH<sub>4</sub> emissions are firstly influence by atmospheric pressure change, with increasing emission when pressure drops, and vice versa. The seasonal variability of CH<sub>4</sub>

fluxes from the reservoir is mostly linked with the changes in the reservoir water level, further probably with temperature at the bottom.

Intensive measurements suggest that ebullition is sensitive to total static pressure and variation in total static pressure due to either water level change or atmospheric pressure. From these parameters, together with bottom temperature, we have constructed an artificial neuron network (ANN) model that is capable to explain up to 50% of variation in bubbling fluxes, which is quite high-quality for such a stochastic process.

CO<sub>2</sub> flux measurement from the different deployments revealed a complex pattern of CO<sub>2</sub> flux which appears to be mainly a result of the interaction of physical processes in the water column and meteorological processes above the water surface. Our results indicate that owing to the turbulent velocity scale due to heat loss, CO<sub>2</sub> fluxes are much higher when  $T_{\text{water}} > T_{\text{air}}$  with thermal and CO<sub>2</sub> gradient in the water column. On the opposite, when the water column is poorly thermal stratified with no CO<sub>2</sub> gradient, then low CO<sub>2</sub> fluxes occur. Our results confirm that during the heat gain in the water column (buoyancy > 0), CO<sub>2</sub> fluxes are linearly dependent on wind speed. While, during heat loss (buoyancy < 0), (1) at low wind speed, fluxes do not follow the wind speed and (2) at high wind speed fluxes increase exponentially with wind speed. As the CO<sub>2</sub> efflux from reservoirs is most likely limited by processes in the water column, the effect of convection in the hydroelectric reservoirs must be investigated in the future works.

As matter of fact each hydroelectric reservoir is unique in terms of physical and chemical dynamics. However this study stresses the need to carry out more EC-measurements in different types and sizes of hydroelectric reservoir to enable a more detailed comparison between different controlling variables of CO<sub>2</sub> and CH<sub>4</sub> emissions.



## Appendix A: Artificial neuron network

$$\text{CH}_{4\text{fluxnorm}} = w_{12} + w_{13} \cdot \tanh(S_1) + w_{14} \cdot \tanh(S_2) + w_{15} \cdot \tanh(S_3) \quad (\text{A1})$$

where  $\text{CH}_{4\text{fluxnorm}}$  is the normalized  $\text{CH}_4$  flux, and

$$S_1 = w_0 + \sum_{i=1}^3 w_i v_{j,\text{norm}} \quad (\text{A2})$$

$$S_2 = w_4 + \sum_{i=5}^7 w_i v_{j,\text{norm}} \quad (\text{A3})$$

$$S_3 = w_8 + \sum_{i=9}^{11} w_i v_{j,\text{norm}} \quad (\text{A4})$$

with  $j=1 \rightarrow 3$

where  $v_1$  to  $v_3$  correspond to change in total static pressure (sum of change in water level and change in atmospheric pressure), total static pressure (water depth + atmospheric pressure) and bottom temperature, respectively; with

$$v_{1,\text{norm}} = x_1 + x_2 * v_1 \quad (\text{A5})$$

$$v_{2,\text{norm}} = x_3 + x_4 * v_2 \quad (\text{A6})$$

$$v_{3,\text{norm}} = x_5 + x_6 * v_3 \quad (\text{A7})$$

All weights  $w_i$  are given in Table 3.A1 the weights  $w_0$ ,  $w_4$ , and  $w_8$  being linked to the bias neuron (constant term equal to 1).

The resulting  $\text{CH}_4$  ebullition flux is finally calculated (in  $\text{mmol} \cdot \text{m}^{-2} \cdot \text{d}^{-1}$ ) using:

$$\text{CH}_{4\text{bubblingflux}} = x_6 + x_8 * \text{CH}_{4\text{fluxnorm}} \quad (\text{A8})$$

where  $x_j$  are the normalization coefficient, given in Table 3.A2

Table 3.A1. Weights for CH<sub>4</sub> bubbling flux modeling with neural network parameterization

Weights	
w <sub>(0)</sub>	-0.26251023
w <sub>(1)</sub>	0.27036778
w <sub>(2)</sub>	-0.18312979
w <sub>(3)</sub>	1.57915236
w <sub>(4)</sub>	-1.28271027
w <sub>(5)</sub>	0.70240626
w <sub>(6)</sub>	-0.07368578
w <sub>(7)</sub>	1.62828297
w <sub>(8)</sub>	-2.29557914
w <sub>(9)</sub>	-1.53963978
w <sub>(10)</sub>	-0.84875177
w <sub>(11)</sub>	-0.40894676
w <sub>(12)</sub>	0.87099919
w <sub>(13)</sub>	0.98768781
w <sub>(14)</sub>	-1.1417559
w <sub>(15)</sub>	1.58234604

Table 3.A2. Normalization coefficients for CH<sub>4</sub> bubbling flux modeling with neural network parameterization

Normalization Coefficients	
x <sub>1</sub>	0.499219
x <sub>2</sub>	15.97745
x <sub>3</sub>	-4.289562
x <sub>4</sub>	0.294832
x <sub>5</sub>	-10.99491
x <sub>6</sub>	0.55589
x <sub>7</sub>	9.538083
x <sub>8</sub>	9.62247

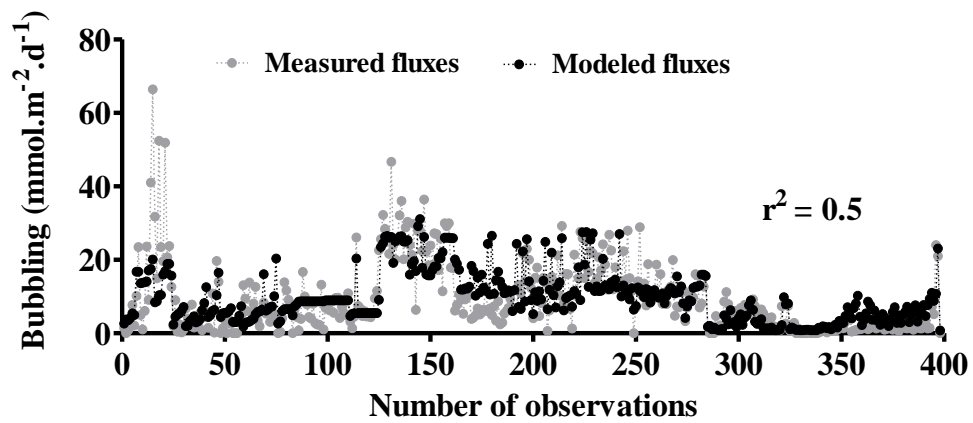


Figure 3A. Measured versus modeled bubbling fluxes.



## Chapter 4

# Methane (CH<sub>4</sub>) dynamics and gross atmospheric emissions from a newly impounded hydroelectric reservoir in subtropical south-east Asia: the Nam Theun 2 Reservoir (Lao PDR)

---

**Abstract:** The Nam Theun 2 (NT2) hydroelectric reservoir, located in subtropical South Asia (Lao PDR) was flooded in April 2008 and first reached its maximum level in October 2009. The turbines were operated 8 months later (March 2010). During the study, the surface area of the reservoir varied from 450 down to 170 km<sup>2</sup> between the wet and the dry seasons. The total methane (CH<sub>4</sub>) emissions were quantified at the reservoir surface, downstream of the dam and the powerhouse and from the drawdown area between April 2009 and December 2011. Based on aerobic incubation of water at different CH<sub>4</sub> concentrations and on anaerobic incubations of soils, we estimated the total production and oxidation of CH<sub>4</sub> in the NT2 system which were compared with the total emissions.

Overall, the total emissions vary seasonally by a factor of two with 50% of the total emissions occurring within 3 to 5 month during the transition between the dry and the wet seasons. Against expectation, the contribution of emissions from the drawdown area was very low (< 4%) although its surface area during the dry season could be as large as the reservoir surface area. The diffusive fluxes contributed only 18% of total emissions ( $2.4 \pm 2.9 \text{ mmol.m}^{-2}.\text{day}^{-1}$ ) but the 2-km<sup>2</sup>-area located at the water intake contributed 32% of the total diffusive fluxes due to the water column mixing as soon as the turbines were operated ( $94 \pm 140 \text{ mmol.m}^{-2}.\text{day}^{-1}$ ). Because of the outgassing before the water reached the water intake, CH<sub>4</sub> emissions below the powerhouse contributed only 13% of total CH<sub>4</sub> emissions in 2011 (first year of normal operation of the reservoir). However, the degassing from spillway release before the power station commissioning and the degassing following the turbine operation were very significant for the year 2010. Ebullition decreased with depth and no bubbling was observed at stations where the water column was deeper than 13 m. It occurred mostly during periods of decreasing water level and contributed 50-70% of total emissions from this young reservoir. Between 2010 and 2011, total CH<sub>4</sub> emissions decreased from  $30.8 \pm 8.2$  to  $19 \pm 3.7 \text{ Gg(CH}_4\text{).year}^{-1}$  because of a significant increase of methanotrophic activity in the reservoir water column. The comparison of the contribution of each pathway to the total emissions from the NT2 Reservoir with other reservoirs evidences that the estimation of worldwide emission from hydroelectric reservoirs is challenging.

### 4.1. Introduction

Methane (CH<sub>4</sub>) is the second major radiatively active greenhouse gas contributing to global warming after carbon dioxide (CO<sub>2</sub>) (Forster et al., 2007). In the context of climate change and global warming, the identification and quantification of natural and anthropogenic sources and sinks of CH<sub>4</sub> have become a major environmental issue. Until the 90', hydropower has been supported as green energy source. Since the last two decades, a large number of scientific studies conducted worldwide have shown that hydroelectric reservoirs could contribute significantly to anthropogenic CH<sub>4</sub> emission (Barros et al., 2011; St. Louis et al., 2000). The current global estimates of CH<sub>4</sub> emission from hydroelectric reservoirs vary

from 4 to 64 TgC-CH<sub>4</sub>.yr<sup>-1</sup> (Barros et al., 2011; St. Louis et al., 2000). This large range of estimates indicates that there are still a lot of uncertainties associated with CH<sub>4</sub> emissions from hydroelectric reservoirs. All estimates confirmed the high potential of CH<sub>4</sub> emissions from reservoirs located in the tropics due to a combination of high temperature and high amount of flooded organic matter, both favoring CH<sub>4</sub> production (Barros et al., 2011; St. Louis et al., 2000). However, these conclusions are based on compilations of results from an important number of reservoirs but only a few studies have included all emission pathways with high spatial and temporal resolution (Abril et al., 2005; Kemenes et al., 2007; Teodoru et al., 2012).

The formation of CH<sub>4</sub> in reservoirs occurs during the degradation of flooded or allochthonous OM in strictly anaerobic conditions at the bottom of the reservoir (Guérin et al., 2008a). A major part of the CH<sub>4</sub> produced is oxidized within the water column and never reaches to the atmosphere (Guérin and Abril, 2007). The remaining portion of produced CH<sub>4</sub> escapes to the atmosphere through several pathways: 1/ CH<sub>4</sub> emitted by ebullition occurs mainly in the shallower part of the reservoir (Chapter 3; DelSontro et al., 2011; Galy-Lacaux et al., 1999; Keller and Stallard, 1994) and almost escapes oxidation (DelSontro et al., 2011, 2010; McGinnis et al., 2006); 2/ diffusive emission occurs at the surface of reservoirs (e.g., Guérin et al., 2006 and references therein); 3/ in hydroelectric reservoirs with large seasonal variation of the reservoir surface area, plant-mediated emissions could occur in vegetated littoral zones (Chen et al., 2009, 2011); 4/ methane-rich water from the reservoir water body passes through turbines, and undergoes both a pressure drop and a turbulence spike downstream of the dam which leads to the so-called degassing (Abril et al., 2005; Galy-Lacaux et al., 1997; Kemenes et al., 2007); 5/ the remaining portion of the CH<sub>4</sub> in the turbinated water is either oxidized or released to the atmosphere by diffusion along the river downstream of the turbines (Guérin and Abril, 2007). The contribution of each pathway to the total CH<sub>4</sub> emission from hydroelectric reservoirs varies seasonally according to the hydrological and meteorological cycles (Abril et al., 2005; Chapter 3; Demarty et al., 2009, 2011; Kemenes et al., 2007) and all along the lifetime of the reservoir (Abril et al., 2005). The total emissions from hydroelectric reservoirs decrease with the age of the reservoir as C-pool decreases (Abril et al., 2005; Barros et al., 2011).

Most of the studies on CH<sub>4</sub> emission from hydroelectric reservoirs have been conducted in Europe (e.g., DelSontro et al., 2010), North America (e.g., Soumis et al., 2004; Teodoru et al., 2012) and South America (e.g., Abril et al., 2005), and there is very little information from Asia (Chanudet et al., 2011; Chen et al., 2009, 2011) where 60% of the total world hydropower potential remains (2795 GW) (Kumar et al., 2011).

The objective of the study is to quantify the gross CH<sub>4</sub> emission and provide a comprehensive CH<sub>4</sub> mass balance in the newly flooded subtropical Nam Theun 2 Reservoir (NT2). Quantification of the emissions through all known pathways, based on fortnightly monitoring and four field campaigns, was conducted for the year 2010, which was the first year after NT2 full impoundment, and for the year 2011. The CH<sub>4</sub> mass balance was obtained by extrapolating results of the CH<sub>4</sub> production and oxidation obtained from laboratory

experiments to the reservoir scale, and by comparison with the total emissions. On the basis of these results, we discuss the seasonal variation of the contribution of each emission pathways, and the difference of total emissions between the two years of monitoring.

## 4.2. Material and methods

### 4.2.1. Study area

The NT2 hydroelectric reservoir was built on the Nam Theun River located in the subtropical region of Lao People's Democratic Republic (Lao PDR). Six turbines deliver a maximum annual production of 6 TWh. Filling of the reservoir began in April 2008, and the full water level was first reached in October 2009. NT2 is a trans-basin diversion scheme that receives water from the Nam Theun watershed and releases it into the Xe Bang Fai River through a 27 km long artificial downstream channel (Fig. 4.1). Below the powerhouse, the turbinated water reaches first the tailrace channel (TRC in Fig. 4.1), then is stored one day in a 8 Mm<sup>3</sup> regulating pond (C in Fig. 4. 1) located a few hundred meters below the powerhouse, and is finally released in the artificial downstream channel. To prevent potential problem of deoxygenation in the turbinated water, an aerating weir was built at midway between the turbines and the release in the Xe Ban Fai River (D in Fig. 4.1). A continuous environmental flow of 2 m<sup>3</sup>.s<sup>-1</sup> (and occasionally spillway release) is discharged from the Nakai Dam (A in Fig. 4.1) to the Nam Theun River. NT2 Reservoir receives around 7527 Mm<sup>3</sup> of water from the Nam Theun watershed, which is more than twice the volume of the reservoir (3530 Mm<sup>3</sup>).

Typical meteorological years are characterized by three seasons: wet (May-September), dry-cold (October-January) and dry-warm (February-April). Daily average air temperature varies between 14°C (cold-dry) to 30°C (warm-dry). The mean annual rainfall is about 2400 mm and occurs mainly between May and September (NTPC, 2005).

During the filling, 450 km<sup>2</sup> of soils and different types of vegetation (see Descloux et al., 2011 for description) were flooded by the end of October 2009 (Fig. 4.2). The water level in the reservoir was nearly constant from October 2009 to March 2010 when the plant was commissioned (Fig. 4.2). After the commissioning, the reservoir surface varies seasonally and reaches its maxima (450 km<sup>2</sup>) and minima (175 km<sup>2</sup>) during the wet (October) and dry (June) season, respectively. As a matter of consequence, a large drawdown area, ranging from 175 km<sup>2</sup> to 275 km<sup>2</sup> depending on the years, is observed around the lake at the end of the dry-warm season (June) (Fig. 4.2).

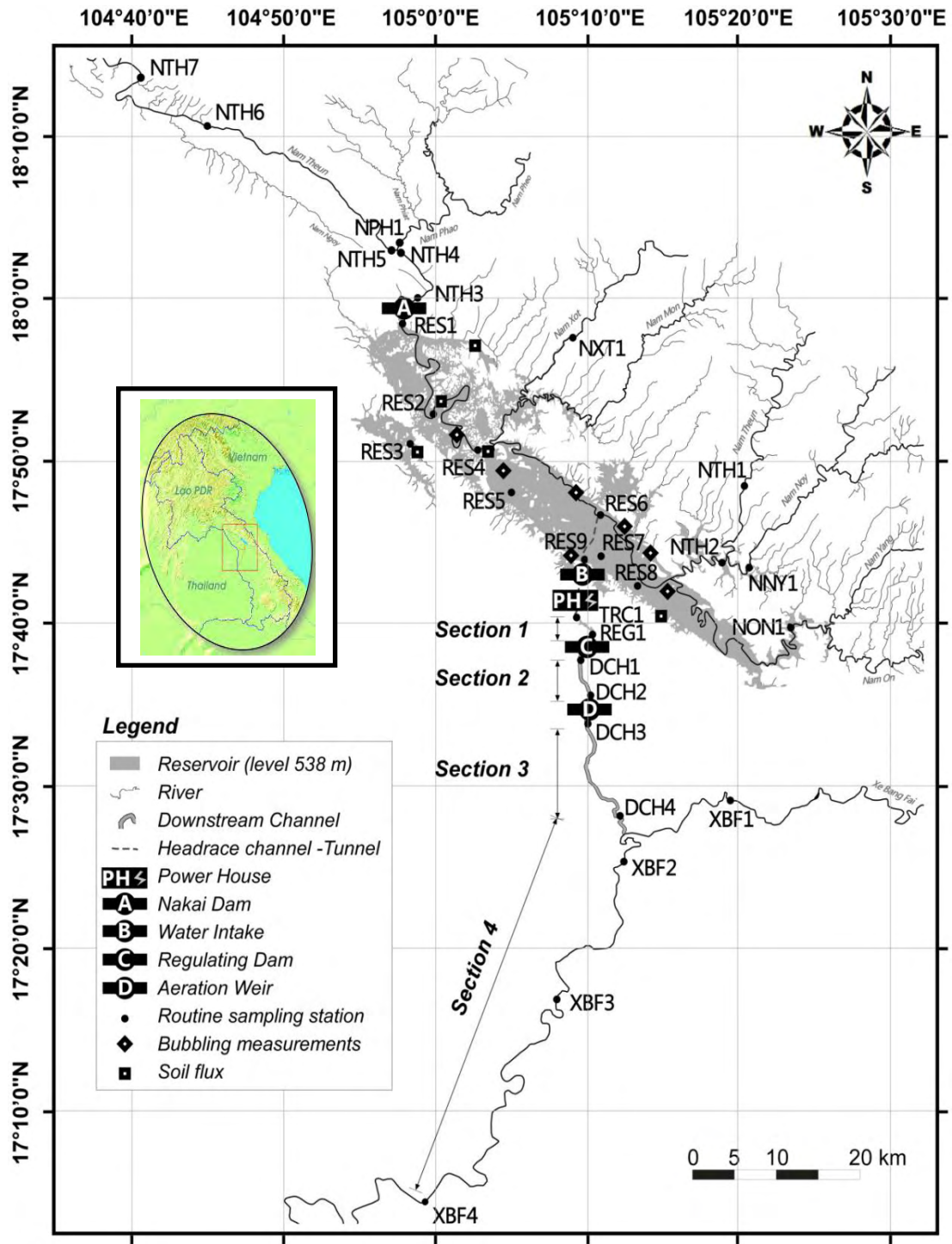


Figure 4.1. Location map showing the different components of the Nam Theun 2 (NT2) reservoir, and the location of the sampling stations. The reservoir is shown at its full capacity (538 m above sea level).



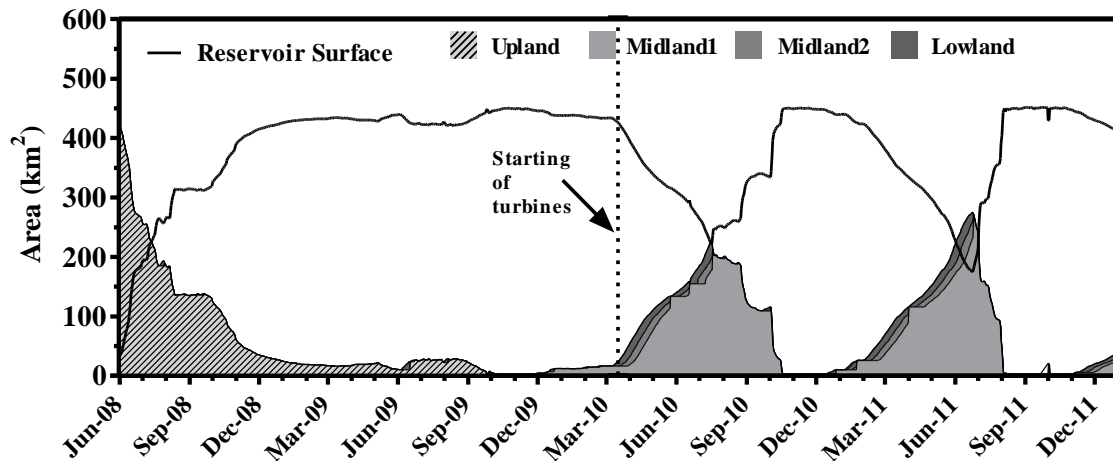


Figure 4.2. Variation in the area of NT2 reservoir surface and different zones of the drawdown area, (i.e. upland, midland1, midland2 and lowland) since beginning of impoundment.

Table 4.1: The main characteristics of the Nam Theun 2 Hydroelectric Reservoir, Lao PDR.

<b>General</b>	Country	Lao People's Democratic Republic (Lao, PDR)
	River	Nam Theun
	Latitude	17°59'49"N
	Longitude	104°57'10"E
	Year of impoundment	2008
	Installed capacity	1070 MW
	Annual Power Production	6000 GWh
	<b>Meteorological</b>	Wind speed
Average relative humidity		63% (Jan) - 89% (Jul)
Precipitation		2400 mm
Air temperature		24.7 °C
<b>Reservoir</b>	Surface at full water level, 538 msl	450 km <sup>2</sup>
	Surface at low water level 525.5 msl	70 km <sup>2</sup>
	Average depth	7.8 m
	Active storage	3530 Mm <sup>3</sup>
	Catchment area	4013 km <sup>2</sup>
<b>Regulating Pond</b>	Maximum turbine water discharge	345 m <sup>3</sup> .s <sup>-1</sup>
	Surface area	0.76 km <sup>2</sup>
<b>Downstream Channel</b>	Length	27 km

#### 4.2.2. Sampling strategy

A total of 29 stations were monitored fortnightly in order to quantify (i) the allochthonous inputs to the reservoir and (ii) CH<sub>4</sub> emissions from the reservoir surface, and from downstream of the dam and the powerhouse. Five stations were located on the main tributaries of the reservoir: the Nam Theun (NTH1, NTH2), the Nam Xot (NXT1), the Nam Noy (NNY1) and the Nam Non (NON1) (Fig. 4.1). In the reservoir, the RES1 (~100 m

upstream of the Nakai Dam), RES2, RES4 and RES6 stations are on the thalweg of the Nam Theun River. RES5, RES7 and RES8 stations are respectively located in the flooded degraded forest, flooded swamp area and flooded agricultural land. RES3 station is located in a small embayment in the flooded primary forest, and RES9 station is located ~100 m upstream of the intake of the turbines.

Below the Nakai Dam, five sampling stations (NTH3-NTH7) were used for the monitoring of the Nam Theun River. Below the powerhouse, the turbinated water was monitored at ten stations and four sections were defined in order to calculate degassing below the powerhouse, the regulating pond and the aeration weir and the diffusive losses (Fig. 4.1).

During each field campaign (March 2010, June 2010, March 2011 and June 2011), we incubated water samples collected from 3 stations in the reservoir (RES1, RES3 and RES7) and 2 stations in the downstream of the dam (NTH3) and the powerhouse (DCH1) in order to determine aerobic methane oxidation rates. Water samples were taken from two depths in the reservoir: (1) in the epilimnion (depth: 1.3 to 4 m) and (2) in the metalimnion (depth: 3 to 8 m). Only surface water samples were taken in the Nam Theun River and in the downstream channel.

During each field campaign, seven stations were used for measurements of ebullition (Chapter 3). In June 2010 and 2011, five sites were used for the estimation of emissions from (i) soils that were never flooded and (ii) from soils in the drawdown area (Fig. 4.1). Sampling sites were selected based on the soil mapping and the representativeness of the flooded ecosystems (Descloux et al., 2011). At each of the five sites, four zones were defined: the upland zone located in an area which was never flooded (soil moisture ~20%); the midland zone 1 which was flooded during high water level ( $20\% \leq \text{moisture} \leq 30\%$ ); the midland zone 2 which was flooded during moderate water level ( $30\% < \text{moisture} < 40\%$ ); and the lowland zone which was close to the shoreline and water-saturated (moisture ~40%). Fig. 4.2 depicts the temporal variations of different zones of the drawdown area.

During the dry season (June 2010), 19 vertical profiles of soil were collected using a soil auger from these sites after the fluxes were measured. Each vertical profile were divided into surface (upper 20 cm soil layer) and subsurface (below 20 cm to 120 cm) soils and collected separately. The soils located in the upland zone were characterized as acrisol, ferralisol and planosol whereas all flooded soils were reductisols. The total twenty two samples (thirteen surface soils and nine subsurface soils) were incubated in anoxic conditions for the determination of their potential methane production rates over a year (November 2010 to October 2011). Soil samples were categorized in FS1 (soils from the primary dense and medium forest), FS2 (soils from light, degraded forest and riparian forest) and AG (soils from agricultural land). Incubations were not performed on AG subsurface soils.

Three sediment cores with length ranging from 13 to 21 cm were collected from the shallow zone (depth < 6 m) in the flooded forest (RES3) and flooded agricultural area (RES8). CH<sub>4</sub> concentrations in pore water were determined for these three cores.

### **4.2.3. Experimental methods**

#### **4.2.3.1. In situ water quality parameter**

Vertical profiles of O<sub>2</sub>, temperature, pH and conductivity were measured in situ at all sampling stations with a multi-parameter probe Quanta<sup>®</sup> (Hydrolab, Austin, Texas) since January 2009. In the reservoir, the vertical resolution was 0.5 m above the oxic–anoxic limit and 1-m in the hypolimnion, whereas only surface waters were analyzed in rivers and in the downstream channel. The oxygen probe was calibrated at 100% in water saturated air.

#### **4.2.3.2. Methane concentration in water**

The evolution of CH<sub>4</sub> concentrations at the reservoir, downstream of the powerhouse and downstream of the Nakai Dam has been monitored since April 2009 on a fortnightly basis. Surface- and deep-water samples for CH<sub>4</sub> concentration were taken with a surface water sampler (Abril et al., 2007) and a peristaltic pump, respectively. Water samples were stored in serum glass vials, capped with butyl stoppers, sealed with aluminum crimps and poisoned (Guérin and Abril, 2007). Before gas chromatography (GC) analysis for CH<sub>4</sub> concentration, a N<sub>2</sub> headspace was created and the vials were vigorously shaken to ensure an equilibration between the liquid and gas phases.

#### **4.2.3.3. Methane concentration in the pore water of the flooded soils**

The flooded soil cores, retrieved with a large bore interface corer (Aquatic Research<sup>®</sup>) corer were cut in 1 cm slices within 15 min of sampling. Two replicates were sampled for each depth. Each slice of these cores was transferred into pre-weighed glass vials containing 20 ml of 1M NaOH that were quickly closed with rubber stoppers, vigorously shaken to break up the sediment (Guérin et al., 2008a). A sub-sample of each slice was immediately sealed in a pre-weighed vial for determination of water content and porosity. The CH<sub>4</sub> concentrations in the headspace were determined by GC (section 4.2.3.9). The concentration in the pore water was calculated using the solubility coefficient of Yamamoto et al. (1976), the volume of NaOH, and the weight and the water content of soil sample.

#### **4.2.3.4. Diffusive fluxes measured by floating chamber**

During the field campaigns, 98 diffusive fluxes across the water-air interface were measured with floating chambers at RES1 to RES8 stations. Flux measurements were performed with two circular chambers, (surface area = 0.15 m<sup>2</sup>; volume = 24.6 L) following the same design as in Guérin et al. (2007). The floating chambers were covered with a reflective surface to limit warming inside the chamber during measurements. Floating chambers were deployed from a boat that was left drifting during measurement to avoid creation of artificial turbulence (Frankignoulle et al., 1998). Within 45 min, four air samples were collected with a syringe from the chambers (duplicates) at 15 min interval. Air samples were collected in 10 ml glass vials which contained 6M NaCl solution capped with butyl stoppers and aluminum seals. All samples were analyzed within 48 h by GC (section 4.2.3.9). Methane fluxes were calculated from the slope of the linear regression of gas concentration in

the chamber versus time. The fluxes were accepted when the determination coefficient ( $r^2$ ) of the linear regression was higher than 0.80 ( $n = 4$ ). Each flux measurement was done together with a determination of the  $\text{CH}_4$  concentration in surface water.

#### **4.2.3.5. Ebullition of $\text{CH}_4$**

Methane bubbling fluxes (ebullition) were measured at various sites with different depths. The selection of the sampling sites was determined by the water depth and the type of flooded ecosystems. The bubbling fluxes were measured with the funnel technique (Keller & Stallard, 1994). Several sets of 5 to 10 funnels (diameter = 26 cm) were positioned at the surface of the water, and attached one to each other at 1 m distance. The sets of funnels were placed above particular water depths, ranging from 0.5 to 15 m and remained on site for 24 to 48 h. The samples were collected and stored in glass vials before being analyzed by GC (section 4.2.3.9).

#### **4.2.3.6. Diffusive fluxes from the soils surrounding the reservoir and from the drawdown area**

The diffusive soil-air exchanges were measured using rectangular metallic static chamber with metallic collar (Serça et al., 1994). At each zones, two chambers (surface area =  $0.08 \text{ m}^2$ ) were deployed on the collars installed in the soil around one hour before the measurements. Sample collection, storage and analysis were performed as described for the floating chamber measurements (section 4.2.3.4). Surface soil moisture content and temperature were measured for each chamber measurement.

#### **4.2.3.7. Potential $\text{CH}_4$ production in flooded soils**

After drying at  $30^\circ\text{C}$  in the laminar flow dryer, soil samples were ground, sieved (2 mm) and homogenized. 750 g of homogenized samples of each type of soil were then redistributed, 250 g in three replicate glass vials (570 ml). After adding 250 ml of de-ionized water in each vial (soil/water ratio = 1), vials were closed with butyl stoppers and aluminum crimps. Vials were covered with aluminum foil to avoid effect of light on any bacterial activity, and flushed with  $\text{N}_2$  for 30 min to create an anaerobic environment. The flushed vials were stored in the dark at  $20^\circ\text{C}$  (average bottom water temperature of NT2). Incubations were performed without agitation to avoid the destruction of symbiotic microbial associations involved in methanogenesis (Dannenberg et al., 1997). Two days before the determination of the production rates, the vials were flushed with  $\text{N}_2$  for 30 min to eliminate accumulated  $\text{CO}_2$  which could increase the methanogenesis (Das and Adhya, 2011 and reference therein) and any volatile compounds inhibiting methanogenesis (Williams and Crawford, 1984). Incubated soils samples were analyzed at a frequency of 1 week to 2 months over a year from November 2010 to October 2011. After six months of experiment, when no measurement was performed for more than a month, the bottles were flushed monthly with  $\text{N}_2$ . Before each GC analysis, vials were vigorously shaken for about 30 seconds to ensure equilibration between the liquid and gas phase. Total  $\text{CH}_4$  concentration in the vials were measured in the headspace of the

vials 3-times a week to calculate the production rate, as the slope of the concentration evolution versus time.

#### **4.2.3.8. Aerobic CH<sub>4</sub> oxidation in the water column**

Water samples for aerobic oxidation rate measurements were collected in HDPE bottles. Water was homogenized and redistributed to twelve serum vials (160 ml). Each vial contained 80 ml of water and 80 ml of air. According to in situ concentration of CH<sub>4</sub> in the water, different amounts of CH<sub>4</sub> and N<sub>2</sub> were added by syringe while withdrawing an equal volume of air from the headspace with a second syringe. Incubations were performed at concentrations ranging from in situ down to ten times lower. Vials were incubated in the dark (Dumestre et al., 1999, Murase and Sugimoto, 2005) at 20°C to 30°C, depending on seasons. Incubations were performed with agitation to ensure continuous equilibrium between gas and water phases. Total CH<sub>4</sub> concentrations in the vials were measured 5-times in a row at a 12 h interval, and oxidation rates were calculated as the total loss of CH<sub>4</sub> in the vial. The oxidation rate for each concentration was the average value of the triplicates with standard deviation ( $\pm$ SD).

#### **4.2.3.9. Gas chromatography**

Analysis of CH<sub>4</sub> concentrations were performed by gas chromatography (SRI 8610C gas chromatograph, Torrance, CA, USA) equipped with a flame ionization detector. A subsample of 0.5 ml from the headspace of water sample vials and 1 ml of air from flux sample vials were injected. Commercial gas standards (2, 10 and 100 ppmv, Air Liquid "crystal" standards and mixture of N<sub>2</sub> with 100% CH<sub>4</sub>) were injected after analysis of every 10 samples for calibration. Duplicate injection of samples showed reproducibility better than 5%. The specific gas solubility for CH<sub>4</sub> as a function of temperature (Yamamoto et al., 1976) was used for calculation of CH<sub>4</sub> concentrations dissolved in water.

### **4.2.4. Calculations**

#### **4.2.4.1. Methane storage in the reservoir water column**

The measurements of the vertical profiles of CH<sub>4</sub> concentrations were performed at the 9 sampling stations in the reservoir (Fig. 4.1). CH<sub>4</sub> concentrations between two sampling depth of profiles were assumed to change linearly. The volume of each layer was calculated using the volume-capacity curve (NTPC, 2005). Dissolved CH<sub>4</sub> was determined for each 1 m layer of water by multiplying the average CH<sub>4</sub> concentrations by the volume of the layer. The total CH<sub>4</sub> storage was the sum of CH<sub>4</sub> stored at all depth intervals.

#### **4.2.4.2. Estimation of diffusive fluxes from surface concentrations**

The diffusive CH<sub>4</sub> fluxes were calculated from the fortnightly monitoring of surface concentrations with thin boundary layer (TBL) equation at all stations in the reservoir and downstream of the powerhouse and the Nakai Dam. Thus, the database of measured and

calculated fluxes includes flux data from open waters, flooded agricultural and different type of forests.

The measured fluxes and concomitant water and air CH<sub>4</sub> concentrations were applied in equation (4.1) to calculate gas transfer velocity:

$$F = k_T \times \Delta C \quad (4.1)$$

where F, the diffusive flux at water-air interface; k<sub>T</sub>, the gas transfer velocity at a given temperature (T);  $\Delta C = C_w - C_a$ , the concentration gradient between the water (C<sub>w</sub>) and the overlying atmosphere (C<sub>a</sub>). Afterward, the k<sub>600</sub> was computed from k<sub>T</sub> with the following equation:

$$k_{600} = k_T \times (600/Sc_T)^{-n} \quad (4.2)$$

with Sc<sub>T</sub>, the Schmidt number of CH<sub>4</sub> at a given temperature (T) (Wanninkhof, 1992); n, a number that is either 2/3 for low wind speed (< 3.7 m.s<sup>-1</sup>) or 1/2 for higher wind speed and turbulent water (Jahne et al., 1987).

We used different formulations of k<sub>600</sub> one obtained from the CH<sub>4</sub> dataset, others from the literature: Guérin et al. (2007) from a tropical hydroelectric reservoir, Crucius and Wanninkhof (2003) and Frost and Upstill-Goddard (2002) from temperate reservoirs, and with the relationship from Cole and Caraco (1998) which encompasses all type of natural aquatic ecosystems. We also used the relationship of MacIntyre et al., (2010), which considers influence of heat loss on diffusion. For calculation purpose, wind speed (at 10 m height) and rainfall from two adjacent meteorological stations located at Nakai and at the Ban Thalang Bridge (close to RES4 station, Fig. 4.1) were used.

At RES9 station, in the Nam Theun River below the dam and in the downstream channel, no measurement was possible for security reason because of strong water currents. We considered a constant value of k<sub>600</sub> (10 cm.hr<sup>-1</sup>) for all these sites.

#### 4.2.4.3. Degassing

At NT2, degassing occurs at four sites: (1) below the turbines (TRC1), (2) below the regulating pond dam (DCH1), (3) below the aeration weir (DCH3) and (4) below the Nakai Dam (NTH3) (Fig. 4.1). In addition, degassing occurs occasionally during spillway release at the Nakai Dam. Degassing was estimated using the difference between concentrations upstream and downstream (C<sub>upstream</sub>-C<sub>downstream</sub>) of the structures multiplied by the discharge (Galy-Lacaux et al., 1997).

At the Nakai Dam and the aeration weir, we considered surface concentrations at RES1 and DCH2 as upstream concentrations (C<sub>upstream</sub>), respectively. The C<sub>upstream</sub> was the average of the vertical profile of concentrations at RES9 and REG1 for the degassing below the turbines (TRC1) and below the regulating pond (DCH1), respectively. When necessary, the degassing due to spillway release was computed at the Nakai Dam. For this latter case, the

degassing was calculated using the average CH<sub>4</sub> concentration in the epilimnion at RES1 (from surface to 10 m depth) and the surface concentration at NTH3. For the outflows (C<sub>downstream</sub>), CH<sub>4</sub> surface concentrations at TRC1, DCH1, DCH3 and NTH3 were considered for the calculations.

#### 4.2.4.4. Extrapolation of fluxes for the estimation of the NT2 total emissions

Based on the statistical analysis, diffusive CH<sub>4</sub> fluxes clustered in three groups: RES1, RES2, RES4, RES5, RES6, RES7 and RES8 behaved similarly, whereas RES3 (located in a small embayment), and RES9 (close to the water intake) had their own seasonal patterns. Based on physical modeling (Chanudet et al., 2012), it has been showed that RES9 is representative of an area of ~2 km<sup>2</sup> in the region of the water intake, whatever the season. This 2 km<sup>2</sup> area was used to extrapolate specific diffusive fluxes from RES9. The embayment where RES3 is located represents a surface area of 6% of the total surface area of the reservoir whatever the season (maximum 26 km<sup>2</sup>), to which were attributed the specific diffusive fluxes from RES3. The average diffusive fluxes calculated for RES1, RES2, RES4, RES5, RES6, RES7 and RES8 stations were attributed to the remaining reservoir surface area, taking into account the seasonal variation of the reservoir surface area from the area-capacity curve.

Ebullition of CH<sub>4</sub> was observed only in area shallower than 13 m water depth. It was found that ebullition depends, among other parameters, on depth (Chapter 3). The surface area corresponding to a particular water level in the reservoir was estimated using the area-capacity curve and bubbling corresponding to the particular level was estimated from the equation given by the artificial neural network (Chapter 3). The surface area below 13 m depth varied from 171 to 386 km<sup>2</sup>, and followed the same pattern as the reservoir water surface.

Diffusive fluxes from the drawdown area depended on the soil moisture contents. The extrapolation of these fluxes required the use of the area-capacity curves and the determination of the time of exposure to air in order to attribute the emission factors corresponding to the soil moisture content. Based on field observations of the drawdown area, we attributed fluxes from “midland 1” soils to the surface of soils exposed to the air for more than 20 days, the average flux observed at “midland 2” soils to the surface of soils exposed to the air between 10 to 20 days and the average flux “lowland” soils to the surface of soils exposed to the air between 1 to 10 days. The diffusive fluxes obtained from “upland soils” (which were never flooded and located at outside the influence of the reservoir) were used to calculate emission from the drawdown area before the reservoir was fully impounded. Fig. 4.2 depicts the temporal evolution of the surface area of each individual sub-zone of the drawdown zone. The upland area disappeared after first full-impoundment of the reservoir (October 2009). The drawdown area consisted mostly of midland 1 after the full impoundment (up to 200 km<sup>2</sup>). The surface areas of midland 2 (0-50 km<sup>2</sup>) and lowland (0-20 km<sup>2</sup>) represented a small portion of the drawdown area.

#### 4.2.5. Statistical analysis

Statistical tests were performed to assess the spatial variation in the surface CH<sub>4</sub> concentrations and diffusive CH<sub>4</sub> fluxes at different sampling stations in the reservoir. The Kolmogorov-Smirnov test indicated the non-normal behavior of CH<sub>4</sub> concentrations and diffusive fluxes at different sampling stations in the reservoir. Hence, the differences in CH<sub>4</sub> concentrations and diffusive fluxes were statistically examined using non-parametric Kruskal-Wallis test. Michaelis-Menten kinetics parameters were derived for aerobic CH<sub>4</sub> oxidation rates. All statistical tests and analysis were performed by using GraphPad Prism (GraphPad Software, Inc., v5.04).

### 4.3. Results

#### 4.3.1. Temperature, O<sub>2</sub> and CH<sub>4</sub> concentrations and CH<sub>4</sub> storage in the reservoir water column

During the two and half year of monitoring, the NT2 was thermally stratified from February to September (dry-warm and wet seasons) and well mixed for the next month (September-February., dry-cold season) as shown for the stations RES2, RES3 and RES7 (Fig. 4.3a, b, c). As already mentioned by Chanudet et al. (2012), the NT2 Reservoir is monomictic. During the periods of stratification, the epilimnic temperatures (dry-warm:  $27.0 \pm 2.6^\circ\text{C}$ ; wet:  $27.9 \pm 1.7^\circ\text{C}$ ) were significantly higher than hypolimnic temperatures (dry-warm:  $18.7 \pm 1.5^\circ\text{C}$ ; wet:  $21.2 \pm 1.6^\circ\text{C}$ ) whereas surface and bottom temperature were  $22.6 \pm 2.0^\circ\text{C}$  and  $19.5 \pm 1.6^\circ\text{C}$  during the lake overturn in dry-cold season, respectively. Thermocline depth was  $4.7 \pm 2.7$  m and  $7.2 \pm 5.5$  m deep during the dry-warm and wet seasons, respectively. Occasionally, sporadic and local destratification occurred during the wet season. Once the turbines went on operation since March 2010, the water column at RES9 located near the water intake got totally mixed as revealed by the homogeneous temperature from the surface to the bottom (Fig. 4.3d).



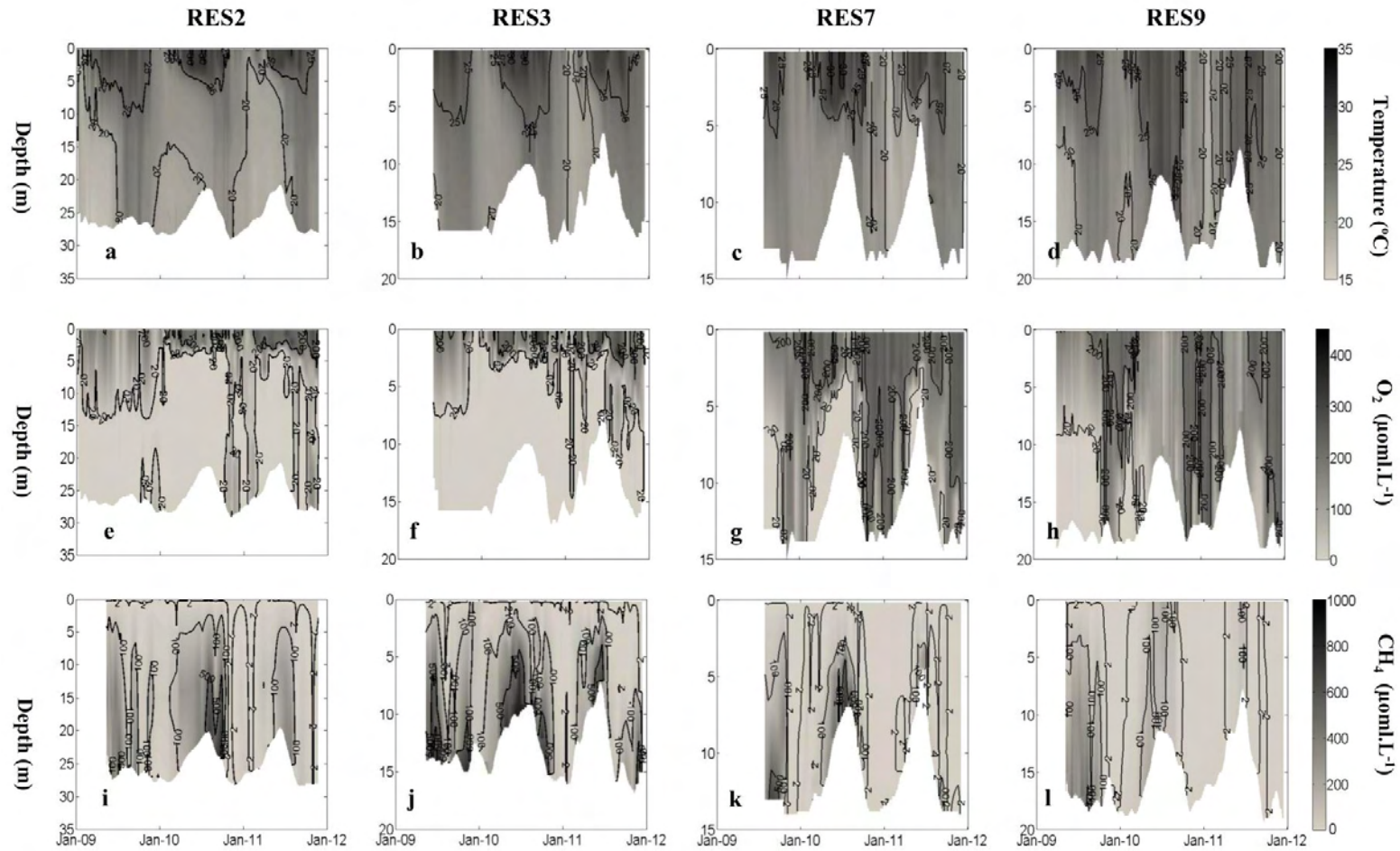


Figure 4.3: Evolution of vertical profiles of temperature (a, b, c, d), oxygen, (e, f, g, h) and CH<sub>4</sub> concentration (i, j, k, l) at RES2 (in the thalweg of the Nam Theun River), RES3 (flooded forest), RES7 (flooded swamp area) and RES9 (close to turbine intake) sampling stations of the NT2 Reservoir.

During the dry-warm season, an oxic-epilimnion and anoxic-hypolimnion were observed at most of the stations as shown in Fig. 4.3e, f, g. During the wet season, the reservoir was generally stratified with an anoxic hypolimnion and a well-oxygenated epilimnion, although O<sub>2</sub> reached occasionally the hypolimnion during the sporadic destratification events. During the dry-cold seasons (reservoir overturn), the water column was often oxygenated from the top to the bottom (i.e., RES2, RES7, November-December, Fig. 4.3g, h and Fig. 4.4a). The depth of the oxycline was concomitant with the thermocline in the warm-dry and the wet season whereas O<sub>2</sub> concentrations decreased smoothly from the surface to the bottom in the cold-dry season. Once the turbines went on operation, the water column at RES9 was always well oxygenated ( $170 \pm 59 \mu\text{mol.L}^{-1}$ , Fig. 4.3h).

The distribution of the CH<sub>4</sub> concentrations is exactly the opposite of that of O<sub>2</sub> (Fig. 4.3i, j, k, l). At the station RES1 to RES8, when the water column is thermally stratified in the dry-warm and in the wet season, CH<sub>4</sub> concentrations are ~200 times higher in the hypolimnion ( $275 \pm 78 \mu\text{mol.L}^{-1}$ ) than in the epilimnion ( $1.5 \pm 0.5 \mu\text{mol.L}^{-1}$ ) (Fig. 4.3i, j, k). The gradient of CH<sub>4</sub> concentration was steeper during the dry-warm season than during the wet season. During the reservoir overturn, the average concentration in the hypolimnion ( $51.4 \pm 38.9 \mu\text{mol.L}^{-1}$ ) was only ~20 times higher than in the epilimnion ( $2.9 \pm 3.6 \mu\text{mol.L}^{-1}$ ) and the concentrations increased progressively from the surface to the bottom. The vertical profiles at the four stations (RES2, RES3, RES7 and RES9) evidenced a high spatial heterogeneity of the CH<sub>4</sub> concentrations. After the turbines were operated, the CH<sub>4</sub> vertical profiles of concentration at RES9 were homogeneous from the surface to the bottom. The average concentrations were  $59 \pm 87$ ,  $49 \pm 76$  and  $5 \pm 39 \mu\text{mol.L}^{-1}$  during the dry-warm, wet and dry-cold season, respectively. A sharp decrease of the average CH<sub>4</sub> concentrations in the water column was observed between the years 2010 and 2011.

In 2010, the CH<sub>4</sub> bottom concentration (Fig. 4.4a) and storage in the reservoir (Fig. 4.4b) increased at the beginning of the dry-warm season concomitantly with the establishment of the reservoir thermal stratification which is illustrated by the difference between surface and bottom temperature ( $\Delta T$ ) in Fig. 4.4c. CH<sub>4</sub> concentration and storage reached their maxima ( $500 \pm 254 \mu\text{mol.L}^{-1}$  and  $3.5 \pm 0.3 \text{ GgCH}_4$ , Fig. 4.4a, b) at the end of the dry-warm-beginning of the wet season when the residence time of water in the reservoir was the lowest (40 days, Fig. 4.4c). During the rainy season, the reservoir was still stratified and the CH<sub>4</sub> concentration and storage decreased (Fig. 4.4a,b) while the residence time of water increased and the reservoir is less and less stratified (Fig. 4.4c). In the dry-cold season, the reservoir overturns as evidenced by the low  $\Delta T$  and the CH<sub>4</sub> concentration and the storage reached their minima ( $5 \pm 12 \mu\text{mol.L}^{-1}$  and  $0.11 \pm 0.04 \text{ Gg(CH}_4)$ , Fig. 4.4a, b) when the residence of water was the highest (Fig. 4.4c). The sharp decrease of CH<sub>4</sub> storage and concentration during the dry-cold season is concomitant with a sharp increase of O<sub>2</sub> concentration at the bottom (up to  $121 \pm 90 \mu\text{mol.L}^{-1}$  in January, Fig. 4.4a). In the year 2011, the same seasonal pattern is observed although the CH<sub>4</sub> bottom concentration and storage were two to four times lower than in the year 2010.

CH<sub>4</sub> concentration in the hypolimnion of NT2 was higher than in reservoirs from the same geographical region (Nam Ngum:  $13.6 \pm 29.1 \mu\text{mol.L}^{-1}$ ; Nam Leuk:  $69 \pm 107 \mu\text{mol.L}^{-1}$ ; Chanudet et al., 2011). However, the average CH<sub>4</sub> concentration in the hypolimnion was lower than in tropical reservoirs located in South America (Petit Saut:  $300 \mu\text{mol.L}^{-1}$ ; Balbina:  $424 \pm 139 \mu\text{mol.L}^{-1}$ ; Abril et al., 2005; Guérin et al., 2006).

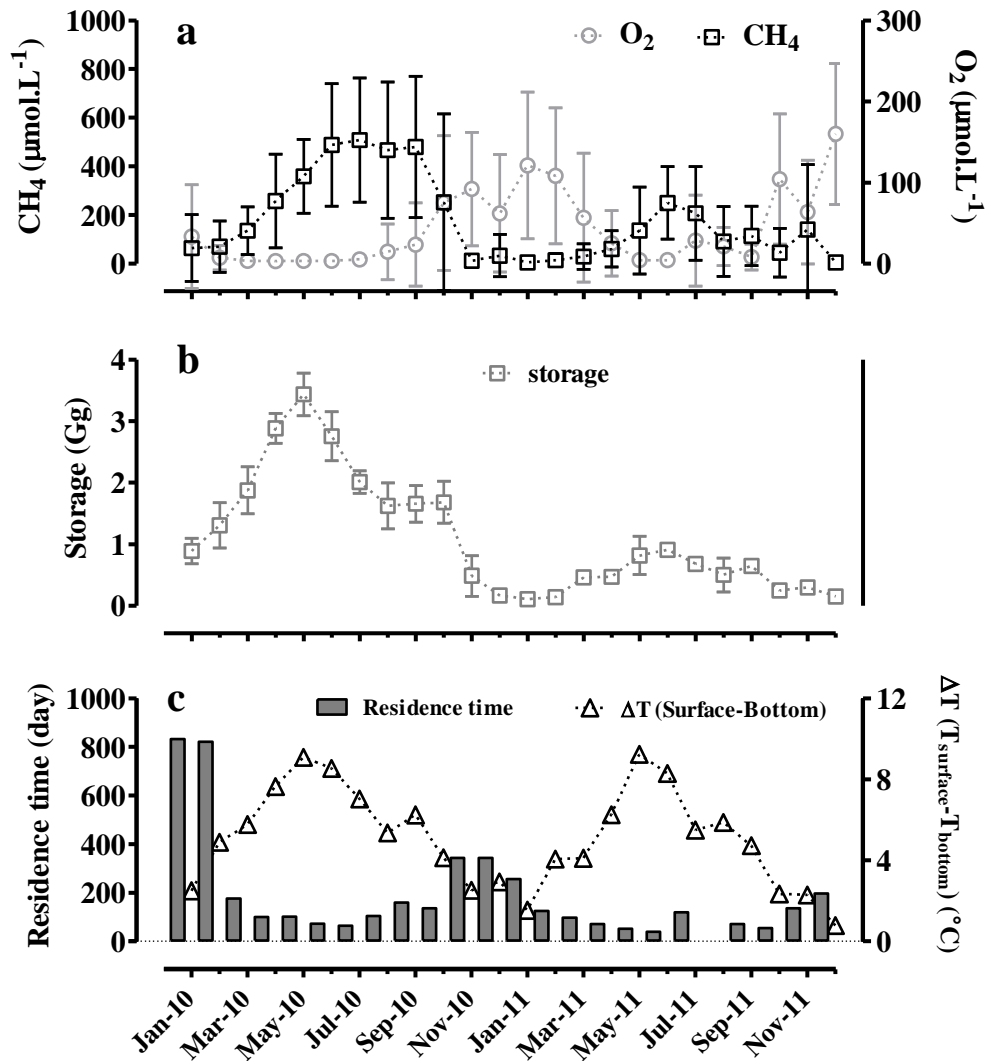


Figure 4.4: (a) CH<sub>4</sub> and O<sub>2</sub> concentrations at the bottom ( $\mu\text{mol.L}^{-1}$ ); (b) dissolved CH<sub>4</sub> storage in the water column (GgCH<sub>4</sub>); (c) residence time (day) and difference between surface and bottom temperature ( $^{\circ}\text{C}$ ).

#### 4.3.2. Methane concentration in the reservoir surface water

CH<sub>4</sub> concentrations in surface water at all sampling stations exceeded saturation levels ( $> 1000 \%$ ) and ranged from 0.01 to  $214 \mu\text{mol.L}^{-1}$  ( $n = 560$ ). Non-parametric statistical test (Kruskal-Wallis,  $p = 0.05$ ) applied on the nine sampling stations showed that the stations RES3 and RES9 behaved differently from the others.

CH<sub>4</sub> surface concentrations of the stations RES1, RES2, RES4, RES5, RES6, RES7 and RES8 did not differ significantly from each other whatever the season and before and after the starting of the turbine. Overall, the average concentration was  $1.9 \pm 9.4 \mu\text{mol.L}^{-1}$  (range:  $0.01\text{-}150 \mu\text{mol.L}^{-1}$ ) whereas 50% of the 426 observations were lower than the median value of  $0.5 \pm 0.03 \mu\text{mol.L}^{-1}$ . Most of the sporadic high concentrations were observed in the wet and cold-dry seasons.

RES3 is statistically different from the other stations ( $p = 0.04$ , Kruskal-Wallis test) due to frequent very high concentrations during the dry-cold season before and after the turbines were operated (before:  $38.9 \pm 54.6 \mu\text{mol.L}^{-1}$ ; after  $3.9 \pm 5.0 \mu\text{mol.L}^{-1}$ ). The average surface CH<sub>4</sub> concentration was  $7.5 \pm 23.61 \mu\text{mol.L}^{-1}$  ( $0.07 - 128 \mu\text{mol.L}^{-1}$ ). For this station, the median for the whole monitoring was  $0.55 \pm 0.19 \mu\text{mol.L}^{-1}$  that is significantly lower than the average value of concentrations at this site.

Before the starting of turbines, the seasonal pattern at RES9 was similar as the one observed at stations RES1, RES2, RES4, RES5, RES6, RES7 and RES8. After the turbines were started, the average concentration observed during the dry-warm season-beginning of the wet season was 40 times higher than the average concentration at all other stations during this period with surface concentrations peaking up to  $215 \mu\text{mol.L}^{-1}$ . Overall, surface concentrations at RES9 after the commissioning of the reservoir were  $64.3 \pm 61.2$  and  $0.19 \pm 0.12 \mu\text{mol.L}^{-1}$  for the warm-dry and cold-dry seasons, respectively. During the wet season following the commissioning (March 2010), the average concentration at RES9 was  $95.45 \pm 76.06$  and only  $1.95 \pm 4.95 \mu\text{mol.L}^{-1}$  in the year 2011.

The average surface concentrations of  $2.8 \pm 6.7 \mu\text{mol.L}^{-1}$  at the stations RES1 to RES8 are four times lower than the surface concentrations at Petit Saut during the first 3 years after impoundment where the average concentration was  $8.29 \pm 11.76 \mu\text{mol.L}^{-1}$  (Galy-Lacaux et al., 1997). Median concentrations are in the same range as those at Petit Saut Reservoir ten years after impoundment (Abril et al., 2005) in older reservoirs located in Brazil (Guérin et al., 2006). To the best of our knowledge, the surface concentrations at RES9 after the commissioning are the highest reported to date for this kind of environment.

#### **4.3.2.1. CH<sub>4</sub> and O<sub>2</sub> concentrations in the Nam Theun River and the artificial downstream channel**

At TRC1 station, the average O<sub>2</sub> concentration was  $169 \pm 62 \mu\text{mol.L}^{-1}$  that is  $64 \pm 24\%$ . During the dry season, the O<sub>2</sub> saturation can be as low as 3% whereas it can be 100% at some occasion during the wet and dry-cold seasons. O<sub>2</sub> level reached around 100% saturation all along the year after 27 km from the turbine outlet, i.e. at the DCH4 sampling station.

CH<sub>4</sub> concentration at TRC1, which receives water from the homogenized water column at RES9, varied from 0.03 (Aug.-Feb., wet season and dry-cold seasons) to  $221 \mu\text{mol.L}^{-1}$  (June, end of the dry-warm season and beginning of the wet season). As shown in Fig. 4.5, CH<sub>4</sub> concentration decreased from TRC1 to DCH4 during the dry-warm (from  $99 \pm 75$  to  $1.3 \pm 1.2 \mu\text{mol.L}^{-1}$ ) and wet (from  $66 \pm 76$  to  $1.3 \pm 1.5 \mu\text{mol.L}^{-1}$  in 2010 and from  $26 \pm$

42 to  $0.6 \pm 0.8 \mu\text{mol.L}^{-1}$  in the year 2011) seasons, whereas concentrations varied in a narrow range along the 27 km long channel in the dry-cold season ( $0.02 - 2 \mu\text{mol.L}^{-1}$ ). Below the confluence with Xe Bang Fai, concentrations decreased down to  $0.4 \pm 0.2 \mu\text{mol.L}^{-1}$  at XBF4 (Fig. 4.5) that is concentrations found in the pristine Nam Xot ( $0.8 \pm 0.6 \mu\text{mol.L}^{-1}$ ), Nam Theun ( $0.6 \pm 0.8 \mu\text{mol.L}^{-1}$ ) upstream pristine tributaries of the reservoir and Xe Band Fai ( $0.8 \pm 0.8 \mu\text{mol.L}^{-1}$ ).

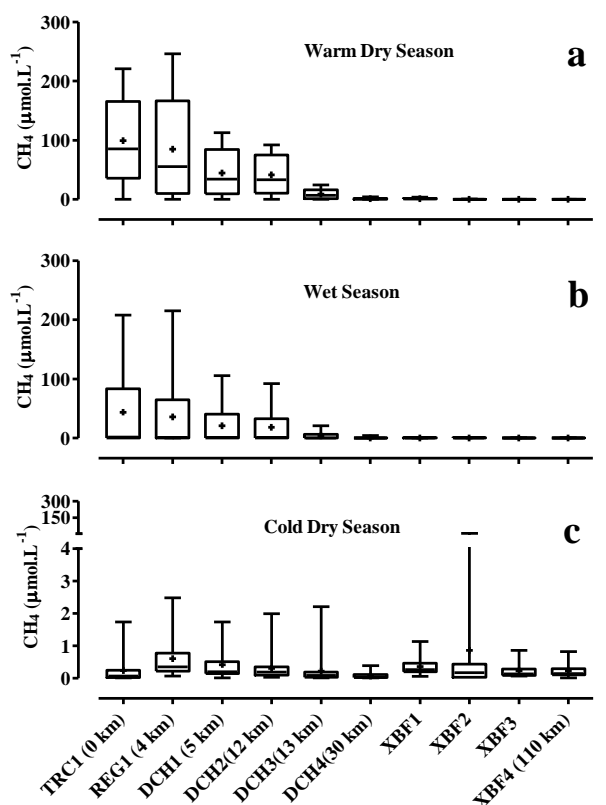


Figure 4.5: Spatial and seasonal variations in  $\text{CH}_4$  surface concentration downstream of the powerhouse (a) dry-warm season, (b) wet season, and (c) cold dry season. Boxes show the median concentration and the interquartile range. Whiskers denote the full range of all values. Plus sign (+) in the box shows the average value.

Downstream of the Nakai Dam (NTH3),  $\text{CH}_4$  concentration varied from  $0.03$  to  $6 \mu\text{mol L}^{-1}$  (average:  $1.2 \pm 1.4 \mu\text{mol.L}^{-1}$ ). High  $\text{CH}_4$  concentrations (up to  $69 \mu\text{mol.L}^{-1}$ ) were also sometimes observed when  $\text{CH}_4$ -rich water was released from spillway. Downstream of the station NTH4,  $\text{CH}_4$  concentration decreased down to  $\text{CH}_4$  concentrations found in the pristine rivers of the watershed ( $< 1 \mu\text{mol.L}^{-1}$ ).

#### 4.3.3. Methane the pore water of flooded soils

There was no clear tendency in the vertical profiles of  $\text{CH}_4$  concentrations in the pore water. For all three cores, mean  $\text{CH}_4$  concentration varied from  $181 \pm 54$  to  $1098 \pm 93 \mu\text{mol.L}^{-1}$ . The concentration in the first 1 cm sediment layer (below the soil-water interface) ranged from  $299 \pm 25$  to  $766 \pm 349 \mu\text{mol.L}^{-1}$ , revealing a high spatial variability. This range

of concentration was up to three times higher than the average concentration at the bottom of the reservoir for the same month (June),  $249 \pm 149 \mu\text{mol.L}^{-1}$ .

#### 4.3.4. Diffusive CH<sub>4</sub> fluxes from the reservoir

During the different field campaigns, 103 floating chamber measurements were made. Percentage of rejection of the measured fluxes was close to 70%. In most of the cases, fluxes were rejected because CH<sub>4</sub>-rich bubbles entered the chambers (86% of rejected fluxes). Such perturbations on the measurements occurred often in the flooded forest (RES3), and above the former floodplain and agricultural land (around RES8), and even more often during the low water level periods. Among the validated data, diffusive measured fluxes ranged from 0.16 to 3.2 mmol.m<sup>-2</sup>.d<sup>-1</sup> ( $0.95 \pm 0.8 \text{ mmol.m}^{-2}.\text{d}^{-1}$ ; n=32; Table 4.3), values that are in the lower range of CH<sub>4</sub> fluxes from tropical hydroelectric reservoir (Abril et al., 2005; Guérin et al., 2006; Kemenes et al., 2007).

Combining the concomitant flux and concentration measurements, an average  $k_{600}$  value of  $3.5 \pm 2.5 \text{ cm.h}^{-1}$  was calculated from measurements performed at wind speed lower than  $5 \text{ m.s}^{-1}$  and rainfall lower than  $10 \text{ mm.h}^{-1}$ . No clear relationship between  $k_{600}$  and wind speed could have been obtained from this dataset alone.

Diffusive fluxes were also calculated from the surface CH<sub>4</sub> concentration dataset from the fortnightly sampling conducted between April 2009 and September 2011 at all sampling stations done by AELab. We used  $k_{600}$ -wind speed relationships from MacIntyre et al., (2010), Cole and Caraco, (1998), Frost and Upstill-Goddard, (2002) and from Guérin et al., (2007). The average  $k_{600}$  calculated from the MacIntyre et al. (2010) relationship is very similar to  $k_{600}$  ( $3.9 \pm 1.5 \text{ cm.h}^{-1}$  vs.  $3.5 \pm 2.5 \text{ cm.h}^{-1}$ ) calculated from flux measurements. As a matter of consequences, calculated fluxes from the MacIntyre et al., (2010) relationship are in the same range as fluxes calculated from the mean of the measured  $k_{600}$  values (Table 4.2). Fluxes calculated from using MacIntyre et al. (2010) for stations RES1-RES8 compare well with fluxes measured on those stations in May 2009 and March 2010 (Table 4.3 and Fig. 4.6a). No fluxes were measured at RES9 because it was impossible to leave the boat drifting towards the water intake, thus fluxes were calculated using TBL technique with a constant  $k_{600}$  values. Fluxes calculated from the MacIntyre et al. (2010) relationship will be used for further description and quantification of CH<sub>4</sub> emissions.

The seasonal pattern of the calculated diffusive fluxes was the same as the one described for the surface concentrations. At RES1, RES2, RES4, RES5, RES6, RES7 and RES8 stations before and after the turbines were operated, no seasonal trend, neither differences before and after the commissioning of NT2 was observed. The average flux was  $2.0 \pm 9.5 \text{ mmol.m}^{-2}.\text{d}^{-1}$  ranging from 0.02 to  $122 \text{ mmol.m}^{-2}.\text{d}^{-1}$  with a median flux of  $0.45 \text{ mmol.m}^{-2}.\text{d}^{-1}$  (Fig. 4.6a, b). At RES3 during the dry-cold season, the fluxes were  $26 \pm 40$  and  $2.3 \pm 3.2 \text{ mmol.m}^{-2}.\text{d}^{-1}$  before and after the commissioning, respectively (Fig. 4.6a, b). The average diffusive flux was  $6.0 \pm 18.0 \text{ mmol.m}^{-2}.\text{d}^{-1}$  ranging from 0.04 to  $108 \text{ mmol.m}^{-2}.\text{d}^{-1}$  with a median of  $0.6 \text{ mmol.m}^{-2}.\text{d}^{-1}$ .

Table 4.2: Measured and calculated diffusive CH<sub>4</sub> fluxes using different k<sub>600</sub> relationships.

Relationships	References	<sup>a</sup> Wind speed (U <sub>10</sub> ), m.s <sup>-1</sup>	<sup>a</sup> Rainfall, (R) mm.h <sup>-1</sup>	<sup>b</sup> k <sub>600</sub> , cm.hr <sup>-1</sup>		<sup>c</sup> Fluxes, mmol.m <sup>-2</sup> .d <sup>-1</sup>	
				Range	Mean ± SD	Range	Mean ± SD (N)
<sup>d</sup> Constant k <sub>600</sub> = 3.5 cm.hr <sup>-1</sup>	This study	0.29-4.2	0-9.7		3.5 ± 2.5	0.02-157	2.4 ± 11 (464)
k <sub>600</sub> = 2.25 (±0.33) · U <sub>10</sub> + 0.16(±1.65)	MacIntyre et al. 2010	-	-	0.8-9.8	3.9 ± 1.5	0.02-122	2.4 ± 10 (464)
k <sub>600</sub> = 1.66 (±0.34) · e <sup>0.26(±0.04) · U<sub>10</sub></sup> + 0.66 (±0.10) · R	Guérin et al., 2007	0.1-4.6	0.6-36	1.7-9.3	2.8 ± 0.9	0.01-76	1.7 ± 7.0 (464)
k <sub>600-mod</sub> = 1.03 + 0.129 · (U <sub>10</sub> ) <sup>2</sup> + 1.999 · R	Frost & Upstill- Goddard, 2002	1-10	-	1.0-21	2.2 ± 2.1	0.01-65	1.2 ± 5.1 (464)
k <sub>600</sub> = 2.07 + 0.215 · U <sub>10</sub> <sup>1.7</sup>	Cole & Caraco, 1998	-	-	2.1-4.5	2.6 ± 0.4	0.01-78	1.6 ± 6.8 (464)
k <sub>600</sub> = 0.228 · U <sub>10</sub> <sup>2.2</sup> + 0.168	Crusius & Wanninkhof, 2003	0.9-5.4	-	0.2-5.5	1.0 ± 0.8	0.01-50	0.6 ± 3.0 (464)

<sup>a</sup>range of wind speed or rainfall at the reservoir/lake for which formulation of k<sub>600</sub> was established.

<sup>b</sup>k<sub>600</sub> calculated from corresponding formulation of k<sub>600</sub> using the wind speed and the rainfall data for the day when water sample was collected.

<sup>c</sup>fluxes calculated from CH<sub>4</sub> surface concentration and using corresponding k<sub>600</sub>.

<sup>d</sup>average k<sub>600</sub> value, obtained from all the measured diffusive CH<sub>4</sub> fluxes over 2 years.

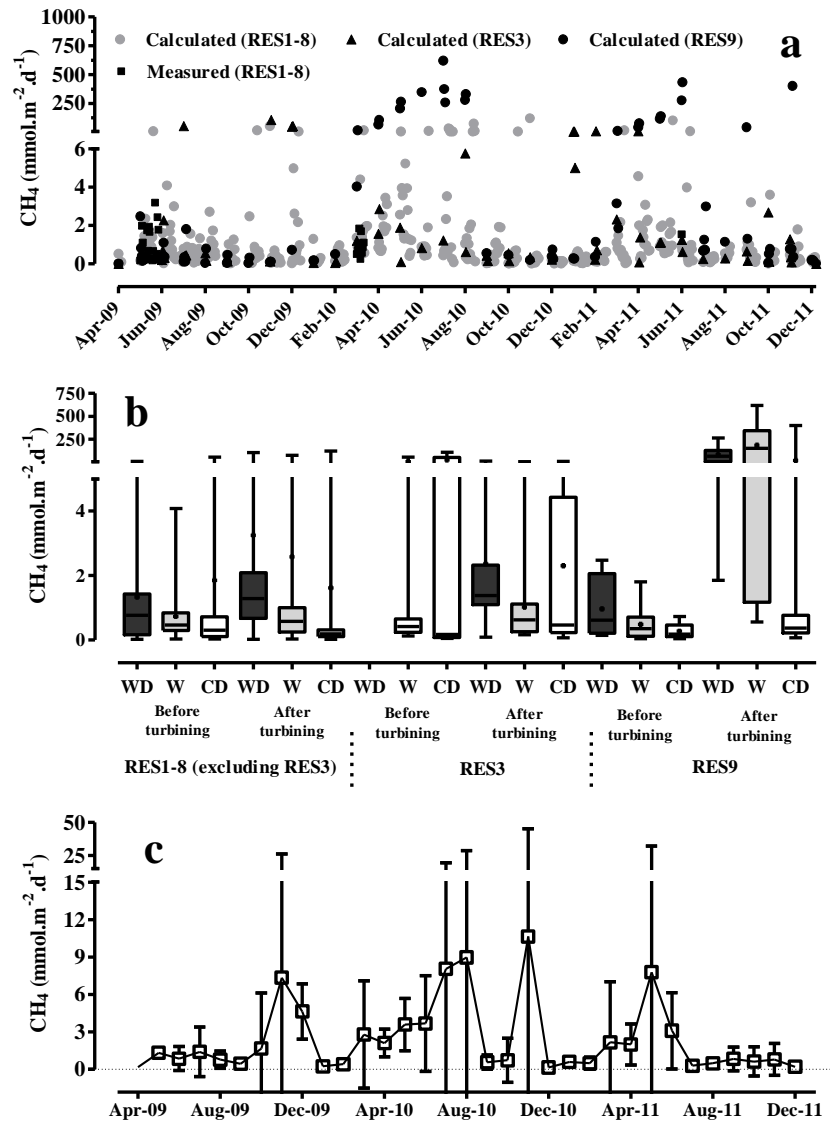


Figure 4.6. (a) Time series of the diffusive CH<sub>4</sub> fluxes at the different sampling stations in the reservoir, (b) spatial and seasonal variation in the diffusive CH<sub>4</sub> fluxes before and after beginning of turbines, (c) area-weighted diffusive CH<sub>4</sub> fluxes. In panel b, boxes show the median concentration and the interquartile range, and whiskers denote the full range of all values. Plus sign (+) in the box is showing the mean value. In panel c, error bar corresponds to  $\pm 1$  standard deviation.

As for the concentrations, the diffusive fluxes before the commissioning at RES9 were similar to those at RES1, RES2, RES4, RES5, RES6, RES7 and RES8 stations (Fig. 4.6a, b). Since the beginning of turbines, the fluxes mimicked the concentrations at this site. The diffusive fluxes were  $82 \pm 83$  and  $20 \pm 89$  mmol.m<sup>-2</sup>.d<sup>-1</sup> for the dry-warm and dry-cold seasons (Fig. 4.6a, b). During the wet season following the commissioning (2010), the average concentration at RES9 was  $316 \pm 183$  and only  $7.5 \pm 16.3$  mmol.m<sup>-2</sup>.d<sup>-1</sup> in the year 2011. Diffusive CH<sub>4</sub> fluxes covered the whole range of fluxes reported for tropical reservoirs, depending on the season. Diffusive CH<sub>4</sub> fluxes at NT2 reservoir were around one order of



magnitude lower than the ones at Petit Saut Reservoir (French Guiana) just after the impoundment (Galy-Lacaux et al., 1997), and but in the same order of magnitude as reported for reservoirs older by 10 to 18 years (Abril et al., 2005; Chanudet et al., 2011; Guérin et al., 2006; Kemenes et al., 2007).

Table 4.3: Statistical comparisons of measured and calculated diffusive CH<sub>4</sub> fluxes.

	May, 2009		March, 2010	
	Calculated	Measured	Calculated	Measured
Number of values	17	22	13	10
Range	0.1 – 9.8	0.2 - 3.2	0.6 - 4.4	0.3 - 1.8
Median	0.7	0.5	1.3	0.9
Mean ± standard deviation	1.4 ± 2.2	0.9 ± 0.9	1.6 ± 1.0	1.0 ± 0.5
Mann Whitney test	P value	0.67	P value	0.06
Are medians significant different? (P < 0.05)		No		No

#### 4.3.5. Ebullition of CH<sub>4</sub>

Ebullition fluxes were measured at different depths (from 0.5 m to 15 m) at 44 locations spread over 7 stations in various parts of the reservoir (Fig. 4.1; Chapter 3). The average ebullition was  $9.5 \pm 9.6 \text{ mmol.m}^{-2}.\text{d}^{-1}$  from the 1489 individual measurements. A strong relationship ( $r^2 = 0.84$ ) is observed between the second order polynomial function of 1-m binned average fluxes and the water depth at the measurement site. Ebullition decreased from 102 to 0  $\text{mmol.m}^{-2}.\text{d}^{-1}$  for water depth ranging from 0.5 to 15 m (Fig. 4.7a), and no bubbling was observed for a water depth higher than 13 m. Fig. 4.7b shows the influence of atmospheric pressure on the ebullition. Ebullition for a given depth-range decreased when the atmospheric pressure increased, as it is visible for measurements from March to June 2012 for instance. Average ebullition at NT2 was about 5 times lower than Petit Saut average ebullition after 2 year of impoundment ( $50 \text{ mmol.m}^{-2}.\text{d}^{-1}$ ; Galy-Lacaux et al., 1999) and almost one orders of magnitude higher than the value found 10 years after impoundment for that same reservoir ( $0.7 \pm 0.5 \text{ mmol m}^{-2} \text{ d}^{-1}$ ; Abril et al., 2005). The average ebullition at NT2 was about two times higher than maximum reported for the temperate Lake Wohlen ( $5 \text{ mmol.m}^{-2}.\text{d}^{-1}$ ; DelSontro et al., 2010). However, the hydroacoustic measurements done by DelSontro et al., (2011) showed that ebullition could vary over several orders of magnitude (up to  $\sim 6000 \text{ mmol m}^{-2} \text{ day}^{-1}$ ) for an African tropical reservoir.

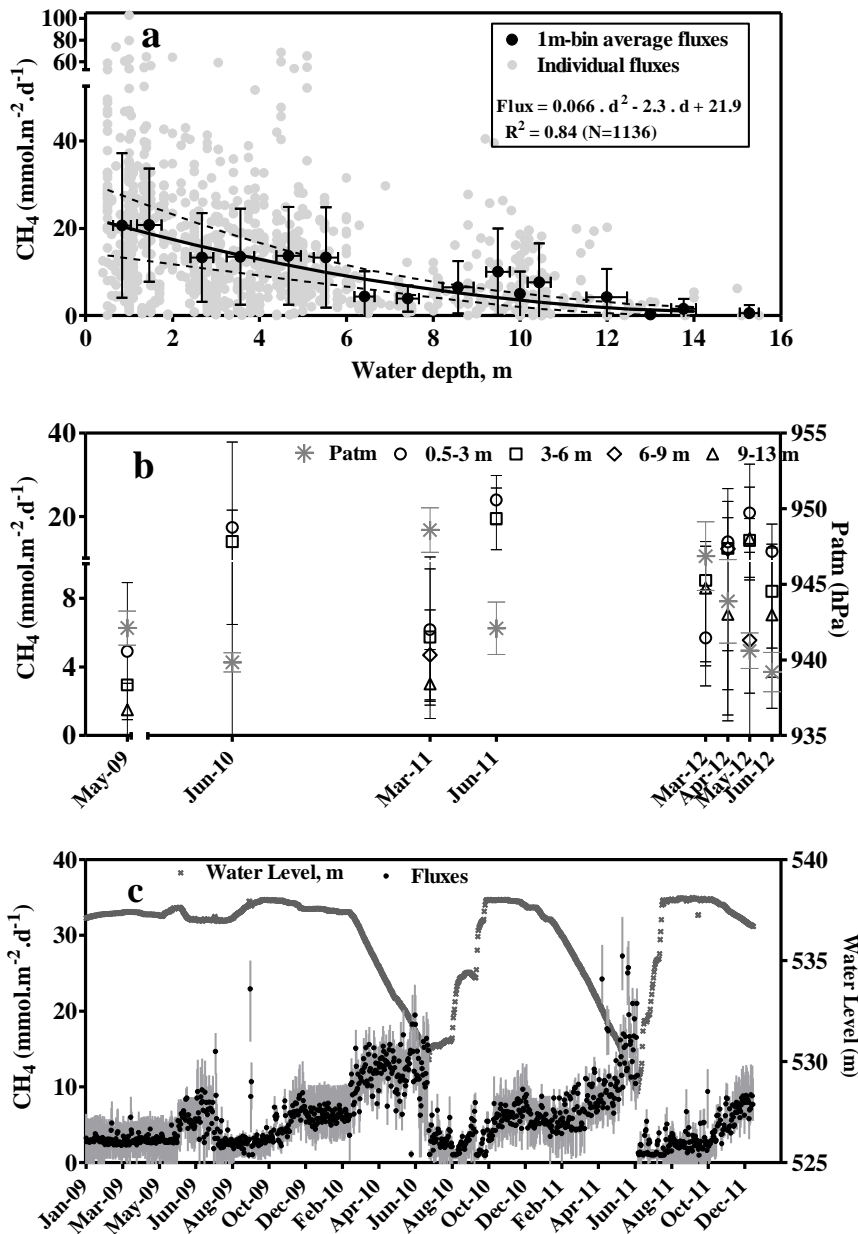


Figure 4.7. (a) Second order polynomial relationship between 1 m-binned average CH<sub>4</sub> bubbling fluxes and water depth (Error bar represents  $\pm 1$  standard deviation), (b) influence of change in atmospheric pressure on the bubbling fluxes, (c) influence of change in water level on the bubbling fluxes obtained from an artificial neuron network model (Chapter 3).

#### 4.3.6. Diffusive fluxes from the drawdown area

Diffusive CH<sub>4</sub> fluxes from the drawdown area ranged from  $-0.43$  to  $124$  mmol.m<sup>-2</sup>.d<sup>-1</sup> for soil temperature ranging from  $24.4$  to  $34.7$ °C. As shown in Fig. 4.8a, with low moisture content ( $20 \pm 7\%$ ), upland soils were acting as a slight sink of CH<sub>4</sub> ( $-0.09 \pm 0.11$  mmol.m<sup>-2</sup>.d<sup>-1</sup>, Fig. 4.8b). Midland soils 1 (moisture:  $21 \pm 5\%$ ) and 2 (moisture:  $38 \pm 8\%$ ), emitted  $0.06 \pm 0.24$  mmol.m<sup>-2</sup>.d<sup>-1</sup> and  $0.06 \pm 0.11$  mmol.m<sup>-2</sup>.d<sup>-1</sup>, respectively (Fig. 4.8b).

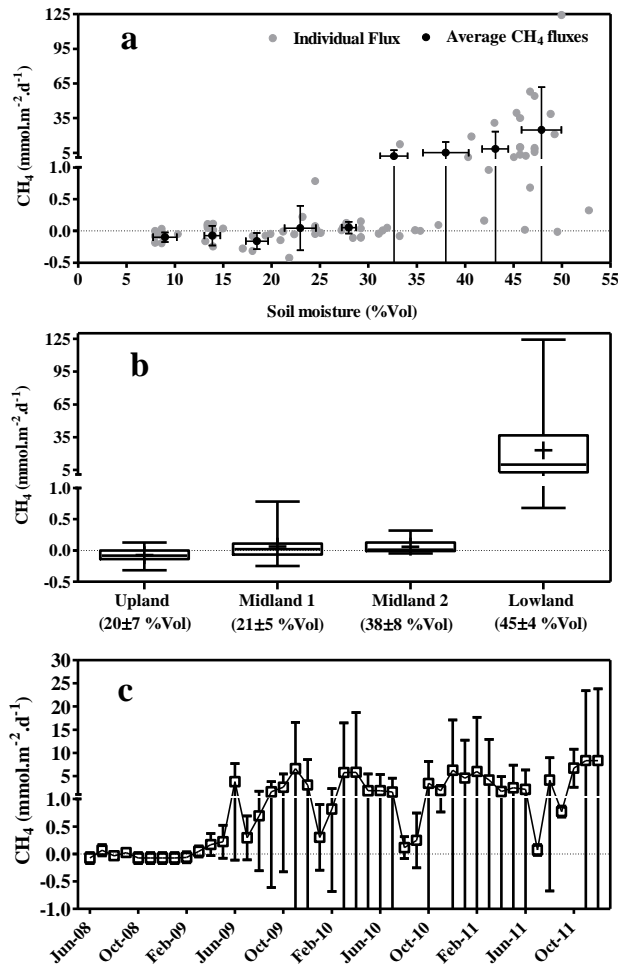


Figure 4.8 (a) diffusive CH<sub>4</sub> fluxes from soils vs. soil moisture contents, (b) diffusive CH<sub>4</sub> fluxes from soils of the drawdown area and from pristine (upland) soils in the watershed (% below the x-axis is average soil moisture content). Boxes show the median concentration and the interquartile range. Whiskers denote the full range of all values. Plus sign (+) in the box is showing the mean value, (c) area-weighted CH<sub>4</sub> diffusive fluxes from the drawdown area.

Emissions from the lowland soils (moisture:  $45 \pm 4\%$ ) were two order of magnitude higher than the other zones ( $23 \pm 29 \text{ mmol.m}^{-2}.\text{d}^{-1}$ , Fig. 4.8b). CH<sub>4</sub> emissions from soils showed a shift between a sink and a source for soil moistures between 20 and 30%, and a shift between moderate and significant source of CH<sub>4</sub> for soil moistures between 30 and 45%. No relation could be evidenced between CH<sub>4</sub> fluxes and the soil temperature (data not shown). Flux range was very similar to those reported for the littoral marshes at Three Gorges Reservoir in China ( $-1.0 - 156 \text{ mmol m}^{-2} \text{ d}^{-1}$ ; Chen et al., 2009).

### 4.3.7. Downstream emissions

#### 4.3.7.1. Degassing and diffusive fluxes from downstream of the turbines

The highest daily degassing emissions (up to 25 Mg(CH<sub>4</sub>) d<sup>-1</sup>) occurred at TRC1 (below the powerhouse) and DCH1 (below the regulating pond) at the end of the dry-warm season and beginning of the wet season in the year 2010, just after the turbines were operated (Fig. 4.9a). Degassing efficiency was 32% at TRC1 and 15% at DCH1. Negligible degassing was observed during the dry-cold season (Oct. to Feb., Fig. 4.9a) and during the wet season in the year 2011 for these two sites.

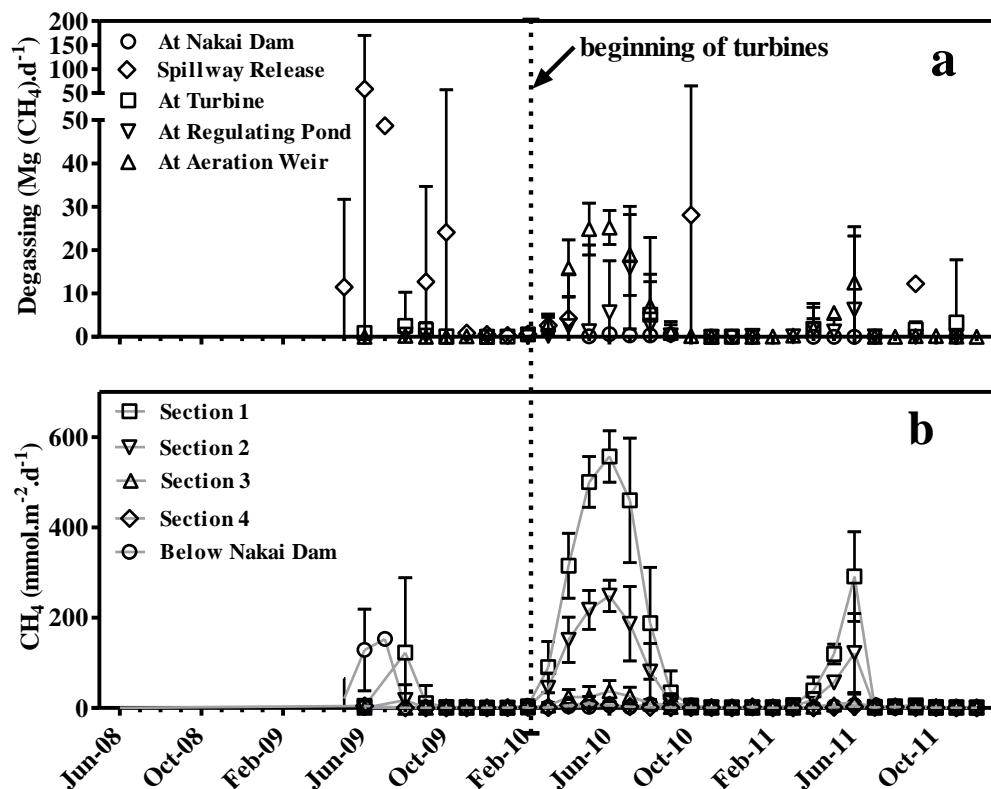


Figure 4.9 (a) Monthly mean degassing in the NT2 Hydroelectric system, (b) diffusive CH<sub>4</sub> fluxes from the artificial downstream channel below the powerhouse and from the Nam Theun River downstream of the Nakai Dam. Error bar represents  $\pm 1$  standard deviation.

The aeration weir showed a degassing efficiency of 80%. Therefore, even if CH<sub>4</sub> concentrations at DCH2 are 50% lower than at TRC1, as much CH<sub>4</sub> was released at the aeration weir (up to 25 Mg (CH<sub>4</sub>).d<sup>-1</sup>) than at TRC1 during the dry season. Degassing at this site during the wet season was higher in 2010 than in the year 2011, and it was negligible during the dry-cold season (October - February, Fig. 4.9a). Degassing below the powerhouse in the year 2010 was twice higher than in the year 2011. Note that in the year 2010 degassing lasted from March to August, whereas it occurred only in May and June in the year 2011.

Downstream of the turbine, diffusive fluxes followed the same seasonal variation as those observed for concentrations and degassing, decreasing with distance from the turbines. Fig. 4.9b plots monthly time series of mean CH<sub>4</sub> diffusive fluxes from the artificial downstream channel below the powerhouse and on the Nam Theun River downstream of the Nakai Dam. In section 1, the flux was  $121 \pm 188 \text{ mmol.m}^{-2}.\text{d}^{-1}$ , which was two times higher than in section 2 ( $56 \pm 81 \text{ mmol.m}^{-2}.\text{d}^{-1}$ ). Further in the downstream channel, at section 3 (below the aeration weir), fluxes were almost twenty times lower than the fluxes in section 1 ( $7.6 \pm 10 \text{ mmol.m}^{-2}.\text{d}^{-1}$ ). After the confluence with the Xe Bang Fai River, CH<sub>4</sub> fluxes drop to  $1.5 \pm 2.3 \text{ mmol.m}^{-2}.\text{d}^{-1}$  for the next 30 km. The area-weighted average diffusive flux along the 110 km reach of downstream of turbine (from TRC to XBF4) was  $20 \pm 31 \text{ mmol.m}^{-2}.\text{d}^{-1}$ , which is 4-5 times lower than the diffusive flux along the 40 km reach below the Petit Saut Dam ( $90 \text{ mmol.m}^{-2}.\text{d}^{-1}$ ; Guérin and Abril et al., 2007) 10 years after impoundment and seven times lower than diffusive flux along the 30 km reach downstream the Balbina Dam ( $140 \text{ mmol.m}^{-2}.\text{d}^{-1}$ ; Kemenes et al., 2007) 18 years after impoundment.

#### **4.3.7.2. Degassing and diffusive CH<sub>4</sub> fluxes from downstream of the Nakai Dam**

Due to the low environmental flow released at the Nakai Dam, these fluxes summed up over one year led to an mean amount  $0.3 \pm 3 \text{ Mg}(\text{CH}_4).\text{d}^{-1}$  degassed at NTH3, a value two orders of magnitude lower than the degassing measured downstream of the powerhouse, Fig. 4.9a). Mean diffusive flux downstream of the Nakai Dam was  $3.2 \pm 3.8 \text{ mmol.m}^{-2}.\text{d}^{-1}$ , that is very similar to diffusive fluxes from the reservoir surface. Further downstream of the Nakai Dam, diffusive fluxes were three times lower (from  $1.0 \pm 0.74$  for NTH4 to  $2.0 \pm 1.2 \text{ mmol.m}^{-2}.\text{d}^{-1}$  for NTH7).

During occasional spillway releases, before or after the commissioning, very high diffusive fluxes (up to  $195 \text{ mmol.m}^{-2}.\text{d}^{-1}$ ) were observed downstream of the Nakai Dam. This led to very intense degassing (up to  $59 \text{ Mg}(\text{CH}_4).\text{d}^{-1}$ , July 2009, Fig. 4.9a).

#### **4.3.8. Potential CH<sub>4</sub> production in flooded soils**

The evolution of CH<sub>4</sub> production rates for flooded and never flooded AG, FS1 and FS2 soils is illustrated in the Fig. 4.10. After reaching the maxima within 10 to 30 weeks, CH<sub>4</sub> production rates decreased as previously reported for Petit Saut Reservoir (Guérin et al., 2008) and for rice field soils (Das and Adhya 2012; and references therein). The highest CH<sub>4</sub> production rates were observed for surface and subsurface soils that were never flooded (Fig. 4.10a, b, e, f).

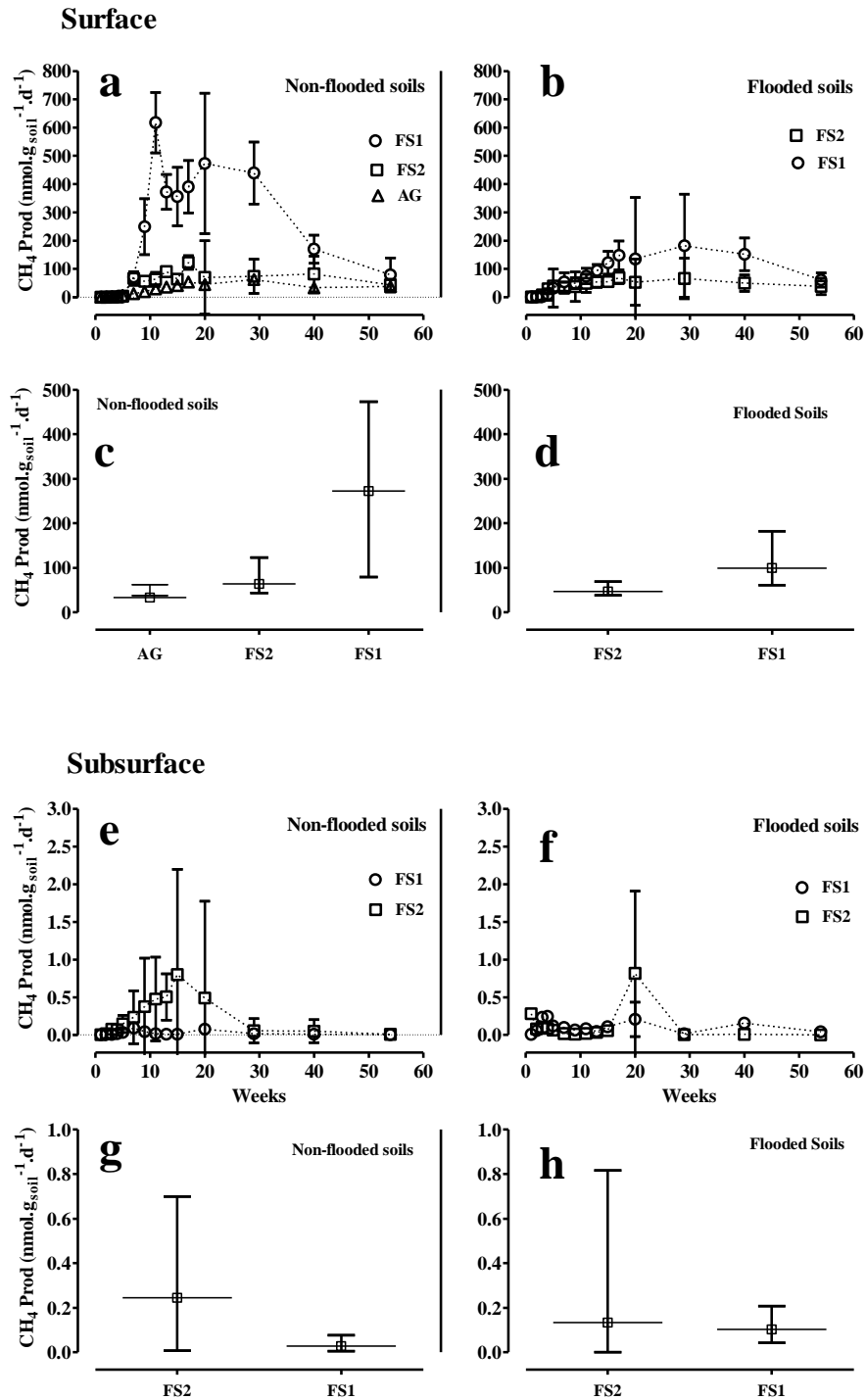


Figure 4.10: Time series and average potential CH<sub>4</sub> production rates from one year soil incubations. Time series of surface (a) non-flooded soils, (b) flooded soils. Average of surface (c) non-flooded soils, (d) flooded soils. Time series of subsurface (e) non-flooded soils, (f) flooded soils. Average of subsurface (g) non-flooded soils, (h) flooded soils. Error bars represent standard deviation. Note: Surface corresponds to soils collected from upper 20 cm layer, and subsurface corresponds to soils collected from between 20 to 120 cm. FS1 represents soils from primary dense and medium forests, FS2 represents soils from light, degraded and riparian forests and AG represents soils from agricultural lands.

Fig. 4.10 (c, d, g, h) shows the average CH<sub>4</sub> production rates for surface and subsurface soils incubated over one year. On average, the highest CH<sub>4</sub> production rates were observed for soils that were never flooded. The average annual CH<sub>4</sub> production in never flooded surface soils ranged from 33 nmol.g<sub>soil</sub><sup>-1</sup>.d<sup>-1</sup> for AG to 273 nmol.g<sub>soil</sub><sup>-1</sup>.d<sup>-1</sup> for FS1, whereas production rates in soils from the drawdown area ranged from 47 nmol.g<sub>soil</sub><sup>-1</sup>.d<sup>-1</sup> for FS2 to 99 nmol.g<sub>soil</sub><sup>-1</sup>.d<sup>-1</sup> for FS1. CH<sub>4</sub> production rates in subsurface soils were 2 to 3 order of magnitude lower than in the surface soils, with production rates ranging from 0.1 to 0.2 nmol.g<sub>soil</sub><sup>-1</sup>.d<sup>-1</sup> in never flooded soils and from 0.03 nmol.g<sub>soil</sub><sup>-1</sup>.d<sup>-1</sup> for FS1 to 0.2 nmol.g<sub>soil</sub><sup>-1</sup>.d<sup>-1</sup> for FS2 in soils from the drawdown area. CH<sub>4</sub> production rates in the surface soils at the NT2 reservoir were one order of magnitude lower than CH<sub>4</sub> production rates found in soils surrounding the Petit Saut Reservoir, where the production rates were up to 1176 ± 1680 nmol.g<sub>soil</sub><sup>-1</sup>.d<sup>-1</sup> (Guérin et al., 2008).

#### 4.3.9. Aerobic CH<sub>4</sub> oxidation in the reservoir, artificial downstream channel and the Nam Theun River

Aerobic methane oxidation (AMO) rates varied by four orders of magnitude within the NT2 system, and increased with the CH<sub>4</sub> concentrations (Fig. 4.11). In the NT2 system, potential AMO rates ranged from 0.02 ± 0.03 at NHT3 to 62.2 ± 3.8 μmol.L<sup>-1</sup>.d<sup>-1</sup> at DCH1 for CH<sub>4</sub> concentrations ranging from 0.003 ± 0.000 to 16.42 ± 0.1 μmol.L<sup>-1</sup>. For similar concentrations, the potential oxidation rates in the epilimnion are up to 8 times higher in the metalimnion than in the epilimnion. At DCH1 where the water originates from RES9, the average oxidation rate at this station was 50% higher than in the metalimnion for the same concentration range. Downstream of the Nakai Dam (NTH3), the water has the physico-chemical characteristics of the whole epilimnion at RES1, and potential AMO is half of the AMO observed in the epilimnion of the reservoir.

In the epilimnion, the AMO rates increased linearly with the CH<sub>4</sub> concentrations (Fig. 4.11a). In 2010, the slope of the linear correlation, or the so-called specific oxidation rate was 4.1 ± 0.1 d<sup>-1</sup> for concentrations ranging from 0.01 ± 0.00 to 1.0 ± 0.0 μmol.L<sup>-1</sup>, and AMO rates ranging from 0.04 ± 0.03 to 3.8 ± 0.4 μmol.L<sup>-1</sup>.d<sup>-1</sup>. In the year 2011, the specific oxidation rate was more than two times lower (1.8 ± 0.1 d<sup>-1</sup>) since the maximum AMO rate of 2.8 ± 0.0 μmol.L<sup>-1</sup>.d<sup>-1</sup> was reached at an initial concentration of 1.1 ± 0.0 μmol.L<sup>-1</sup>. On the opposite, in the metalimnion, the AMO rates were higher in the year 2011 than in the year 2010 for a similar range of concentration. (Fig. 4.11b). We obtained typical Michaelis-Menten kinetics specific for the two years. In 2010, the half saturation constant K<sub>m</sub>(CH<sub>4</sub>) was 7.3 ± 1.4 μmol.L<sup>-1</sup> and the maximum oxidation rate V<sub>max</sub> was 51.6 ± 4.7 μmol.L<sup>-1</sup>.d<sup>-1</sup> (r<sup>2</sup>=0.97). In 2011, the K<sub>m</sub>(CH<sub>4</sub>) was 1.0±0.3 μmol.L<sup>-1</sup> and the V<sub>max</sub> was 33.3 ± 3.4 μmol.L<sup>-1</sup>.d<sup>-1</sup> (r<sup>2</sup>=0.93). At NTH3, we obtained different relationships between AMO rates and the initial CH<sub>4</sub> concentrations at each sampling dates. For further calculation, the average specific oxidation rate of 2.8 ± 2.2 d<sup>-1</sup> will be used. At DCH1, our sampling strategy did not allow the calculation of Michaelis-Menten kinetics parameters for the two years separately or by season. Therefore, all AMO rates from the years 2010 and 2011 were plotted together and a

single Michaelis-Menten relationship was obtained with mean  $K_m(\text{CH}_4)$  equal to  $12.0 \pm 6.7 \mu\text{mol.L}^{-1}$  and mean  $V_{\text{max}}$  equal to  $95.2 \pm 30.6 \mu\text{mol.L}^{-1}.\text{d}^{-1}$ . ( $r^2=0.87$ ).

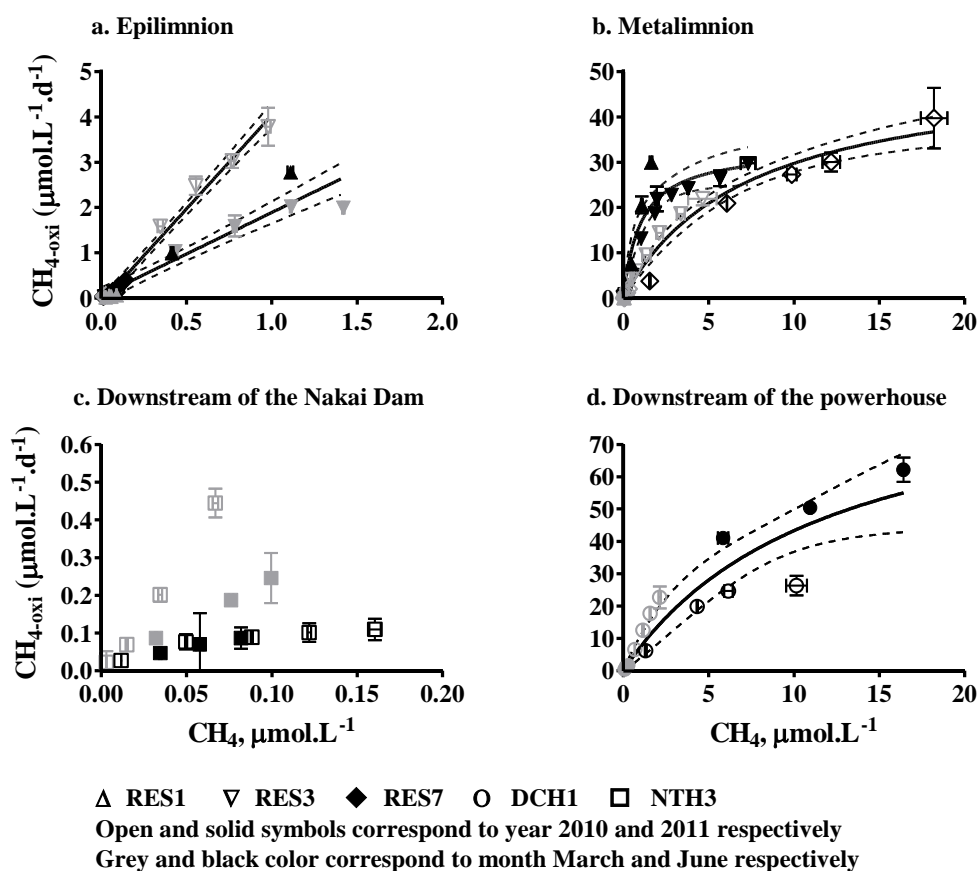


Figure 4.11: Aerobic methane oxidation rate ( $\mu\text{mol.L}^{-1}.\text{d}^{-1}$ ) versus  $\text{CH}_4$  concentration ( $\mu\text{mol.L}^{-1}$ ) obtained in incubations of water samples from (a) the epilimnion, (b) metalimnion, (c) downstream of the Nakai Dam, (d) downstream of the powerhouse. Error bars correspond to SD of triplicates bottles.

In the metalimnion and at NTH3,  $K_m(\text{CH}_4)$  values are very low compare to the potential in situ concentrations observed at these sites (up to  $100 \mu\text{mol.L}^{-1}$ ). However, they are well in the range of  $K_m(\text{CH}_4)$  reported from pure culture (Dunfield and Conrad, 2000, Segers, 1998) in lakes with similar  $\text{CH}_4$  concentration ranges (Bédard and Knowles, 1997, Rudd and Hamilton, 1975) and are one order of magnitude higher than in marine environment (Ward and Kilpatrick, 1990).  $V_{\text{max}}$  at NT2 was more than twice the  $V_{\text{max}}$  in Lake St Georges (Canada, Bédard and Knowles, 1997). Specific oxidation rates observed NT2 were twice higher than those obtained at the Petit Saut Reservoir, and one order of magnitude higher than in natural lakes and rivers (Guérin and Abril, 2007, and reference therein).



## **4.4. Discussion**

### **4.4.1. CH<sub>4</sub> dynamic in the reservoir water column**

The regular decrease of the CH<sub>4</sub> concentration from the bottom of the anoxic water column to the metalimnion and the sharp decrease around the oxicleine in the metalimnion (Fig. 4.3) is typical in lakes and reservoirs where CH<sub>4</sub> is produced in the anoxic sediments and flooded soils, and where most of it is oxidized at the oxic-anoxic interface (e.g., Bastviken et al., 2004; Bédard and Knowles, 1997; Guérin and Abril, 2007; Guérin et al., 2006). The occurrence of methanogenesis in the flooded soils was confirmed by the CH<sub>4</sub> concentrations in pore water of the cores that was significantly higher than in the water column at the same period and by the potential CH<sub>4</sub> production incubation in the soils that were artificially flooded during incubations in anoxic conditions (Fig. 4.10). The occurrence of methanotrophy in oxygenated epilimnic water and mainly at the oxic-anoxic interface was also evidenced by the incubations of water in aerobic conditions at different CH<sub>4</sub> concentrations (Fig. 4.11a, b).

CH<sub>4</sub> concentrations and storage increase concomitantly with the water temperature and the establishment of the thermal stratification during the dry-warm season and peak at the end of the dry-warm season-beginning of the wet season (Fig. 4.3 and 4.4). During the wet season, concentrations and storage decrease slowly while they decrease sharply at the beginning of the dry-cold season when the reservoir overturns (Fig. 4.4b). The overturn favors the penetration of oxygen up to the bottom (Fig. 4.3, Fig. 4.4a). The sharp decrease of the CH<sub>4</sub> concentrations and CH<sub>4</sub> storage during this period might be explain by a sudden outgassing together with an enhancement of the aerobic CH<sub>4</sub> oxidation as already observed in a monomictic lake in Switzerland (Schubert et al., 2012). Therefore, the lowest CH<sub>4</sub> concentrations of the year were observed during the period with the longest residence time. Owing to the monomictic nature of NT2, the seasonal dynamics of the CH<sub>4</sub> differs from the permanently stratified Petit Saut Reservoir where CH<sub>4</sub> concentration increased with retention time (Abril et al., 2005).

### **4.4.2. Diffusive fluxes from the reservoir surface**

#### **4.4.2.1. At the RES1, RES2, and RES4 to RES8 monitoring stations**

CH<sub>4</sub> concentrations exhibited a high spatial and temporal variability in the hypolimnion of NT2. The seven investigated stations are located above contrasting flooded ecosystems (agricultural soils, primary dense to degraded forest, swamps...) where potential production rates could vary by 2 orders of magnitude from one to another (Fig. 4.10). In addition, the distance between these stations and the thalweg, the tributaries and the Nakai Dam significantly influence the hydrodynamics/hydrology and therefore the dilution of hypolimnic waters by CH<sub>4</sub>-poor water coming from the watershed, the O<sub>2</sub> supply and the stability of the thermal stratification. Despite such contrasting characteristics and the resulting high range of CH<sub>4</sub> concentrations reaching the metalimnion, the surface concentrations and thus the diffusive fluxes at the seven stations were not significantly different. A hypothesis to explain the high homogeneity of surface concentrations and thus fluxes (at the exception of

the sporadic events during the wet season and the reservoir overturn) would be that methanotrophic bacteria could consume CH<sub>4</sub> until it reaches a threshold value corresponding to the surface concentrations. This hypothesis was not validated in laboratory conditions during the quantification of CH<sub>4</sub> oxidation in metalimnic water since no threshold was observed even at concentrations as low as 0.01 μmol.L<sup>-1</sup>, which is the lowest concentration observed in surface water. In situ and laboratory conditions differed only by the absence or the presence of light which was already shown to inhibit methanotrophy in a tropical reservoir (Dumestre et al., 1999) and in a natural lake (Murase and Sugimoto, 2005). The experiment of Murase and Sugimoto (2005) suggests that methanotrophic bacteria have a higher threshold in the presence of light than in the dark. The potential presence of a threshold of methanotrophic activity in the surface water could explain the absence of seasonal and spatial variability of the diffusive fluxes.

#### **4.4.2.2. At the RES3 monitoring station (flooded forest)**

Among all the studied soils, the one sampled at flooded forest station (RES3) is characterized by the highest potential for CH<sub>4</sub> production (FS1 samples, Fig. 4.10). In addition, this station is located in a small embayment preventing efficient water mixing with the rest of the reservoir, thereby not being part of the reservoir outflow or inflows and becoming more stagnant as a result. At RES3, CH<sub>4</sub> concentrations in the hypolimnion were 2 to 14 times higher than those from other stations during the wet season and at the beginning of the dry-cold season in the year 2011. This evidences that the dilution of hypolimnic waters during the wet season is not as effective as in the other stations. Therefore, large amount of CH<sub>4</sub> accumulated at the bottom of the water column of this small embayment is emitted during the reservoir overturn in the dry-cold season. During these events, the water column could be occasionally anoxic and CH<sub>4</sub>-enriched from the surface to the bottom (e.g., Fig. 4g, j, October-November 2009).

#### **4.4.2.3. At the RES9 monitoring station (water intake)**

The different behavior of CH<sub>4</sub> concentrations and fluxes at RES9 after the turbines were operated is explained by the artificial water mixing caused by the presence of the water intake. After the commissioning of NT2, the water column was permanently mixed at this site (Fig. 4.3d, h, l and Chanudet et al., 2012). Therefore, CH<sub>4</sub>-rich water from the hypolimnion reached the surface and led to diffusive fluxes up to 600 mmol.m<sup>-2</sup>.d<sup>-1</sup> in the dry-warm season (June 2010, Fig. 4.6a). After the commissioning, the surface concentrations at this site followed the same seasonal pattern as the average concentration in the reservoir water column.

By identifying a new type hotspot of CH<sub>4</sub> emissions in hydroelectric reservoirs designed such as in NT2, our results show that the dam and water intake design could have a significant influence on emissions. In addition, this intense degassing before the water goes through the turbines has a significant influence on emissions downstream of the dam (see section 4.4.5).

#### 4.4.2.4. Estimation of total diffusive fluxes from the reservoir

Area weighted average diffusive fluxes were calculated for the whole reservoir water surface (section 4.2.4.4; Fig. 4.6c). The average diffusive flux during the monitoring was  $2.4 \pm 2.9 \text{ mmol.m}^{-2}.\text{d}^{-1}$ . The lowest fluxes were always observed during the wet season. The average diffusive fluxes peaked during the reservoir overturns in November-December 2009 ( $7.3 \pm 18.7 \text{ mmol.m}^{-2}.\text{d}^{-1}$ ) and in November 2010 ( $10.6 \pm 34.6 \text{ mmol.m}^{-2}.\text{d}^{-1}$ ). In the year 2010, a slight increase of the diffusive fluxes was also observed during the reservoir overturn in the cold dry season. Since the  $\text{CH}_4$  stock in the water column was 2 times lower in the year 2011 than in the year 2010 for instance, diffusive fluxes were significantly lower than in 2011 ( $1.6 \pm 2.1 \text{ mmol.m}^{-2}.\text{d}^{-1}$ ) during this period. On average, diffusive fluxes during the reservoir overturn accounted for ~60% of the total diffusive fluxes since the beginning of the monitoring. The average diffusive fluxes increased all through the dry warm season in 2010 and 2011 and reached  $8.0 \pm 11.4 \text{ mmol.m}^{-2}.\text{d}^{-1}$  and  $7.7 \pm 24 \text{ mmol.m}^{-2}.\text{d}^{-1}$  in July 2010 and May 2011 respectively. During these periods, emissions from RES9 resulting from the destratification of the water column at the water intake contributed to up to 70% of the total diffusive fluxes from the reservoir even if RES9 represents only 2% of the total reservoir water surface. On a yearly basis, RES9 contributes to 32% of the diffusive fluxes at the air-water interface of the NT2 Reservoir.

We clearly show that hotspots (RES9) and moments of high emission (reservoir overturn, and short and sudden destratification) could have a significant impact on total emissions (McClain et al., 2003).

#### 4.4.3. Ebullition of $\text{CH}_4$

Our results clearly show that  $\text{CH}_4$  ebullition decreases with depth and depends on atmospheric pressure (Fig. 4.7a, b). The influence of these two parameters on ebullition was frequently documented in various aquatic environments like lakes (Bastviken et al., 2004, Casper et al., 2000) and hydroelectric reservoirs (Galy-Lacaux et al., 1999; Keller and Stallard, 1994).

As explained in Chapter 3, we used water level, water level variation, atmospheric pressure, change in atmospheric pressure and bottom temperature to model the bubbling fluxes using an ANN equation. The input parameters used in the equation are easily measurable in the field, and provide an equation that can be easily generalized. Fig. 4.7c shows the daily time series of the estimated area-weighted average bubbling fluxes at the NT2 reservoir since January 2009. The total ebullition was calculated following the methodology described in section 4.2.4.4. Ebullition exhibits large seasonal variation well correlated with water level variations (mainly decrease), fluxes peaking at  $27 \pm 4 \text{ mmol.m}^{-2}.\text{d}^{-1}$  in between the end of the cold dry season and warm dry season. Within 4 months, it contributed around 40-50% of the total annual ebullition even if the reservoir exhibits the lowest water surface area at that period (Fig. 4.2). This underlines that the estimation of bubbling from an aquatic ecosystem with large water level variations requires high frequency measurements (e.g. eddy

covariance, Chapter 3) over the period of water level decrease since the water level as well as its variations and the concomitant temperature variations have a strong impact on bubbling.

#### 4.4.4. Diffusive fluxes from the drawdown area

The soil moisture mainly governed diffusive fluxes from the drawdown area as shown in Fig. 4.8b. The moisture content plays a key role to control the methanogenesis and the methanotrophic activities in the soil (Le Mer and Roger, 2001). When soil moisture is low, oxygen penetrates deeper in the soil, enhancing CH<sub>4</sub> oxidation. In that case, soils act as either a slight source or sink of atmospheric CH<sub>4</sub>. When soil moisture is high, aerobic CH<sub>4</sub> oxidation is annihilated due to the absence of O<sub>2</sub>. This favors methanogenesis and CH<sub>4</sub> fluxes could be higher than diffusive fluxes from the reservoir surface in some occasions (soil moisture contents > 35%).

For upscaling of the discrete diffusive flux measurements at the drawdown area scale, values were clustered in four groups (section 4.2.4.4). Before the reservoir was first flooded, the drawdown area was acting as a CH<sub>4</sub> sink ( $-0.07 \pm 0.10 \text{ mmol.m}^{-2}.\text{d}^{-1}$ ; Fig. 4.8c). Gradually, the whole ecosystem became a source of CH<sub>4</sub>, with an average flux of  $3.3 \text{ mmol.m}^{-2}.\text{d}^{-1}$  ranging from  $0.8 \text{ mmol.m}^{-2}.\text{d}^{-1}$  (in the end of dry season) to  $8.3 \text{ mmol.m}^{-2}.\text{d}^{-1}$  (in the wet season). Logically, the CH<sub>4</sub> fluxes reached their maximum during the phases of decrease of the water level (maximum extension of the drawdown area). Since the water level rises irregularly, fluctuating at the scale of days to weeks, water saturated soils are also exposed to air and increase CH<sub>4</sub> oxidation.

#### 4.4.5. Downstream emissions

Total CH<sub>4</sub> emission below the dam and the powerhouse varies by four orders of magnitude within a year and 90% of the annual emissions from this pathway occur within 5 months in the year 2010 and within 3 months in the year 2011. 80% of downstream emissions occurred downstream of the powerhouse and less than 2% occurred below the Nakai Dam, not including degassing from spillway release (see below). This is mainly due to the difference in type and amount of water discharged at the two sites ( $2 \text{ m}^3.\text{s}^{-1}$  of surface water exported at the Nakai Dam vs.  $220 \text{ m}^3.\text{s}^{-1}$  of CH<sub>4</sub>-rich water at the powerhouse to the artificial downstream channel in the warm dry season). Most of downstream emissions occurred via degassing at the aerating weir.

Downstream of the turbines and the dam, the emissions decrease sharply with the distance from the structure due to a continuous outgassing by (1) degassing at the aeration weir and (2) diffusive fluxes from the river and channel surface water as already observed at the Petit Saut Reservoir (Guérin and Abril, 2007). The occurrence of aerobic CH<sub>4</sub> oxidation below the dam and the turbines was confirmed by the strong methanotrophic activity found during the incubations of downstream water at different CH<sub>4</sub> concentrations (Fig 4.11c, d). The diffusive fluxes below the dam contributed only to 15 % of total downstream emissions.

During spillway release (June-July 2009; Fig. 4.9a), degassing reached up to 59  $\text{Mg}(\text{CH}_4)\cdot\text{d}^{-1}$ , which is 30% higher than the maximum degassing occurring at TRC1. Even if these emissions are occasional and generally occur within a few days, spillway releases have contributed about 18% of total degassing since the beginning of the monitoring, and need to be accounted for when calculating the total  $\text{CH}_4$  emissions from a reservoir. This observation stresses the fact that dam operations can significantly influence emissions.

#### 4.4.6. Total gross emissions and comparison with other tropical reservoirs

Figure 4.12 summarizes the monthly  $\text{CH}_4$  emissions to the atmosphere from all identified pathways from May 2009 (when the monitoring started) to December 2011.

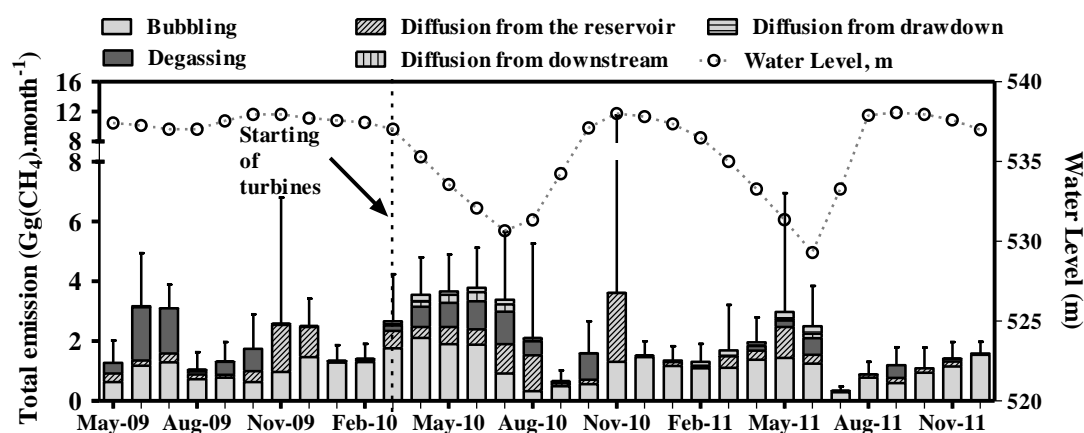


Figure 4.12. Time series of the monthly  $\text{CH}_4$  emissions from the whole NT2 system. Figure shows each individual pathways (bubbling, diffusion from the reservoir surface, diffusion from drawdown area, degassing, and diffusion from downstream).

It shows that the contribution of all identified pathways varied significantly throughout the two and half years of monitoring. Overall, total  $\text{CH}_4$  emissions reached their maximum at the end of the warm dry season-beginning of the wet season when ebullition, diffusive fluxes at RES9 and downstream emissions increase because of decreasing water level due to high releases compared to water inputs. Throughout the year, ebullition was the main pathway to the atmosphere, although it decreases during the rise in water level (Figure 4.12). The annual budgets for the year 2010, the first year after full impoundment and the year 2011, the first year of normal operation, are summed up in Table 4.4. Total  $\text{CH}_4$  emissions to the atmosphere decreased by 38% between 2010 and 2011 due to low diffusive emission from reservoir water surface and degassing emissions. Total  $\text{CH}_4$  emissions at NT2 are 2 to 5 times lower than at Petit Saut Reservoir (Abril et al., 2005), for an amount of flooded carbon 2-3 times lower (Descloux et al., 2011). This suggests that total emissions are closely related to the amount of flooded carbon (Abril et al., 2005; Guérin et al., 2008). Temperature might also influence methanogenesis and subsequent emissions, as suggested by the relationship between  $\text{CH}_4$  emission factor and latitude given by Barros et al., (2011). With total  $\text{CH}_4$  emissions ranging from 115 to 187  $\text{mg}\cdot\text{m}^{-2}\cdot\text{d}^{-1}$ , NT2 is in the upper range of emission factors given by Barros et al., (2011).

Table 4.4. Annual CH<sub>4</sub> budget for the years 2010 and 2011.

Emission Gg (CH <sub>4</sub> ).year <sup>-1</sup>		Upstream emission		Downstream emission		Total
Pathways	Bubbling (water depth < 13m)	Diffusive fluxes from reservoir surface	Diffusive fluxes from drawdown Area	Degassing	Diffusive fluxes from downstream	
2010	15.3 ± 1.1 (50%)	6.9 ± 8.1 (22%)	0.8 ± 0.7 (3%)	6.6 ± 0.7 (21%)	1.1 ± 0.3 (4%)	<b>30.8 ± 8.2</b>
2011	12.7 ± 1.0 (67%)	2.9 ± 3.4 (15%)	0.9 ± 0.8 (5%)	2.2 ± 0.3 (12%)	0.2 ± 0.1 (1%)	<b>19.0 ± 3.7</b>

Ebullition contributed 50 and 67% to the total emissions in the years 2010 and 2011, respectively. This was the major CH<sub>4</sub> pathway to the atmosphere from this flat bottom and shallow reservoir with large variation in the water level (up to 9 m during the study period). The increase of the proportional contribution of this pathway between the years 2010 and 2011 was due to both the sharp decrease of the contribution of downstream emissions, and the larger water level variations on the second year (Fig. 4.2). The absolute value of the ebullition is low compare to some other tropical reservoirs (DelSontro et al., 2011; Galy-Lacaux et al., 1999) but the contribution of this pathway to the total emission is very significant. This is consistent with results reported for temperate natural lakes (Casper et al. 2000) or reservoirs (DelSontro et al., 2010) and for tropical reservoir (DelSontro et al., 2011). We hypothesize that the high contribution of ebullition could result from the combination of (1) the rapid degradation of above ground vegetation and litter since this type of labile OM could produce very high amount of CH<sub>4</sub> during the initial phase of the mineralization in anoxic conditions (Guérin et al., 2008), and (2) high water level variations associated to the flat morphology of the reservoir. As a matter of consequence, ebullition is probably common in young flat reservoirs, especially if located in the tropics-subtropics where the high temperature enhances the CH<sub>4</sub> production and thereby bubble formation.

Total downstream emission (degassing + diffusive fluxes) was the second main pathway for 2010 (25% of total emissions), and the third main pathway in 2011 (13%). Downstream emissions in 2010 were significantly influenced by the spillway releases and the degassing of CH<sub>4</sub> stock resulting from the long residence time of water (Fig. 4.9). The moderate contribution of the emissions downstream of the dam and powerhouse at NT2 compared to South American tropical hydroelectric reservoirs (Abril et al., 2005; Kemenes et al., 2007) could be explained by the outgassing of the reservoir water column (1) during the dry-cold and wet season destratification of the reservoir, and mostly by (2) the outgassing of the water at the water intake (RES9) before the water reaches the turbines.

Despite the effect of the seasonal destratification events in the wet and cold-dry seasons (RES1, RES2, RES3, RES7 and RES8 in November 2009, 2010 and 2011) and the very high contribution of the outgassing at RES9 (July-August 2010, 2011; Fig 4.9), the contribution of diffusive fluxes from the reservoir surface (22 and 15%) is smaller than at Petit Saut Reservoir during the first two years after impoundment (20-40%; Abril et al., 2005)

and at Balbina 18 years after impoundment (> 50%; Kemenes et al., 2007). According to the sporadic nature of the destratification events occurring in the wet season, we do not exclude that emissions resulting from this period could have been underestimated during the monitoring.

At the beginning of the project, the contribution of the CH<sub>4</sub> emissions from the drawdown area was expected to be higher than a few percent (3-5%) owing the large surface area of this zone at NT2. Actually, only water-saturated soils located along the shoreline (width of ~3 m) emit up to ten times more CH<sub>4</sub> than the water surface and this zone represents only 1% of the total area of the reservoir. It was planned that the drawdown area would extend up to 80% of the total surface of the reservoir during its operation and only 61% were reached during the years 2009 to 2011. Our estimate is probably in the lower range of contribution of the drawdown zone during normal operation. In addition, the soils from the drawdown area are currently bare soils without vegetation. If vegetation would take over in the future, then enhanced CH<sub>4</sub> fluxes towards the atmosphere from this seasonal wetland could be observed due to enhanced methanogenesis fueled by increased fluxes of fresh OM into the soils.

#### **4.4.7. CH<sub>4</sub> mass balance in the NT2 Reservoir**

##### **4.4.7.1. Estimation of the CH<sub>4</sub> production during the mineralization of the flooded soils**

The incubations in anoxic conditions showed that CH<sub>4</sub> production rates were 2-4 order of magnitude higher in the surface soils (OC: 25.1 ± 10.7%, C:N=15.8 ± 3.4) than in the subsurface soils (OC: 7.7 ± 5.8%, C:N=13.5 ± 3.0). This is consistent with the decrease in CH<sub>4</sub> production with depth in previous studies in lake sediment (Rothfuss et al., 1997), tropical soils (Guérin et al., 2008) and in marine sediment in the Baltic Sea (Piker et al., 1998). We confirm that methanogenesis is controlled by the organic carbon content as reported for rice field soils (Wassmann et al., 1998; Yao et al., 1999), peat soils (Magnusson, 1993; Moore and Dalva, 1993) river sediments (Gebert et al., 2006), and reservoir (Guérin et al., 2008a; Sobek et al., 2012). Although NT2 OC content and C:N are in the same range as the one observed in the Petit Saut Reservoir, the production rates are 20 times lower. The difference between the production rates obtained at 30°C for Petit Saut (Guerin et al., 2008a) and 20°C for NT2 is very consistent with a Q<sub>10</sub> of 1.5-28 for methanogenesis (Borrel et al., 2011; Segers 1998).

The potential CH<sub>4</sub> production rates were extrapolated to compute the potential CH<sub>4</sub> production during soil mineralization in the reservoir. It was estimated using following equation:

$$\text{CH}_4\text{-Production} = \text{CH}_4\text{-Prod-rate} \times \rho \times (1-\phi) \times A \times d \quad (4.3)$$

with CH<sub>4</sub>-Prod-rate, the potential production rates. For the calculation purpose, average (average over the one year period of incubation), maximum (maximum production rate achieved during the one year period of incubation) and stabilized (stabilized production rate

after achieving maximum at 54 week) CH<sub>4</sub> production rates were used for each group of soils (Table 4.5). The production rates of the never flooded and already flooded soils were averaged together in order to include the effect of first flooding in these calculations. For subsurface soils, we used average value of FS1 and FS2 for the AG area. The quartz density  $\rho$  is 2.65 g cm<sup>-3</sup>. Because of soil compaction by hydrostatic pressure, we considered that the porosity of the soil  $\phi$  was 50% lower than the porosity reported by Chanudet and Descloux (2008). The following soil porosities were used: for surface soils- 24%, 32%, 31% for FS1, FS2 and AG respectively; and for subsurface soils - 50% of surface soils densities. The flooded area (km<sup>2</sup>) was calculated daily based on the area-capacity curve from NTPC (Chanudet, personal communication, EDF) and the surface area of the three types of soils were calculated from Descloux et al. (2011). The depth of the soil layer  $d$  was 0.2 m for surface and 1.0 m for subsurface soils.

Table 4.5: Average CH<sub>4</sub> production rates (nmol.g<sub>soil</sub><sup>-1</sup>.d<sup>-1</sup>) from the soil samples incubated over a period of one year.

CH <sub>4</sub> -prod nmol.g <sub>soil</sub> <sup>-1</sup> .d <sup>-1</sup>	<sup>d</sup> FS1		<sup>e</sup> FS2		<sup>f</sup> AG
	Subsurface	Surface	Subsurface	Surface	Surface
<sup>a</sup> Average CH <sub>4</sub> -prod	0.07 ± 0.04	171 ± 152	0.2 ± 0.2	54 ± 50	33 ± 20
<sup>b</sup> Maximum CH <sub>4</sub> -prod	0.14 ± 0.1	285 ± 71	0.7 ± 0.7	90 ± 12	62 ± 10
<sup>c</sup> Stabilized CH <sub>4</sub> -prod (at 54 weeks)	0.02 ± 0.02	68 ± 16	0.01 ± 0.01	40 ± 8	38 ± 1

<sup>a</sup>Average over the one year period of incubation.

<sup>b</sup>Maximum production rate achieved during the one year period of incubation.

<sup>c</sup>Stabilized production rate after achieving maximum.

<sup>d</sup>FS1, soils from the primary dense and medium forest.

<sup>e</sup>FS2, soils from light, degraded forest and riparian forest.

<sup>f</sup>AG, soils from agricultural land.

Time series of the monthly CH<sub>4</sub> productions calculated from Equation 4.3 shown in Fig. 4.13, with maximum and stabilized production as upper and lower limits. The CH<sub>4</sub> production varied with the seasonal changes in the flooded area. On average, the production by the mineralization of the flooded soils could produce 2.8 to 10.4 Gg(CH<sub>4</sub>).month<sup>-1</sup> during the dry and the wet seasons, respectively. Even if the volume of the subsurface soils is 5 times higher than the volume of surface soils, 99% of the CH<sub>4</sub> is produced from the surface soils according to our calculation. It has to be noted that these production rates are probably in the lower range of the total production rate in the reservoir since the production of CH<sub>4</sub> resulting from the degradation of above ground biomass was not included. This latter was shown to contribute to up to 10% of the total CH<sub>4</sub> production in the Petit Saut Reservoir (Guérin et al., 2008).



#### 4.4.7.2. Estimation of the aerobic CH<sub>4</sub> oxidation (AMO) in the NT2 waters

A clear decrease of  $K_m(\text{CH}_4)$  in the metalimnion and the specific oxidation rates in the epilimnion was observed between the year 2010 and 2011 (Fig. 4.12a, b). Since no bacteria identification and counting were performed we do not know whether (1) the methanotrophs adapted their metabolism to the amount of substrate available in the water column by modifying their  $K_m(\text{CH}_4)$  as it was observed by Dunfield and Conrad (2000) during starvation of bacteria in pure culture of methanotrophs, or if (2) the evolution of CH<sub>4</sub> concentration induced a change in the bacterial assemblage (Dumestre et al., 2001). Below the turbines and the dam, no temporal tendency could be drawn since (1) the specific oxidation rates were different at each campaign at NTH3 without any correlation with the in situ concentrations, and (2) only one single relationship was obtained at DCH1 because of a limited dataset on the whole range of concentration.

The AMO was measured in order to determine the potential contribution of methanotrophy to the CH<sub>4</sub> cycle in the NT2 reservoir. Based on 102 vertical profiles of in situ CH<sub>4</sub> and O<sub>2</sub> concentration at all stations in the reservoir, AMO was integrated in the oxic layer of the reservoir water column. In the metalimnion, equation 4.4 adapted from Guérin and Abril (2007) was used. It takes into account the inhibitory effect of light on methane oxidation (Dumestre et al., 1999; Murase and Sugimoto, 2005), and the availability of oxygen (Lidstrom and Somers, 1984).

$$\text{CH}_4\text{-Oxidized} = C_{\text{CH}_4} \times V_{\text{max}} / (C_{\text{CH}_4} + K_m(\text{CH}_4)) \times I(z) \times C_{\text{O}_2} / (C_{\text{O}_2} + K_m(\text{O}_2)) \times V \quad (4.4)$$

with  $C_{\text{CH}_4}$ , the CH<sub>4</sub> concentrations in the water layer;  $V_{\text{max}}$ , the specific maximum oxidation rate;  $K_m(\text{CH}_4)$ , the half saturation constant for AMO;  $C_{\text{O}_2}$ , the oxygen concentration; and  $K_m(\text{O}_2)$ , the half-saturation constants of O<sub>2</sub> for CH<sub>4</sub> oxidation. For calculation purpose, we considered two different  $K_m(\text{O}_2)$  from the literature: 20  $\mu\text{mol.L}^{-1}$  observed in sediments at Lake Washington (Lidstrom and Somers, 1984) and 58  $\mu\text{mol.L}^{-1}$  observed in landfill incubations (Gebert et al., 2003). The function of inhibition of methanotrophy by light  $I(z)$  is from Dumestre et al. (1999), and was quantified at the Petit Saut Reservoir. The volume of the water layer ( $V$ ) was calculated using volume-capacity curve (Chanudet, personal communication, EDF). In the epilimnion, the equation was adapted to consider the average specific oxidation rate obtained from our incubations instead of the Michaëlis-Menten parameters. In the downstream Nam Theun River and in the artificial downstream channel, the effects of light inhibition and oxygen limitations were neglected because of the high turbidity (data not shown), and oxygen concentrations significantly higher than the available  $K_m(\text{O}_2)$  from the literature.

The monthly amounts of total oxidized CH<sub>4</sub> are presented in Fig. 4.13. For the year 2010 and 2011, the amount of oxidized CH<sub>4</sub> was on average  $7 \pm 6 \text{ Gg}(\text{CH}_4).\text{month}^{-1}$  ranging from  $0.5 \pm 0.2$  to  $22 \pm 5 \text{ Gg}(\text{CH}_4).\text{month}^{-1}$ .

#### 4.4.7.3. Comparison of the total CH<sub>4</sub> source and sinks in the NT2 system

All estimated terms of the CH<sub>4</sub> mass balance in the NT2 system are given in Fig. 4.13 and in Table 4.6. Inputs from the watershed and the production are considered as sources to the NT2 system and total emissions, oxidation in the reservoir and in the downstream river and artificial downstream channel are considered as sinks. Overall, the sum of monthly CH<sub>4</sub> sinks follows the same pattern as the CH<sub>4</sub> production from the degradation of soil organic matter in anoxic conditions (Fig. 4.13).

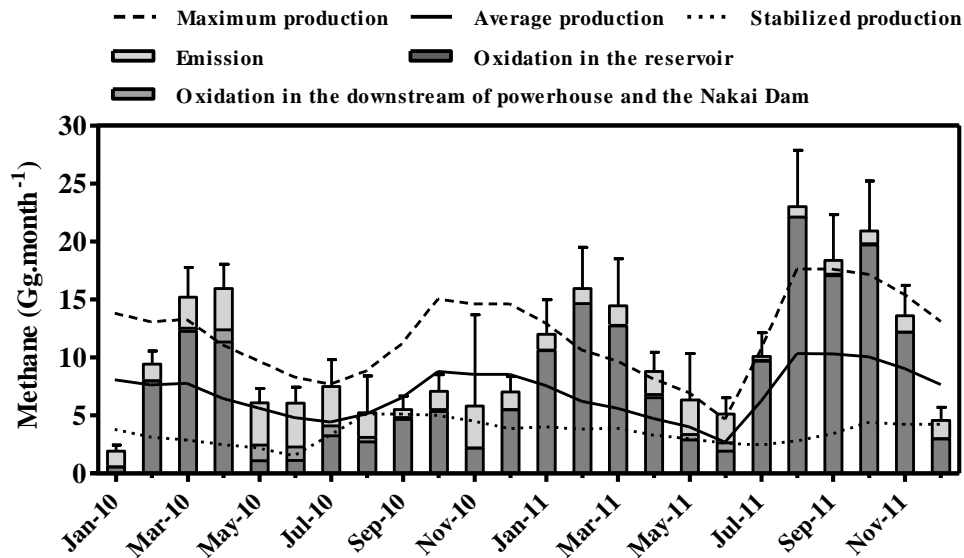


Figure 4.13: Time series of the different components of the CH<sub>4</sub> mass balance (oxidation in the reservoir and downstream, emission and production) on a monthly basis for the years 2010 and 2011.

In 2010, the amount of oxidized CH<sub>4</sub> was  $58 \pm 10$  Gg(CH<sub>4</sub>), that is 2 times less than in 2011 ( $132 \pm 31$  Gg(CH<sub>4</sub>)) (Table 4.6). In the year 2010, the methanotrophic activity was at its maximum in March-April when the stock of CH<sub>4</sub> in the water column was at its maximum. In the year 2011, the CH<sub>4</sub> was mostly consumed at the beginning of the wet season (August) and during the dry-cold season (January-February and October-November) showing that the supply of water from the watershed, the sporadic destratification and the reservoir overturn occurring during these two seasons could enhance CH<sub>4</sub> oxidation by increasing the penetration of O<sub>2</sub> in the reservoir water column. This result indicates that the decrease of gross emissions observed between the years 2010 and 2011 is due to an increase of methanotrophic activity in the reservoir water column (Table 4.6).

Table 4.6: CH<sub>4</sub> budget (production, storage, oxidation, emissions and exports) for the years 2010 and 2011 at the NT2 Reservoir (all values in Gg (CH<sub>4</sub>).year<sup>-1</sup>).

		Year 2010	Year 2011
Input	Total	0.1 ± 0.02	0.1 ± 0.02
Production <sup>a</sup>	At stabilized production rates	43	44
	At average production rates	83	86
	At maximum production rates	145	141
Oxidation <sup>b</sup>	Pelagic CH <sub>4</sub> oxidation in Lake	58 ± 10	132 ± 31
	Downstream	5.5 ± 0.6	2.0 ± 0.2
Emissions <sup>c</sup>	Total	30.8 ± 8.2	19.0 ± 3.6
Change in storage		-0.8	-0.02
Export <sup>d</sup>	Export to downstream	0.1 ± 0.2	Negligible

<sup>a</sup>Production obtained from surface (upper 20 cm layer) and subsurface (from 20 to 120 cm deep layer) soils using the area-weighted average production rates over a period of one year.

<sup>b</sup>Pelagic aerobic methane oxidation in lake and oxidation downstream.

<sup>c</sup>Emissions from all the major pathways at NT2 Reservoir.

<sup>d</sup>Export from the downstream releases from the Nakai Dam and at the powerhouse.

For the year 2010, the sum of the sinks is  $94.3 \pm 18.8$  Gg(CH<sub>4</sub>).year<sup>-1</sup>, that is very close to the average CH<sub>4</sub> production rate. In the year 2011, the sum of the sinks is  $153 \pm 35$  Gg(CH<sub>4</sub>).year<sup>-1</sup>, that is very close to the maximum CH<sub>4</sub> production rate. This mass balance implies that emissions could have decreased between the years 2010 and 2011 while both the production and the oxidation could have increased in the reservoir. Although we cannot be conclusive on the increase of the production between the years 2010 and 2011, this hypothesis seems reasonable for the following two reasons. (1) The incubation for CH<sub>4</sub> production showed that the maximum production rates are never reached immediately after flooding of the soils but systematically several weeks or months later (Fig. 4.10, Das and Adhya 2012; and cited therein; Guérin et al., 2008). In all the studies cited previously including this study, the incubations for CH<sub>4</sub> productions were always performed on ground soils. Grinding of soils could have enhanced and accelerated the microbial decomposition of soil OM compare to the in situ conditions by increasing the accessibility of soil OM to bacteria (Powlson, 1980). (2) In the year 2010, the long residence time of water could have led to the accumulation of inhibitory volatile compounds for CH<sub>4</sub> production in the pore water of flooded soils as observed in closed incubations (Williams and Crawford, 1984) which were flushed after the commissioning of the reservoir allowing higher production rates.

Although the emissions decreased sharply between the years 2010 and 2011, we cannot confirm the decrease of CH<sub>4</sub> emission with the age of the reservoirs (Abril et al., 2005; Barros et al., 2011). The total emissions in the year 2010 were enhanced by the long residence time of water (470 days) before the reservoir commissioning and the total emissions decreased in the year 2011 because of a high methanotrophic activity due to a high O<sub>2</sub> availability in the reservoir. On the other hand, we cannot be conclusive on the evolution of the total CH<sub>4</sub> production in the NT2 reservoir between the years 2010 and 2011 and for future years on the basis of the anoxic incubations of soils. Therefore, a third year of monitoring is needed to be conclusive on the decrease of emissions at the NT2 with age.

## 4.5. Conclusion

This is the first study on CH<sub>4</sub> emissions from a newly flooded sub-tropical hydroelectric reservoir which includes all known emission pathways. We confirm that the seasonal variation of the emissions is very significant (Abril et al., 2005; Chen et al., 2011; Kemenes et al., 2007) with more than 50% of diffusive fluxes and downstream emissions occurring within 3 to 5 months. It stresses that accurate estimation of emissions from such man-made ecosystems cannot be based on short field experiment but requires at least a first year of monthly monitoring (or better) to identify the period of high emissions. We also confirmed that emissions from (sub) tropical hydroelectric reservoir outside the Amazonian watershed are lower than emission from Amazonian reservoirs (Barros et al., 2011; Chen et al., 2011). On the other hand, we were unable to confirm the decrease of the emissions with the age of the reservoir on the basis of a two and half years of monitoring and a comprehensive CH<sub>4</sub> mass balance because of a lack of constraint on the term of CH<sub>4</sub> production in the reservoir. The decrease of the emissions with the age of the reservoir has to be confirmed by extending the monitoring by one or two more years.

Based on an original approach for the extrapolation of the ebullition at the reservoir scale, we evidenced a very high contribution of this term compared to previous studies in the tropics. We hypothesize that ebullition could be a common phenomenon in young flat reservoirs, especially if located in the tropics-subtropics where high mean temperature enhances bubble formation.

We evidenced a new hotspot of emission by diffusive fluxes at the water intake of turbines. Its existence in other reservoirs depends both on the design of the water intake and the physics of the water column upstream of the structure. In reservoirs with well mixed water column, the occurrence of mixing upstream of the turbines should not have impact on diffusive emissions at the reservoir surface. In stratified reservoir with high hypolimnetic CH<sub>4</sub> concentration such as NT2 in the warm dry season, CH<sub>4</sub> diffusive fluxes could be overlooked if such stations are not included in the monitoring. The design of the water intake leads to a very low contribution of downstream emissions compare to Amazonian reservoirs since the mixing of the water before it enters the water intake both enhance the outgassing of CH<sub>4</sub> and its oxidation.

The comparison of the contribution of each pathway to the total emissions from the NT2 Reservoir with other reservoirs evidences that the estimation of worldwide emission from hydroelectric reservoirs is challenging.

## Chapter 5

# Gross carbon dioxide (CO<sub>2</sub>) emissions and carbon budget for a subtropical hydroelectric reservoir: case of Nam Theun 2, Lao PDR

**Abstract:** Gross carbon dioxide (CO<sub>2</sub>) emissions and the carbon budgets were assessed in a newly flooded sub-tropical reservoir, Nam Theun 2 (NT2) in Lao PDR in Southeast Asia for first two years after full impoundment (2010 and 2011). Gross CO<sub>2</sub> emissions included all known major pathways of emissions: diffusion from the reservoir water surface, ebullition (bubbling), emissions from downstreams (diffusion and degassing) and emissions from the drawdown area (up to 275 km<sup>2</sup> for a total flooded area of 450 km<sup>2</sup> during studied period). Vertical profiles of dissolved CO<sub>2</sub>, inorganic carbon (IC) and total organic carbon (TOC) were determined in the reservoir at nine sampling stations. Import and export of dissolved CO<sub>2</sub>, IC and TOC were estimated through surface water sampling at twenty sampling sites in the pristine inflowing tributaries and, downstream release at the power house and the Nakai Dam. The laboratory work in controlled conditions allowed assessing the benthic production of CO<sub>2</sub> at the bottom of the reservoir. Additional, *chlorophyll-a* concentrations were measured at five sampling stations in the reservoir to quantify the primary production in the upper water column.

On average, diffusive CO<sub>2</sub> flux from reservoir was  $179 \pm 73 \text{ mmol.m}^{-2}.\text{day}^{-1}$ , which is in the upper range of diffusive fluxes from the tropical hydroelectric reservoirs. Notably, after the full impoundment, diffusive CO<sub>2</sub> fluxes from the drawdown area were in the same range as observed at the water surface and had a mean value of  $225 \pm 73 \text{ mmol.m}^{-2}.\text{day}^{-1}$ . For the year 2010 and 2011, our results show that diffusive emission from water surface was the main contributor (68-77%) to total CO<sub>2</sub> emissions. Whereas, the drawdown area contributed up to 25% total annual CO<sub>2</sub> emissions. Owing to physical dynamics of the reservoir and structural design, downstream (degassing and diffusion) emissions were in the lower range (~7%) as reported for tropical reservoirs. There was a slight enhance in total annual gross CO<sub>2</sub> emissions in the year 2011 than the year 2010, i.e.  $1307 \pm 243$  and  $1551 \pm 197 \text{ Gg CO}_2.\text{year}^{-1}$  for 2010 and 2011 respectively. The increase in the CO<sub>2</sub> for the year 2011 was probably because of increase in the CH<sub>4</sub> oxidation, increase in the aerobic respiration and the decrease in the photosynthesis activities.

Taking account of CH<sub>4</sub> mass balance (Chapter 4), the annual carbon budgets for 2010 and 2011 indicates that NT2 reservoir was a carbon source with annual carbon exports (atmosphere + downstream) of about  $401 \pm 120$  and  $437 \pm 108 \text{ GgC}.\text{year}^{-1}$  for the years 2010 and 2011 respectively. Magnitudes of carbon inputs from the watershed revealed that around 85-90% of total carbon release was fueled by flooded carbon stock at the reservoir bottom. Our results showed that the total carbon release during first two years corresponds to around 15% of total flooded carbon in above ground biomass and a soil thickness of 30 cm of the NT2 Reservoir.

### 5.1. Introduction

More than half of the carbon annually entering inland waters is thought to be processed therein (i.e., photosynthesis, respiration/decomposition, sedimentation), the remaining reaching the ocean (Aufdenkampe et al., 2011; Cole et al., 2007; Tranvik et al., 2009). Some studies have shown that emissions of CO<sub>2</sub> from inland aquatic ecosystems are in the same order of magnitude as emissions from fossil fuel combustion, deforestation and carbon uptake by ocean (e.g. Burgermeister, 2007; Tranvik et al., 2009).

Creation of a hydroelectric reservoir by damming a river for power generation converts a terrestrial ecosystem into an aquatic ecosystem. Subsequent decomposition of flooded terrestrial soil organic matter stimulates CO<sub>2</sub> productions and thereby CO<sub>2</sub> emissions to atmosphere. Several studies have confirmed that, converse to the past perception of hydroelectric reservoirs as C-free alternatives to fossil-fuel power generation (Hoffert et al., 1998; Victor, 1998), hydroelectric reservoirs may contribute significantly to global anthropogenic CO<sub>2</sub> (Barros et al., 2011; St. Louis et al., 2000). Recently, a meta-analysis on 85 published data on carbon emissions from reservoirs (Barros et al., 2011) has shown that processes leading to CO<sub>2</sub> production are probably enhanced in the tropics when compared to boreal or temperate regions. Studies based on carbon emission from hydroelectric reservoirs have not been equally distributed on the globe; most of the studies have been conducted in South American and Canadian reservoirs. The information on carbon emissions is especially crucial in Asian tropical regions where many new hydroelectric reservoirs are projected to be built (IPCC, 2012).

Compared to the primary production in the water column, higher benthic and pelagic respiration rates sustained by flooded soil organic carbon and terrestrial inputs from the watershed can often lead to supersaturated levels of CO<sub>2</sub> as observed in most of the world's hydroelectric reservoirs in both boreal (Diem et al., 2012, Duchemin, et al., 1995; Demarty et al., 2009; 2011; Teodoru et al., 2010) and tropical areas (Abril et al., 2005; Guérin et al., 2007; Kemenes et al., 2011; Roland et al., 2010). However, recently, some studies reported that hydroelectric reservoirs can be undersaturated with CO<sub>2</sub> if primary production exceeds total respiration (Chanudet et al., 2011; Ometto et al., 2010). It is believed that initial CO<sub>2</sub> emissions in a reservoir is largely supported by the decomposition of organic carbon stored in the flooded terrestrial ecosystem (Abril et al., 2005; Bodaly et al., 2004; Demarty et al., 2011; Galy-Lacaux et al., 1997; Guérin et al., 2008; Rosenberg et al., 1997; Teodoru et al., 2010). Emission of CO<sub>2</sub> decreases with the age of the impoundment as C-pool decreases (Abril et al., 2005; Demarty et al., 2011; Galy-Lacaux et al., 1999; Barros et al., 2011; Teodoru et al., 2010). Further, CO<sub>2</sub> emissions rates also vary within a reservoir in the initial years after flooding (Teodoru et al., 2010, Demarty et al., 2011).

Once produced, CO<sub>2</sub> can be emitted by the following major pathways: (1) diffusion at the reservoir surface (Abril et al., 2005; Galy-Lacaux et al., 1997; Guérin et al., 2006; Chanudet et al., 2011); (2) bubbles produced at the sediment-water interface that migrate through the water column and reaches to the atmosphere (Abril, et al., 2005; Galy-Lacaux et al., 1997; Kemenes et al., 2011); (3) downstream emissions, which include degassing and diffusion downstream of the powerhouse (Abril et al., 2005; Galy-Lacaux et al., 1997; Guérin et al., 2006; Kemenes et al., 2011). Contribution of each pathway to the total CO<sub>2</sub> emission varies over time (Abril et al., 2005), and it is likely that proportion of emission among the pathways depends upon the physical dynamics, operational and structural design of the hydroelectric reservoirs.

Nevertheless, only few studies have considered all the potential pathways of CO<sub>2</sub> emission in hydroelectric systems. For example, many studies do not report downstream

emissions measurements, but are using CO<sub>2</sub> emission estimates from other hydroelectric reservoirs. Furthermore, hydroelectric reservoir can exhibit a seasonal surface variation, with large drawdown area uncovered in the dry season. No measurements are reported yet on CO<sub>2</sub> emissions from this drawdown area, whereas CO<sub>2</sub> emissions could there be significant due to soil respiration.

In this context, the main objectives of this study were to implement a set of techniques and approaches to quantify gross CO<sub>2</sub> emissions from the subtropical Nam Theun 2 (NT2) hydroelectric reservoir, Lao PDR in South Asia. In order to reduce the uncertainty in the estimates, our sampling strategy took into consideration of the spatial and temporal variability. This was done by increasing the spatial coverage of measurements (35 sampling stations with a fortnightly sampling frequency, starting from April 2009 till December 2012). Our dataset includes also results from five intensive field campaigns conducted in between April 2009 and June 2011, and additional laboratory experiments on CO<sub>2</sub> production in controlled condition. These latter were conducted to assess production of CO<sub>2</sub> at the bottom of the reservoir. Measurements of *chlorophyll a* were performed to derive estimates of primary production in the water column of the reservoir. From these we have established the carbon balance, i.e., the following terms: gross emissions of CO<sub>2</sub> and CH<sub>4</sub>, import and export of CO<sub>2</sub>, CH<sub>4</sub>, organic and inorganic carbon, and primary production in the water column. All terms of the CH<sub>4</sub> mass balance are from Chapter 4.

Sampling strategies, determination of dissolved CO<sub>2</sub> concentrations and other physical and chemical parameters and methodology to assess emissions on reservoirs scale have been detailed in the Chapter 2. Kinetics of potential CO<sub>2</sub> production rates were determined in controlled laboratory conditions as described for CH<sub>4</sub> (Chapter 2). In the coming section, we present the results on carbon dynamics in reservoir water column, and thereby emissions of CO<sub>2</sub> from different pathways at the NT2 reservoir.

## **5.2. Results**

### **5.2.1. Dissolved CO<sub>2</sub> along with physico-chemical parameters in the reservoir**

Vertical profiles of CO<sub>2</sub> and other carbon species i.e. total carbon (TC), inorganic carbon (IC), total organic carbon (TOC), dissolved organic carbon (DOC) and particulate organic carbon (POC) were measured in the water column of the NT2 reservoir at 9 different sampling stations (Figure 2.1 in Chapter 2). An example of vertical profiles of CO<sub>2</sub>, IC, DOC and POC along with temperature and pH is shown in Figure 5.1.

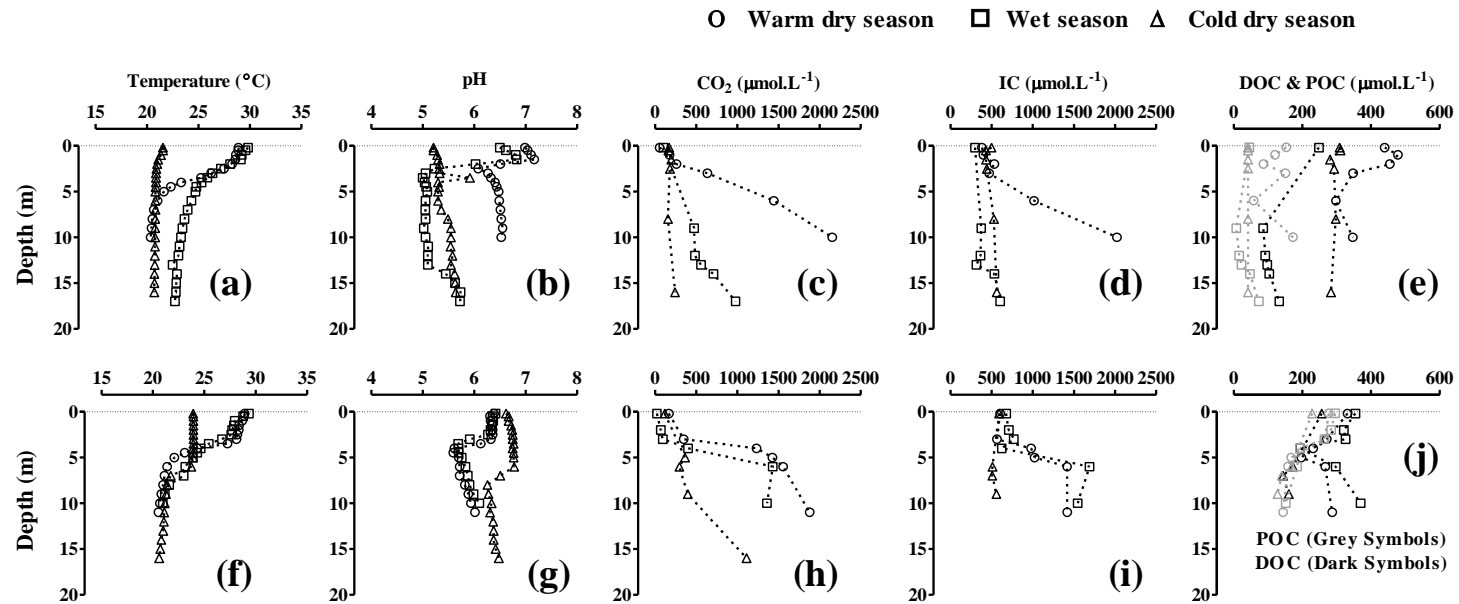


Figure 5.1. An example of vertical profiles of temperature (a, f), pH (b, g), carbon dioxide ( $\text{CO}_2$ ) (c, h), inorganic carbon (IC) (d, i), dissolved organic carbon (DOC) and particulate organic carbon (e, j) at RES3 (upper panel) and RES5 (lower panel) in the water column of the NT2 reservoir.



During the stratification, the water column exhibited clearly thermal and chemical gradient, resulting in a higher concentrations of CO<sub>2</sub> and IC in the hypolimnion than in the epilimnion water (Figure 5.1c, d, h, i). Notably, TOC and DOC concentrations were higher in the surface water than in the bottom water of the reservoir. Vertical profiles were more homogenous from surface to bottom during the cold period (October-February) than the warm dry (March-May) and the wet (June-September) seasons. In the bottom waters, we observed higher CO<sub>2</sub>, IC and DOC concentration at RES3 and RES5 than at other sampling stations in all the seasons, whereas RES8 and RES9 exhibited the lowest CO<sub>2</sub> and IC concentration in the bottom water. Spatial heterogeneity in the surface CO<sub>2</sub> concentrations was not significant as opposed to the bottom waters (Figure 5.2). On the seasonal basis, surface CO<sub>2</sub> concentrations at RES3 and RES5 were similar to those observed at other stations. Excepted for RES9 ( $p = 0.03$ , one way ANOVA test), dissolved CO<sub>2</sub> in the surface water at all other sampling stations behaved similarly ( $p = 0.62$ , one way ANOVA test) during the warm dry season. During wet season, dissolved CO<sub>2</sub> in the surface water at all sampling sites behaved similarly, and their average values were not significantly different ( $p = 0.14$ , one way ANOVA test). During the cold dry season, statistical analysis suggested 3 clusters in the sampling stations, cluster 1: RES1 and RES3 ( $p = 0.86$ , t-test), cluster 2: RES2, RES4, RES5, and RES6 ( $p = 0.86$ , one way ANOVA test), and cluster 3: RES7, RES8, and RES9 ( $p = 0.84$ , one way ANOVA test).

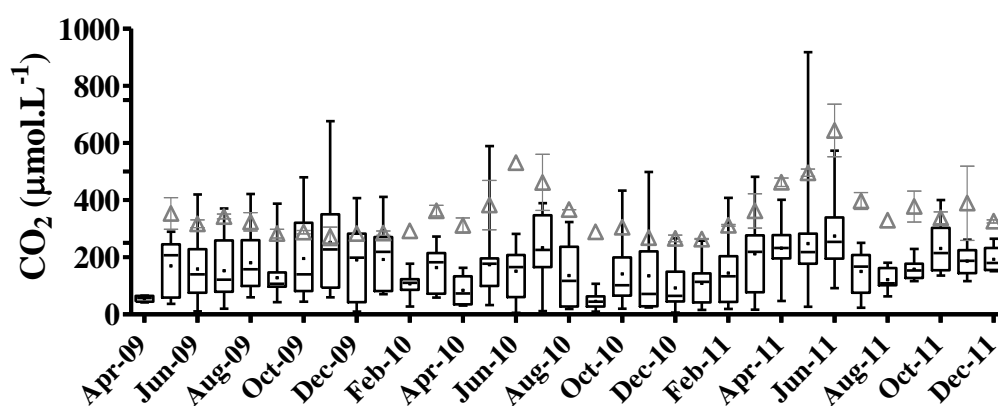


Figure 5.2. CO<sub>2</sub> concentration in surface water at the NT2 reservoir. CO<sub>2</sub> concentrations at RES1 to RES8 are shown using whisker-box plot whereas triangle symbol corresponds to the concentrations at RES9.

Dissolved CO<sub>2</sub> concentrations and other physico-chemical parameters in the reservoir (surface and bottom water) are summarized in Table 5.1. Overall, in the bottom water, maximum CO<sub>2</sub>, IC and DOC were observed during the stratified period, whereas minimum values occurred in the cold dry season. Average CO<sub>2</sub> concentrations in the bottom water were  $838 \pm 564 \mu\text{mol.L}^{-1}$  and  $1118 \pm 837 \mu\text{mol.L}^{-1}$  respectively for the warm and the wet season, and were significantly lower in the cold dry season (average value of  $297 \pm 347 \mu\text{mol.L}^{-1}$ ).

Similar to CO<sub>2</sub> concentration, seasonal average of IC and DOC were higher in the warm dry and wet seasons than in the cold dry season (Table 5.1).

Table 5.1 Dissolved CO<sub>2</sub> and physico-chemical parameters in the NT2 reservoir.  
SD: standard deviation.

	Depth level	Warm Dry Season		Wet Season		Cold Dry Season	
		Range	Average $\pm$ SD	Range	Average $\pm$ SD	Range	Average $\pm$ SD
O <sub>2</sub> ( $\mu\text{mol.L}^{-1}$ )	Surface	204-563	436 $\pm$ 57	34-708	418 $\pm$ 102	35-600	407 $\pm$ 122
	Bottom	3-494	30 $\pm$ 77	4-420	60 $\pm$ 115	4-545	189 $\pm$ 164
O <sub>2</sub> saturation (%)	Surface	37-117	89 $\pm$ 13	7-137	86 $\pm$ 21	6-119	77 $\pm$ 24
	Bottom	1-82	5 $\pm$ 13	1-77	11 $\pm$ 21	1-90	33 $\pm$ 28
Temperature ( $^{\circ}\text{C}$ )	Surface	17.5-31.1	27.4 $\pm$ 2.9	23.2-31.7	28.0 $\pm$ 1.9	17.0-31.8	23.0 $\pm$ 2.6
	Bottom	16.0-21.7	19.1 $\pm$ 1.2	18.1-26.6	21.5 $\pm$ 1.7	15.7-22.8	19.7 $\pm$ 1.4
pH	Surface	6.0-8.4	6.8 $\pm$ 0.6	5.4-8.4	6.5 $\pm$ 0.6	5.2-7.9	6.3 $\pm$ 0.5
	Bottom	5.5-8.0	6.5 $\pm$ 0.4	5.1-7.3	6.2 $\pm$ 0.5	4.9-7.3	5.9 $\pm$ 0.4
CO <sub>2</sub> ( $\mu\text{mol.L}^{-1}$ )	Surface	16-918	193 $\pm$ 141	6-573	160 $\pm$ 106	6-499	139 $\pm$ 92
	Bottom	50-2947	838 $\pm$ 564	94-4771	1118 $\pm$ 837	27-1966	297 $\pm$ 347
TC ( $\mu\text{mol.L}^{-1}$ )	Surface	45-977	606 $\pm$ 139	301-1136	585 $\pm$ 183	292-836	470 $\pm$ 128
	Bottom	407-2726	944 $\pm$ 435	99-3639	1190 $\pm$ 769	178-4091	568 $\pm$ 492
IC ( $\mu\text{mol.L}^{-1}$ )	Surface	42-650	320 $\pm$ 80	119-1059	305 $\pm$ 122	119-516	272 $\pm$ 83
	Bottom	268-2223	712 $\pm$ 364	106-3010	912 $\pm$ 654	120-3133	391 $\pm$ 374
TOC ( $\mu\text{mol.L}^{-1}$ )	Surface	42-593	287 $\pm$ 90	76-635	280 $\pm$ 114	91-416	198 $\pm$ 67
	Bottom	42-520	233 $\pm$ 91	68-785	287 $\pm$ 129	55-957	176 $\pm$ 129
DOC ( $\mu\text{mol.L}^{-1}$ )	Surface	42-453	266 $\pm$ 75	61-518	247 $\pm$ 97	88-410	190 $\pm$ 67
	Bottom	42-349	175 $\pm$ 67	48-471	185 $\pm$ 74	43-340	148 $\pm$ 69
POC ( $\mu\text{mol.L}^{-1}$ )	Surface	42-153	47 $\pm$ 17	4-312	45 $\pm$ 36	0-61	36 $\pm$ 12
	Bottom	42-217	72 $\pm$ 40	6-365	107 $\pm$ 78	4-713	55 $\pm$ 91

Dissolved CO<sub>2</sub> in the pristine inflowing tributaries varied from 4 to 483  $\mu\text{mol.L}^{-1}$ . CO<sub>2</sub> concentrations were the highest in the warm dry season (247  $\pm$  129  $\mu\text{mol.L}^{-1}$ ), whereas mean values were 197  $\pm$  138  $\mu\text{mol.L}^{-1}$  and 158  $\pm$  91  $\mu\text{mol.L}^{-1}$  for the wet and the cold dry season respectively. Similar to CO<sub>2</sub> concentration, highest IC concentrations were observed in the warm dry season, with an average of 300  $\pm$  133  $\mu\text{mol.L}^{-1}$ . With an average of 125  $\pm$  92  $\mu\text{mol.L}^{-1}$ , TOC was supplied from the watershed mostly in the DOC form (average of 116  $\pm$  83  $\mu\text{mol.L}^{-1}$ ).

### 5.2.2. CO<sub>2</sub> concentrations downstream of the powerhouse and downstream of the Nakai Dam

Downstream of the powerhouse, measurements mostly reflected the water composition at the RES9 (water intake of the turbines) sampling station. In the turbined water, dissolved CO<sub>2</sub> varied from 5 to 1023  $\mu\text{mol.L}^{-1}$ , suggesting seasonality with maximum at the end of the dry season, and minimum at the end of the cold dry season.

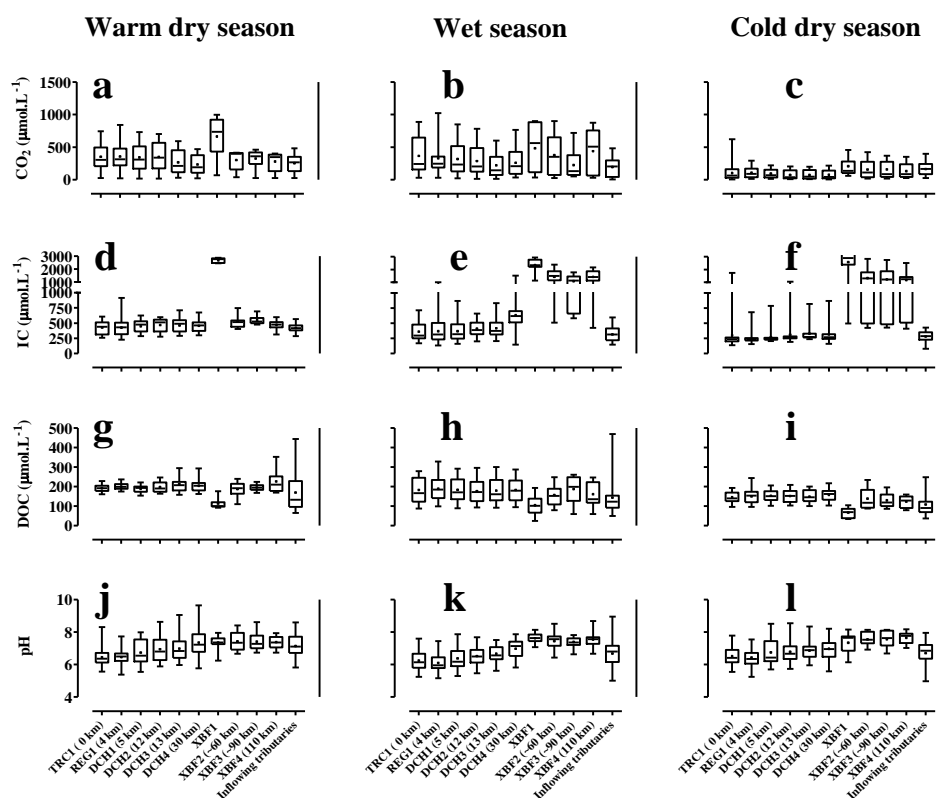


Figure 5.3. Evolution of carbon dioxide (a, b, c), inorganic carbon (IC) (d, e, f), dissolved organic carbon DOC (g, h, i) and pH (j, k, l) downstream of the powerhouse for the warm dry, the wet and the cold dry seasons.

CO<sub>2</sub>-poor waters released from the turbines and CO<sub>2</sub> concentration downstream of the powerhouse dropped to  $120 \pm 93 \mu\text{mol.L}^{-1}$  in the cold dry season. CO<sub>2</sub> concentration decreased gradually within a length of 12 km (i.e. section 1 and section 2). At DCH4, after a distance of 30 km from the turbine outlet, CO<sub>2</sub> concentration dropped significantly due to aeration weir in the section 3 (area between DCH2 and DCH3). In section 3, the CO<sub>2</sub> concentration were very close to the level observed in the pristine inflowing tributaries with seasonal averages of  $247 \pm 129 \mu\text{mol.L}^{-1}$ ,  $197 \pm 138 \mu\text{mol.L}^{-1}$  and  $158 \pm 91 \mu\text{mol.L}^{-1}$  respectively for the warm dry, wet and the cold dry seasons.

Owing to high CO<sub>2</sub> inputs from the Xe Bang Fai River, CO<sub>2</sub> concentration increased again in the section 4 (area between DCH4 and XBF4). Further 110 km downstream at XBF4, CO<sub>2</sub> concentration decreased in both the warm and cold dry seasons, whereas an increase occurred in the wet season, probably due to CO<sub>2</sub> inputs from the surrounding areas. In the cold season, IC concentration was at their lowest level. Due to the decrease in CO<sub>2</sub> concentration along with the distance from turbine outlet, an increase in the pH was observed (Figure 5.3j, k, l). IC inputs from the Xe Bang Fai River were significantly higher  $2683 \pm 181 \mu\text{mol.L}^{-1}$  than the release from the reservoir (Figure 5.3d, e, f).

Water releases from the Nakai Dam (either through spillway or continuous  $2 \text{ m}^3 \cdot \text{s}^{-1}$  ecological flow outlet) contained from 8 to  $451 \mu\text{mol} \cdot \text{L}^{-1}$  of dissolved  $\text{CO}_2$ . Similar to downstream of the powerhouse, highest concentrations were released during the warm and wet season, whereas minimum occurred in the cold the season. TOC ranged from 33 to  $300 \mu\text{mol} \cdot \text{L}^{-1}$  with an average of  $166 \pm 66 \mu\text{mol} \cdot \text{L}^{-1}$ . DOC was much higher ( $150 \pm 66 \mu\text{mol} \cdot \text{L}^{-1}$ ) than POC ( $16 \pm 32 \mu\text{mol} \cdot \text{L}^{-1}$ ). Water released from the Nakai Dam held comparatively higher TOC and DOC than turbined water. This is because water released from the Nakai Dam is from the epilimnion water, with higher TOC and DOC than in the hypolimnion water.

### 5.2.3. The kinetics of potential $\text{CO}_2$ production rate at the bottom of the reservoir

For all soils (FS1: dense and primary forest, FS2: riparian and degraded forest and AG: agricultural land) and whatever the depth (surface: upper 20 cm layer of soil and subsurface: sub-layer of soil between 20 to 100 cm), production rates were maximum in the beginning of the incubation experiment.  $\text{CO}_2$  production rates decreased over time as previously observed for Petit Saut Reservoir (Gu erin et al., 2008a). Table 5.2 summarizes the average  $\text{CO}_2$  production rates for surface and subsurface soils. Laboratory experiments showed that  $\text{CO}_2$  production rates were higher in the surface soils than in the subsurface soils. The average annual  $\text{CO}_2$  production in surface soils ranged from  $99 \pm 69$  (FS2) to  $327 \pm 256$  (FS1)  $\text{nmol} \cdot \text{g}_{\text{soil}}^{-1} \cdot \text{d}^{-1}$ , and had a lower range for subsurface soils ( $41 \pm 37$  (FS1) to  $61 \pm 36$  (FS2)  $\text{nmol} \cdot \text{g}_{\text{soil}}^{-1} \cdot \text{d}^{-1}$ ).

Table 5.2: Average  $\text{CO}_2$  production rates ( $\text{nmol} \cdot \text{g}_{\text{soil}}^{-1} \cdot \text{d}^{-1}$ ) from the soil samples incubated over a period of one year.

$\text{CO}_{2\text{-prod}}, \text{nmol} \cdot \text{g}_{\text{soil}}^{-1} \cdot \text{d}^{-1}$	FS1		FS2		AG
	Subsurface	Surface	Subsurface	Surface	Surface
Average $\text{CO}_{2\text{-prod}}$ <sup>a</sup>	$61 \pm 36$	$327 \pm 256$	$41 \pm 37$	$99 \pm 69$	$132 \pm 113$
Maximum $\text{CO}_{2\text{-prod}}$ <sup>b</sup>	$137 \pm 9$	$749 \pm 172$	$61 \pm 11$	$185 \pm 43$	$230 \pm 8$
Stabilized $\text{CO}_{2\text{-prod}}$ <sup>c</sup> (at 54 weeks)	$35 \pm 5$	$89 \pm 14$	$18 \pm 3$	$34 \pm 8$	$59 \pm 9$

<sup>a</sup>Average over the one year period of incubation.

<sup>b</sup>Maximum production rate achieved over the one year period of incubation.

<sup>c</sup>Stabilized production rate after achieving maximum at 54 week.

However, these  $\text{CO}_2$  production rates are lower than values reported for Petit Saut Reservoir in French Guiana (Guerin et al., 2008). These low  $\text{CO}_2$  production rates could be linked to lower area-weighted average carbon density ( $115 \pm 15 \text{ tC} \cdot \text{ha}^{-1}$ ) at the NT2 reservoir than the carbon density for some South American tropical hydroelectric reservoirs ( $251$  to  $326 \text{ tC} \cdot \text{ha}^{-1}$ , (Descloux et al., 2011). Another probable reason would be the lower incubation temperature in this study ( $20^\circ\text{C}$ ), compared to incubation temperature ( $30^\circ\text{C}$ ) in the Petit Saut Reservoir study (Gu erin et al., 2008a).

Potential  $\text{CO}_2$  production rates were used to compute the potential  $\text{CO}_2$  production during soil mineralization at the reservoir scale. Total  $\text{CO}_2$  production was estimated using the same approach as discussed for  $\text{CH}_4$  (Chapter 4).

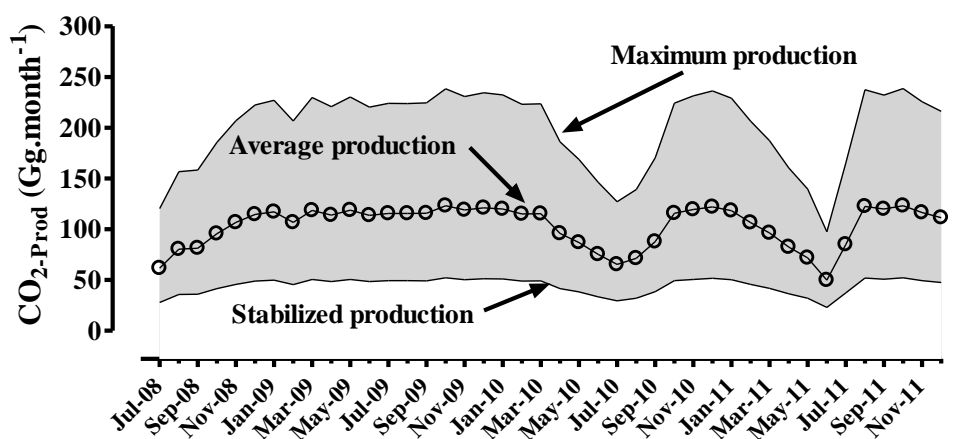


Figure 5.4. Time series of monthly average CO<sub>2</sub> production with maximum and stabilized production as upper and lower limits. Average, maximum and stabilized production are calculated using the average production rate over the one year period of incubation, maximum production rate during the period of incubation and stabilized production rate after achieving maximum at 54 week, respectively.

The time series of average CO<sub>2</sub> production is depicted in Figure 5.4, with maximum and stabilized production as upper and lower limits. CO<sub>2</sub> production varied with the seasonal changes in the flooded area, with maximum production during the wet season when reservoir was at its maximal surface level.

#### 5.2.4. Bubbling flux from the reservoir water surface

Bubbling fluxes were measured at stations representative to different water column depths (from 1 to 15 m). Due to the high CO<sub>2</sub> solubility of in the water, CO<sub>2</sub> content in the sampled bubbles was not significant. With a mean value of  $0.08 \pm 0.09 \text{ mmol.m}^{-2}.\text{day}^{-1}$ , emission of CO<sub>2</sub> through ebullition was almost negligible.

#### 5.2.5. Diffusive CO<sub>2</sub> flux from the reservoir water surface

Surface water samples were collected from nine stations to measure the concentration of CO<sub>2</sub> by AELab. These concentrations were applied on the thin boundary layer equation to calculate diffusive fluxes using a formulation of  $k_{600}$  from MacIntyre et al., (2010) study. Time series of calculated CO<sub>2</sub> diffusive fluxes since April 2009 till December 2011 is shown in Figure 5.5.

During the wet and the warm dry seasons, all sampling sites, excepted RES9 ( $p = 0.0001$ , one way ANOVA test), behaved similarly with their average diffusive flux values not significantly different ( $p = 0.24$ , one way ANOVA test). However, during the cold dry season, one way ANOVA test ( $p < 0.05$ ) suggests 3 groups in the sampling stations, group 1: RES1, RES2, RES3, RES4, RES5 and RES6; group 2: RES7 and RES8 and, group 3: RES9. CO<sub>2</sub> fluxes ranged from 5 to  $1522 \text{ mmol.m}^{-2}.\text{day}^{-1}$  for RES1 to RES8 sampling stations, with seasonal average for the warm dry and the wet seasons of  $234 \pm 199$  and  $168 \pm 133 \text{ mmol.m}^{-2}.\text{day}^{-1}$ , respectively. In the cold dry season, fluxes were lower at RES7 and RES8 and with an

average of  $106 \pm 87 \text{ mmol.m}^{-2}.\text{day}^{-1}$ , whereas the average flux was  $186 \pm 138 \text{ mmol.m}^{-2}.\text{day}^{-1}$  for RES1-RES6 sampling stations. At RES9 sampling station, diffusive  $\text{CO}_2$  fluxes ranged between 1 to  $2492 \text{ mmol.m}^{-2}.\text{day}^{-1}$ , with seasonal average of  $644 \pm 419$ ,  $643 \pm 628$ , and  $285 \pm 359 \text{ mmol.m}^{-2}.\text{day}^{-1}$  for the warm dry, the wet and the cold dry season, respectively.

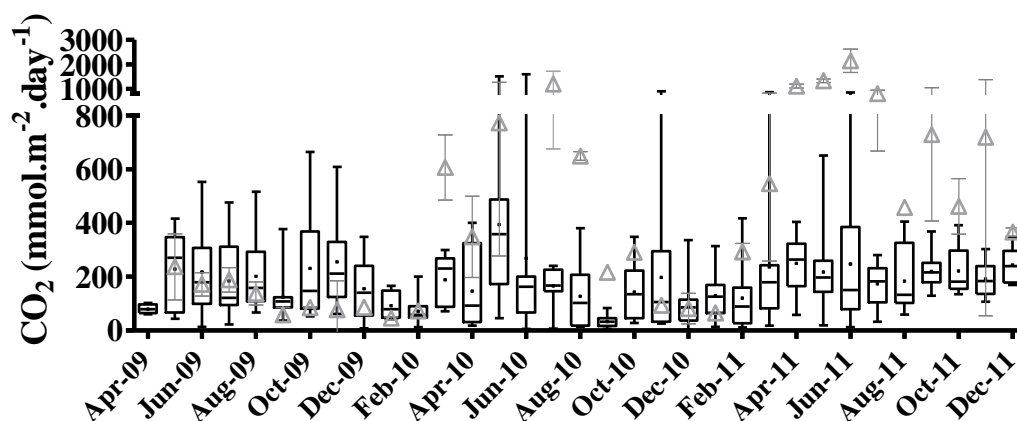


Figure 5.5. Time series of diffusive  $\text{CO}_2$  fluxes from reservoir surface since April 2009 till December 2011. Diffusive  $\text{CO}_2$  fluxes at RES1 to RES8 are shown using whisker-box plot whereas triangle corresponds to the fluxes at RES9.

Considering that RES9 station is representative of surface of about 2 all along the year. RES3 covers 6% of the total reservoir surface and values from the other sampling stations are attributed to the remaining of the reservoir surface. With a global average of  $179 \pm 73 \text{ mmol.m}^{-2}.\text{day}^{-1}$ , the area weighted average  $\text{CO}_2$  fluxes varied from 35 to  $418 \text{ mmol.m}^{-2}.\text{day}^{-1}$ , comparatively higher during the warm dry season than during the wet and the cold seasons. Diffusive  $\text{CO}_2$  fluxes at NT2 were reasonably higher than fluxes from older reservoirs located in the same geographical region; i.e. Nam Ngum and Nam Leuk reservoirs (Chanudet et al., 2011). In comparison to South American reservoirs, these fluxes are two times higher than those at Petit Saut 10 year after flooding (Abril et al., 2005; Guerin et al., 2006) and around 2 times lower than those at Balbina ( $315 \text{ mmol.m}^{-2}.\text{day}^{-1}$ ; Kemenes et al., 2011) 18 years after flooding. NT2 fluxes are comparable to those from Tucurui ( $237 \text{ mmol.m}^{-2}.\text{day}^{-1}$ ), Xingo ( $223 \text{ mmol.m}^{-2}.\text{day}^{-1}$ ), and Samuel ( $184 \text{ mmol.m}^{-2}.\text{day}^{-1}$ ), and, comparatively higher than the ones from other Amazonian reservoirs studied by dos Santos et al. (2005; 2006).

The reservoir water surface area was multiplied by area-weighted diffusive  $\text{CO}_2$  fluxes on a monthly basis to obtain total  $\text{CO}_2$  emission. Time series of monthly  $\text{CO}_2$  diffusive emissions since April 2009 till December is shown in Figure 5.6.

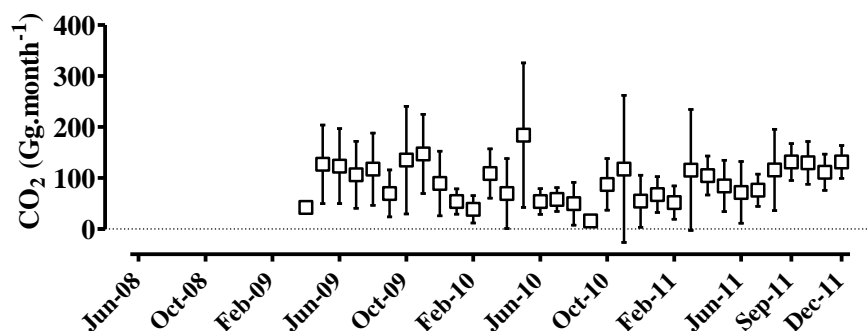


Figure 5.6. Time series of monthly diffusive CO<sub>2</sub> emissions from reservoir surface since April 2009 till December 2011.

### 5.2.6. Diffusive CO<sub>2</sub> fluxes from the drawdown area

During the two minimum water level periods i.e. June 2010 and June 2011, we measured diffusive CO<sub>2</sub> fluxes from the drawdown area which, by definition, was flooded during the high water level periods.

Diffusive CO<sub>2</sub> fluxes from the drawdown area ranged from 20 to 589 mmol.m<sup>-2</sup>.day<sup>-1</sup>. As shown in Figure 5.7, we observed slightly higher fluxes from never flooded (i.e. upland, 255 ± 90 mmol.m<sup>-2</sup>.day<sup>-1</sup>) and saturated soils (i.e. lowland, 248 ± 169 mmol.m<sup>-2</sup>.day<sup>-1</sup>) than from soils which were flooded during high water level (i.e. midland, 192 ± 118 mmol.m<sup>-2</sup>.day<sup>-1</sup>). Diffusive CO<sub>2</sub> fluxes were not correlated with the soil moisture contents (Figure 5.7). Soil temperature ranged similarly for all the soils between 24.4 to 34.7°C, and CO<sub>2</sub> fluxes were not linked with soil temperature (data not shown).

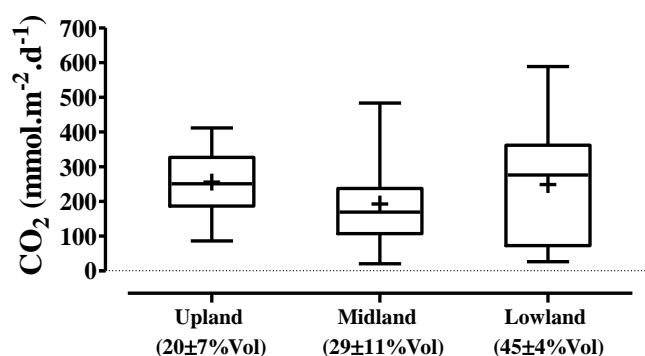


Figure 5.7. CO<sub>2</sub> fluxes from soils of three zones defined in the drawdown area. Average soil moisture content (in % Vol) is indicated for each zone.

Time series of monthly area-weighted average diffusive CO<sub>2</sub> fluxes is shown in Figure 5.8a. For the estimate of CO<sub>2</sub> fluxes from the drawdown area before the first full impoundment, value of the net ecosystem production (NEP) was considered as reported in Luysaert et al, 2007 for different kind of forests (-403 ± 102 gC.m<sup>-2</sup>.year<sup>-1</sup>). CO<sub>2</sub> fluxes from the water surface were estimated at sampling station located in the pristine inflowing

tributaries Nam Xot, Nam Theun and Nam On. We estimated an average annual CO<sub>2</sub> flux of  $9393 \pm 9403 \text{ gCO}_2\text{-}^2\text{.year}^{-1}$  from the water surface without considering the seasonal variability in CO<sub>2</sub> fluxes. For the swamp area,  $1963 \pm 2164 \text{ gCO}_2\text{-}^2\text{.year}^{-1}$  was considered (Jauhiainen et al, 2005; Hirano et al, 2007). For agricultural land,  $-1710 \pm 927 \text{ gCO}_2\text{-}^2\text{.year}^{-1}$  were used (measured by eddy covariance, Chapter 7). Depending on the reservoir water level, proportional areal converge of different ecosystems was applied to calculate the area-weighted average CO<sub>2</sub> exchange from the drawdown area before the first full impoundment of the reservoir in October 2009 (Figure 5.8a, b).

After the first full impoundment of the reservoir in October 2009, field observations suggested that there were no vegetation left in the drawdown area, i.e. no carbon uptake during photosynthesis activities. Therefore, measured diffusive CO<sub>2</sub> fluxes from the soils were used to calculate the area-weighted average fluxes from the drawdown area. For extrapolation purpose, the whole drawdown area was divided into upland, midland 1, midland 2, and lowland zones. Assumptions and details of the defined zones have been discussed in Chapter 2 and Chapter 4.

In the beginning of flooding, drawdown area was a net sink of CO<sub>2</sub> (Figure 5.8a). After full-impoundment, monthly area-weighted average CO<sub>2</sub> diffusive rates were more or less constant, around  $250 \text{ mmol.m}^{-2}\text{.day}^{-1}$  (Figure 5.8a). Corresponding area weighted exchanges were multiply by the surface area of the drawdown to calculate the net CO<sub>2</sub> exchange (Figure 5.8b). After full impoundment of NT2, the maximum monthly emission ( $83.6 \pm 34 \text{ Gg CO}_2\text{.month}^{-1}$ ) was observed in June 2011 (dry season) when the area of soil exposed to air was at its maximum ( $275 \text{ km}^2$ ) for the first time after full impoundment. On an annual basis, total CO<sub>2</sub> emissions from the drawdown area were  $324 \pm 48$  and  $243 \pm 48 \text{ Gg CO}_2\text{.year}^{-1}$  for 2010 and 2011, respectively.

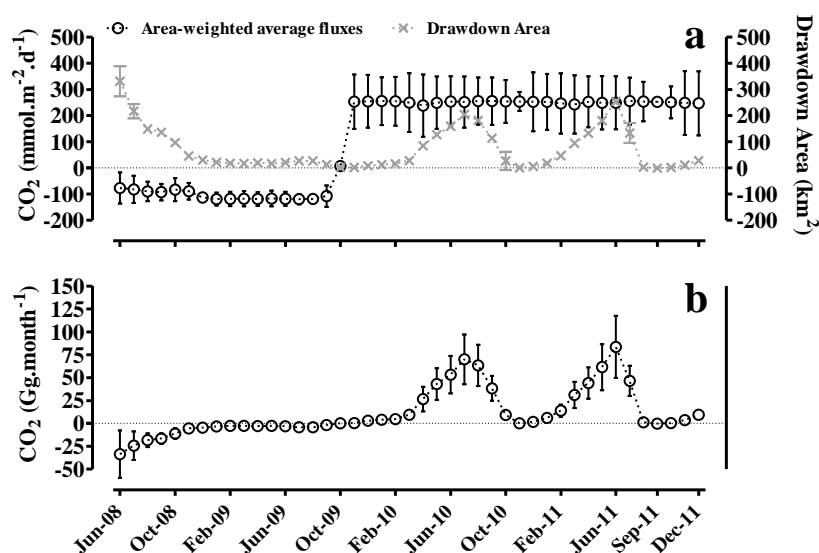


Figure 5.8. Times series of diffusive CO<sub>2</sub> fluxes from the drawdown area at NT2 hydroelectric reservoir.



## 5.2.7. Emissions from downstream

### 5.2.7.1. Degassing

In the NT2 hydroelectric system, there were five degassing sites, four continuous: at the outlet of the Nakai Dam, below the turbines, below the Regulating Pond Dam, and at the Aeration Weir, and one occasional: from spillway release. Monthly degassing of CO<sub>2</sub> at each of these sites was estimated by multiplying the difference between monthly averaged CO<sub>2</sub> concentrations in the incoming and outgoing water, by the average monthly water discharge through the relevant structures. Figure 5.9 shows time series of monthly total continuous degassing (sum of degassing from the continuous releases) and occasional releases (spillway). Along the year, both continuous and occasional CO<sub>2</sub> degassing varied by 2 orders of magnitude between the dry and the wet seasons. Even if water discharge varies seasonally, the CO<sub>2</sub> degassing varies during the year with the lowest values occurring after the rainy period (November-January, in Figure 5.9) when the CO<sub>2</sub> concentrations were the lowest in the released water. The highest degassing occurred at the very end of the dry season (April-July in Figure 5.9) when the CO<sub>2</sub> concentrations were the highest. At the turbine outlet, daily degassing emission was maximum in the warm dry season with  $82 \pm 63$  Mg(CO<sub>2</sub>), whereas daily degassing emission dropped to  $12 \pm 1$  Mg CO<sub>2</sub> in the cold dry season. . Maximum daily degassing emissions at outlet of regulating pond and aeration weir were respectively  $73 \pm 56$  and  $74 \pm 67$  Mg CO<sub>2</sub> in the late warm dry season.

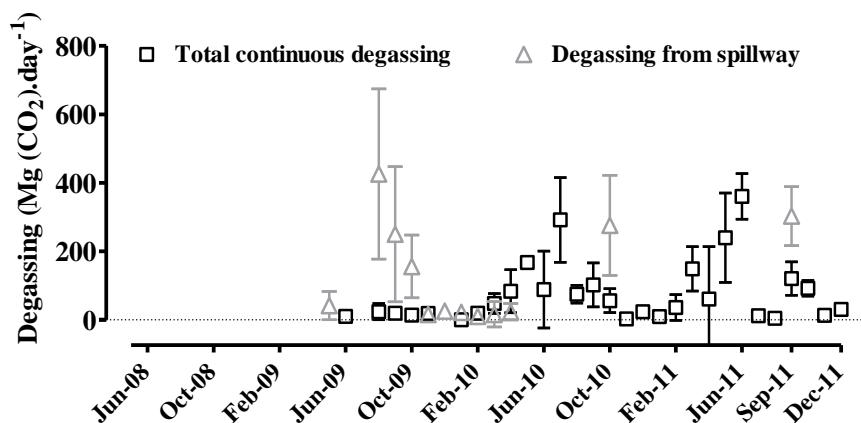


Figure 5.9. Evolution of degassing emissions of CO<sub>2</sub> over time.

It has been observed that during infrequent (and for a short time) high release of water from the spillway in the wet season, up to  $425 \pm 326$  Mg CO<sub>2</sub>.day<sup>-1</sup> could be emitted to the atmosphere. Sometime high increase in CO<sub>2</sub> concentration after the turbine was observed, this is compensated by a decrease in IC concentration between upstream and downstream concentrations. Therefore, the degassing, if any, was probably not significant.

The lower degassing at turbines outlet could be principally due to turbulent mixing before the turbine intake. Further, the turbines discharge is released underneath the water surface level and discharge at the Regulating Pond is released from the bottom sluices. This is likely to reduce turbulence/eddy-formation and subsequently, the degassing efficiency (6-

8%). On the opposite, the well in purpose designed U-shape Aeration Weir (L = 200 m, H = 4.7 m, and as wide as the artificial downstream channel) exhibits slightly higher degassing efficiency (18%). Degassing efficiency at Nakai Dam is around 54%, as the released water creates very high turbulence due to the height of release.

### 5.2.7.2. Diffusive fluxes

The remaining discharge of dissolved CO<sub>2</sub>, not released by degassing is transported downstream, and gradually released to the atmosphere by diffusion. Owing to presence of different kind of civil structures downstream of the powerhouse, we divided this area in four sections (for details see Chapter 2). Monthly CO<sub>2</sub> diffusive emissions in those four sections downstream of the powerhouse and the Nakai Dam are shown in Figure 5.10. Diffusive CO<sub>2</sub> emissions show strong seasonal variations. Diffusive emissions till the section 3 were at their maximum in the late warm dry season (March to July in Figure 5.10), when the CO<sub>2</sub> concentrations were at its maximum, and were at their minimum in the cold dry season (October to January in Figure 5.10).

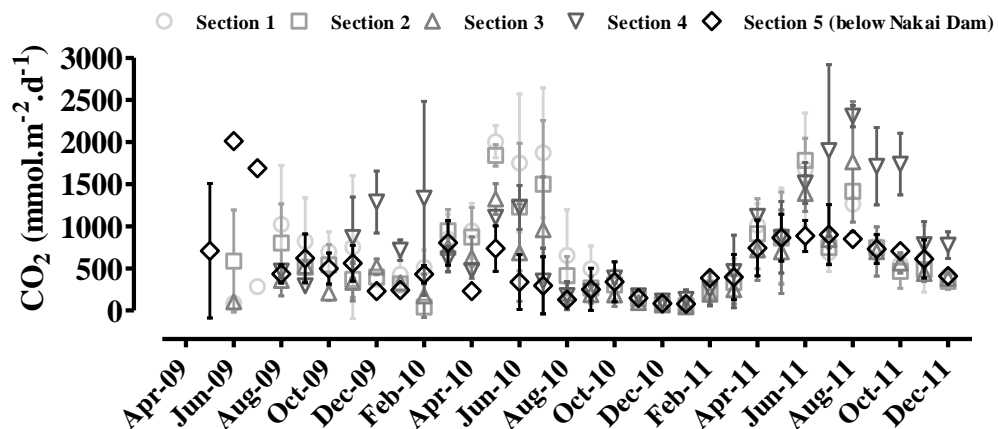


Figure 5.10. Times series of diffusive CO<sub>2</sub> fluxes downstream of NT2 reservoir.

Downstream of the powerhouse, CO<sub>2</sub> diffusive fluxes ranged from 79 to 2919 mmol.m<sup>-2</sup>.day<sup>-1</sup> in section 1. Due to high inflow from the tributaries in the wet season, downstream of the power house receive CO<sub>2</sub>-poor water and therefore, CO<sub>2</sub> fluxes dropped to 307±247 mmol.m<sup>-2</sup>.day<sup>-1</sup> in the cold dry season. CO<sub>2</sub> Fluxes were more or less in the same range with a small decrease along a 12 km-stretch (i.e. section 1 and section 2). CO<sub>2</sub> production from CH<sub>4</sub> oxidation probably compensated the diffusive loss of CO<sub>2</sub> in these sections. In section 3, the CO<sub>2</sub> fluxes were very close to the level observed in the pristine inflowing tributaries with seasonal averages of 693±429 mmol.m<sup>-2</sup>.day<sup>-1</sup>, 707±570 mmol.m<sup>-2</sup>.day<sup>-1</sup> and 225 ± 197 mmol.m<sup>-2</sup>.day<sup>-1</sup> respectively for the warm dry, the wet and the cold dry seasons. After 30 km, in the end of the section 3 at DCH4, CO<sub>2</sub> fluxes dropped significantly due to aeration weir in the section 3. Owing to high CO<sub>2</sub> inputs from the Xe Bang Fai River, CO<sub>2</sub> fluxes increased in the section 4. In the Nam Theun River (section 5 in Figure 5.10), downstream of the Nakai Dam, diffusive CO<sub>2</sub> fluxes ranged from 17 to 1415 mmol.m<sup>-2</sup>.day<sup>-1</sup>,

with seasonal average of  $640 \pm 336$ ,  $503 \pm 383$  and  $313 \pm 243$   $\text{mmol.m}^{-2}.\text{day}^{-1}$  for the warm dry, the wet and the cold dry season respectively.

In the first 30 km downstream from the turbines, the area-weighted diffusive  $\text{CO}_2$  fluxes are  $609 \pm 445$   $\text{mmol.m}^{-2}.\text{day}^{-1}$ , which is around two thirds lower than the value reported by Abril et al. (2005) for the first 40 km of the Sinnamary river downstream of the Petit Saut Dam ( $950$   $\text{mmol.m}^{-2}.\text{day}^{-1}$ ). These fluxes are two thirds higher than those reported by Kemenes et al. (2011) for the first 30 km of the Uatumã River downstream of the Balbina Dam,  $400$   $\text{mmol.m}^{-2}.\text{day}^{-1}$ .

Monthly diffusive  $\text{CO}_2$  emissions downstream of the powerhouse and the Nakai Dam were derived by multiplying the areal diffusive rate of given section by the surface area of corresponding section (Figure 5.11). The highest  $\text{CO}_2$  emissions occurred during periods between the warm-dry and the wet seasons (Figure 5.11), whereas lowest  $\text{CO}_2$  emissions occurred during the cold dry season.

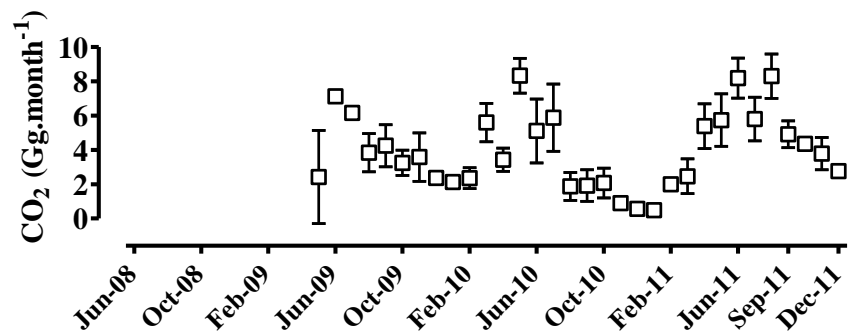


Figure 5.11. Time series of downstream diffusive  $\text{CO}_2$  fluxes.

### 5.3. Discussion

#### 5.3.1. Dissolved $\text{CO}_2$ and physico-chemical parameters

Our study shows that all nine sampling stations at the NT2 reservoir are predominately supersaturated, and in general sources of  $\text{CO}_2$  to the atmosphere. Lower concentrations of  $\text{CO}_2$  in the epilimnion than in the hypolimnion can be explained by the evasion that occurs at the air-water interface and photosynthesis activity in upper water column of the reservoir. Our results suggest that the shapes of the vertical profiles depend on the physical and hydrodynamical conditions in the water column (Figure 5.1).

In bottom waters, positive correlation coefficients between dissolved  $\text{CO}_2$  and carbon species suggest a dependency of heterotrophic pelagic and benthic respiration on availability of main substrates, i.e. organic carbon. Positive relationship between dissolved  $\text{CO}_2$  and, total nitrogen and ammonium concentrations suggests a positive feedback of nutrients on biogenic heterotrophic respiration. High dissolved  $\text{CO}_2$  with high conductivity might indicate high bacterial activities.

Surface CO<sub>2</sub> concentrations were negatively correlated ( $r^2 = -0.2$ ) with secchi depth and euphotic layer depth, indicating consumption of CO<sub>2</sub> in the euphotic layer during photosynthesis activity. Negative correlation ( $r^2 = -0.4$ ) of CO<sub>2</sub> concentration with O<sub>2</sub> saturation in the surface water could also suggest production of O<sub>2</sub> and consumption of CO<sub>2</sub> during photosynthesis in the euphotic layer of epilimnion water column. Higher *chlorophyll a* and DOC concentration in the surface water than in the hypolimnion water suggest that organic matter produced during the photosynthesis releases DOC in the water column. However, even if primary production could lower significantly the CO<sub>2</sub> concentration in the epilimnion, no CO<sub>2</sub> absorption was observed at the NT2 reservoir surface.

Low concentration of CO<sub>2</sub> and other physico-chemical parameters during the wet season reveals dilution because of high water inputs. Further, lowering bottom temperature could also decrease the respiration and decomposition rates. During the warm dry season, increasing bottom temperature and low water inputs builds up high concentrations in the hypolimnion. During the warm dry season, CH<sub>4</sub>/CO<sub>2</sub> ratios in the hypolimnion were higher than in the wet season suggesting a shift toward methanogenesis probably due to higher temperature and complete anoxia at the reservoir's bottom.

The spatial variability among sampling stations is probably linked to pre-impoundment landscape. The higher bottom CO<sub>2</sub> concentrations at RES3 and RES5 sampling stations is most likely linked with high soil organic matter and therefore high CO<sub>2</sub> production rates (Table 5.2). It seems that high photosynthesis activities reduce CO<sub>2</sub> concentration in surface water at these sampling stations since high DOC and *chlorophyll a* concentration were observed on in the surface water at RES3 and RES5. Further, hydrological and physical conditions are expected to vary substantially among different parts of the reservoir. For example RES7 and RES8 sampling station are more prone to be affected by river water inflows than other sampling station. On the other hand, RES3 is located in an isolated area and receive very low influence from the main river inflow. Accurate estimates of physical and hydrological conditions for specific areas are difficult to obtain without additional data. In the warm dry season, owing to the mixing of CO<sub>2</sub>-rich hypolimnion water and epilimnion water before the turbine intake, RES9 exhibited the highest surface CO<sub>2</sub> concentration after the starting of turbines. To conclude, CO<sub>2</sub> concentrations in the water column of the NT2 reservoir are jointly regulated by physical and biological processes: temperature, uptake of CO<sub>2</sub> photosynthesis, supply of CO<sub>2</sub> from the pelagic and benthic decomposition of the carbon, and physico-hydrodynamical mixing of the water column.

### **5.3.2. Estimates of different components of gross CO<sub>2</sub> emissions**

Monthly estimates of the different components of gross CO<sub>2</sub> emissions to the atmosphere from the whole NT2 system since May 2009 till December 2011 are depicted in Figure 5.12. Diffusion from the reservoir water surface has been the main source of CO<sub>2</sub> emissions and can contributed up to > 95% of the total monthly emissions (Figure 5.12). Interestingly, as matter of fact, during the low water periods in the dry seasons, CO<sub>2</sub> emissions from the drawdown soils can contribute up to 50% of the total monthly emissions.

Rest of the emission pathways i.e. bubbling and downstream emissions contributed relatively a little (< 10%) to the total monthly emissions.

Annual estimates of the different components of gross CO<sub>2</sub> emissions to the atmosphere for the years 2010 and 2011 are summarized in Table 5.3. Results for the year 2010 and 2011 show that diffusive emission from the reservoir water surface (68-77%) was the main contributor to total CO<sub>2</sub> emissions from the NT2 reservoir. Our results suggest that the drawdown area, when it represents a large portion of the reservoir surface like in NT2, can be a significant source of carbon (16-25% of total annual CO<sub>2</sub> emissions). CO<sub>2</sub> bubbling emission was negligible because of its high solubility (Abril et al., 2005). Downstream emissions, including both degassing and diffusive emissions, contributed around 7% of the total CO<sub>2</sub> emissions, a percentage lower than values reported for other reservoirs (Abril et al., 2005; Kemenes et al., 2007). This lower downstream emission percentage is linked to the turbulent mixing and thereby outgassing before the turbine intake

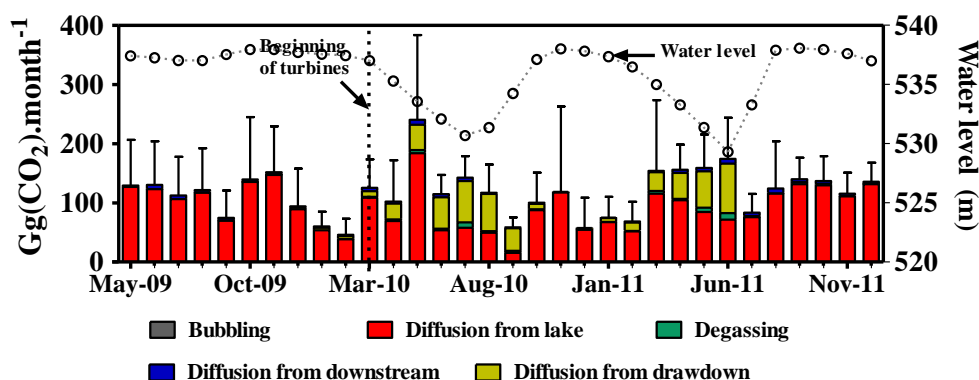


Figure 5.12. Time series of the monthly CO<sub>2</sub> emissions from the whole NT2 system. Figure shows each individual pathway (bubbling, degassing, diffusion from the lake, diffusion from downstream and diffusion from drawdown area).

Table 5.3. Estimates of gross CO<sub>2</sub> emissions (in GgCO<sub>2</sub>.year<sup>-1</sup>) from the NT2 hydroelectric reservoir for the years 2010 and 2011. Percentages between brackets represent the proportion of each component to the total annual emission.

Years	Diffusive emission from drawdown area	Bubbling	Diffusive emission from reservoir water surface	Degassing	Diffusive emission from downstream	Total
2010	324 ± 48 (25%)	Negligible	892 ± 239 (68%)	51 ± 7.7(4%)	40 ± 3.5 (3%)	1307 ± 243
2011	243 ± 48 (16%)	Negligible	1192 ± 191 (77%)	62 ± 7.5(4%)	54 ± 3.4 (3%)	1551 ± 197

Total annual CO<sub>2</sub> emissions for the NT2 hydroelectric system, including emissions from the reservoir water surface, drawdown area, degassing facilities and downstream for 2010 and 2011 were respectively 2.9 ± 0.5 and 3.4 ± 0.4 Gg CO<sub>2</sub>.km<sup>-2</sup>.year<sup>-1</sup>, similar to the

gross CO<sub>2</sub> emissions estimated for Petit Saut reservoir for first (1994) and second (1995) years after impoundment (3.4 and 3.7 Gg CO<sub>2</sub>.km<sup>-2</sup>.year<sup>-1</sup>; Abril et al., 2005). However, 18 years after its impoundment, Balbina reservoir was still emitting 5.2 Gg CO<sub>2</sub>.km<sup>-2</sup>.year<sup>-1</sup> (Kemenes et al., 2011). One should note that emissions from the drawdown area were not assessed in any of these studies. Taking into consideration this latter pathway would lead to higher (up to one fourth) total CO<sub>2</sub> emissions.

The estimate of gross CO<sub>2</sub> emissions for the year 2010 was a bit lower than the 2011 ones. This is consistent with previous studies in a tropical reservoir where CO<sub>2</sub> emissions increased during first 3 years (Abril et al., 2005). The initial CO<sub>2</sub> emission rates tend to decline in the years after flooding (St. Louis et al., 2000; Teodoru et al., 2010; Tremblay et al., 2005). At NT2 reservoir, it can be expected that after the trophic-upsurge occurring in the year 2011, gross CO<sub>2</sub> emissions would decline as observed at Petit Saut reservoir (Abril et al., 2005). The initial exponential decline in total CO<sub>2</sub> emissions is driven primarily by the patterns of decomposition of surface plant biomass, whereas at later stages, emission is increasingly dominated by sediment and pelagic respiration, which decline in time at a slower rate (Barros et al., 2000; St. Louis et al., 2000; Teodoru et al., 2010; Tremblay et al., 2005).

### 5.3.3. Tentative carbon budget for the years 2010 and 2011

Tentative CO<sub>2</sub> and carbon budgets for the year 2010 and 2011 are presented in Table 5.4, which includes carbon supply from the watershed, internal cycling of carbon (CH<sub>4</sub> oxidation and photosynthesis activities), carbon emissions (gross CH<sub>4</sub> and gross CO<sub>2</sub> emissions from the reservoir water surface, the drawdown area and the downstream), and carbon export downstream the reservoir. Estimates of CO<sub>2</sub> emissions (Table 5.3) and CH<sub>4</sub> emissions (Chapter 4) have been converted into carbon equivalent. Estimate of the carbon inflow was from the major pristine inflowing tributaries, whereas export of carbon was calculated downstream of the Nakai Dam (NTH3) and at the powerhouse (TRC1). Assuming a methanotrophic bacterial growth efficiency (BGE) of 50%, aerobic CH<sub>4</sub> oxidation corresponds to a CO<sub>2</sub> production of 24 ± 4 GgC.year<sup>-1</sup> and 50 ± 12 GgC.year<sup>-1</sup> for the years 2010 and 2011, respectively (Chapter 4). BGE varies between 5% and 80% among different lakes and seasons in the boreal environment (Bastviken et al., 2003). This estimate is therefore highly dependent on the assumption on BGE that is not documented at the NT2 hydroelectric system. Primary production (PP) was estimated using the published relationship between *Chlorophyll a* concentration (mg.m<sup>-3</sup>) and volumetric rates of PP (mgC.m<sup>-3</sup>.d<sup>-1</sup>) described in del Giorgio and Peters (1993) for lakes worldwide (PP = 10.3 × Chl<sup>1.19</sup>). Those rates were converted into areal rates (mgC.m<sup>-2</sup>.d<sup>-1</sup>) by multiplying the volumetric PP with the depth of the euphotic zone. Following this methodology, annual consumptions of CO<sub>2</sub> during photosynthesis activities 116 GgC.year<sup>-1</sup> and 71 GgC.year<sup>-1</sup> were calculated for the years 2010 and 2011, respectively.

The sums of annual CO<sub>2</sub> import, CO<sub>2</sub> emissions, CO<sub>2</sub> consumption during photosynthesis, supply from CH<sub>4</sub> oxidation and export were 365 ± 75 and 370 ± 70 GgC.year<sup>-1</sup> for year 2010 and 2011 respectively. These values are close to the annual average CO<sub>2</sub>

production in the flooded soil ( $324$  and  $328 \text{ GgC}\cdot\text{year}^{-1}$  for year 2010 and 2011 respectively, Table 5.4).

For year 2010, annual total carbon inputs from the watershed were around  $39 \pm 16 \text{ Gg C}\cdot\text{year}^{-1}$ , with a total gaseous carbon inputs around  $8.0 \pm 0.6 \text{ Gg C}\cdot\text{year}^{-1}$ . Around two thirds of the total carbon inputs ( $20.6 \pm 12.6 \text{ Gg C}\cdot\text{year}^{-1}$ ) contributed in the form of inorganic carbon. In year 2011, annual carbon input from watershed was almost double ( $72 \pm 20 \text{ Gg C}\cdot\text{year}^{-1}$ ) than of year 2010, with a significant amount of input as  $\text{CO}_2$  ( $26 \pm 1.6 \text{ Gg C}\cdot\text{year}^{-1}$ ). Around  $63.6 \pm 9.9 \text{ Gg C}\cdot\text{year}^{-1}$  and  $70 \pm 12 \text{ Gg C}\cdot\text{year}^{-1}$  were exported downstream for years 2010 and 2011. This is twice the carbon inputs from the watershed, and an amount equal to the carbon input in the year 2011.

Total atmospheric carbon emissions from the reservoir were  $378 \pm 89 \text{ GgC}\cdot\text{year}^{-1}$ , and around  $437 \pm 72 \text{ GgC}\cdot\text{year}^{-1}$  for year 2010 and 2011 respectively. In overall for the years 2010 and 2011,  $\text{CO}_2$  contributed for around 95% of the total atmospheric carbon emissions, whereas  $\text{CH}_4$  contributed for only 5%. Figure 5.13 show the carbon balance for the year 2010. For the year 2010, comparison between total supply of carbon from the watershed is compared with the total carbon release (i.e. emissions to atmosphere and export to the downstream) suggest that around 90% of the carbon release was fuelled by the supply from the bottom of reservoir. The annual carbon balance calculation indicates that this reservoir was a carbon source with an annual carbon export (atmosphere + downstream river) of about  $401 \pm 120 \text{ GgC year}^{-1}$  and  $437 \pm 108 \text{ GgC year}^{-1}$  for year 2010 and 2011 respectively. A total of about  $5100 \pm 700 \text{ GgC}$  has been flooded in the uppermost 30 cm of the NT2 reservoir area during the impoundment (Descloux et al., 2011). This flooded carbon stock includes  $2200 \text{ GgC}$  and  $2900 \text{ GgC}$  for respectively above ground and belowground biomass and soil organic carbon (Descloux et al., 2011). This component of the soil carbon is supposed to be transformed following the flooding and, therefore the most probable source of soil organic carbon to the reservoir in the initial years following impoundment. An additional organic matter from below 30 cm depth soils can be expected to be available over long time periods (i.e. decades). Our results suggest that within first two years after flooding of NT2 reservoir, a significant amount of carbon has been released which corresponds to around 15% of the total flooded carbon in above ground biomass and in upper 30 cm soil layer.

In newly flooded reservoirs, such as NT2,  $\text{CO}_2$  is derived from the decomposition during impoundments of flooded organic matters from vegetation and soils (Abril et al., 2005; Galy-Lacaux et al., 1999; Guérin et al., 2008a). The most labile components of flooded organic matters (tree crowns, palms, vines, seedlings, litters/root mat) are believed to be decomposed quickly and likely to be the source of organic carbon for the reservoir in the years immediately following the impoundment. Meanwhile, the most refractory flooded materials (trunks or ligneous matters) and isolated components can be released to the reservoir over the following decades (Campo and Sancholuz, 1998).

Table 5.4: CH<sub>4</sub>, CO<sub>2</sub> and Carbon budget for the years 2010 and 2011 at the NT2 Reservoir (all values given in GgC.year<sup>-1</sup>)

Year		CH <sub>4</sub>		CO <sub>2</sub>		Inorganic Carbon		Total organic carbon	
		2010	2011	2010	2011	2010	2011	2010	2011
Production <sup>a</sup>	Stabilized	32	33	140	141				
	Average	62	65	324	328				
	Maximum	108	105	630	637				
Input		0.08 ± 0.01	0.05 ± 0.05	8 ± 0.6	26 ± 1.6	20.6 ± 12.6	32.7 ± 14.4	10.1 ± 3.2	13 ± 3.6
Methane oxidation <sup>b</sup>		-48 ± 8	-100 ± 24	24 ± 4 <sup>c</sup>	50 ± 12 <sup>c</sup>				
Primary production <sup>d</sup>				-116	-71				
Emissions <sup>e</sup>	Bubbling	-11 ± 1	-9.5 ± 0.8						
	Diffusion from lake	-5 ± 6	-2.2 ± 2.6	-243 ± 65	-325 ± 52				
	Diffusion from drawdown area	-0.5 ± 0.5	-0.7 ± 0.6	-88 ± 13	-66 ± 13				
	Degassing	-5 ± 0.5	-1.7 ± 0.2	-14 ± 2	-17 ± 2				
	Diffusion from downstream	-0.8 ± 0.2	-0.2 ± 0.1	-11 ± 1	-15 ± 1				
Export to downstream <sup>f</sup>		-0.1 ± 0.01	-0.01 ± 0.01	-11 ± 1.1	-20 ± 1.1	-34.7 ± 7.8	-32.8 ± 9.4	-17.8 ± 1	-17.3 ± 2.1
Change in storage		-1.1 ± 0.7	0.7 ± 0.7	-2.8 ± 1.6	1.3 ± 0.7	2.2 ± 1.5	-1.0 ± 1.7	2.9 ± 0.6	-2.6 ± 0.7
<b><i>Annual carbon release (downstream + atmosphere)</i></b>								<b><i>-401 ± 120</i></b>	<b><i>-437 ± 108</i></b>

<sup>a</sup>Production obtained from surface (upper 20 cm layer) and subsurface (between 20 to 120 cm deep layers) soils using the area-weighted average production rates over a period of one year.

<sup>b</sup>Pelagic aerobic methane oxidation in the reservoir and oxidation downstream of the reservoir.

<sup>c</sup>Calculated assuming a bacterial growth efficiency of 50% for CO<sub>2</sub> production by aerobic CH<sub>4</sub> oxidation.

<sup>d</sup>Primary production in the euphotic layer.

<sup>e</sup>Emissions from all the major pathways at NT2 Reservoir.

<sup>f</sup>Export from downstream releases at the Nakai Dam and the powerhouse.



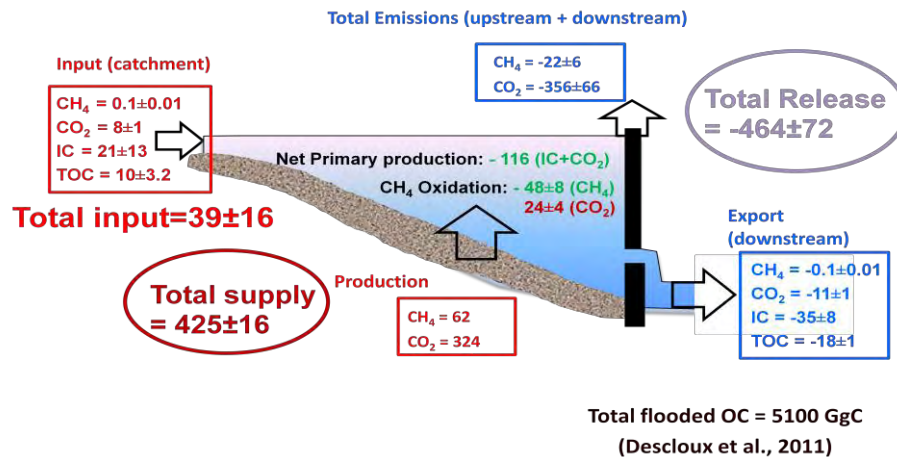


Figure: 5.13. CH<sub>4</sub>, CO<sub>2</sub> and carbon budget for the year 2010 at the NT2 Reservoir (all values given in GgC.year<sup>-1</sup>).

#### 5.4. Conclusion

Our results suggest that CO<sub>2</sub> emissions from upstream of the dam (drawdown area, diffusion from the reservoir water surface) contribute to around 93% of the gross CO<sub>2</sub> emissions for the year 2010 and 2011, while 7% come from downstream (degassing and diffusion) emissions. Our results suggest that most of the CO<sub>2</sub> is emitted through diffusive pathway from reservoir water surface and secondly from the drawdown area. Compared to upstream emissions, downstream CO<sub>2</sub> emissions are lower because of physical dynamics and structural design of the NT2 hydroelectric system which generates a physical mixing of the hypolimnetic and epilimnetic waters and thereby outgassing of CO<sub>2</sub> before the turbine intakes.

Results suggest that around 95% of atmospheric carbon is emitted as CO<sub>2</sub>, and only 5% as CH<sub>4</sub>. The annual carbon balance calculation indicates that this reservoir was a carbon source with an annual carbon release (atmosphere + downstream river) of about 401 ± 120 Gg C year<sup>-1</sup> and 437 ± 108 Gg C year<sup>-1</sup> for year 2010 and 2011 respectively. Import and export balance reveals that around 95% of total annual carbon export is fuelled by organic carbon flooded at the bottom of the reservoir during impoundment. Our results suggest that carbon release in the first two years after flooding of the NT2 Reservoir corresponds around 15% of initial total flooded organic carbon in the above ground biomass and in a upper 30 cm soil layer.



## Chapter 6

# Nitrous oxide (N<sub>2</sub>O) dynamics and gross atmospheric emissions

---

**Abstract:** Dynamics of nitrous oxide (N<sub>2</sub>O), along with inorganic nitrogen compounds i.e. ammonium (NH<sub>4</sub><sup>+</sup>), nitrate (NO<sub>3</sub><sup>-</sup>) and nitrite (NO<sub>2</sub><sup>-</sup>) have been studied in a newly flooded subtropical hydroelectric reservoir (impounded in 2009), Nam Theun 2 (NT2), in Lao PDR, Asia. The atmospheric gross N<sub>2</sub>O emissions were quantified for the first two years after full-impoundment. The main quantified pathways of N<sub>2</sub>O emission included diffusion from the reservoir water surface, downstream emissions (diffusion and degassing) and emissions from the drawdown area (up to 275 km<sup>2</sup> for a 450 km<sup>2</sup> in the case of NT2). We found that seasonal variation in the N<sub>2</sub>O emissions was stronger than spatial one. An important parameter affecting N<sub>2</sub>O concentration in the reservoir was rainfall inflow from the watershed, inducing a hot moment of high N<sub>2</sub>O concentration in the wet season and thereby N<sub>2</sub>O fluxes of up to  $191 \pm 335 \mu\text{mol.m}^{-2}.\text{day}^{-1}$  while the mean daily flux was 10 times lower ( $19 \pm 17 \mu\text{mol.m}^{-2}.\text{day}^{-1}$ ). In addition to significant N<sub>2</sub>O inputs from watershed in the wet season, it seems that flooding of drawdown area during the water level rising facilitates the denitrification process in the littoral soils which contributes to N<sub>2</sub>O concentrations. Further, at the same time, hydrodynamical mixing of NH<sub>4</sub><sup>+</sup>-rich hypolimnetic water and oxygenated epilimnetic water during the wet season could also lead to enhanced nitrification and high N<sub>2</sub>O emissions. Results show that up to 60% of the diffusive emissions from the reservoir water surface and downstream occurred in the high water inflow from watershed in the wet season (June-September).

This study represents the first assessment of N<sub>2</sub>O emission from drawdown area and revealed that the zone between upland and water saturated lowland was a significant hot spot of N<sub>2</sub>O emissions, with a mean flux of  $590 \pm 507 \mu\text{mol.m}^{-2}.\text{day}^{-1}$ . Whereas, other parts of the drawdown area emitted around four times lower and had a mean of  $162 \pm 227 \mu\text{mol.m}^{-2}.\text{day}^{-1}$ .

Our results for the major quantified emissions pathways reveal that NT2 reservoir was a source of N<sub>2</sub>O and emitted around  $312 \pm 544$  and  $366 \pm 571$  Mg of N<sub>2</sub>O respectively during the years 2010 and 2011. N<sub>2</sub>O emissions from the drawdown area represent around 53-69% of the total annual N<sub>2</sub>O emissions from the whole NT2 hydroelectric system. The remainder by and large (26-44%) comes from the reservoir water surface via diffusive fluxes. Our results suggest that considering the drawdown area while making N<sub>2</sub>O emissions inventory is essential, whereas downstream and ebullitive emissions are non-significant.

### 6.1. Introduction

Nitrous oxide (N<sub>2</sub>O) is the third major radiatively active greenhouse gas contributing to global warming (IPCC, 2007). Atmospheric concentration of N<sub>2</sub>O, which can alter the Earth's climate, has risen dramatically since industrialization. Hence, this has resulted in an urgent need for process-based understanding of the main factors influencing the emissions of N<sub>2</sub>O from various anthropogenic activities.

Studies on N<sub>2</sub>O emissions have been exclusively carried out on the terrestrial ecosystems (Andersson et al., 2003; Bremner, 1997; Cardenas et al., 1993; Conen et al.,

2000; Davidson, 1995; Groffman et al., 2000; Hou et al., 2000; Keller et al., 1986; McSwiney et al., 2001; Schindlbacher et al., 2004; Smith et al., 1998; Zheng et al., 2000). Even though, significant N<sub>2</sub>O emissions have been reported from N-rich freshwaters (Chen et al., 2010; García-Ruiz et al., 1999; Garnier et al., 2009; Hendzel et al., 2005; Kroeze et al., 2010; Liu et al., 2011; McCrackin and Elser 2011; McMahon and Dennehy, 1999; Stow et al., 2005; Wang et al., 2009), N<sub>2</sub>O emissions from inland aquatic systems have received less attention.

In last decades, many studies have revealed that hydroelectric reservoirs are responsible for significant GHG emissions to the atmosphere, though different estimates of GHG emissions have been reported (Barros et al., 2011; St. Louis et al., 2000). As a matter of fact, none of these estimates have included N<sub>2</sub>O emissions from the hydroelectric reservoirs, when numerous studies were devoted to CO<sub>2</sub> and CH<sub>4</sub> emissions in both boreal or temperate region (Chen et al., 2011; DelSontro et al., 2010, Diem et al., 2012; Demarty et al., 2011; Teodoru et al., 2010), and tropical or subtropical areas (Abril et al., 2005; Chanudet et al., 2011; DelSontro et al., 2011; Galy-Lacaux et al., 1997; Galy-Lacaux et al., 1999; Guérin et al., 2007; Kemenes et al., 2007, 2011; Roland et al., 2010).

Owing to high global warming potential of N<sub>2</sub>O (298 times that of CO<sub>2</sub>, IPCC 2007), and to stratospheric ozone depletion, the increasing concentrations of N<sub>2</sub>O in the atmosphere have received considerable attention (e.g., IPCC 2007; Ravishankara et al., 2009; Wuebbles, 2009). But there is little known about how existing and newly constructed hydroelectric reservoir are impacting current atmospheric N<sub>2</sub>O concentrations. Relatively few direct studies investigating N<sub>2</sub>O dynamics in hydroelectric reservoirs have suggested that hydroelectric reservoirs are not significant source of N<sub>2</sub>O compare to CO<sub>2</sub> and CH<sub>4</sub> (Diem et al., 2012; Guerin et al., 2008b; Hendzel et al., 2005; Huttunen et al., 2003a, 2003b; Lima et al., 2002; Liu et al., 2011). It is important to note that most of the studies of N<sub>2</sub>O dynamics in the reservoirs have been conducted in the Northern Hemisphere in temperate and boreal climates, and that data for regions such as tropics are lacking, whereas these regions hold most of the remaining global hydropower potential (Kumar et al., 2012). Further, it is however still unclear if N<sub>2</sub>O emission from tropical reservoirs is an environmental issue, because data are sparse and the contribution of fluxes downstream of the dams and drawdown area are not documented.

N<sub>2</sub>O is produced as an intermediate product during nitrification and denitrification (Bouwman et al., 1995). Nitrification is an oxidative aerobic process, i.e. it needs the availability of molecular O<sub>2</sub>, during which NH<sub>4</sub><sup>+</sup> is oxidized to NO<sub>2</sub><sup>-</sup> and NO<sub>3</sub><sup>-</sup>. In contrast, denitrification is a reductive anaerobic process, i.e. it takes place in O<sub>2</sub>-depleted zones. These processes are primarily controlled by temperature, pH, O<sub>2</sub> level, inorganic N, and the shift of oxic-anoxic interface (Garnier et al., 2006; Hendzel et al., 2005; Mengis et al., 1997; Stow et al., 2005).

Both nitrification and denitrification can take place concurrently in complex soil microsites with different access to O<sub>2</sub>. The continuous cycle of flooding and draining of soils affects important soil parameters such as their O<sub>2</sub> content, pH, and redox potential and

thereby modulates the biogeochemical processes involved in production and emissions of N<sub>2</sub>O (Baldwin and Mitchell, 2000). This hydrological pulse effect is well known in systems influenced by anthropogenic input of nitrogen, where hotspots or hot moments (McClain et al., 2003) of N<sub>2</sub>O emissions are induced by temporal and spatial oxic-anoxic transitions as reported for marches (Hernandez and Mitsch, 2006), agricultural soil (Markfoged et al., 2011), mangrove sediment (Allen et al., 2007) and tropical wetland soils (Lienggaard et al., 2013). Hot spots often occur where hydrological flowpaths intersect, or where flowpaths encounter a substrate containing complementary reactants (McClain et al., 2003). In the soil medium, movement of water plays an important role (McClain et al., 2003). Similar cycle of flooding and draining occurs in the drawdown area of hydroelectric reservoir, but influence of water level rising and falling in such ecosystem has not yet explored. Besides this, soils in the tropics and sub-tropics are known to be predominant sources of N<sub>2</sub>O emissions (Bremner, 1997; Houghton et al., 2001). Therefore, a hydroelectric reservoir like NT2, which exhibits a large drawdown area (up to 275 km<sup>2</sup> for a 450 km<sup>2</sup> in the case of NT2 during the studied period), could be a potential source of N<sub>2</sub>O.

Further, hydroelectric reservoirs in tropical or subtropical region are often characterized by an oxic epilimnion, an anoxic water bottom, an oxic-anoxic interface (Chanudet et al., 2012), and a high ammonium (NH<sub>4</sub><sup>+</sup>) turnover (Collos et al., 2001). It has been reported that N<sub>2</sub>O production can be maximum around oxic-anoxic interface (Mengis et al., 1997). As a consequence, these water bodies seem to be favorable environments for N<sub>2</sub>O production. Hence, the potential for hydroelectric reservoirs to contribute substantial amounts of N<sub>2</sub>O to the atmosphere is high.

In this context, we studied the Nam Theun 2 (NT2) hydroelectric reservoir in a subtropical region of Lao PDR with following main objectives (1) to have an understanding of N<sub>2</sub>O dynamics in the reservoir water column and in the downstream of power house and the downstream of the dam (2) thereby, to assess gross N<sub>2</sub>O emissions and understanding of the main factors influencing the emissions from the subtropical NT2 reservoir. Here first, we present an analysis of the significance of NH<sub>4</sub><sup>+</sup>, NO<sub>3</sub><sup>-</sup> and NO<sub>2</sub><sup>-</sup> concentrations on N<sub>2</sub>O concentrations in the pristine inflowing tributaries, in the reservoir water column, and in the downstream water. Then, we report gross N<sub>2</sub>O emissions from the NT2 reservoir including reservoir water surface, downstream emissions, and emissions from the drawdown area for the year 2010 and 2011, i.e. first two years after full-impoundment.

## **6.2. Study area and methodology**

### **6.2.1. The Nam Theun 2 Hydroelectric Reservoir**

The NT2 reservoir (17°59.50'N, 104°57.08'E) is built on the Nam Theun River by EDF, and is now operated by Nam Theun 2 Power Company (NTPC) in the subtropical region of Lao People's Democratic Republic. Main features of NT2 reservoir have been discussed in the Chapter 2.

### 6.2.2. Strategies (stations design)

All the sampling stations mentioned in the CH<sub>4</sub> dynamics assessment (Chapter 4) were monitored for N<sub>2</sub>O, NH<sub>4</sub><sup>+</sup>, NO<sub>3</sub><sup>-</sup> and NO<sub>2</sub><sup>-</sup> sampling in the pristine inflowing tributaries, reservoir and downstream of power house and the Nakai Dam. The importances of each sampling station have been discussed in chapter 2.

### 6.2.3. Methodology

The evolution of the dissolved N<sub>2</sub>O concentration has been monitored since April 2009 till December 2011. Sampling procedure for dissolved N<sub>2</sub>O concentration is similar to the one described for determination of dissolved CH<sub>4</sub> concentrations in Chapter 4. Determination of physical and water chemistry variables has already been detailed in Chapter 2.

Diffusive N<sub>2</sub>O fluxes were derived from thin boundary layer (TBL) using N<sub>2</sub>O concentration gradient between water and air at nine sampling stations (RES1-RES9) in the reservoir water surface. Gas transfer velocities were calculated using a formulation of  $k_{600}$  from MacIntyre et al. (2010). In the pristine inflowing tributaries, RES9 and the downstream waters, a constant  $k_{600}$  (10 cm.hr<sup>-1</sup>, Guerin et al., 2007) was used. Additional measurements of diffusive N<sub>2</sub>O fluxes using floating chamber technique were performed in a field campaign in June 2011 excepted at RES9 sampling station for practical access. During estimation of N<sub>2</sub>O fluxes using thin boundary layer equation, we used an average value of atmospheric concentrations measured during the floating chamber measurements, i.e. 327 ppb.

Bubbling N<sub>2</sub>O fluxes were measured at various sites with different depths, mostly during field campaigns (not part of the monitoring sampling). Sample collection, storage, analysis and bubbling flux calculation have been detailed in Chapter 4. Sampling strategy and procedure for diffusive N<sub>2</sub>O fluxes determination from the drawdown area was the same as discussed in the chapter 4 for CH<sub>4</sub> and sample collection, storage and analysis were performed with the same methodology as described for floating chamber technique (Chapter 4). N<sub>2</sub>O degassing emissions were measured at five sites mentioned in Chapter 4, sampling strategy and calculation procedure were similar to those described for CH<sub>4</sub> degassing emission in Chapter 4. Downstream of the power house and the Nakai Dam, diffusive fluxes were measured with the same approach as described for CH<sub>4</sub> in Chapter 4.

### 6.2.4. Gas Chromatography

Analysis of N<sub>2</sub>O concentrations were performed by gas chromatography on a SRI 8610C gas chromatograph (SRI, Torrance, CA, USA) equipped with an *electron capture detector* (ECD). 0.5 mL gas volume from the headspace for water sample vials and 1 mL gas volume for flux sample vials were injected. Commercial gas standards (320, 347, 1000 and 1020 ppbv, Air Liquid, "crystal" standards, uncertainties less than 10%) were injected after analysis of every 10 samples to calibrate and control the GC. Duplicate injections of samples showed results to be reproducible within ±5%. The specific gas solubility for N<sub>2</sub>O as a

function of temperature (Weiss and Price, 1980) was used for calculation of N<sub>2</sub>O concentrations dissolved in water.

### 6.2.5. Statistical analysis

One way ANOVA statistical tests were performed to assess the spatial variation in the surface N<sub>2</sub>O concentrations and diffusive N<sub>2</sub>O fluxes at different sampling stations in the reservoir. This was done using GraphPad Prism (GraphPad Software, Inc., v5.04).

## 6.3. Results and discussion

### 6.3.1. N<sub>2</sub>O concentrations in water column along with physico-chemical parameters

Vertical profiles of N<sub>2</sub>O concentrations, nitrogen compounds (i.e. NH<sub>4</sub><sup>+</sup>, NO<sub>3</sub><sup>-</sup>, NO<sub>2</sub><sup>-</sup> and N<sub>tot</sub>), temperature and O<sub>2</sub> were measured in the reservoir water column. Table 6.1 summarizes N<sub>2</sub>O concentrations along with inorganic nitrogen compounds, O<sub>2</sub> and temperature in the surface and the bottom water for the three different seasons. The shapes of the vertical profile showed seasonal change (Figure 6.1).

During the two and half year of monitoring, NT2 was thermally stratified from February to September (dry-warm and wet seasons) and well mixed for the next month (October-January in the cold dry season). As already mentioned by Chanudet et al. (2012), the NT2 Reservoir is monomictic. During the periods of stratification, the epilimnetic temperatures were significantly higher than hypolimnetic temperatures whereas surface and bottom temperature were  $22.6 \pm 2.0^{\circ}\text{C}$  and  $19.5 \pm 1.6^{\circ}\text{C}$  during the lake overturn in dry-cold season, respectively. Thermocline was  $4.7 \pm 2.7\text{m}$  and  $7.2 \pm 5.5\text{m}$  deep during the dry-warm and wet seasons, respectively. Occasionally, sporadic and local destratification occurred during the wet season. Once the turbines went on operation in March 2010, the water column at RES9 located near the water intake got totally mixed as revealed by the homogeneous temperature from the surface to the bottom.

During the dry-warm season, an oxic-epilimnion and anoxic-hypolimnion were observed at most of the stations as shown in Figure 6.1a. During the wet season, the reservoir was generally stratified with an anoxic hypolimnion and a well-oxygenated epilimnion, although O<sub>2</sub> reached occasionally the hypolimnion during the sporadic destratification events. During the dry-cold seasons, the water column was often oxygenated from the top to the bottom. The depth of the oxycline was concomitant with the thermocline in the warm dry and wet season whereas O<sub>2</sub> concentrations decreased smoothly from the surface to the bottom in the cold dry season. Once the turbines went on operation, the water column at RES9 was always well oxygenated.

During the stratified periods, NH<sub>4</sub><sup>+</sup> was trapped in the anoxic hypolimnion, therefore, considerably higher NH<sub>4</sub><sup>+</sup> was observed in the hypolimnion water in the warm dry ( $45 \pm 44\ \mu\text{mol.L}^{-1}$ ) and the wet season ( $70 \pm 80\ \mu\text{mol.L}^{-1}$ ) than in the epilimnion waters (Table 6.1 and Figure 6.1b). The nitrification is faster in the oxic water layer and does not support a build-up of NH<sub>4</sub><sup>+</sup>, hence significantly lower NH<sub>4</sub><sup>+</sup> occurred during the cold dry season in the whole

water column, with  $5.3 \pm 7.1$  and  $9.4 \pm 22.7 \mu\text{mol.L}^{-1}$  in the epilimnion and the hypolimnion water, respectively.

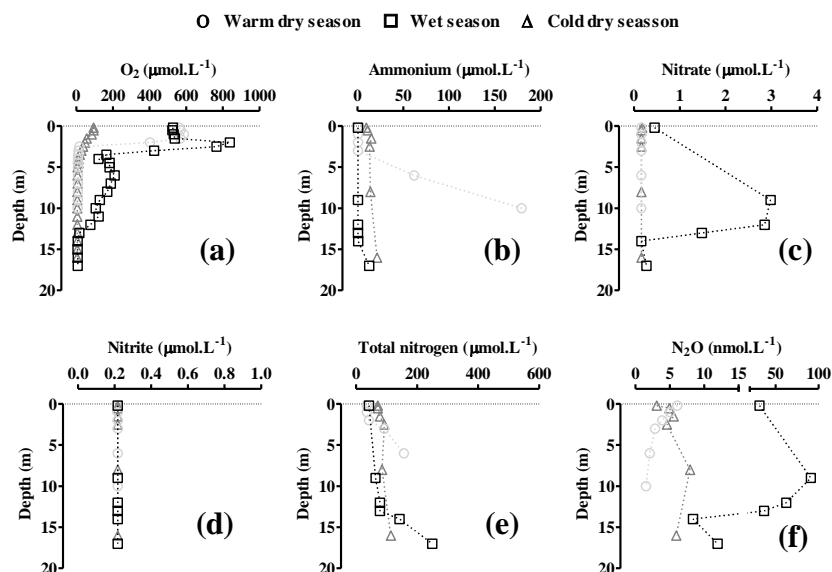


Figure 6.1. Vertical profiles of (a) oxygen ( $\text{O}_2$ ), (b) ammonium ( $\text{NH}_4^+$ ), (c) nitrate ( $\text{NO}_3^-$ ), (d) nitrite ( $\text{NO}_2^-$ ), (e) total nitrogen ( $\text{N}_{\text{tot}}$ ), and (f) nitrous oxide ( $\text{N}_2\text{O}$ ) in the water column of NT2 hydroelectric reservoir.

During the stratified periods,  $\text{NO}_3^-$  concentrations were comparatively higher in the epilimnion water than hypolimnion waters, but sometimes also found around the oxicleine (Figure 6.1c). Whereas the lowest  $\text{NO}_3^-$  ( $1.5 \pm 4.6 \mu\text{mol.L}^{-1}$ ) in the hypolimnion of the reservoir during the stratified period (warm dry season). An increase in the  $\text{NO}_3^-$  concentration occurred during the non-stratified periods (wet season and cold dry season, Table 6.1).

$\text{NO}_2^-$  concentrations were at the low level in the whole water column and often close to detection limit of the analyzer ( $0.2 \mu\text{mol.L}^{-1}$ , Figure 6.1d). Significantly higher  $\text{N}_{\text{tot}}$  occurred during the warm dry and the wet seasons than the cold dry season in the hypolimnetic water (Table 6.1). Further, throughout the year,  $\text{N}_{\text{tot}}$  concentrations were higher in the hypolimnion water than in the epilimnion water (Figure 6.1e). In the water column of NT2 reservoir, we observed minimum  $\text{NO}_3^-$  in the bottom of the reservoir during the stratified period (warm dry season). It suggests that the anoxia at the hypolimnion would have suppressed the production of  $\text{NO}_3^-$  from nitrification and further low availability of  $\text{NH}_4^+$  in the epilimnion could lead low production of  $\text{NO}_3^-$  in the surface water. We observed high  $\text{NO}_3^-$  in the non-stratified periods (wet season and cold dry season, Table 6.1). It is likely that high input of  $\text{NO}_3^-$  with water inputs might increase the level of  $\text{NO}_3^-$  in the reservoir water. Further high  $\text{NO}_3^-$  concentrations in the water column during the wet season were due to nitrification during the mixing of  $\text{NH}_4^+$ -rich hypolimnion water with  $\text{O}_2$ -rich epilimnion water column.



Table 6.1: Dissolved N<sub>2</sub>O and physico-chemical parameters in the water column of the NT2 reservoir. Avg: average; SD: standard deviation.

		Warm Dry Season			Wet Season			Cold Dry Season		
		Range	Median	Average ± SD	Range	Median	Average ± SD	Range	Median	Average ± SD
O <sub>2</sub> (μmol.L <sup>-1</sup> )	Surface	203-563	438	424±64	33-707	430	407±104	35-600	447.2	412±119
	Bottom	3-493	7.5	46±96	3.8-420	7.5	81±126	4.4-545	203.1	213±170
O <sub>2</sub> saturation (%)	Surface	37-117	90.4	86±14	6.6-137	89	84±22	6.2-119	83.7	77±22
	Bottom	0.6-82	1.3	8±16	0.7-77	1.5	15±23	0.8-90	35.2	37±29
NH <sub>4</sub> <sup>+</sup> (μmol.L <sup>-1</sup> )	Surface	0.6-11	0.6	1.3±1.7	0.6-41	0.6	4.2±7.3	0.6-31	1.2	5.3±7.1
	Bottom	0.6-179	35.3	44±44	0.6-276	24	69±79	0.6-138	1.1	9.4±22
NO <sub>2</sub> <sup>-</sup> (μmol.L <sup>-1</sup> )	Surface	0.2-0.9	0.2	0.3±0.1	0.2-2.8	0.2	0.3±0.3	0.2-3.6	0.2	0.4±0.6
	Bottom	0.2-1.3	0.2	0.3±0.2	0.2-3.7	0.2	0.3±0.4	0.2-4.4	0.2	0.5±0.8
NO <sub>3</sub> <sup>-</sup> (μmol.L <sup>-1</sup> )	Surface	0.2-13	0.2	1.1±2.4	0.2-84	1.3	6.0±12	0.2-16	1.6	3.7±4.2
	Bottom	0.2-31	0.2	1.5±4.6	0.2-29	0.3	4.1±7.0	0.2-25	7.0	6.7±6
N <sub>tot</sub> (μmol.L <sup>-1</sup> )	Surface	35-207	35.7	42±24.	42-507	57	79±65	35-107	35.7	53±23
	Bottom	35-771	164.3	205±149	57-892	250	273±187	35-1342	71.4	128±212
N <sub>2</sub> O (nmol.L <sup>-1</sup> )	Surface	4-30	10	11±5	6-1300	24	52±135	1-66	14	17±12
	Bottom	2-960	6	11±15	2-589	20	48±82	1-81	18	23±17

During the stratified periods, the vertical N<sub>2</sub>O profiles show high concentration close to the surface or sometimes close to the oxicle depth (Figure 6.1f). In the whole water column, N<sub>2</sub>O concentrations were significantly higher ( $52 \pm 135 \text{ nmol.L}^{-1}$ ) during the wet season than during the warm and cold dry seasons ( $11 \pm 5 \text{ nmol.L}^{-1}$  and  $17 \pm 12 \text{ nmol.L}^{-1}$  respectively). Alike to epilimnion water column, hypolimnion water column exhibited significantly higher N<sub>2</sub>O concentrations in wet season ( $48 \pm 82 \text{ nmol.L}^{-1}$ ) than in the cold dry and warm seasons. Hence, the N<sub>2</sub>O concentration in water column of NT2 reservoir suggested a strong seasonal variation.

The average of N<sub>2</sub>O concentration in the inflowing tributaries was around 4 times higher in the wet season ( $75 \pm 92 \text{ nmol.L}^{-1}$ ) than in the warm ( $17 \pm 10 \text{ nmol.L}^{-1}$ ) and cold season ( $18 \pm 11 \text{ nmol.L}^{-1}$ ) (Figure 6.2a). In the wet season, a significant amount of N<sub>2</sub>O carried in to the reservoir with high water inflow (Figure 6.2b). It should be noticed that on monthly basis, a significant percentages of reservoir water (up to 75%) is renewed during high water inflows. It suggests that high inputs of N<sub>2</sub>O from the watershed increase the N<sub>2</sub>O concentrations in the reservoir water column (Figure 6.2c). Further, high N<sub>2</sub>O concentration during the wet season could also be associated with the rapid microbial consumption of NH<sub>4</sub><sup>+</sup> accumulated in the hypolimnion water during stratified periods which were in turn partly oxidized into N<sub>2</sub>O (Mengis et al., 1997). During the increase in the water level, flooding of the drawdown area can also support the denitrification at the flooded soils in the drawdown area. Experimental wetting of the soils from the tropical wetland emitted significantly higher N<sub>2</sub>O (Liengaard et al., 2013).

The accumulations of NH<sub>4</sub><sup>+</sup> in the anoxic water were also indicated by low levels of nitrification processes (Knowles et al., 1981; Mengis et al., 1997). Laboratory experiments on lake littoral sediments have indicated that N<sub>2</sub>O production is limited by low NO<sub>3</sub><sup>-</sup> availability due to low nitrification activity (Liikanen et al., 2003). During the stratified periods, low N<sub>2</sub>O concentration in anoxic water suggested a low denitrification activity or the reductions of N<sub>2</sub>O to N<sub>2</sub> in the complete denitrification, or both. The nitrification is the faster in the oxic-surface water layer and does not support a build-up of NH<sub>4</sub><sup>+</sup> in the surface water layer. The higher N<sub>2</sub>O concentration in the surface water suggests that there could be lateral flow of the NH<sub>4</sub><sup>+</sup> from the drawdown area to the reservoir water column. Further, N<sub>2</sub>O can be produced in the surface water by green algae (Weathers, 1984), or denitrifying bacteria living on the surface of macroalgae (Law et al., 1993). Maximum N<sub>2</sub>O concentrations around oxycline reveal that various bacteria e.g. nitrifiers, denitrifiers (Mengis et al., 1997), methanotrophs (Yoshinari 1985), nitrate ammonifiers (Smith 1982) contribute to N<sub>2</sub>O concentrations.

From the ANOVA test, our results reveal that the different sampling stations in the reservoir were not significantly different in terms of N<sub>2</sub>O concentration in surface water ( $p = 0.61$  for the warm dry,  $p = 0.71$  for the wet season,  $p = 0.13$  for the cold season; one way ANOVA test,  $p < 0.05$ ). It seems that physical and bacterial processes responsible for N<sub>2</sub>O concentrations in the surface water were quite similar at all the sampling stations.

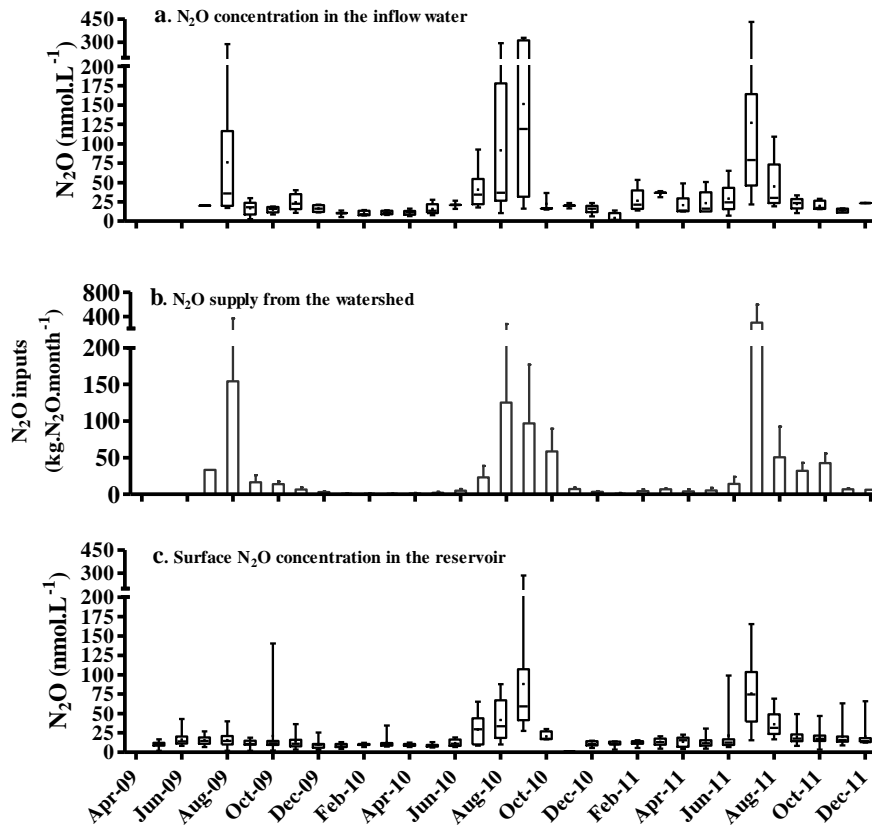


Figure 6.2. (a)  $N_2O$  concentration in the inflow water, (b) amount of  $N_2O$  supply from the watershed and, (c) surface  $N_2O$  concentration in the reservoir at NT2 hydroelectric reservoir.

The influence of physico-chemical variables on  $N_2O$  concentration were also accessed by correlation analysis (Figure 6.3). On the both (epilimnion and hypolimnion waters),  $N_2O$  concentrations were positively correlated with  $NO_3^-$  and  $O_2$  level.

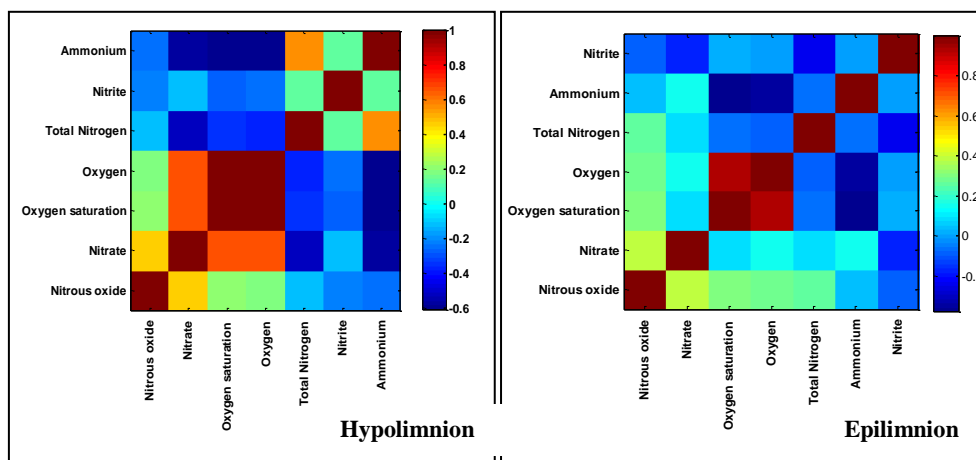


Figure 6.3: The correlation coefficients between dissolved  $N_2O$  and physico-chemical parameters at the hypolimnion and the epilimnion water.

The highest N<sub>2</sub>O concentrations in the hypolimnetic waters have been found in the water with high O<sub>2</sub> and NO<sub>3</sub><sup>-</sup>, suggesting a link between N<sub>2</sub>O concentrations and nitrification activity in the water column (McCrackin and Elser, 2011; Mengis et al., 1996, 1997). A negative correlation coefficient between NH<sub>4</sub><sup>+</sup> and N<sub>2</sub>O concentration reveals that accumulation of NH<sub>4</sub><sup>+</sup> occurs in the anoxic waters where N<sub>2</sub>O production is insignificant at the NT2.

### **6.3.2. N<sub>2</sub>O concentrations in the downstream of powerhouse and the downstream of the Nakai Dam**

In the downstream of the power house, concentrations of N<sub>2</sub>O, NH<sub>4</sub><sup>+</sup> and NO<sub>3</sub><sup>-</sup> also showed seasonality (Figure 6.4). N<sub>2</sub>O concentrations were at the maximum level during the wet season when high N<sub>2</sub>O was released from the turbines (Figure 6.4 a, b, c). Comparatively low N<sub>2</sub>O concentrations occurred during the cold dry season in the downstream of the power house.

With the distance from the turbine outlet, N<sub>2</sub>O concentrations decrease in the downstream channel. It is likely due to diffusive emission and degassing at the aeration weir. After confluence with the Xe Bang Fai River, N<sub>2</sub>O concentration increased because of comparatively often high N<sub>2</sub>O concentration in the Xe Bang Fai River (Figure 6.4 a, b, c). In the warm dry and the wet seasons, relatively higher NH<sub>4</sub><sup>+</sup> concentrations were released in the downstream the reservoir (Figure 6.4 d, e). Further in the downstream at the distance of 110 km (XBF4), a clear decrease in the NH<sub>4</sub><sup>+</sup> concentration and increase in the N<sub>2</sub>O and NO<sub>3</sub><sup>-</sup> concentration occurred, suggesting the nitrification process in the turbined water during the warm and the wet season (Figure 6.4 a, b, d, e). In the cold season, it seems that most of the NH<sub>4</sub><sup>+</sup> would have already been oxidized within the reservoir, leading to minimal NH<sub>4</sub><sup>+</sup> concentration release (Figure 6.4 f).

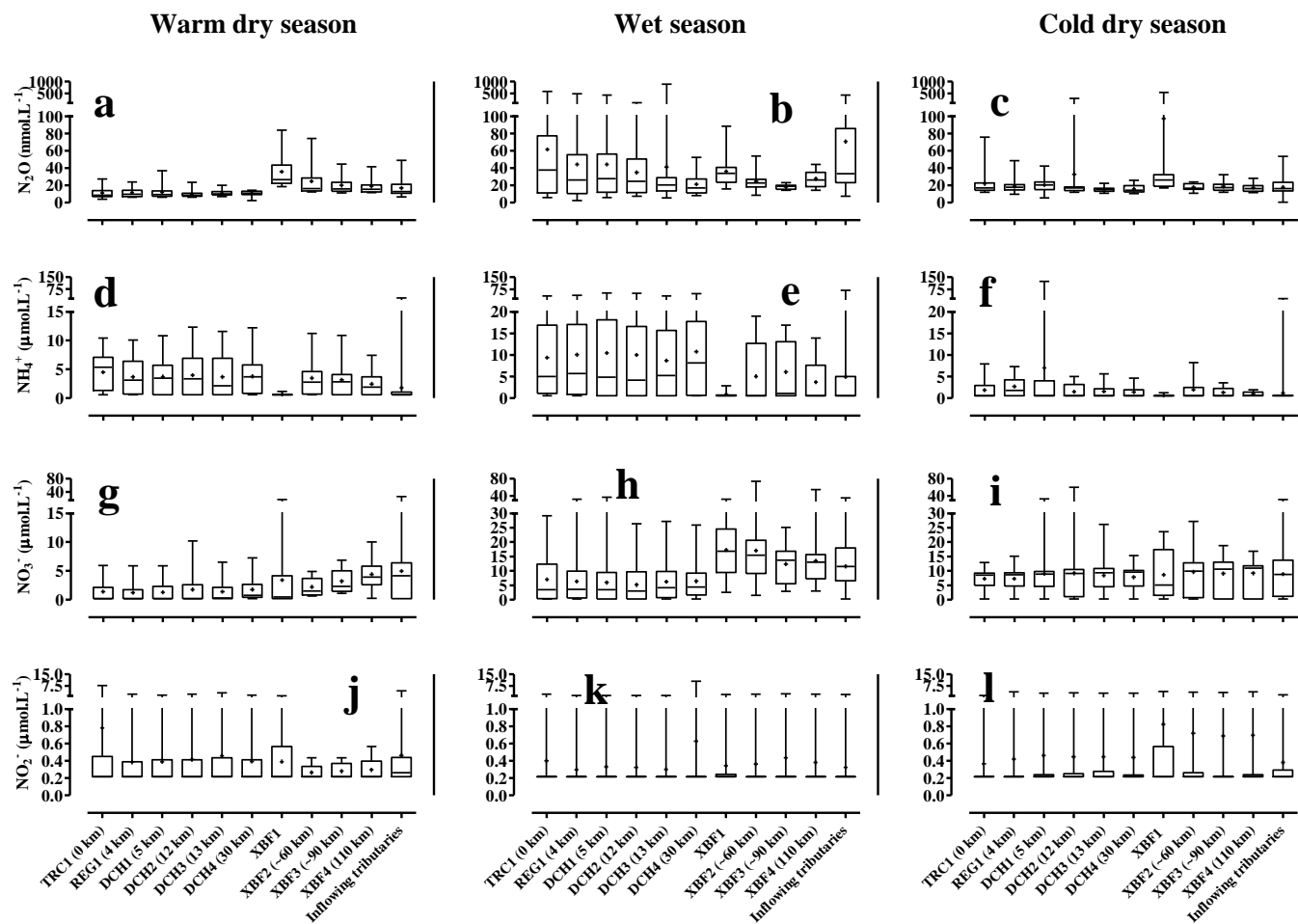


Figure 6.4: The spatial and seasonal changes in the concentration of nitrous oxide ( $N_2O$ ) (a, b, c), ammonium ( $NH_4^+$ ) (d, e, f), nitrate ( $NO_3^-$ ) (g, h, i), and nitrite ( $NO_2^-$ ) (j, k, l) in the NT2 reservoir and the downstream of the power house.

### 6.3.3. Emissions from upstream

#### 6.3.3.1. Bubbling N<sub>2</sub>O flux

N<sub>2</sub>O concentrations in the bubbles ranged from 340 to 1181 ppbv (average = 584 ± 194 ppbv), i.e. always greater than atmospheric N<sub>2</sub>O concentration (327 ppbv initial concentration in the floating chamber measurements), suggesting N<sub>2</sub>O emission to atmosphere. Calculations led to N<sub>2</sub>O flux ranging from 0.0005 to 0.9 μmol.m<sup>-2</sup>.day<sup>-1</sup>, with an average of 0.03 ± 0.05 μmol.m<sup>-2</sup>.day<sup>-1</sup>. Even when considering the high global warming potential of N<sub>2</sub>O, N<sub>2</sub>O emission through bubbling is not significant at the NT2 reservoir.

#### 6.3.3.2. Diffusive N<sub>2</sub>O flux from the reservoir water surface

Measured and calculated fluxes are summarized in Table 6.2. The spatial differences in calculated diffusive N<sub>2</sub>O fluxes were statistically examined using one way ANOVA test. Our results reveal that sampling station RES9 in the reservoir was significantly different from other sampling stations in terms of diffusive N<sub>2</sub>O fluxes (p = 0.013 for the warm dry, p < 0.0001 for the wet season and the cold season; one way ANOVA test, p < 0.05). This is because of considering high k<sub>600</sub> for RES9 sampling station (water intake) as the area exhibits very high water current velocity (Chanudet et al., 2012). But, rest of the sampling stations (RES1 to RES8) were not significantly different from each other in terms of diffusive N<sub>2</sub>O fluxes (p = 0.58 for the warm dry, p = 0.57 for the wet season, p = 0.33 for the cold season; one way ANOVA test, p < 0.05).

Measured N<sub>2</sub>O diffusive fluxes ranged from 1 to 58 μmol.m<sup>-2</sup>.day<sup>-1</sup> at RES1-RES8 sampling stations. For the same month (June 2011), calculated N<sub>2</sub>O diffusive fluxes ranged from 0 to 49 μmol.m<sup>-2</sup>.day<sup>-1</sup> and had a mean value of 12 ± 13 μmol.m<sup>-2</sup>.day<sup>-1</sup> at RES1-RES8 sampling stations. The medians of fluxes measured using floating chamber and calculated using k<sub>600</sub> are in a good agreement for June 2011 (p = 0.8, Mann Whitney test). Globally, at the NT2, calculated N<sub>2</sub>O diffusive fluxes ranged from 0.4 to 803 μmol.m<sup>-2</sup>.day<sup>-1</sup> (Table 6.2).

Table 6.2: Diffusive N<sub>2</sub>O fluxes from the NT2 reservoir. SD: standard deviation; FC: floating chamber measurements; TBL: thin boundary layer technique. Values are in μmol.m<sup>-2</sup>.day<sup>-1</sup>.

	Technique	RES1-RES8			RES9		
		Average ± SD	Range	Median	Average ± SD	Range	Median
Warm Dry Season	TBL	14±7.3	1.9-42	12.2	24±12	11-58	21
	FC	13 ± 13	1 - 58	9.6			
Wet Season	TBL	28±32	0.4-193	17.3	112±162	8-803	41
Cold Dry Season	TBL	13±16	1.2-138	10.4	35±26	5.8-117	33

Considering the spatial coverage of 2 km<sup>2</sup> and 26 km<sup>2</sup> for RES9 and RES3 respectively, and rest area of the reservoir is equally shared by other sampling stations, area weighted average flux was  $19 \pm 17 \mu\text{mol.m}^{-2}.\text{day}^{-1}$ . The average N<sub>2</sub>O diffusive fluxes are lower than at the Petit Saut Reservoir ( $97 \pm 61 \mu\text{mol.m}^{-2}.\text{day}^{-1}$ ; Guerin et al., 2008b). While area-weighted average flux was comparable to diffusive N<sub>2</sub>O fluxes (15 and 10  $\mu\text{mol.m}^{-2}.\text{day}^{-1}$ ) from two subtropical reservoirs located in China (PRC) (Liu et al., 2011).

Monthly reservoir surface areas were multiplied by area-weighted average fluxes for each month. Figure 6.5 shows the monthly time series of N<sub>2</sub>O emission from the reservoir water surface.

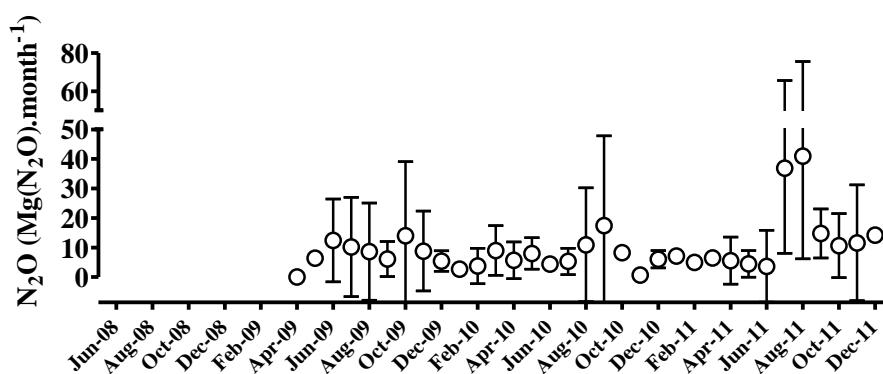


Figure 6.5: Evolution of diffusive N<sub>2</sub>O emissions from the reservoir water surface of NT2 reservoir since beginning of impoundment.

On the other hand, seasonal variation of N<sub>2</sub>O diffusive fluxes is clearer and stronger than the spatial variation, with maximum during wet season (June - September) and minimum during the cold dry season at all the sampling stations (Table 6.2). The seasonality of N<sub>2</sub>O fluxes is thus different from the one observed for both CO<sub>2</sub> and CH<sub>4</sub> (mostly high in the warm dry season; Chapter 4 and 5). Results suggest that during the wet season, a significant amount of N<sub>2</sub>O is supplied from the watershed area (Figure 6.2.a, b). During the increase in the reservoir level, a significant amount of N<sub>2</sub>O can be produced from the flooded soils via denitrification process (Liengaard et al., 2013). Further, oxic environments and supply of trapped NH<sub>4</sub><sup>+</sup> in the hypolimnion water column during the stratified period enhanced nitrification process and thereby N<sub>2</sub>O concentration in the surface water.

Owing to thermal stratification in the warm dry season, most of the NH<sub>4</sub><sup>+</sup> is accumulated in the hypolimnion waters. It seems that the lower availability of NH<sub>4</sub><sup>+</sup> could be the possible reason for lower nitrification rates and low N<sub>2</sub>O concentration in the surface water and thereby low N<sub>2</sub>O emissions from the reservoir water surface. During the cold season, it seems that lower temperature might have lowered the bacterial degradation of organic matter and supply of NH<sub>4</sub><sup>+</sup>. Consequently, low nitrification activity in the whole water column causes low N<sub>2</sub>O concentrations. In addition, there is low supply of the N<sub>2</sub>O and other N compound from the watershed in the warm dry and the cold dry periods (Figure 6.2).

### 6.3.3.3. N<sub>2</sub>O fluxes from the drawdown area

During the two field campaigns (June 2010 and June 2011, beginning of the wet season), when reservoir was at its minimum water level, we measured fluxes in the soils at upland (never flooded) and drawdown area (flooded during the high reservoir water level). Soil fluxes were measured in four different zones defined by their mean soil moisture contents (see details in sampling strategy in Chapter 2).

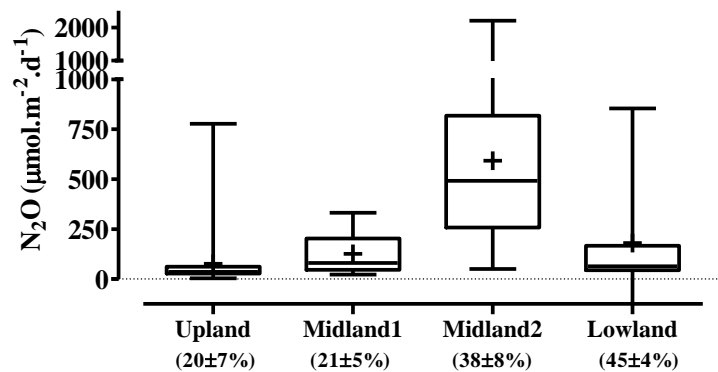


Figure 6.6: Diffusive N<sub>2</sub>O fluxes from soils from the upland and the drawdown area. Averages soil moisture are given in brackets.

N<sub>2</sub>O fluxes from soils from the upland and the drawdown area are depicted in Figure 6.6. The well-aerated upland soils were behaving as a source of N<sub>2</sub>O ( $80 \pm 160 \mu\text{mol.m}^{-2}.\text{day}^{-1}$ ) though emission were the smallest of the four soil types. Considering the low soil moisture for these soils, nitrification-based emission can occur. Intermediate N<sub>2</sub>O fluxes ( $180 \pm 270 \mu\text{mol.m}^{-2}.\text{day}^{-1}$ ) were measured in water saturated lowland soils. Nitrification is most likely inexistent at saturated soil moisture levels, and N<sub>2</sub>O production is supposed to come mainly from denitrification activity. In the upper drawdown zone, midland 1, on average fluxes were  $126 \pm 98 \mu\text{mol.m}^{-2}.\text{day}^{-1}$  with soil moisture of around 21% vol.

With a mid-range of moisture content ( $38 \pm 8\%$  vol), midland2 soils were the most significant source of nitrous oxide up to  $2200 \mu\text{mol.m}^{-2}.\text{day}^{-1}$  and had a mean value of  $590 \pm 507 \mu\text{mol.m}^{-2}.\text{day}^{-1}$ . Although nitrification and denitrification are characterized by different environmental controls and have optima under different environmental conditions, it is well known that these processes may occur simultaneously in the soil, thus giving rise to duplicate sources for N<sub>2</sub>O (Davidson et al., 2000). Kiese et al., (2002) also reported a linear correlation between N<sub>2</sub>O emissions and water field pore space for values less than 60%, but noted a decline in N<sub>2</sub>O emissions at higher moisture levels, which is most likely due to the increasing formation of N<sub>2</sub> rather than N<sub>2</sub>O, suggesting that the denitrification process begins to dominate, as has been shown elsewhere (Butterbach-Bahl et al., 2002). The average value of diffusive N<sub>2</sub>O fluxes at midland2 is slightly higher than the average value reported at tropical wetland soil in South America ( $430 \pm 30 \mu\text{mol.m}^{-2}.\text{day}^{-1}$ , Liengard et al., 2013).



Here, we propose a hypothesis to explain the high fluxes of  $N_2O$  in midland2 zone. A schematic illustration of high  $N_2O$  emission from the midland 2 soils is depicted in the Figure 6.8. Considering that water level and associated oxic-anoxic interface (OAI) in the drawdown soil layer is linked with reservoir water level (WL) and follows the same upward and downward movements.

Hot spot 1 is supposed to take place when water level in the reservoir decreases from  $WL_0$  to  $WL_{falling}$ , i.e. the case in the cold dry and the warm dry seasons when reservoir water level drops. A decrease in the reservoir water level would drop the oxic-anoxic interface from  $OAI_0$  to  $OAI_{falling}$  in the drawdown area (Figure 6.8). This would create oxic condition in the hot spot 1. In this case, anoxic soil holding electron donors ( $NH_4^+$  and  $CH_4$ ) is exposed to oxic condition and allows rapid oxidation of accumulated  $NH_4^+$ . Thus hot spot 1 not only emits  $N_2O$  as a by-product but also produces  $NO_3^-$  as final product. Liengaard et al., (2013) found a significant increase of  $NO_3^-$  in drained soil than in water logged soil, indicating the importance of dynamic shifts between denitrification and nitrification.

Hot spot 2 can occur when water level in the reservoir increases from  $WL_0$  to  $WL_{rising}$ , i.e. case of the wet season. An increase in the reservoir water level would raise the oxic-anoxic interface from  $OAI_0$  to  $OAI_{rising}$  in the drawdown area. This would create anoxic condition in the hot spot 2. In this case, oxic soil holding electron acceptors ( $NO_3^-$ ) is experienced the anoxic condition and creating a zone of high denitrification rates. It is well known that sudden onset of anoxia (Bollmann and Conrad, 1998) and high concentration of  $NO_3^-$  (Blackmer and Bremner, 1978) can increase the emissions of  $N_2O$ . Such hot spots have been reported in the riparian zones (Hill et al., 2000), in wetlands (Johnston et al., 2001, Liengaard et al., 2013), hyporheic zones (Holmes et al., 1996; Triska et al., 1989), and individual soil profiles (Parkin, 1987).

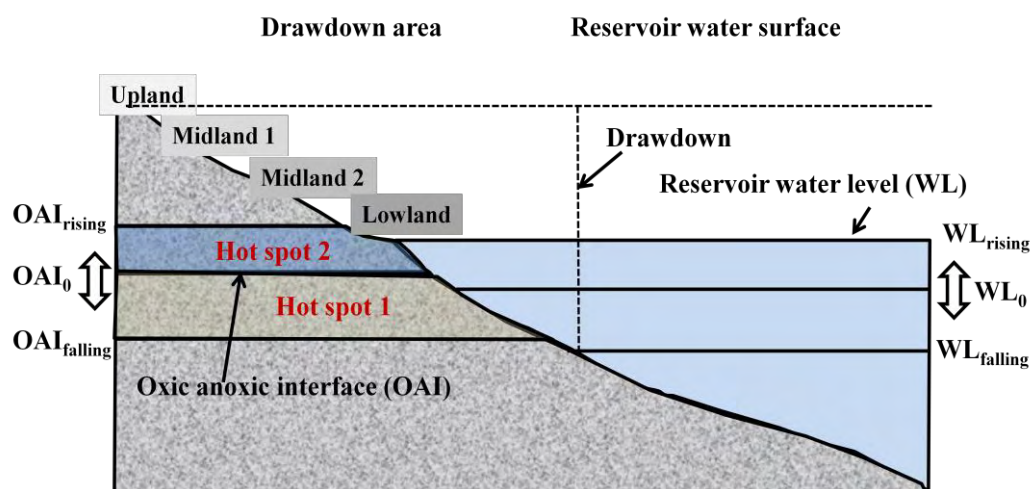


Figure 6.8 Schematic illustration of hot spot formation in the drawdown area

In most cases, the hot spots for denitrification are at most a few meters (circa 100–1000 m) wide at the upland boundary (Groffman et al., 1992; Pinay et al., 1993), although

they can occur at the riverbed wetland interface (Johnston et al., 2001) or within the wetland or riparian zone, depending on the location of ground water flowpaths (Hill et al., 2000).

Nevertheless, during rainfall, percolation of rain water can leach  $\text{NH}_4^+$  or  $\text{NO}_3^-$  to the subsurface anoxic layer or lateral flow can supply  $\text{NH}_4^+$  or  $\text{NO}_3^-$  to the reservoir water column. On the other hand, the reservoir can be a supplier of N-compound to the soils through lateral flow during the dry seasons.

However, the measured fluxes of  $\text{N}_2\text{O}$  from the drawdown area and upland soils had a high spatial variability. Our measured diffusive  $\text{N}_2\text{O}$  fluxes were well related to  $\text{NH}_4^+$  and  $\text{NO}_3^-$  content in the soils where  $\text{N}_2\text{O}$  flux measurements were made (Figure 6.7). The availability of  $\text{NH}_4^+$  could be a controlling factor for the  $\text{N}_2\text{O}$  and  $\text{NO}_3^-$  production in the soil. The diffusive  $\text{N}_2\text{O}$  fluxes were higher in the soils which exhibited high contents of  $\text{NH}_4^+$  and  $\text{NO}_3^-$  (Figure 6.7).

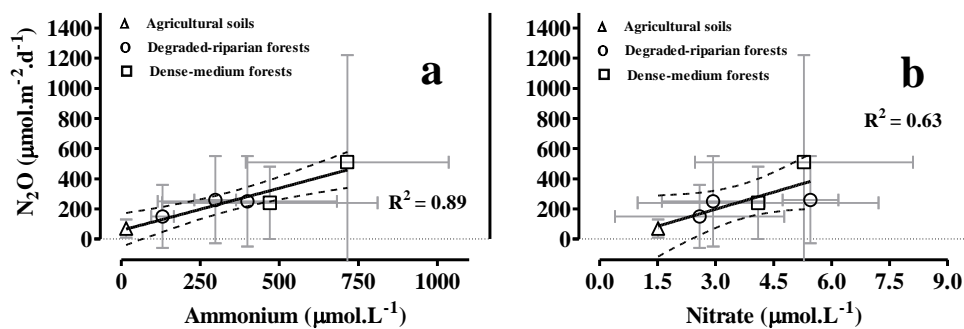


Figure 6.7: Diffusive  $\text{N}_2\text{O}$  fluxes versus ammonium ( $\text{NH}_4^+$ ) and nitrate ( $\text{NO}_3^-$ ) concentration in the soils.

Thus, the variability in  $\text{N}_2\text{O}$  fluxes is generally caused by the underlying biogeological processes (e.g. nitrification, denitrification and mineralization), which are controlled by environmental factors such as soil moisture, soil temperature and nutrient availability (Bandibas et al., 1994; Bateman et al., 2005; Cardenas et al., 1993; Conen, et al., 2000; Davidson, 1992; Hou et al., 2000; Maag and Vinther, 1996; Schindlbacher et al., 2004; Smith et al., 1998; Zheng et al., 2000). Soil moisture is clearly a very important and sensitive factor regulating  $\text{N}_2\text{O}$  emission from drawdown area.

For upscaling the diffusive  $\text{N}_2\text{O}$  fluxes at the whole drawdown area scale, this area has been divided in to four zones (see the Chapter 4 for definition of these zones). Hence, for flux extrapolation purpose, following considerations were made: 1. lowland area is characterized by moisture content around 45%; 2. midland2 area retains the moisture content around 38%; 3. midland1 area retains the moisture content around 20%; and 4. upland area retains the moisture content around 20%. For extrapolation purpose, average fluxes in upland, midland1, midland2 and lowland were applied to the corresponding area of different zones. It is to be mentioned that since  $\text{N}_2\text{O}$  fluxes were measured in the beginning of the rainy season, the soils moisture content must have been in an intermediate range. During the dry season midland1

and upland might be the place of smaller sources than the one measured if we would have done the measurements in the dry season. As a matter of consequence, net  $N_2O$  flux presented has to be considered as a value in the upper range.

In order to calculate the integrated  $N_2O$  flux from the drawdown area, daily surfaces of the different zones were multiplied by the mean corresponding flux and summed up on a daily basis. Figure 6.9 depicts the time series of monthly  $N_2O$  emissions from the drawdown area.

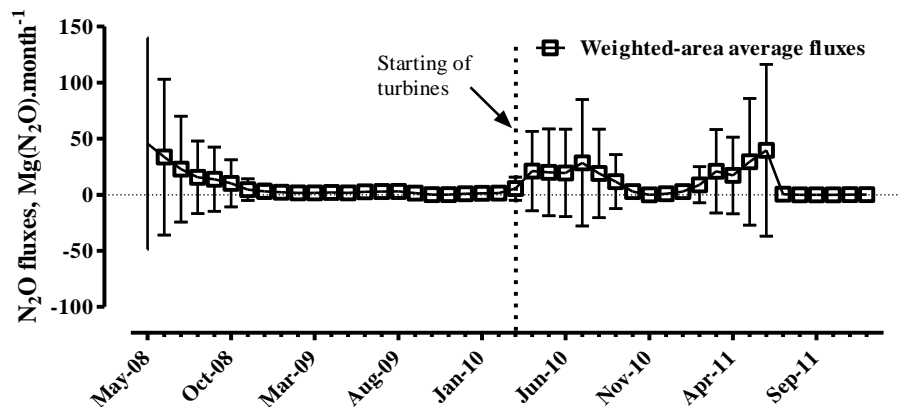


Figure 6.9: Time series of diffusive  $N_2O$  fluxes from drawdown area since beginning of impoundment.

It shows that before the first full impoundment, the drawdown area was acting as a  $N_2O$  source, up to  $45 \text{ Mg (N}_2\text{O).month}^{-1}$ . After the turbine starting, the whole system became alternatively a source of  $N_2O$  during the dry season (February-September) when reservoir exhibits maximum drawdown area, and an almost null source during the late wet season (October-January) when reservoir is at its maximal level. Evidently, contribution of  $N_2O$  emissions from the drawdown area is directly proportional to its areal coverage.

### 6.3.4. Emissions from downstream

#### 6.3.4.1. Degassing

No clear  $N_2O$  degassing was observed in the downstream of the powerhouse and the Nakai Dam. Some negative values were sometime observed. This could be attributed to the production of  $N_2O$  downstream of the structure where ammonium-rich water released to downstream channel could be nitrified.  $N_2O$  production could also be related to nitrification by methanotrophs (Roy and Knowles, 1994) as we observed simultaneously high aerobic methane oxidation rate in the turbined water. Thus emission of  $N_2O$  from degassing was not significant.

#### 6.3.4.2. Diffusive $N_2O$ fluxes from downstream of the power house and downstream of the Nakai Dam

In the downstream of the power house and downstream of the Nakai Dam,  $N_2O$  diffusive fluxes were calculated using surface  $N_2O$  concentration database and constant  $k_{600}$

(10 cm.hr<sup>-1</sup>, a conservative value of gas transfer velocity in river downstream of a dam; Guerin et al., 2007).

Table 6.3. Diffusive N<sub>2</sub>O fluxes from downstream of the power house (Section 1 - Section 4) and the Nakai Dam (Section 5). SD: Standard deviation, IQR: Interquartile range. All values are in  $\mu\text{mol.m}^{-2}.\text{day}^{-1}$ .

Season		Section 1	Section 2	Section 3	XBF1	Section 4	Inflowing tributaries	Section 5
<b>Warm Dry</b>	Range	10-80	20-60	05-50	50-320	30-220	20-150	20-130
	Average $\pm$ SD	30 $\pm$ 10	30 $\pm$ 10	30 $\pm$ 10	110 $\pm$ 90	60 $\pm$ 40	50 $\pm$ 30	40 $\pm$ 20
	Median(IQR)	20(20)	20(10)	30(10)	80(30)	40(30)	40(30)	30(20)
<b>Wet</b>	Range	10-1570	10-1220	10-2440	40-240	20-150	20-1250	30-280
	Average $\pm$ SD	190 $\pm$ 280	120 $\pm$ 150	100 $\pm$ 290	100 $\pm$ 50	70 $\pm$ 30	200 $\pm$ 260	80 $\pm$ 50
	Median(IQR)	110(190)	90(120)	50(50)	90(30)	60(20)	90(210)	50(80)
<b>Cold Dry</b>	Range	20-200	10-700	20-80	40-1340	30-100	001-130	5-60
	Average $\pm$ SD	60 $\pm$ 30	60 $\pm$ 100	40 $\pm$ 10	210 $\pm$ 420	50 $\pm$ 20	40 $\pm$ 30	30 $\pm$ 10
	Median(IQR)	50(20)	40(20)	40(20)	70(30)	40(20)	40(20)	30(10)

Diffusive N<sub>2</sub>O fluxes were higher in the wet season than in the warm dry and cold season (Table 6.3). In the wet season, average diffusive N<sub>2</sub>O flux was  $190 \pm 280 \mu\text{mol.m}^{-2}.\text{day}^{-1}$  in the Section1 and then dropped in Section2 and Section3. Diffusive N<sub>2</sub>O fluxes are more or less constant in section1 and section2 during the warm dry season and cold dry season (Table 6.3). As a matter of fact, diffusive emission occurs in the previous sections. It seems that N<sub>2</sub>O emission is compensated by the attribution of N<sub>2</sub>O from the production of N<sub>2</sub>O downstream during nitrification when NH<sub>4</sub><sup>+</sup>-rich water releases to downstream channel in the warm dry season. As mentioned before, N<sub>2</sub>O production could also be linked to nitrification by methanotrophs (Roy and Knowles, 1994) since high aerobic methane oxidation rate has been observed in the turbinated water in the warm dry season. Further downstream in Section3 (located after the aeration weir), fluxes were similar as observed the fluxes in Section1 and Section2. After confluence with Xe Bang Fai River, diffusive N<sub>2</sub>O fluxes increased in the section 4 because of the high N<sub>2</sub>O supply from the Xe Bang Fai River.

In the downstream of the Nakai Dam (Section5), N<sub>2</sub>O diffusive fluxes ranged from 20 to 220  $\mu\text{mol.m}^{-2}.\text{day}^{-1}$ . Similar to the downstream of power house, higher diffusive N<sub>2</sub>O fluxes were observed in the wet season ( $70 \pm 30 \mu\text{mol.m}^{-2}.\text{day}^{-1}$ ) than in the warm and cold dry season (Table 6.3).

In order to calculate the integrated N<sub>2</sub>O emissions from the downstream, the surface areas of individual downstream sections were multiplied by the corresponding mean areal flux.

#### 6.4. Estimates of different components of gross N<sub>2</sub>O emissions

Time series of the monthly N<sub>2</sub>O emissions from the whole NT2 system is depicted in the Figure 6.10. Our results show that each N<sub>2</sub>O emission pathways significantly varies seasonally (Figure 6.10). During the wet season, diffusive N<sub>2</sub>O emissions from the reservoir water surface and downstream occurred during the wet season (June-September) and contributed up to 90% of total monthly N<sub>2</sub>O emissions. On the other hand, during the dry season diffusive N<sub>2</sub>O emissions from the drawdown area added more than 90% of the total monthly N<sub>2</sub>O emissions and maximum emissions occurred during the dry months (January-June) when water level decreases. Bubbling and degassing emissions were almost negligible all year long.

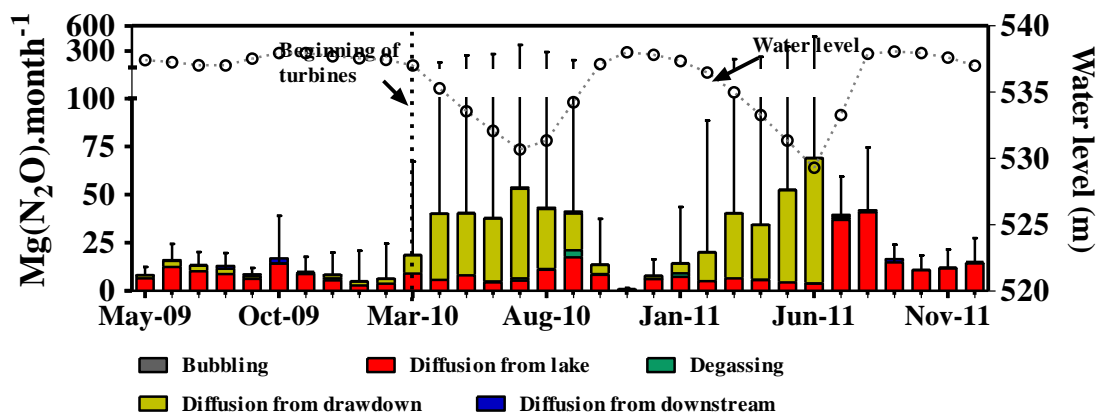


Figure 6.10. Time series of the monthly N<sub>2</sub>O emissions from the whole NT2 system. Figure shows each individual pathways (bubbling, diffusion from the reservoir water surface, diffusion from drawdown area, degassing, and diffusion from downstream).

Table 6.4: Estimates of gross N<sub>2</sub>O emissions (in Mg N<sub>2</sub>O.year<sup>-1</sup>) for the years 2010 and 2011. The percentage in between brackets represents the proportion of each component to the total emission.

Years	Diffusive emission from drawdown area	Bubbling	Diffusive emission from reservoir water surface	Degassing	Diffusive emission from downstream	Total
2010	216 ± 543 (69%)	Negligible	82 ± 38 (26%)	5.5 ± 6.8 (2%)	8.8 ± 0.8 (3%)	312 ± 544
2011	196 ± 569 (53%)	Negligible	161 ± 63 (44%)	Negligible	9.7 ± 1.6 (3%)	366 ± 571

Table 6.4 sums up the annual budget for the years 2010 and 2011, the first two years after full impoundment. Our results show that diffusive emission is the leading atmospheric N<sub>2</sub>O pathways at the NT2 reservoir scale. For both years, the major contributions come from drawdown area, around 53 to 69% of the total annual N<sub>2</sub>O emissions. Diffusive emissions from the reservoir water surface were also significant, up to 44% of the total annual N<sub>2</sub>O emissions. Contribution to total downstream N<sub>2</sub>O emission is minor (i.e. diffusive + degassing, 5% at the most). Finally the total N<sub>2</sub>O emission, from all the quantified N<sub>2</sub>O

emissions pathways at the NT2, reaches  $312 \pm 544$  and  $366 \pm 571$  Mg (N<sub>2</sub>O).yr<sup>-1</sup> for the years 2010 and 2011, respectively.

## 6.5. Conclusions

Our study reveals that seasonal variation in the N<sub>2</sub>O emissions was stronger than spatial one. An important parameter affecting N<sub>2</sub>O concentration in the reservoir was rainfall inflow from the watershed, inducing a hot moment of high N<sub>2</sub>O concentration in the wet season and thereby N<sub>2</sub>O fluxes. It is noteworthy to point out that most of the diffusive emissions from the reservoir water surface and from the downstream waters occur during the wet season (~ 60%). Here we show that seasonality of N<sub>2</sub>O diffusive fluxes in the reservoir and the downstream is different from the one observed for both CO<sub>2</sub> and CH<sub>4</sub> (mostly high emissions in the dry season). Therefore measurements should be performed in all seasons.

This study represents the first assessment of N<sub>2</sub>O emission from drawdown area and revealed that the zone between upland and water saturated lowland was a significant hot spot of N<sub>2</sub>O emissions. Notably, up to 70% of total N<sub>2</sub>O emissions were emitted from the drawdown area at NT2 reservoir. Our results suggest that if drawdown area represents a large portion of the reservoir surface like in the NT2 case, then it can emit a significant amount of N<sub>2</sub>O to the atmosphere. This is an important new result, specially keeping in mind that all previous studies never measured fluxes from the drawdown area. In this study we extrapolated N<sub>2</sub>O diffusive fluxes on total drawdown area using soil moisture content, considering this being the main controlling factor of nitrification and denitrification. We encourage future studies focusing on linking the other environmental variables to N<sub>2</sub>O emissions from the drawdown area. This would help to better quantify emissions from the drawdown area while extrapolating on the global area of the reservoir.

## Chapter 7

# Net GHG footprint of a newly impounded subtropical hydroelectric reservoir: Nam Theun 2 case study

**Abstract:** Rising concern over the contribution of hydroelectric reservoirs to increased atmospheric concentration of greenhouse gases (GHGs) led to quantify the net GHG footprint of a hydroelectric reservoir. We present here the first comprehensive assessment of GHGs footprint associated with the creation of a hydroelectric reservoir Nam Theun 2 (NT2) in subtropical region of the Lao People's Democratic Republic. This is the results of a large scale study that have been conducted over 4 year (2008-to date). The major GHG sources and sinks of the terrestrial and aquatic components of the pre-impoundment landscape where quantified. Similar estimate of these various emission pathways were made at the reservoir scale since the May 2009.

Ecosystems existing on the reservoir footprint before flooding were a sink of carbon dioxide ( $-73 \pm 225 \text{ GgCO}_2\text{eq. year}^{-1}$ ), roughly neutral in terms of methane ( $7 \pm 11 \text{ GgCO}_2\text{eq. year}^{-1}$ ), and a source of nitrous oxide ( $345 \pm 158 \text{ GgCO}_2\text{eq. year}^{-1}$ ). Post-impoundment GHG budget reveal that the same footprint has become a more significant source of  $\text{CO}_2$  and  $\text{CH}_4$ , and a much smaller source of  $\text{N}_2\text{O}$ . For the year 2010, with  $1307 \pm 244 \text{ GgCO}_2\text{eq. year}^{-1}$  and  $768 \pm 206 \text{ GgCO}_2\text{eq. year}^{-1}$  respectively,  $\text{CH}_4$  and  $\text{CO}_2$  have contributed around 60% and 35%) to the total GHG budget. With  $93 \pm 163 \text{ GgCO}_2\text{eq. year}^{-1}$ ,  $\text{N}_2\text{O}$  accounts for less than 5% of the total emission. While  $\text{CH}_4$  emissions declined a bit the second year of study ( $473 \pm 91 \text{ GgCO}_2\text{eq. year}^{-1}$  in the year 2011),  $\text{CO}_2$  emissions increased ( $1551 \pm 197 \text{ GgCO}_2\text{eq. year}^{-1}$ ) in the same time, while  $\text{N}_2\text{O}$  emissions remained constant. Our results indicate that upstream GHG emissions (emissions from the reservoir water surface and drawdown area) contributed around 87% and 92% of total GHG emissions for the years 2010 and 2011, respectively. Remaining total GHG emissions were contributed from downstream emissions (degassing and diffusive emissions from the downstream), a percentage lower than reported for tropical reservoirs.

With a total gross emissions of  $2168 \pm 358$  and  $2133 \pm 276 \text{ GgCO}_2\text{eq. year}^{-1}$  for the years 2010 and 2011, gross NT2 emissions are about an order of magnitude higher than pre-impoundment emissions ( $276 \pm 343 \text{ GgCO}_2\text{eq. year}^{-1}$ ). With a net GHG emissions of  $1889 \pm 496$  (2010) and  $1854 \pm 440$  (2011)  $\text{GgCO}_2\text{eq. year}^{-1}$ , and an annual power generation of about 6 TWh, GHG emission factor equal to 0.31 (2010) and 0.30 (2011)  $\text{MgCO}_2\text{eq. MWh}^{-1}$  for the NT2 Reservoir. This is lower than a typical thermal coal based power plant emission factor of 0.96  $\text{Mg}$  of  $\text{CO}_2\text{eq. MWh}^{-1}$ . GHG emission factor for the year 2010 corresponds to the initial years after impoundment for NT2, and as such, can be considered as the maximum value that would be reached for this reservoir. Work is in progress to predict the trends of GHG emissions over the projected life span (e.g. 100 years) of the reservoir yields integrated long-term net GHG emissions per energy generation. It will allow comparing with alternate energy sources over the projected life span (100 years) of the reservoir.

### 7.1. Introduction

The identification and accurate quantification of sinks or sources of greenhouse gases (GHGs) have become a key challenge for scientific and policy makers groups working on climate change or global warming. The contribution of freshwater hydroelectric reservoirs to

the increasing atmospheric GHGs concentrations is of rising concern. The major GHGs related to reservoir creation are carbon dioxide (CO<sub>2</sub>), methane (CH<sub>4</sub>) and nitrous oxide (N<sub>2</sub>O) (Eggleton et al., 2006). A recent meta-analysis of published data on GHG emissions from hydroelectric reservoirs covering a worldwide distribution suggests that globally, hydroelectric reservoirs emit annually about 48 TgC-CO<sub>2</sub>, and 3 TgC-CH<sub>4</sub> (Barros et al., 2011). This is significantly less than previous estimates (St. Louis et al. 2000), mostly due to differences in the estimate of global reservoir surface (0.34 vs. 1.50 Million km<sup>2</sup>). The second main reason of the large range of GHG emissions estimates is lack of representative regional GHG areal flux.

Most current estimates are based on gross GHG fluxes from reservoirs alone. They may be biased because they do not consider the pre-impoundment GHG sinks and sources (St. Louis et al., 2000; Teodoru et al., 2012; Tremblay et al., 2005, 2010). A realistic assessment of the net GHG footprint of hydroelectric reservoirs requires, in addition to reliable estimates of reservoir GHG emissions taken over space and time, robust estimates of the GHG sinks and sources from the terrestrial and natural aquatic ecosystems that existed in the pre-impoundment landscape, and which disappear due to flooding (Teodoru et al., 2012; Tremblay et al., 2010), i.e. net emissions = post impoundment emissions - pre impoundment emission. Thus, to predict the impact on emissions of greenhouse gases needed to be measured precisely, before and after the impoundment of reservoirs. In spite of the increasing awareness of the significance of reservoir GHG emissions for these two last decades, only one such pre-and-post impoundment GHG balance has ever been carried out (Eastmain 1 Reservoir, Quebec; Teodoru et al., 2012; Tremblay et al., 2010).

For the governing bodies (e.g. Intergovernmental Panel on Climate Change (IPCC), United Nations Educational, Scientific and Cultural Organization (UNESCO), etc.) and the energy sector (International Hydropower Association (IHA), International Energy Agency (IEA), etc.), the evaluation of net GHG emissions from hydroelectric reservoirs is becoming more and more relevant to ensure that methods of energy production are adequately compared. This is a necessary step for assessing carbon credits.

Around 25% of the existing 45000 large dams are used for electricity production, while the other 75% are used exclusively for other purposes (e.g., irrigation, flood control, navigation and urban water supply schemes). The number of reservoirs continues to increase at fast pace specially in the tropical or sub-tropical regions which still hold significant amount of undeveloped hydropower resources to be exploited (Kumar et al., 2012). As a matter of fact, tropical or subtropical hydroelectric reservoirs have been considered as more significant source of GHG than boreal or temperate one (Barros et al., 2011; St. Louis et al., 2000; Varis et al., 2012). Notably, no study dedicated to “net emissions” has ever been conducted in tropical or subtropical regions which is believed to be the “hot spot” for GHG emissions (Barros et al, 2011; DelSontro et al, 2011; Demarty and Bastien, 2011; Kemenes et al, 2011; St. Louis et al., 2000).

In this context, we studied a subtropical hydroelectric reservoir, Nam Theun 2 (NT2), a complex-structural-designed, created on the Nam Theun River in Laos PDR. This reservoir



has 1070 MW installed capacity, and an annual production of about 6 TWh. The overall aims of our study were to: (1) determine the complete GHG budget of the pre-impoundment landscapes; (2) determine the post-impoundment GHG budget including spatial and temporal variability; and finally, (3) combine these two estimates to assess the net GHG footprint of the NT2 reservoir.

Considering the above objectives, a major part of this chapter deals with the quantification of pre-impoundment GHG budget. Afterwards, net GHG emissions were quantified by combining this pre-impoundment GHG emission assessment with gross post GHG emissions estimated in Chapter 4, Chapter 5 and Chapter 6. Finally, we compared the net NT2 GHG emissions with alternative conventional energy sources.

These results represent, to the best of our knowledge, the first comprehensive, pre- and post-flooding net GHG balances ever carried out for a tropical/subtropical hydroelectric reservoir, and provide a robust estimate of the net GHG footprint directly associated with hydroelectricity generation.

## **7.2. Site description and methodology**

### **7.2.1. Site description**

The Nam Theun 2 (NT2) hydroelectric dam (17°59'49" N, 104°57'08" E) is built on the Nam Theun River in the subtropical region of Lao People's Democratic Republic (Figure 7.1). NT2 hydroelectric plant delivers an annual production of 6 TWh with a maximum flooded area of 450 km<sup>2</sup> at full water level (538 m msl). This leads to a high ratio of energy density (or annual production by maximum flooded area) of 13.34 GWh.km<sup>-2</sup>. The project area experiences a tropical monsoon climate with distinct wet and dry (initial cold, then warm) seasons. Since the water inputs are directly related to rainfall, filling typically occurs during the wet season (mainly May to September). Owing to the hydrological conditions and reservoir operation planning, a large drawdown area, up to 80% of total 450 km<sup>2</sup> can be observed in normal years during the dry season (March to June) when the reservoir is at its minimal operating level (525.5 m msl).

With an annual average rainfall of 2400 mm, NT2 reservoir receives an average annual runoff of 7527 million m<sup>3</sup> from six major tributaries (Nam Xot, Nam Mon, Nam Theun, Nam Noy, Nam Yang and Nam On), an amount that represent more than twice the NT2 reservoir full capacity (3530 Mm<sup>3</sup>).

Filling of the reservoir began in April 2008 and full water level (538 m msl) was first reached in October 2009. Commercial operation of the NT2 hydroelectric plant began in March 2010. The 450 km<sup>2</sup> area of terrestrial landscape was originally covered by dense, medium, light, degraded and riparian forests, as well as agricultural soils and swamps (Descoux et al., 2011). Dense, medium, and light forests represented 59% of the 450 km<sup>2</sup>, whereas agricultural lands and swamps accounted only for 11% and 2% respectively. A small fraction of the vegetation was partially burnt or removed before the impoundment. The total amount of flooded organic carbon was around 5.1 ± 0.7 MtC, with 2.2 MtC from above

ground biomass, litter and dead wood, and 2.9 MtC from below ground biomass and soil organic carbon (Descloux et al., 2011).

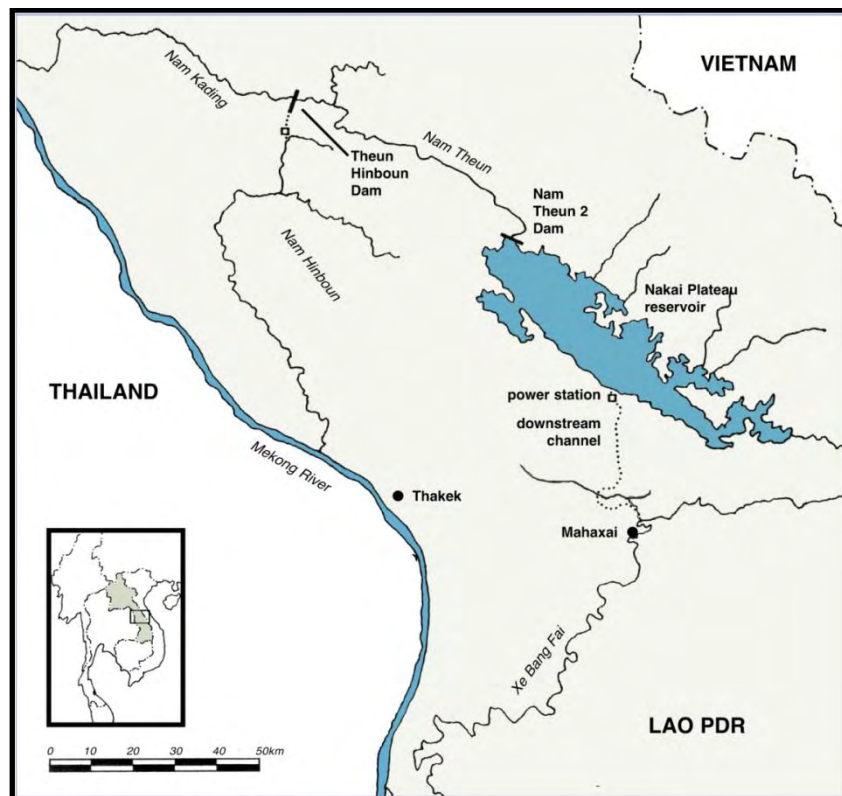


Figure 7.1. Location map of the Nam Theun 2 (NT2) Reservoir. The reservoir is shown at its full capacity (538 m above sea level). Map available on International Rivers Organization website (<http://www.internationalrivers.org/campaigns/nam-theun-2-dam>)

The NT2 reservoir is characterized as a warm monomictic lake, completely mixed from top to bottom once a year (Chanudet et al., 2012). During the dry season, the lake water body remains stratified with an oxic epilimnion overlying an anoxic hypolimnion, destratification occurring during the wet and cold dry season (Chanudet et al., 2012). An important feature of the reservoir concern is the turbine intake. This intake is located at the bottom of the reservoir between 506 and 524 m msl and receives a mixture of epilimnetic and hypolimnetic water due to its conceptual design. NT2 reservoir is a trans-basin diversion hydroelectric reservoir that takes water from the Nam Theun River and turbines release it after turbines into the Xe Bang Fai River through a 27 km long artificial downstream channel (Figure 7.1). Before being released into the Xe Bang Fai River, and to control the flow, turbined water is stored in an 8 Mm<sup>3</sup> artificial regulating pond. A continuous ecological flow ( $2 \text{ m}^3 \cdot \text{s}^{-1}$ ), and occasionally spillway release is released from the Nakai Dam to the Nam Theun River.

### 7.2.2. General approach

The net reservoir GHG footprint corresponds to the net changes in GHG flux. This includes the GHG emissions after impoundment to which are subtracted the sinks or sources

of GHG that were present in the pre-impoundment landscape. This represents the “excess” emissions directly associated with the creation of the reservoir (UNESCO-IHA, 2009; World Commission on Dams, 2000). CO<sub>2</sub>, CH<sub>4</sub> and N<sub>2</sub>O emissions to the atmosphere were quantified and estimated for each of the individual ecosystems existing in the pre-impoundment landscape. Similarly, GHG emissions from the NT2 system (reservoir water surface + drawdown area + downstream) were estimated post-impoundment (see Chapter 4, Chapter 5 and Chapter 6). The overall impact of reservoir creation on the GHG source/sink balance, i.e. net GHG footprint of the reservoir, is calculated as:

Net reservoir GHG footprint = reservoir GHG sink/source balance - pre-impoundment GHG sink/source balance (Teodoru et al., 2012; Tremblay et al., 2010).

The quantification of pre-impoundment and post-impoundment GHG emissions is elaborated from six intensive field campaigns (one before, and five after impoundment, between May 2008 and June 2011) measurements, and from a continuous fortnightly monitoring program on going since the NT2 flooding. Pre-impoundments GHG balance was quantified for year 2008, and reservoir GHG sink/source balance was calculated for first two years after full-impoundment i.e. year of 2010 and 2011.

There is an imbalance in the sampling effort pre-impoundment and post-impoundment, with in the order of ten days of sampling during one season and using a limited number of techniques before flooding and a much more ambitious sampling program during all seasons and using multiple methods after flooding. It was because of the severe practical constraints in terms of funding, timing and access that have caused this imbalance. However, forests occupied about 80% of the surface area prior to the filling of the reservoir and that the pre-impoundment CO<sub>2</sub> budget for forests was derived from a literature value, it could be apparent that the pre-impoundment values are highly tentative. It is to be mentioned that our estimate of CH<sub>4</sub>, CO<sub>2</sub> and N<sub>2</sub>O exchanges were in the upper range. CH<sub>4</sub> exchange has very low contribution to GHG pre-impoundment emissions. Globally, estimates of CO<sub>2</sub> (sink) and N<sub>2</sub>O (source) exchanges were probably compensated by each other. Therefore, our estimates on GHG pre-impoundment emissions can be considered as conservative values.

Next section deals with the GHG budget assessment for the pre-impoundment period.

### **7.2.3. Pre-impoundment GHG exchange**

GHG emission from the different pre-impoundment ecosystems were estimated during a field campaign conducted from 11<sup>th</sup> to 21<sup>st</sup> May 2008, at the beginning of the wet season, together with some additional N<sub>2</sub>O flux measurements conducted in June 2010. GHG emission from pre-impoundment riverine ecosystems were derived using the thin boundary layer technique from GHG concentrations in the surface water sampled from the pristine rivers sampled by AELab within the continuous monitoring program (see details on that technique in Chapter 2).

### 7.2.3.1. CO<sub>2</sub> exchange

CO<sub>2</sub> exchange, or more exactly the Net Ecosystem Exchanges (NEE) were measured using the Eddy Covariance (EC) technique, a direct micrometeorological method (see details in Chapter 2). Given the various constraints (see below) related to the implementation of the EC technique, CO<sub>2</sub> flux measurements were conducted primarily in the former Nam Theun River floodplain. This area was used for agriculture (rice cultivation) before the impoundment. Estimate of the NEE for the different types of forest was beyond our possibility in the context of this program. Indeed, among others, eddy covariance technique requires measurements to be done above a flat and horizontal uniform surface. Forests in the reservoir footprint were on sloppy terrain, and would a tower exceeding the forest canopy has not been present, measurements would have not complied with EC constraints. Literature values were used to complete the database on different forest types, extracted from the study on CO<sub>2</sub> fluxes in the tropical forests from the most comprehensive study currently available (Luyssaert et al., 2007).

### 7.2.3.2. CH<sub>4</sub> exchange

CH<sub>4</sub> emissions were measured using static chamber technique (see the detail in Chapter 2). These measurements were done on six of the most representative ecosystems (primary forest, degraded forest, riparian forest, slash and burnt, agricultural land, swamps, see locations in Figure 7.2) in the reservoir footprint.

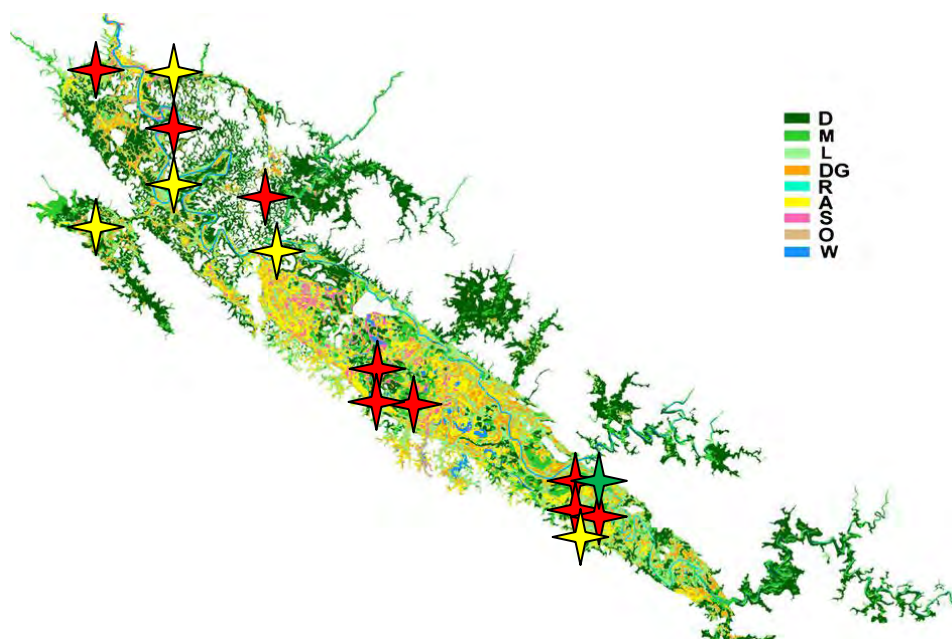


Figure 7.2. Locations of the sampling sites investigated for CH<sub>4</sub> (red symbol), CO<sub>2</sub> (green symbol) and N<sub>2</sub>O (yellow symbol) fluxes pre-impoundment of the NT2 reservoir (source of the map: Descloux et al., 2011). Note: D: dense forest, M: medium forest, L: light forest, DG: degraded forest, R: riparian forest, AG: agricultural land, SW: swamps, S: soils, and W: water.

The sum of the investigated ecosystems represented 96.6% of the total area flooded by the reservoir creation (Table 7.1, Descloux et al, 2011).

A total of nine different sampling stations were investigated (2 swamps sites, 3 degraded forest sites and one site each in other ecosystems, see locations in Figure 7.2). Similar to CO<sub>2</sub>, CH<sub>4</sub> emissions from the water surface were determined from surface CH<sub>4</sub> concentration measured in pristine river sites of the monitoring network and estimated via the thin boundary layer technique.

Table 7.1. Distribution of the major ecosystems existing before flooding the NT2 Reservoir and the number of flux measurements of CO<sub>2</sub>, CH<sub>4</sub> and N<sub>2</sub>O. SC: static chamber flux measurements; EC - eddy covariance flux measurement; TBL - thin boundary layer flux calculation.

Type of ecosystem	Surface area (km <sup>2</sup> )	Surface (%)	No. of flux measurements (technique used)		
			CO <sub>2</sub>	CH <sub>4</sub>	N <sub>2</sub> O
Primary forest	154.5	34.6	-	3 (SC)	12 (SC)
Degraded forest	207.9	46.6	-	19 (SC)	20 (SC)
Agricultural land	48.7	10.9	218 (EC)	45 (SC)	6 (SC)
Swamps	10.7	2.4	-	38 (SC)	-
Bare Soils	5.3	1.2	-	8 (SC)	-
Riparian forest	4.0	0.9	-	8 (SC)	-
Water	15.3	3.4	150 (TBL)	150 (TBL)	150 (TBL)
<b>Total</b>	<b>450</b>	<b>100</b>	<b>368</b>	<b>271</b>	<b>188</b>

### 7.2.3.3. N<sub>2</sub>O exchange

N<sub>2</sub>O emissions were measured in June 2010 using static chamber technique. Measurements were performed on three types of ecosystems present in the pre-impoundment landscape: primary forest, degraded forest and agricultural land. The sum of the investigated ecosystems represented 92.1% of the total flooded area. Flux measurements were done together with soil moisture content and temperature measurements. Note that N<sub>2</sub>O flux measurements were not done on bare soil and in riparian forest. For this latter ecosystem, data from the literature (Groffman et al, 2000, McSwiney et al, 2001) were used to complete the assessment. For bare soils, it was assumed that N<sub>2</sub>O emissions were null because moisture conditions on such soil types are generally not favorable to denitrification, the process primarily responsible for emissions of N<sub>2</sub>O in such ecosystem. Similar to CO<sub>2</sub> and CH<sub>4</sub>, N<sub>2</sub>O emission from the water surface were determined from surface N<sub>2</sub>O concentration measured in pristine river sites of the monitoring network and estimated via the thin boundary layer technique.

## 7.3. Results

### 7.3.1. Pre-impoundment GHG exchange

### 7.3.1.1. CO<sub>2</sub> exchanges

Figure 7.3 shows half-hour CO<sub>2</sub> fluxes measured in the Nam Theun River floodplain during the May 2008 field campaign. A total of 234 half-hours (about 5 days of measurements) were acquired. After post processing and quality control on the measured fluxes, 218 half-hour samples were considered for the final calculation of the CO<sub>2</sub> fluxes (see Figure 7.3).

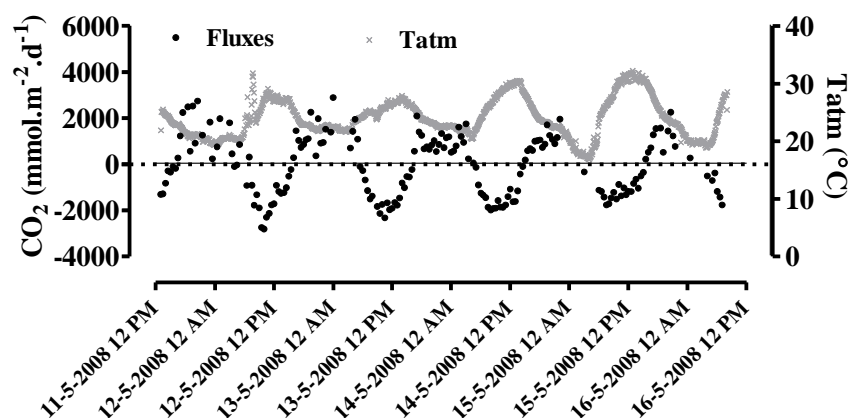


Figure 7.3. Diurnal pattern of CO<sub>2</sub> fluxes measured in May 2008 using eddy covariance technique at the floodplain of the Nam Theun River.

### 7.3.1.2. CH<sub>4</sub> exchange

A total of 121 hourly measurements of CH<sub>4</sub> fluxes were conducted, only 119 fluxes were actually considered for the final calculation (Figure 7.4). For each measurement site (excepted for the primary forest and bare soil sites), a minimum of 8 replicates of flux measurements were performed, which allows us to obtain a reliable and robust statistically mean.

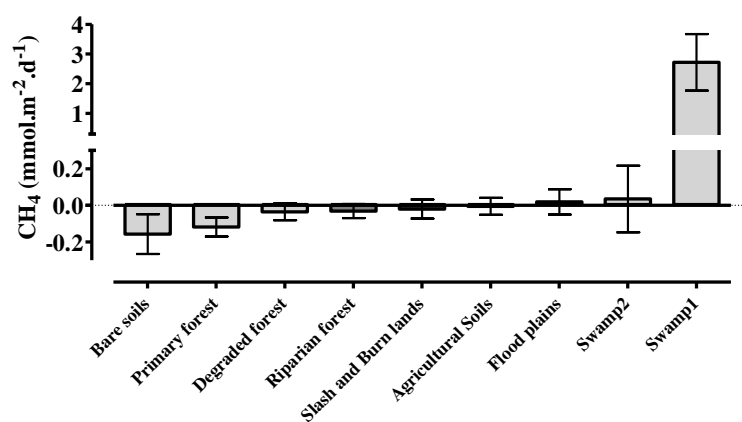


Figure 7.4. Average ( $\pm$  standard deviation) CH<sub>4</sub> fluxes at the nine sampling sites investigated in the pre-impoundment landscape of NT2 reservoir.

A statistical analysis showed that among the 6 sampling sites with mean negative fluxes, only two sites (bare soil and primary forest) were significant sinks of CH<sub>4</sub>, which was not the case for the other four sites (degraded forest, riparian forest, slash and burn farming, rice fields). From the three sites showing positive mean CH<sub>4</sub> flux, only Swamp 1 was a significant source of CH<sub>4</sub>, while the two other sites (floodplain and Swamp 2) were not significantly source of CH<sub>4</sub> at the time of measurement.

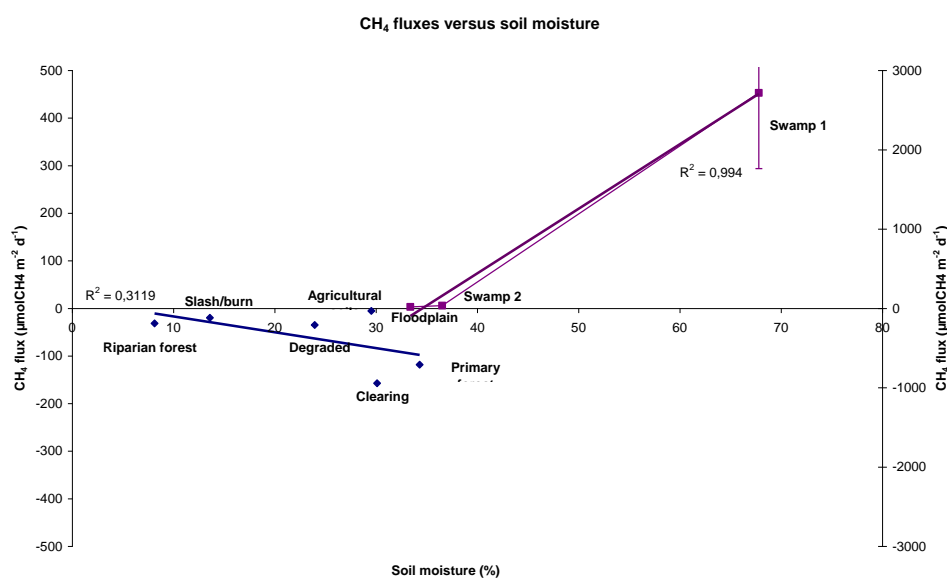


Figure 7.5. Average fluxes of CH<sub>4</sub> for each type of flooded ecosystems depending on the soil moisture content. Fluxes from swamps are plotted on the right Y-axis.

A significant relationship between CH<sub>4</sub> fluxes and soil moisture content was found for sampling sites that were acting as a source of CH<sub>4</sub> (see Figure 7.5, right Y-axis). CH<sub>4</sub> emission was positively correlated with the soil moisture content in 35 to 68% soil moisture range ( $r^2 = 0.998$ ), while CH<sub>4</sub> sink appears to be more or less independent from soil moisture content ( $r^2 = 0.3$ ) in the 10 to 35% soil moisture range. It seems that comparatively low CH<sub>4</sub> emission from swamp 2 (36.5% soil moisture content) than from swamp 1 (68% soil moisture content) appears to be linked to soil moisture, rather than ecosystem differences.

### 7.3.1.3. N<sub>2</sub>O exchanges

A total of 39 hourly N<sub>2</sub>O flux measurements were conducted, 38 of them being considered for final calculation (Table 7.2). According to the soil moisture contents at the time of the measurements, three different groups can be defined: dry soils ( $20 \pm 7\%$  vol.), representing the warm dry season; intermediate soils ( $29 \pm 11\%$  vol.) representing the cold dry; saturated soils ( $45 \pm 4\%$  vol.), representing average condition of the wet season. Since we could not perform the measurement over swamps, we considered N<sub>2</sub>O fluxes from saturated agricultural soils for swamp areas in the subsequent flux up-scaling.

Table 7.2. N<sub>2</sub>O mean flux values in the four investigated ecosystems.

Sites	Dry soils (20 ± 7% vol.)	Intermediate moisture content (29 ± 11% vol.)	Saturated Soils (45 ± 4% vol.)
Degraded forest	38 ± 22	195 ± 129	214 ± 274
Primary forest	35 ± 21	708 ± 171	62 ± 6
Agricultural soils	64 ± 86	103 ± 75	29 ± 48
Swamp	29 ± 48	29 ± 48	29 ± 48

### 7.3.1.4. Spatial and temporal integration of fluxes

Several assumptions were made for each GHG to extrapolate measured fluxes at the scale of the total flooded area. Note that all calculations of spatial and temporal integration fluxes were made at the scale of the reservoir footprint at its full level i.e. 450 km<sup>2</sup>.

#### 7.3.1.4.1. CO<sub>2</sub> budget

It has been considered that evolution of the swamp area along the wet season was the result of agricultural soils flooding (Chanudet, personal communication, EDF) of the Nam Theun river floodplain. Areas of all other ecosystems remain constant throughout the year. All types of forests (primary, medium, light, degraded and riparian) listed in the inventory (Descloux et al., 2011) are lumped in a same "forest" category (362.4 km<sup>2</sup> or 81% of the total area). For the "forest" category, CO<sub>2</sub> fluxes of  $-403 \pm 102$  gC-CO<sub>2</sub>.m<sup>-2</sup>.year<sup>-1</sup> were considered from Luysaert et al, 2007. CO<sub>2</sub> flux for the water surface was calculated from CO<sub>2</sub> surface concentrations determined in sampling stations NXT0, NXT1, NTH2 and NON1 (pristine sections of the Nam Xot, Nam Theun and Nam On rivers respectively). These fluxes were calculated via the thin boundary layer technique using a constant  $k_{600}$  of 10 cm.hr<sup>-1</sup>. From this, an average annual CO<sub>2</sub> flux of  $9393 \pm 9403$  gC-CO<sub>2</sub>.m<sup>-2</sup>.year<sup>-1</sup> from the water surface was estimated. One should note that this estimate does not consider any seasonal variability in CO<sub>2</sub> fluxes since we used annual mean surface water concentrations for this purpose. CO<sub>2</sub> fluxes used for interpolation on the whole pre-impoundment landscape are summarized in Table 7.3.

Table 7.3. Average (± standard deviation) CO<sub>2</sub> flux values used for spatial extrapolation (all fluxes in gC-CO<sub>2</sub>.m<sup>-2</sup>.year<sup>-1</sup>).

Type of ecosystem	Average ± SD	References
All type of forests	-403 ± 102	Luysaert et al., 2007, Global Change Biology
Agricultural soils	-1710 ± 927	this study (measured by eddy covariance)
Swamp	1963 ± 2164	Jauhiainen et al, 2005, Hirano et al, 2007
Water	9393 ± 9403	this study



Figure 7.6 shows integrated CO<sub>2</sub> exchanges for the different major ecosystems investigated, namely forest, agricultural land, swamp and water surface, using CO<sub>2</sub> exchanges and surface area of the different ecosystems.

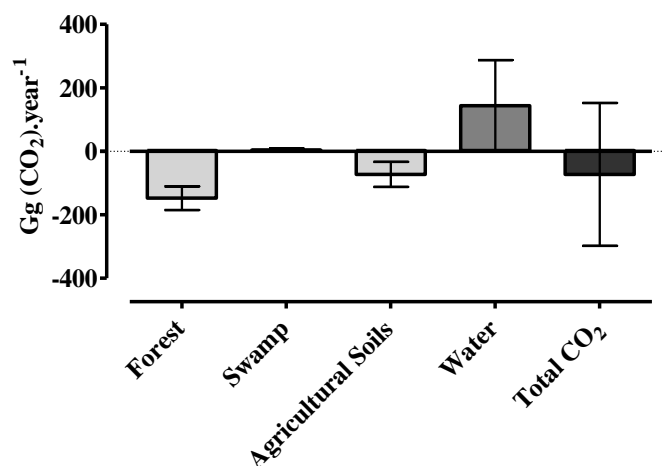


Figure 7.6. Average ( $\pm$  standard deviation) CO<sub>2</sub> fluxes for forest ecosystems, swamp, agricultural soils, surface water, and total emissions (all fluxes given in GgCO<sub>2</sub>.year<sup>-1</sup>).

At the whole pre-impoundment landscape, CO<sub>2</sub> uptake from the forest ecosystems was almost offset the CO<sub>2</sub> emissions from the river ecosystems, while CO<sub>2</sub> emission from the swamp is almost negligible. As a matter of consequences, total CO<sub>2</sub> fluxes are very similar to the CO<sub>2</sub> flux from the agricultural soils. Pre-impoundment NT2 footprint represents an annual sink of  $72.6 \pm 225$  GgCO<sub>2</sub>.year<sup>-1</sup>), i.e. an average CO<sub>2</sub> uptake of  $-169 \pm 504$  gC-CO<sub>2</sub>.m<sup>-2</sup>.year<sup>-1</sup>) (Figure 7.6).

#### 7.3.1.4.2. CH<sub>4</sub> budget

Similar to CO<sub>2</sub>, it has been considered that evolution of the swamp area along the wet season was the results of agricultural soils flooding. We considered that all the swamp area was in saturated conditions, and then attributed the emission value from swamp 1 sampling site. No seasonal variation in the area of primary forest (154.5 km<sup>2</sup>, 34.6% of total flooded area) was considered. All ecosystems acting as CH<sub>4</sub> sinks (that is light, medium and degraded forests) are clustered in the category of degraded forest which represents then an area of 207.9 km<sup>2</sup> (or 46.6% of total flooded area). Statistically, this area is neutral in term of CH<sub>4</sub> exchange. CH<sub>4</sub> fluxes for the water surface was calculated from CH<sub>4</sub> surface concentrations determined in sampling stations NXT0, NXT1, NTH2 and NON1 (pristine sections of the Nam Xot, Nam Theun and Nam On rivers respectively). These fluxes were calculated via the thin boundary layer technique using surface CH<sub>4</sub> concentrations and a constant  $k_{600}$  of 10 cm.hr<sup>-1</sup>. From this, we estimated an average daily CH<sub>4</sub> flux from the water surface of  $1.44 \pm 3.14$  mmol.m<sup>-2</sup>.d<sup>-1</sup>. One should note that a probable seasonal variability in CH<sub>4</sub> fluxes was not considered for any of the studied ecosystems.

Since CH<sub>4</sub> fluxes were measured in the beginning of the rainy season, the soils moisture content must have been in an intermediate range. The sinks of CH<sub>4</sub> (bare soil and primary forest) might be the place, during the dry season, of a stronger (significant) consumption than the one measured. Further, ecosystems that were not significant sinks of CH<sub>4</sub> emission (degraded forest, riparian forest, burnt forest, rice fields) could be larger sinks of CH<sub>4</sub> (that is to say significant in the case of ecosystems neutral) if we would have done the measurements in the dry season. As a matter of consequence, net CH<sub>4</sub> flux presented here has to be considered as a value in the upper range. Table 7.4 summarizes the average fluxes from the different ecosystems used for spatial extrapolation.

Table 7.4. Average ( $\pm$  standard deviation) CH<sub>4</sub> flux values used for spatial extrapolation (all fluxes in mmol.m<sup>-2</sup>.d<sup>-1</sup>).

Type of Ecosystem	CH <sub>4</sub> flux
Bare soil	-0.16 $\pm$ 0.11
Primary forest	-0.12 $\pm$ 0.05
Swamp	2.70 $\pm$ 0.95
Water	1.44 $\pm$ 3.14

Figure 7.7 shows the annual CH<sub>4</sub> exchange from the different ecosystem prior to flooding. CH<sub>4</sub> uptake occurring in the primary forest soils is almost counterbalanced by CH<sub>4</sub> emissions from the water surface, while CH<sub>4</sub> exchange in the bare soils ecosystem is almost negligible. Therefore, total CH<sub>4</sub> emission is very close to the CH<sub>4</sub> emissions from the swamp area (i.e. 0.28  $\pm$  0.43 Gg CH<sub>4</sub>.year<sup>-1</sup>).

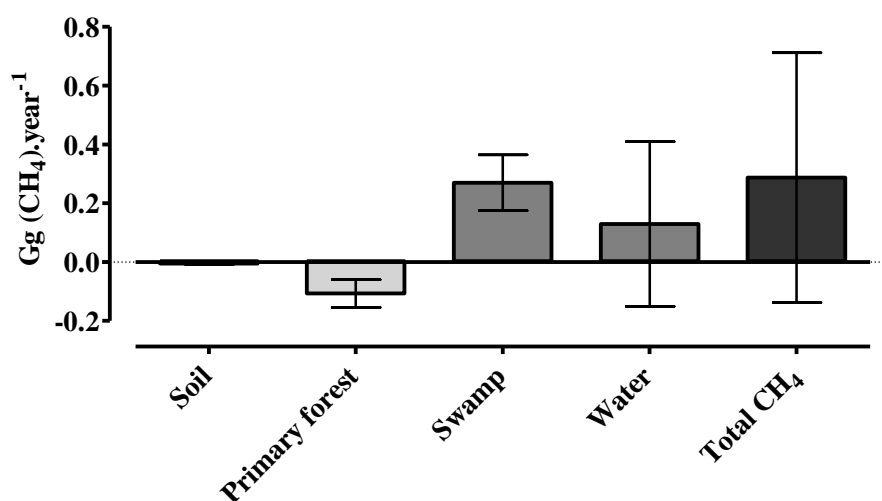


Figure 7.7. Average ( $\pm$  standard deviation) annual CH<sub>4</sub> exchanges in source (swamp, water surface), and sinks (primary forest, bare soil) ecosystems, and total budget.

### 7.3.1.4.3. N<sub>2</sub>O budget

As for CH<sub>4</sub>, we considered that all the swamp areas were in saturated conditions, and then attributed the emission value from swamp 1 site to the entire swamps surface. Evolution of the swamp area along the wet season was the result of agricultural soils flooding. No seasonal variation in the area of primary forest (154.5 km<sup>2</sup>, 34.6% of total flooded area) was considered. Light, medium and degraded forest ecosystems were clustered into the degraded forest category which represents an area of 207.9 km<sup>2</sup> (or 46.6% of total flooded area). For the riparian forest ecosystem, an average flux of  $0.61 \pm 0.31 \text{ mgN}_2\text{O}\cdot\text{m}^{-2}\cdot\text{d}^{-1}$  from the literature (Groffman et al, 2000; McSwiney et al, 2001) was used. N<sub>2</sub>O flux for the water surface was calculated from N<sub>2</sub>O surface concentrations determined in sampling stations NXT0, NXT1, NTH2 and NON1 (pristine sections of the Nam Xot, Nam Theun and Nam On rivers respectively). Fluxes were calculated via the thin boundary layer technique using a constant  $k_{600}$  of  $10 \text{ cm}\cdot\text{hr}^{-1}$ . From this, we estimated an average N<sub>2</sub>O flux from the water surface of  $4.8 \pm 9.8 \text{ mgN}_2\text{O}\cdot\text{m}^{-2}\cdot\text{day}^{-1}$ . A possible seasonal variability of the flux from the water surface has not been taken into account since we used annual mean surface water concentrations for this purpose.

Soil moisture is a very important and sensitive factor regulating N<sub>2</sub>O emission from soils. Many studies have suggested that the soil moisture directly regulates oxygen availability in soil pores, which in turn determines the status of nitrification and denitrification and the ratios of N<sub>2</sub>O to final products (Bandibas et al., 1994; Bateman et al., 2005; Cardenas et al., 1993; Conen, et al., 2000; Davidson, 1992; Hou et al., 2000; Maag and Vinther, 1996; Schindlbacher et al., 2004; Smith et al., 1998; Zheng et al., 2000). For N<sub>2</sub>O fluxes up scaling at the whole pre-impoundment landscape, we considered that for all sampling sites, the fluxes measured in the driest soils (high toposequence) were representative of the dry season. The emissions measured under conditions of intermediate soil moisture (middle toposequence) were assigned to conditions during the wet season. The measurements made at the bottom of toposequence (saturated soils) were assigned to an area representing 10% of the area of primary forest ecosystems and degraded forest in the wet season, and 100% of swamp area.

The length of the season is determined from known statistics of precipitation over the past ten years. Around 5% of the annual precipitation occurs in the dry season (January, February, March, April, October, November and December, or 212 days). Around 80 to 90% of the rainfall occurs in the wet season (May to September, or 153 days). Table 7.5 summarizes the average flux values for different ecosystems deduced from these assumptions, and used for the spatial integration of N<sub>2</sub>O emissions.

Figure 7.8 shows the annual N<sub>2</sub>O emissions from the different ecosystems prior to flooding. This budget is dominated by emissions from primary and degraded forests, agricultural soils and surface water, whereas wetlands and riparian forests are only minor sources for N<sub>2</sub>O. Pre-impoundment NT2 footprint was an annual N<sub>2</sub>O source of  $1156 \pm 558 \text{ Mg N}_2\text{O}\cdot\text{year}^{-1}$ .

Table 7.5. Average ( $\pm$  standard deviation)  $N_2O$  fluxes used for spatial extrapolation (all fluxes given in  $mgN_2O.m^{-2}.d^{-1}$ )

Type of ecosystem	Dry soil	Soil with intermediate moisture level	Saturated soils	References
Primary forest	$1.6 \pm 0.9$	$31.1 \pm 7.5$	$2.7 \pm 0.2$	This study
Degraded forest	$1.7 \pm 1.0$	$8.6 \pm 5.7$	$9.4 \pm 12.1$	This study
Riparian forest	$0.6 \pm 0.3$	$0.6 \pm 0.3$	$0.6 \pm 0.3$	Groffman et al., 2000; McSwinney et al., 2001
Agricultural soil	$2.8 \pm 3.8$	$4.5 \pm 3.3$	$1.3 \pm 2.1$	This study
Swamp	$1.3 \pm 2.1$	$1.3 \pm 2.1$	$1.3 \pm 2.1$	This study
Water	$4.8 \pm 9.8$	$4.8 \pm 9.8$	$4.8 \pm 9.8$	This study

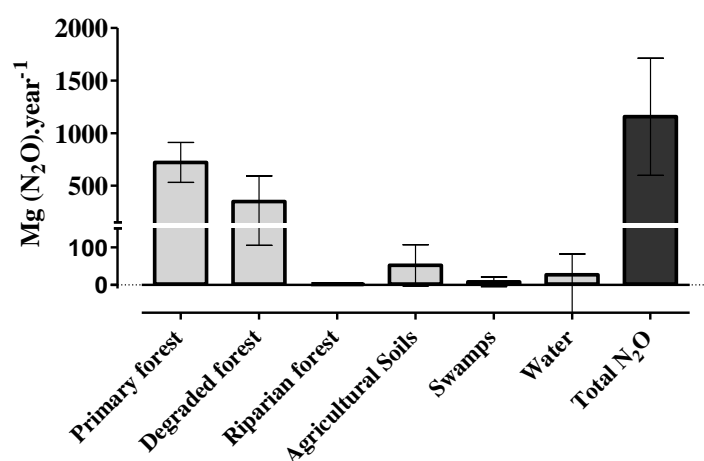


Figure 7.8. Average ( $\pm$  standard deviation) annual  $N_2O$  emitted by forests, swamp, agricultural ecosystems, water surface, and total budget (all terms in  $MgN_2O.year^{-1}$ ).

### 7.3.1.5. Assessment of GHG exchange in $CO_2$ equivalent

The  $CH_4$  and  $N_2O$  budgets were converted into  $CO_2$ -equivalent by multiplying the global warming potentials (GWPs) of  $CH_4$  and  $N_2O$ . For this calculation, GWP values of 25 and 298 for  $CH_4$  and  $N_2O$  respectively were used (IPCC 2007, 100 years time scale).

Table 7.6. Annual  $CO_2$ ,  $CH_4$ , and  $N_2O$  budgets converted into  $CO_2$ -equivalent (all terms given in  $Gg CO_2-eq.year^{-1}$ )

GHG	Exchange, $GgCO_{2eq}.year^{-1}$
Total $CH_4-CO_{2eq}$	$7 \pm 11$
Total $N_2O-CO_{2eq}$	$345 \pm 158$
Total $CO_2$	$-73 \pm 225$
<b>Total <math>CO_{2eq}</math></b>	<b><math>279 \pm 343</math></b>

Emissions of greenhouse gas from the pre-impoundment ecosystems within the NT2 footprint would represent a total of  $279 \pm 343 \text{ GgCO}_2\text{-eq. year}^{-1}$  (see Table 7.6), or an average flux of  $620 \pm 881 \text{ gCO}_2\text{-eq. m}^{-2}\text{. yr}^{-1}$ . Table 7.6 shows that the two most significant terms in the total GHG budget are exchanges of  $\text{N}_2\text{O}$  and  $\text{CO}_2$ , while the influence of  $\text{CH}_4$  is of secondary importance.

### 7.3.2. Post-impoundment GHG exchange

After the flooding of the NT2 Reservoir, the different GHG emission pathway terms from the NT2 reservoir footprint were quantified by integrating detailed spatial and temporal variability (see Chapter 3, Chapter 4, Chapter 5, and Chapter 6). This includes estimates of emissions from the drawdown area, diffusive and bubbling emissions from the reservoir water surface, and degassing and diffusive emissions from downstream (of the Nakai dam and the powerhouse). Sampling strategies with methodologies and results have been discussed in the previous chapters. Here are summarized the major findings regarding gross GHG emissions.

To calculate the post-impoundment gross GHG emissions from the NT2 Reservoir, estimates of the following pathways were established:

- a. Upstream GHG emissions
  1. Diffusive GHG emissions from the reservoir water surface
  2. Diffusive GHG emissions from the drawdown area
  3. Ebullitive (bubbling) GHG emissions from the reservoir surface area corresponding to less than 13 m water depth
- b. Downstream GHG emissions
  1. Diffusive GHG emissions downstream of the powerhouse (initial 30 km) and the Nakai Dam (initial 30 km)
  2. Degassing GHG emissions at five facilities: at the Nakai Dam (ecological flow and occasional spillway release), turbines outlet, regulating pond outlet, and aeration weir

In order to compare the contribution of each gas to gross GHG emissions,  $\text{CH}_4$  and  $\text{N}_2\text{O}$  emissions were converted to  $\text{CO}_2$  equivalent using GWPs as stated in pre-impoundment section. Estimates of post impoundment GHG budget for the different pathways of  $\text{CO}_2$ ,  $\text{CH}_4$  and  $\text{N}_2\text{O}$  are summarized in Table 7.7. Our results indicate that upstream GHG emissions (emissions from reservoir water surface and drawdown area) contributed around 87% and 92% of total GHG emissions for 2010 and 2011 respectively. With 13% and 8% for the year 2010 and 2011, downstream emissions (degassing and diffusion) show a percentage lower than reported for other reservoirs.

Table 7.7. Annual gross GHG budgets for the year 2010 and 2011 (GgCO<sub>2</sub>eq.year<sup>-1</sup>).

Year	Pathways	Upstream emission			Downstream emission		Total
		Diffusive fluxes from the drawdown area	Bubbling (water depth < 13m)	Diffusive fluxes from the reservoir water surface	Degassing	Diffusive fluxes from the downstream	
<b>2010</b>	CO <sub>2</sub>	324 ± 48		892 ± 239	51 ± 8	40 ± 4	1307 ± 244 <b>(60%)</b>
	CH <sub>4</sub>	20 ± 18	383 ± 28	173 ± 203	165 ± 18	28 ± 8	768 ± 206 <b>(35%)</b>
	N <sub>2</sub> O	64 ± 162		24 ± 11	2 ± 2	3 ± 0.2	93 ± 162 <b>(4%)</b>
	<b>All GHG</b>	408 ± 170 <b>(19%)</b>	383 ± 28 <b>(18%)</b>	1089 ± 313 <b>(50%)</b>	218 ± 19 <b>(10%)</b>	70 ± 8 <b>(3%)</b>	<b>2168 ± 358</b>
<b>2011</b>	CO <sub>2</sub>	243 ± 48		1192 ± 191	62 ± 8	54 ± 3	1551 ± 197 <b>(73%)</b>
	CH <sub>4</sub>	23 ± 20	318 ± 25	73 ± 85	55 ± 8	5 ± 3	473 ± 91 <b>(22%)</b>
	N <sub>2</sub> O	58 ± 170		48 ± 16		3 ± 0.5	109 ± 170 <b>(5%)</b>
	<b>All GHG</b>	324 ± 177 <b>(15%)</b>	318 ± 25 <b>(15%)</b>	1312 ± 210 <b>(62%)</b>	117 ± 11 <b>(5%)</b>	62 ± 4 <b>(3%)</b>	<b>2133 ± 276</b>

The following conclusions can be drawn from Table 7.7.

**a. Major emission pathways for different GHGs:**

1. CO<sub>2</sub>: Diffusive fluxes from reservoir water surface and from drawdown area
2. CH<sub>4</sub>: Bubbling, diffusive fluxes from the reservoir water surface and degassing.
3. N<sub>2</sub>O: Diffusive fluxes from the drawdown area and from the reservoir water surface.

**b. Significance of each gas to gross GHG emissions:** CH<sub>4</sub> and CO<sub>2</sub> emissions contribute significantly to total gross GHG emissions, while N<sub>2</sub>O has a small contribution.

**c. Upstream vs. downstream GHG emission:** most of the gross GHG emissions is contributed from upstream (emissions from drawdown, diffusion from reservoir water surface and bubbling), while relatively low GHG emissions come from the downstream (degassing and diffusion from downstream).

One can notice that pre-impoundment budget for CO<sub>2</sub> correspond to a sink, when the net footprint budget is a source for CH<sub>4</sub> and N<sub>2</sub>O (Figure 7.9). Our GHG budget reveals that the NT2 Reservoir is a significant source of CO<sub>2</sub> and CH<sub>4</sub>, and a much smaller source of N<sub>2</sub>O

(Figure 7.9). For the year 2010, with  $1307 \pm 244$  GgCO<sub>2</sub>eq.year<sup>-1</sup> and  $768 \pm 206$  GgCO<sub>2</sub>eq.year<sup>-1</sup> respectively, CH<sub>4</sub> and CO<sub>2</sub> have contributed around 60% and 35% to the total GHG budget, N<sub>2</sub>O accounting for less than 5% with  $93 \pm 162$  GgCO<sub>2</sub>eq.year<sup>-1</sup>. While CH<sub>4</sub> emissions show around 40% decrease from the year 2010 to 2011 ( $473 \pm 91$  GgCO<sub>2</sub>eq.year<sup>-1</sup> in the year 2011), CO<sub>2</sub> emissions increased around 15% ( $1551 \pm 197$  GgCO<sub>2</sub>eq.year<sup>-1</sup>) in the same time, when N<sub>2</sub>O emissions remained constant.

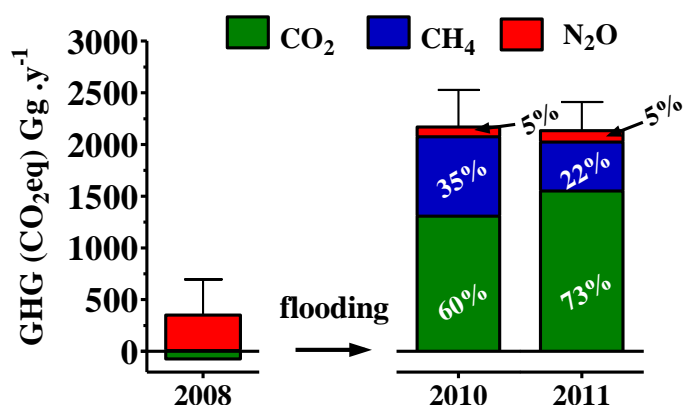


Figure. 7.9. Annual gross GHG budgets for the years 2008, 2010 and 2011.

Total GHG budget suggests that the footprint turned from a small source of total CO<sub>2</sub>eq emissions ( $279 \pm 343$  GgCO<sub>2</sub>eq.year<sup>-1</sup> in the year 2008) in pre-impoundment conditions, to a significant post impoundment source ( $2168 \pm 358$  and  $2133 \pm 276$  GgCO<sub>2</sub>eq.year<sup>-1</sup> for the years 2010 and 2011 respectively) (Figure 7.9).

#### 7.4. Net GHG Emissions

The net GHG footprint of the NT2 Reservoir represents the actual CO<sub>2</sub>, CH<sub>4</sub> and N<sub>2</sub>O fluxes to the atmosphere that can be directly attributed to the creation and existence of the reservoir. As stated in the methodology section, annual net budgets were calculated by subtracting the pre-impoundment GHG budget from the post-impoundment GHG budget. Table 7.8 summarizes the estimates of net budgets for the different GHGs.

Table 7.8. Annual net GHG budgets for the years 2010 and 2011 (all values given in Gg CO<sub>2</sub>eq.year<sup>-1</sup>).

GHG	Pre-impoundment exchange	Post-impoundment exchange		Net GHG footprint	
	2008	2010	2011	2010	2011
<b>Total CO<sub>2</sub></b>	$-73 \pm 225$	$1307 \pm 244$	$1551 \pm 197$	$1380 \pm 332$	$1624 \pm 299$
<b>Total CH<sub>4</sub>-CO<sub>2</sub>eq</b>	$7 \pm 11$	$768 \pm 206$	$473 \pm 91$	$761 \pm 206$	$466 \pm 92$
<b>Total N<sub>2</sub>O-CO<sub>2</sub>eq</b>	$345 \pm 258$	$93 \pm 162$	$109 \pm 170$	$-252 \pm 305$	$-236 \pm 309$
<b>Total CO<sub>2</sub>eq</b>	$279 \pm 343$	$2168 \pm 358$	$2133 \pm 276$	$1889 \pm 496$	$1854 \pm 440$

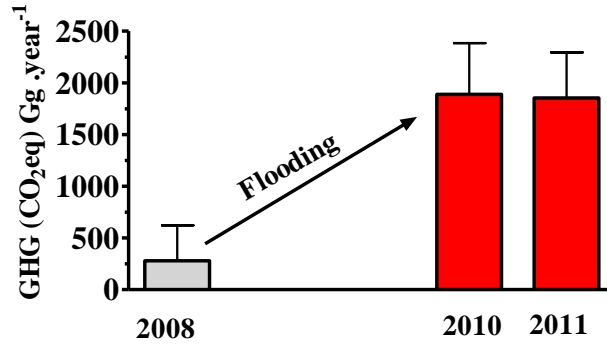


Figure. 7.10. Annual net GHG budgets for the years 2010 and 2011.

The difference between the pre-impoundment and post-impoundment emissions indicates that the net NT2 reservoir footprint is a 10 times large source of GHG ( $1889 \pm 496$  and  $1854 \pm 440$  Gg CO<sub>2</sub>eq.year<sup>-1</sup> respectively for the years 2010 and 2011; Table 7.8).

### 7.5. Net GHG emissions and energy generation

From the net GHG footprint of the NT2 Reservoir calculated in the previous section, and the annual power generation (6TWh), GHG emission factors of 310 and 300 gCO<sub>2</sub> eq.kWh<sup>-1</sup> are calculated for the years 2010 and 2011, respectively. One can conclude that the net GHG emission factor from NT2 reservoir is significantly lower than the emission factors of power plants running on natural gas and all other current fossil-fuel based technologies (Figure 7.11).

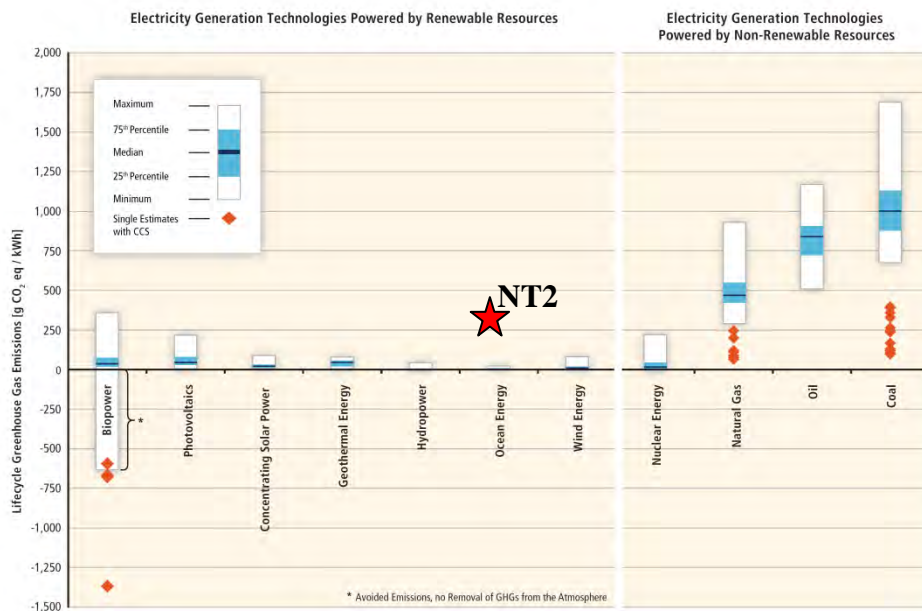


Figure 7.11: Estimates of lifecycle GHG emissions (gCO<sub>2</sub>eq.kWh<sup>-1</sup>) for broad categories of electricity generation technologies, plus some technologies integrated with CCS (IPCC, 2012). It must be noted that red star corresponds to GHG emissions factor for the first 2 years after impoundment of the NT2 Reservoir (which is not the lifecycle GHG emissions).



Those rate are about more than 3 times lower than the mean emission factor of thermal power plant using coal (generator types with scrubbing), and 1.5 times lower than of the GHG emission factor of thermal power plant using natural-gas combined cycle (Figure 7.11).

For more direct comparison of GHG emission factors related to power generation, it is more relevant to use the cumulative GHG emissions throughout the lifespan of the generating facilities (e.g. 100 years for reservoirs). Literature suggests that these emissions will decline over the next following years (Barros et al., 2011; St. Louis et al., 2000). It is difficult at this point to accurately estimate the trend of the NT2 reservoir net GHG budget over the next 100 years, and this is the next step to be undertaken.

GHG emission factors from hydroelectricity vary from one climatic region to another. This result should only be attributed to sub-tropical or tropical reservoir, and not to temperate or boreal reservoirs. Further, GHG emission can also vary within a climatic region from one reservoir to another. This is related to differences in abiotic and biotic parameters in the reservoirs such as availability of carbon and nitrogen, residence time, average water depth, reservoir shape, design and location of the turbine intake (influence on downstream emissions). These estimated GHG emissions related to energy production are likely to vary with the actual reservoir operation and management (time, duration, seasonality of water release for example).

As a conclusion, one should note that the creation of the NT2 sub-tropical reservoir resulted in a significant shift in the GHG budget of the footprint that was flooded. The results of this work project highlights the importance of well documenting (both in term of assessment and process understanding) the GHG exchanges of the natural landscapes prior to flooding, and the post-impoundment GHG budget when determining the net GHG footprint of a hydroelectric reservoir.



## Chapter 8

### Conclusion and outlook

---

#### 8.1. Methane (CH<sub>4</sub>)

##### 8.1.1. CH<sub>4</sub> dynamics

Experiments on the methanogenesis have shown that the CH<sub>4</sub> production rates were lower in the soils from the NT2 Reservoir as compared to some hydroelectric reservoirs studied in the Amazonian region. Our results hint that comparatively low flooded carbon leads to lower CH<sub>4</sub> production in the reservoir. Aerobic CH<sub>4</sub> oxidation at the top of the hypolimnion during the stratified period effectively regulates the CH<sub>4</sub> levels in the epilimnion. The fortnightly continuous monitoring of the CH<sub>4</sub> concentrations on the water column revealed that those concentrations and subsequent emissions to the atmosphere varied over four orders of magnitude. Maximum concentrations were observed during the warm dry season and minimum ones during the cold dry seasons. Our study clearly shows that the physical dynamics of the water column along with dissolved O<sub>2</sub> level in the water are the most important determinants of CH<sub>4</sub> concentration in the water column, rather than methanogenesis (production) at the bottom itself.

Our results show that seven out of nine sampling stations behaved similarly, suggesting a not strong spatial variation compared to the complexity in the system (i.e. different flooded ecosystems). However, embayment(s)/flooded forest (i.e. RES3 in our study) behaved differently than other sampling stations and had higher CH<sub>4</sub> concentration in the water column. Often such sampling stations have been overlooked. Interestingly, artificial mixing due to structural design (i.e. RES9 in our study) can build up very high surface CH<sub>4</sub> concentrations, and allows CH<sub>4</sub> outgassing and increase CH<sub>4</sub> oxidation via penetrating O<sub>2</sub> to the bottom of the water column. Therefore, it's very important to examine the whole reservoir considering the physical dynamics and pre-flooded ecosystems.

Owing to the large seasonal variation in the CH<sub>4</sub> concentrations, our sampling strategy warns that irregular/interrupted sampling could lead to a misunderstanding and wrong assessment of CH<sub>4</sub> emissions. A recommendation to avoid such errors is that sampling should be performed, at least, for all seasons.

##### 8.1.2. Techniques for assessing CH<sub>4</sub> emissions

In the course of assessing CH<sub>4</sub> emissions from the water surface of the reservoir and their variations at different time scales, multiple approaches and techniques have been investigated. The micrometeorological technique, namely the one based on eddy covariance (EC) calculation was deployed during four field campaigns (between May 2009 and June 2011). Direct field measurement techniques included traditional ones, such as floating chambers (FC) for diffusive fluxes and submerged funnels (SF) for bubbling fluxes were

performed simultaneously. The EC method is a less invasive that was used for one of the first time on sub-tropical hydroelectric reservoir. The two approaches, the EC one on one side, and the FC and SF on the other one, are complimentary. Floating chamber and submerged funnel techniques are reliable and inexpensive, but they need continuous manpower. Their results are representative of small scale, which is interesting to study spatial heterogeneity, though inconvenient to extrapolate the results at a larger scale. On the other hand, EC technique is costly and some caution need to be taken for the deployment, for post-processing data and quality control criteria. First advantage of EC technique is the high spatial coverage it offers. Second, it allows for high temporal resolution and long-term automated monitoring - two factors not easy to reach with other traditional techniques. High frequent and long term measurements are useful to investigate the link between CH<sub>4</sub> emissions and their drivers (see next section). This may increase our understanding of the underlying processes regulating CH<sub>4</sub> fluxes on different time scales. When matching EC footprint with floating chamber and funnel measurements, it was observed that our EC methodology was able to capture both diffusive and bubbling fluxes together. For all the field campaigns, EC fluxes were very consistent with the sum of the two terms measured independently (diffusive fluxes + bubbling fluxes = EC fluxes). From the EC measurements, it was found that there is a clear semidiurnal pattern in the CH<sub>4</sub> emissions. Therefore, one should perform submerged funnel measurement on at least 24 hr time period to cover the entire daily variation, as done in this study. Short time measurement of bubbling can be overestimated or underestimated the CH<sub>4</sub> emissions significantly. Semidiurnal pattern warns that only day time measurement can lead an overestimation of CH<sub>4</sub> emissions.

### **8.1.3. Environmental drivers of CH<sub>4</sub> flux variability**

The continuous and high resolution flux sampling provided by EC allowed us to evidence peak periods of CH<sub>4</sub> emissions on daily and seasonal time scales. It was revealed that atmospheric pressure changes, water depth, and water level changes played a critical role in temporal variability of CH<sub>4</sub> emission. We observed a semidiurnal variation of EC fluxes during all four campaigns. These two peaks per day - one in early morning and one in the afternoon, were clearly linked to the semi-diurnal atmospheric pressure variation (late morning and night pressure drop). Our daily EC CH<sub>4</sub> fluxes were weakly linked with near-surface temperature. This is not surprising since temperature did not affect emissions as strongly on daily/short-term basis as temperature could concern on seasonal basis. As for the seasonal variability, CH<sub>4</sub> fluxes from the reservoir were found to be mostly linked with the changes in the reservoir water level.

A comprehensive dataset allowed us to examine the factors regulating the ebullitive emissions of CH<sub>4</sub>. Ebullitive CH<sub>4</sub> emission decreased non-linearly with the depth and atmospheric pressure. Further, it was discovered that ebullitive CH<sub>4</sub> emission was sensitive to changes in the water depth, change in the atmospheric pressure, and bottom temperature. All these factors changing concurrently in an environment such as a hydroelectric reservoir, consequently CH<sub>4</sub> ebullitive emission becomes a non-linear stochastic process. To explore such a process, we chose to develop an artificial neuron network model (ANN) which can

explain up to 50% of the ebullitive fluxes variability using water depth, atmospheric pressure, variations in the water level, atmospheric pressure change and bottom temperature as inputs.

#### **8.1.4. Gross CH<sub>4</sub> emissions**

We reported here the first assessment of gross CH<sub>4</sub> emissions from a newly flooded sub-tropical hydroelectric reservoir including all major emission pathways. Total gross emissions from NT2 were found to be lower than emissions reported in previous studies available, mainly conducted in South America. Our result confirms that CH<sub>4</sub> emissions experience a significant seasonal variability (see previous section).

Among the all emission pathways at the NT2 Reservoir, we have first evidenced a dominant contribution from ebullition, proportionally higher when compared to previously studied (sub) tropical reservoirs. We have evidenced a new hotspot of emission by diffusion just before the turbines water intake. Its existence in other reservoirs depends both on the design of the water intake and the physics of the water column upstream of the structure. In reservoirs with well mixed water column, the occurrence of mixing upstream of the turbines should not have impacted, whereas in stratified reservoir with high hypolimnetic CH<sub>4</sub> concentration such in the NT2 during the warm dry season, CH<sub>4</sub> diffusive fluxes could be overlooked if such stations are not included in the monitoring. The design of the water intake together with the design of the water release below the powerhouse (and regulating pond in the NT2 case) leads to a very low contribution of the downstream emissions compared to South American reservoirs.

Around 38% decrease of the emissions from the year 2010 to 2011 is probably because of significant increase in the CH<sub>4</sub> oxidation in the reservoir and thereby low diffusive and degassing emission. Further, higher emissions for the year 2010 resulted from the accumulation of CH<sub>4</sub> before the turbines went on operation in March 2010. The comparison of the contribution of each emission pathway to the total emissions from the NT2 Reservoir with other reservoirs evidences that the estimation of worldwide emission from hydroelectric reservoirs is challenging.

## **8.2. Carbon dioxide (CO<sub>2</sub>)**

### **8.2.1. Techniques for assessing CO<sub>2</sub> emissions**

Direct flux measurements of CO<sub>2</sub> fluxes using the eddy covariance (EC) technique were consistent with CO<sub>2</sub> emissions measured with the conventional floating chamber (FC) (based on *in-situ* measurements and gas chromatography as well). This provided a cross-validation of the three methods for assessing diffusive CO<sub>2</sub> emissions. FC appears to be a reliable and inexpensive technique to measure diffusive CO<sub>2</sub> emissions when operated properly. This implies avoiding the creation of artificial turbulence by having FCs with walls extending into the water and performing measurements while drifting. Owing to continuous 30 min integration intervals, the eddy covariance technique allowed to capture all the temporal variability contained in biophysical processes and the linkage with their drivers.

### **8.2.2. Environmental drivers of CO<sub>2</sub> flux variability**

CO<sub>2</sub> flux measurement from different deployments revealed a complex pattern which appears to be mainly a result of the interaction of physical processes in the water column and meteorological processes above the water surface. CO<sub>2</sub> fluxes appeared to be time-dependent over the NT2 Reservoir and changes from one season to another. Our results indicate that owing to the contribution of turbulent velocity scale to the turbulence at the water-air interface, CO<sub>2</sub> fluxes are much higher when  $T_{\text{water}} > T_{\text{air}}$  with thermal and CO<sub>2</sub> gradient in the water column. On the opposite, when the water column exhibits a poor thermal stratification together with no CO<sub>2</sub> gradient, low CO<sub>2</sub> fluxes occur. Our results confirm that during heat gain by the water column (buoyancy > 0), CO<sub>2</sub> fluxes are linearly dependent on wind speed. Whereas, during heat loss from the water column (buoyancy < 0), (1) at low wind speed, fluxes do not show a clear dependency on the wind speed, and (2) at higher wind speed, fluxes increase exponentially with the wind speed.

### **8.2.3. Gross CO<sub>2</sub> emissions and carbon budget**

From the gross CO<sub>2</sub> emissions assessment, it was found that emissions from upstream of the dam (drawdown area and diffusion from the reservoir water surface) contribute around 93% of the total gross CO<sub>2</sub> emissions for the years 2010 and 2011, while only 7% were coming from the downstream area (degassing and diffusion). The annual carbon balance calculation indicated that this reservoir was a significant carbon source to the atmosphere. Import and export carbon balance has revealed that around 85-90% of total annual carbon release (atmosphere + downstream) is fuelled by organic carbon flooded at the bottom of the reservoir during impoundment. Our results suggest that total carbon release within the first two years after impoundment correspond to around 15% of the initial flooded organic carbon in the first 30 cm layer of soils and above-ground biomass.

Our results show that the magnitude of diffusive CO<sub>2</sub> fluxes from the drawdown area varied in the same range as observed at the reservoir water surface, a pathway never investigated in previous CO<sub>2</sub> emissions studies. Considering the strong proportion of the drawdown area to the total reservoir surface, we suggest that this pathway should be accountable for future studies to avoid underestimate in assessing gross CO<sub>2</sub> emission from the hydroelectric reservoirs.

### **8.3. Nitrous oxide (N<sub>2</sub>O) dynamics and gross emissions**

We observed the wet season as a hot moment for the N<sub>2</sub>O concentration in the reservoir water column. It was found that during the wet season, a significant amount of N<sub>2</sub>O was carried in to the reservoir with the high water inflow from the watershed. Further, it seems that during water level rising, flooding of soils could increase the denitrification process in the flooded drawdown soils. Another probable reason could be an enhanced nitrification process during hydrodynamical mixing of NH<sub>4</sub><sup>+</sup>-rich hypolimnetic water with oxygenated epilimnetic water.

Further, notably, it was discovered that soils of the drawdown area can be significant hot spot of N<sub>2</sub>O emission. Significantly higher fluxes were observed in the mid zone of the drawdown area, this could be due to an enhanced nitrification process during water level falling when NH<sub>4</sub><sup>+</sup>-rich anoxic soil are exposed to the air. During the increase in the water level, NO<sub>3</sub><sup>-</sup>-rich oxic soil becomes anoxic, both conditions that favor denitrification. This suggests that if the drawdown area represents a large portion of the reservoir surface, like in the NT2 case, it can represent a significant proportion (53-67% for the NT2) of the total N<sub>2</sub>O emission. This is an important new result, specially keeping in mind that fluxes from the drawdown area have never been considered in previous studies.

#### **8.4. Net GHG footprint**

Our study has shown that natural ecosystems pre-existing of flooding were overall a low source of GHG. After flooding, the whole ecosystem has an almost ten times higher GHG footprint. This highlights the importance of understanding the GHG exchanges of the natural landscapes prior to flooding, and the post-impoundment GHG budget when determining the net GHG footprint of a hydroelectric reservoir.

For the two first years after impoundment (2010 and 2011), it was observed that CO<sub>2</sub> and CH<sub>4</sub> emissions contributed mostly to the total gross GHG emissions, 60-73% and 22-35% of the total gross GHG emission for CO<sub>2</sub> and CH<sub>4</sub> respectively. This study clearly indicates that N<sub>2</sub>O emissions did not significantly contribute to the gross GHG emissions (~5%). N<sub>2</sub>O emissions are probably not an issue in hydroelectric reservoirs with low nitrogen inputs like the NT2 Reservoir. In contrast to results from other large tropical reservoirs, we found that design of the water intake and the physics of the water column upstream of the turbine intake significantly lowered downstream GHG emissions. Indeed, most of the gross GHG emissions in NT2 were attributed to upstream (emissions from drawdown, diffusion from reservoir water surface and bubbling).

With net GHG emissions of  $1889 \pm 496$  and  $1854 \pm 440$  GgCO<sub>2</sub>eq.year<sup>-1</sup>, and an annual power generation of 6 TWh, net GHG emission factors of 0.31 and 0.30 Mg-CO<sub>2</sub> eq.MWh<sup>-1</sup> were calculated for the years 2010 and 2011 respectively. These GHG emission factors represent about one third of the mean emission factor (0.96 Mg-CO<sub>2</sub> eq.MWh<sup>-1</sup>) of thermal power plant using coal (generator types with scrubbing) and generally, is well below the emissions of the power plant running on natural gas and all other current fossil fuel based technologies. If the results were extrapolated to the entire watershed, net emissions from the NT2 would have been even lower. Though NT2 net GHG emission factor is not negligible, it is considerably lower than emission factors for some South American reservoirs. This comes from a combination of higher annual power production and lower net emissions.

#### **8.5. Outlook and implications for future GHG emission research**

We have identified short and long term causes for temporal changes in CH<sub>4</sub> emissions that should be considered when attempting to predict or estimate CH<sub>4</sub> emissions from a hydroelectric reservoir. Ebullitive CH<sub>4</sub> emission is sensitive to change in the water level and

atmospheric pressure, normally such daily variation as seen at the NT2 are expected to cause large variations in CH<sub>4</sub> emissions; therefore, it appears that they must be taken into consideration when estimating emissions from a hydroelectric reservoir. Water depth and probably also temperature (as a proxy for CH<sub>4</sub> production) vary CH<sub>4</sub> emissions on seasonal or yearly timescale. Here only physical variables have been linked to CH<sub>4</sub> emissions. One should keep in mind that biological activity occurring at the sediment (i.e. decomposition of organic matter in the sediments) is responsible for the CH<sub>4</sub> fluxes observed over a period of reservoir life.

It is very clear from our study that ebullition deserves a lot more attention while assessing CH<sub>4</sub> emissions from hydroelectric reservoirs. We developed an ANN model to quantify the ebullition using water depth, atmospheric pressure, water level change, change in atmospheric pressure and bottom temperature of the reservoir. It would be beneficial to use our model in other (sub) tropical reservoirs to further develop the ANN ability to parameterize CH<sub>4</sub> ebullition in a wider range of conditions. However, in order to quantify the spatial variability in the bubble characteristics and their release in a better way, approaches based on hydroacoustics should be encouraged in such aquatic ecosystem. Measurements coupling submerged funnels and hydroacoustics on one hand, along with floating chambers and EC on the other hand should be tested in the future for intercomparison and cross validation.

A permanent and continuous deployment of eddy covariance and equilibrators would be appreciated to provide continuous discrimination of bubbling and diffusion. Further, it will allow us to examine the hot moments: (1) bubbling burst when total static pressure drops (e.g. water level drop in the warm dry season or sudden atmospheric pressure drop), (2) sudden and large outgassing by diffusion during overturn (e.g., thermal over turn in cold dry season or hydrological mixing in the wet seasons when a large mass of water enters in the reservoir).

We stress that our laboratory experiments aiming at the quantification of CH<sub>4</sub> production did not consider the seasonal changes in the temperature. For this reason, we used constant Q<sub>10</sub> value for methanogenesis to mimic the seasonal changes in the temperature occurring in the sediment layer at reservoir bottom. We encourage that future work should consider such seasonal variation in temperature since methanogenesis is significantly influenced by temperature.

It is very important to precisely identify the processes fuelling the GHG emissions for better prediction of GHG emissions from the reservoir. The internal cycling of C and N either in the water column or in the flooded soils and sediments has to be well understood. Therefore identification of sources of OM using isotopes and OM tracers would be appreciated in the future works.

We found that the NT2 Reservoir does not exhibit stratification throughout the year. It exhibits an oxic upper layer of the sediment during wet season, leading to CH<sub>4</sub> oxidation in the upper layer of sediment which was not accounted for in this study. For future work, we suggest to consider CH<sub>4</sub> oxidation at the sediments for reservoirs that do not exhibit stratification throughout the year such as NT2.



Further, high frequency continuous monitoring of CO<sub>2</sub> concentration in the whole water column would be appreciated to improve the understanding on CO<sub>2</sub> dynamics in the water column at small time scale. A permanent and continuous deployment of eddy covariance, series of thermocouples and equilibrators which are capable to provide continuous measurements of temperature and GHG concentration at different depths in the water column would be appreciated. It will allow us to examine (1) sudden and large diffusion during overturn (e.g., thermal over turn in cold dry season or hydrological mixing in the wet seasons when a large mass of water enters in the reservoir (2) examine the proportional contribution of convective velocity scale and shear velocity scale to the actual turbulence at the water surface must be included to improve our understanding on buoyancy influence on gas exchange in the tropical hydroelectric reservoirs.

In this study we extrapolated the N<sub>2</sub>O fluxes from the whole drawdown area by using soil moisture content, considering moisture content being the main controlling factor of the nitrification and denitrification processes responsible for N<sub>2</sub>O emissions. We encourage future studies focusing on linking the other environmental variables in addition to soil moisture content to N<sub>2</sub>O emissions and such assumptions should be better checked. This would help to better quantify the contribution of the drawdown area to the total N<sub>2</sub>O emission at the reservoir scale.

Further, the comparison of the contribution of each pathway to the total emissions from the NT2 Reservoir with other reservoirs evidences that the estimation of worldwide emission from hydroelectric reservoirs is challenging because of following reasons: (1) is very high proportional contribution of bubbling to the total CH<sub>4</sub> emissions a common phenomenon in young reservoirs or was it overlooked in others studied done in older reservoir? (2) comparison of different emission pathways with other reservoirs suggest that each emission pathways vary significantly from one reservoir to another (3) unfortunately, very few detailed studies (i.e. considering spatial and temporal variability) are available.

For direct comparison of GHG emission factors related to power generation, it would be more relevant to calculate lifecycle GHG emissions of the generating facilities (e.g. 100 years for reservoirs). Literature suggests that these emissions will decline over the next following years (Barros et al., 2011; St. Louis et al., 2000). It is difficult at this point to accurately estimate the trend of the NT2 net GHG footprint over the next 100 years. This shall be the next step to be undertaken.

We estimated the GHG emissions for a newly flooded subtropical reservoir. This estimate corresponds to the period of the life cycle of the hydroelectric reservoir when maximum GHG emissions are expected. While comparing the hydroelectric power with alternative energy sources, these estimates can be considered as the upper values that would be reached for this reservoir. Knowing that GHG emission factors from hydroelectricity vary from one climatic region to another, the calculated GHG emission factor should only be attributed to sub-tropical or tropical reservoir.

There is an urgent demand from the industry, financial institutions and decision makers for reliable predictive tools able to estimate GHG emissions from unmonitored and/or future hydroelectric reservoirs. Development of this kind of tools will rely on comprehensive data set of GHG emission and proxies. This is particularly true for reservoirs from the tropical climatic region. This is even more sensitive for the Asian continent where data are particularly scarce, though this region has the potential of many new hydroelectric projects to come in the future. We hope that the whole data set built all along this three-year study will be used to validate those predictive models. First step could be to test our data set against the predictive tool developed under the UNESCO/IHA umbrella. The UNESCO/IHA predictive tool might not reproduce NT2 emission with the full spatial and temporal resolution acquired during this study, but rather produce a risk indicator (e.g. probable range of emissions with defined thresholds). After the development of the predictive tools, the development of guidance and assessment tools for mitigation should be pursued. Indeed, there is an urgent need to couple process-based model on greenhouse gases (i.e. biogeochemistry) and water quality (i.e. hydrodynamics).

## References

---

- Aberg, J., A. K. Bergstrom, G. Algesten, K. Soderback and M. Jansson. 2004. A comparison of the carbon balances of a natural lake (L. Ortrasket) and a hydroelectric reservoir (L. Skinnmuddselet) in northern Sweden. *Water Research*, Vol.38. No.3, Feb, pp. 531- 538, 0043-1354.
- Abril, G., and N. Iversen. 2002. Methane dynamics in a shallow non-tidal estuary Randers Fjord, Denmark. *Mar. Ecol. Prog. Ser.* 230, 171-181.
- Abril, G., F. Guerin, S. Richard, R. Delmas, C. Galy-Lacaux, P. Gosse, A. Tremblay, L. Varfalvy, M.A. Dos Santos and B. Matvienko. 2005. Carbon dioxide and methane emissions and the carbon budget of a 10-year old tropical reservoir (Petit Saut, French Guiana). *Global Biogeochem. Cycles*, Vol.19. No.4, Oct, 0886-6236.
- Abril, G., M. V. Commarieu, A. Sottolichio, P. Bretel, and F. Guerin. 2009. Turbidity limits gas exchange in a large macrotidal estuary. *Estuar. Coast. Shelf Sci.* 83: 342-348, doi:10.1016/j.ecss.2009.03.006.
- Abril, G., M. V., Commarieu, and F. Guérin. 2007. Enhanced methane oxidation in an estuarine turbidity maximum. *Limnol. Oceanogr.* 52:470-5.
- Acht nich, C., F. Bak, and R. Conrad. 1995. Competition for electron donors among nitrate reducers, ferric iron reducers, sulfate reducers, and methanogens in anoxic paddy soil. *Biol. Fertil. Soils* 19, 65-72.
- Algar, C. K., and B. P. Boudreau. 2010. Stability of bubbles in a linear elastic medium: Implications for bubble growth in marine sediments. *J. Geophys. Res.* 115: F03012.
- Allen, D. E., R. C. Dalal, H. Rennenberg, R. L. Meyer, S. Reeves, and S. Schmidt. 2007. Spatial and temporal variation of nitrous oxide and methane flux between subtropical mangrove sediments and the atmosphere. *Soil Biol. Biochem.* 39, 622-631.
- Aller, R. C. 2004. Conceptual models of early diagenetic processes: the muddy seafloor as an unsteady, batch reactor. *J. Mar. Res.* 62, 815- 835.
- Amorocho, J., and J. J. DeVries. 1980. A new evaluation of the wind stress coefficient over water surfaces. *J. Geophys. Res.* 85, 433-442.
- Anderson, D. E., R. G. Striegl, D. I. Stannard, C. M. Micherhuizen, T. A. McConnaughey, and J. W. LaBaugh. 1999. Estimating lake-atmosphere CO<sub>2</sub> exchange. *Limnol. Oceanogr.* 44:988-1001.
- Andersson, M., A. Kjøller, and S. Struwe. 2003. Soil emissions of nitrous oxide in fire prone African savannas. *J. Geophys. Res.* 108, 4630-4639.
- Anis, A., and G. Singhal. 2006. Mixing in the surface boundary layer of a tropical freshwater reservoir. *J. Mar. Sys.* 63: 225-243.
- Aubinet, M., A. Grelle, A. Ibrom, Rannik, J. Moncrieff, T. Foken, A. S. Kowalski, P. H. Martin, P. Berbigier, C. Bernhofer, R. Clement, J. Elbers, A. Granier, T. Grünwald, K. Morgenstern, K. Pilegaard, C. Rebmann, W. Snijders, R. Valentini, T. Vesala. 1999. Estimates of the annual net carbon and water exchange of forests: the EUROFLUX methodology. *Adv. Ecol. Res.* 30, 113-175.
- Aufdenkampe, A., E. Mayorga, P. Raymond, J. Melack, S. Doney, S. Alin, R. Aalto, K. Yoo. 2011. Riverine coupling of biogeochemical cycles between land, oceans, and atmosphere. *Front. Ecol. Environ.* 9(1), 53-60, doi:10.1890/100014.
- Baer, D. S., J. B. Paul, J. B. Gupta, and A. O'Keefe. 2002. Sensitive absorption measurements in the near-infrared region using off-axis integrated-cavity-output spectroscopy. *Appl. Phy. B.* 75 2-3, 261-265.

- Baldocchi, D., E. Falge, L.H. Gu, R. Olson, D. Hollinger, S. Running, P. Anthoni, C. Bernhofer, K. Davis, R. Evans, J. Fuentes, A. Goldstein, G. Katul, B. Law, X.H. Lee, Y. Malhi, T. Meyers, W. Munger, W. Oechel, K.T. Paw U, K. Pilegaard, H.P. Schmid, R. Valentini, S. Verma, T. Vesala, K. Wilson, and S. Wofsy. 2001. FLUXNET: a new tool to study the temporal and spatial variability of ecosystem-scale carbon dioxide, water vapor, and energy flux densities. *Bulletin of the American Meteorological Society* 82 11, 2415-2434.
- Baldocchi, D., M. Detto, O. Sonnentag, J. Verfaillie, Y. Teh, W. Silver, and N. M. Kelly. 2012. The challenges of measuring methane fluxes and concentrations over a peatland pasture. *Agric. Forest Meteorol.* v.153, Feb 15, p.177 11.
- Baldwin, D. S., and A. M. Mitchell. 2000. The effects of drying and re-flooding on the sediment and soil nutrient dynamics of lowland river-floodplain systems: a synthesis. *Regul. Rivers Res. Manage.* 16, 457-467.
- Bandibas, J., A. Vermoesen, C.J. De Groot, and O.V. Cleemput. 1994. The effect of different moisture regimes and soil characteristics on nitrous oxide emission and consumption by different soils. *Soil Science* 158 2, 106-114.
- Banerjee, S., and S. MacIntyre. 2004. The air-water interface: Turbulence and scalar exchange, in *Advances in Coastal and Ocean Engineering*, vol. 9, edited by J. Grue et al., pp. 181-237, World Sci., Hackensack, N. J.
- Barros, N., J. J. Cole, L. J. Tranvik, Y. T. Prairie, D. Bastviken, V.L.M. Huszar, P. Del Giorgio, and F. Roland. 2011. Carbon emission from hydroelectric reservoirs linked to reservoir age and latitude. *Nature Geoscience*, Vol.4. No.9, Sep, pp. 593-596, 1752- 0894
- Bartlett, K. B., and R. C. Harriss. 1993. Review and assessment of methane emissions from wetland. *Chemosphere*. 26: 261-320.
- Bastviken, D., J. Ejlertsson, I. Sundh, and L. Tranvik. 2003. Methane as a source of carbon and energy for lake pelagic food webs. *Ecology*. 84: 969-981.
- Bastviken, D., J. J. Cole, M. L. Pace, and M. C. Van De Bogert. 2008. Fates of methane from different lake habitats: Connecting whole-lake budgets and CH<sub>4</sub> emissions. *J. Geophys. Res.* 113: G02024.
- Bastviken, D., J., Cole, M. Pace, and L. Tranvik. 2004. Methane emissions from lakes: dependence of lake characteristics, two regional assessments, and a global estimate. *Global Biogeochem. Cycles*; 18:GB4009. Doi: 10.1029/2004GB002238.
- Bastviken, D., L. J. Tranvik, J. A. Downing, P. M. Crill, and A. Enrich-Prast. 2011. Freshwater methane emissions offset the continental carbon sink. *Science*. 7; 3316013:50.
- Bateman, E. J., and E. M. Baggs. 2005. Contributions of nitrification and denitrification to N<sub>2</sub>O emissions from soils at different water-filled pore space. *Biol. Fert. Soils*. 41: 379-388.
- Bedard, C., and R. Knowles. 1997. Some properties of methane oxidation in a thermally stratified lake, *Can. J. Aquat. Sci.*, 54, 1639-1645.
- Bender, M., and R., Conrad. 1994. Methane oxidation activity in various soils and fresh-water sediments - occurrence, characteristics, vertical profiles, and distribution on grain-size fractions. *J. Geophys. Res.-Atmos.* 99, 16531-16540.
- Bergstrom, A.K., G. Algesten, S. Sobek, L. Tranvik, and M. Jansson. 2004. Emission of CO<sub>2</sub> from hydroelectric reservoirs in northern Sweden. *Archiv. Fur. Hydrobiologie*, Vol.159. No.1, Jan, pp. 25-42, 0003-9136

- Bertilsson, S., and Allard, B. 1996. Sequential photochemical and microbial degradation of refractory dissolved organic matter in a humic freshwater system. *Arch. Hydrobiol. Beih. Ergebn. Limnol.* 48:133-141.
- Blackmer, A. M., and J. M. Bremner. 1978. Inhibitory effects of nitrate on reduction of N<sub>2</sub>O to N<sub>2</sub> by soil microorganisms. *Soil Biol. Biochem.* 10, 187-191.
- Bleakly, B.H., and J.M. Tiedje. 1982. Nitrous oxide production by organisms other than nitrifiers or denitrifiers. *Appl. Environ. Microbiol.*, 44: 1342-1348.
- Bodaly, R.A., K.G. Beaty, L.H. Hendzel, A.R. Majewski, M.J. Paterson, K.R. Rolffhus, A.F. Penn, V.L. St Louis, B.D. Hall, C.J.D. Matthews, K.A. Cherewyk, M. Mailman, J.P. Hurley, S.L. Schiff, and J.J. Venkiteswaran. 2004. Experimenting with hydroelectric reservoirs. *Environ. Sci. Technol.* 38, 346A-352A.
- Bollmann, A., and R. Conrad. 1998. Influence of O<sub>2</sub> availability on NO and N<sub>2</sub>O release by nitrification and denitrification in soils. *Glob. Change Biol.* 4, 387-396.
- Boon, P.I., 2000. Carbon cycling in Australian wetlands: the importance of methane. *Verh. Internat. Verein. Limnol.* 27:37-50
- Boon, P.I., and B.K. Sorrell. 1995. Methane fluxes from an Australian floodplain wetland: the importance of emergent macrophytes. *Journal of North American Benthological Society* 14, 582-598.
- Borges, A.V., B. Delille, L.-S. Schiettecatte, F. Gazeau, G. Abril, and M. Frankignoulle. 2004. Gas transfer velocities of CO<sub>2</sub> in three European estuaries Randers Fjord, Scheldt and Thames. *Limnol. Oceanogr.* 49, 1630-1641.
- Borrel, G., D., Jezequel, C., Biderre-Petit, N., Morel-Desrosiers, J. P., Morel, P., Peyret, G., Fonty, and A. C., Lehours. 2011. Production and consumption of methane in freshwater lake ecosystems. *Res. Microbiol.* 162, 832-847.
- Bosse, U., P. Frenzel, and R. Conrad. 1993. Inhibition of methane oxidation by ammonium in the surface layer of a littoral sediment. *FEMS Microbiol. Ecol.* 13, 123-134.
- Bouwman, A. F., K. W. van der Hoek, and J. G. J. Oliver. 1995. Uncertainties in the global source distribution of nitrous oxide, *J. Geophys. Res.*, 100, 2785-2800.
- Bremner, J.M. 1997. Sources of nitrous oxide in soils. *Nutrient Cycling in Agroecosystems* 49, 7-16.
- Brothers, S., P. A. del Giorgio, C. R. Teodoru, and Y. T. Prairie. 2012. Landscape heterogeneity influences CO<sub>2</sub> production in a young boreal reservoir. *Can J Fish Aquat Sci* 69:447-456. doi:10.1139/f2011-174.
- Burchard, H., 2002. Applied turbulence modelling in marine waters. Springer-Verlag, Berlin.
- Burgermeister, J., 2007. Missing carbon mystery: Case solved? *Nat. Rep.* 3: 36-37.
- Butterbach-Bahl, K., G. Willibald, and H. Papen. 2002. Soil core method for direct simultaneous determination of N<sub>2</sub> and N<sub>2</sub>O emissions from forest soils. *Plant and Soil*, 240: 105-116.
- Calleja, M. L., C. M. Duarte, Y. T. Prairie, S. Agusti, and G. J. Herndl. 2009. Evidence for surface organic matter modulation of air-sea CO<sub>2</sub> gas exchange. *Biogeosciences* 6: 1105-1114, doi:10.5194/bg-6-1105-2009.
- Campo, J., and L. Sancholuz. 1998. Biogeochemical impacts of submerging forests through large dams in the Rio Negro, Uruguay. *J. Environ. Manag.* 54:59-66.

- Cardenas, L., A. Rondon, C. Johansson, and E. Sanhueza. 1993. Effects of soil moisture, temperature, and inorganic nitrogen on nitric oxide emissions from acidic tropical savannah soils. *J. Geophys. Res.*, 98: 14783-14790.
- Casper, P., S. C. Maberly, G. H. Hall, and B. J. Finlay. 2000. Fluxes of methane and carbon dioxide from a small productive lake to the atmosphere. *Biogeochemistry* 49, 1-19.
- Chanton, J.P., C.S. Martens, and C.A. Kelley, 1989. Gas transport from methane saturated, tidal freshwater and wetland sediments. *Limnol. Oceanogr.*, 34:807-819.
- Chanudet, V and S. Descloux. 2008. Pre-impoundment estimation of the above and below ground carbon stocks of the Nam Theun 2 reservoir. EDF report n° IH.NT-WQ.ENV.00021.A, pp 21.
- Chanudet, V., S. Descloux, A. Harby, H. Sundt, B.H. Hansen, O. Brakstad, D. Serça, and F. Guérin. 2011. Gross CO<sub>2</sub> and CH<sub>4</sub> emissions from the Nam Ngum and Nam Leuk sub-tropical reservoirs in Lao PDR. *Sci. Total Environ.*, 409, 5382-5391.
- Chanudet, V., V. Fabre, and T. Kaaij. 2012. Application of a three-dimensional hydrodynamic model to the Nam Theun 2 Reservoir Lao PDR. *J. Great Lakes Res.* 382: 260-269.
- Chartrand, N., R. Schetagne, and R. Verdon. 1994. Enseignements tires du suivi environnemental au complexe La Grande. In : *Dix-huitieme Congres international des Grands Barrages, Comptes rendus*, 7-11 novembre 1994, Durban (South Africa). Paris: Commission Internationale des Grands Barrages, pp 165-190.
- Chen, H., N. Wu, S. Yao, Y. Gao, D. Zhu, Y. Wang, W. Xions, and X. Yuan. 2009. High methane emissions from a littoral zone on the Qinghai-Tibetan Plateau, *Atmospheric Environ.* 43, 4995-5000.
- Chen, H., X. Yuan, Y. Gao, N. Wu, D. Zhu, and J. Wang. 2010. Nitrous oxide emissions from newly created littoral marshes in the drawdown area of the three Gorges reservoir, China. *Water, Air, & Soil Pollution*, 1-9.
- Chen, H., X. Yuan, Z. Chen, Y. Wu, X. Liu, and D. Zhu. 2011. Methane emissions from the surface of the Three Gorges Reservoir. *J. Geophys. Res.*, 9; 116:5.
- Chen, H., Y. Wu, X. Yuan, Y. Gao, N. Wu, and D. Zhu. 2009. Methane emissions from newly created marshes in the drawdown area of the Three Gorges Reservoir, *J. Geophys. Res.*, 114, D18301, doi:10.1029/2009JD012410.
- Chin, K. J., and R. Conrad. 1995. Intermediary metabolism in methanogenic paddy soil and the influence of temperature. *FEMS Microbiol. Ecol.* 18, 85-102.
- Cicerone, R. J., and R. S. Oremland. 1988. Biogeochemical aspects of atmospheric methane. *Global Biogeochem. Cycles*, 2: 299-327.
- Clark, J. F., R. Wanninkhof, P. Schlosser, and H. J. Simpson. 1994. Gas exchange rates in the tidal Hudson River using a dual tracer technique. *Tellus* 46B:274-285.
- Clein, J. S., A. D. McGuire, and X. Zhang. 2002. Historical and projected carbon balance of mature black spruce ecosystems across North America: the role of carbon-nitrogen interactions. *Plant and Soil* 242:15-32.
- Cole, J. J., and N. F. Caraco. 1998. Atmospheric exchange of carbon dioxide in a low-wind oligotrophic lake measured by the addition of SF<sub>6</sub>. *Limnol. Oceanogr.* 43, 647-656.
- Cole, J. J., and N. F. Caraco. 2001. Emissions of nitrous oxide N<sub>2</sub>O from a tidal, freshwater river, the Hudson River, New York. *Environ. Sci. Technol.* 35, 991-996.

Cole, J. J., N. F. Caraco, G. W., Kling, and T. K. Kratz. 1994. Carbon dioxide supersaturation in the surface waters of lakes, *Science*, 265, 1568-1570.

Cole, J. J., Y. T. Prairie, N. F. Caraco, W. H. McDowell, L. J. Tranvik, R. G. Striegl, C. M. Duarte, P. Kortelainen, J. A. Downing, J. J. Middelburg and J. Melack. 2007. Plumbing the global carbon cycle: Integrating inland waters into the terrestrial carbon budget, *Ecosystems*, doi:10.1007/s10021-006-9013-8.

Collos, Y., A. Vaquer, A. M. Johnston, V. Pons, B. Bibent, and S. Richard. 2001. Carbon fixation, ammonium uptake and regeneration in an equatorial Lake: Biological versus physical control, *J. Plankton Res.*, 23, 263- 270.

Conen, F., K. E. Dobbie, and K. A. Smith. 2000. Predicting N<sub>2</sub>O emissions from agricultural land through related soil parameters. *Glob. Change Biol.* 6: 417-426.

Conrad, R. 1989. Control of methane production in terrestrial ecosystems. Pages 39-58. In M.O. Andrea and D.S. Schimel eds. *Exchange of Trace Gases between Terrestrial Ecosystems and the Atmosphere*. J.Wiley & Sons.

Conrad, R. 2002. Microbiological and biochemical background of production and consumption of NO and N<sub>2</sub>O in soil. In: *Trace Gas Exchange in Forest Ecosystems* eds.: Gasche, R., Papen, H., Rennenberg, H. 3-33. Kluwer Academic Publishers, Dordrecht, Netherlands.

Crill, P.M., K.B. Bartlett, J.O. Wilson, D.I. Sebacher, and R.C. Harriss. 1988. Tropospheric methane from an Amazonian floodplain lake. *J. Geophys. Res.* 93, 1564-1570.

Crucius, J. and R. Wanninkhof. 2003. Gas transfer velocities measured at low wind speed over a lake. *Limnol. Oceanogr.*, 48, 1010-1017.

Dannenberg, S., J. Wulderl, and R. Conrad. 1997. Agitation of anoxic paddy soil slurries affects the performance of the methanogenic microbial community. *FEMS Microbiol. Ecol.* 22, 257-263.

Das, S. and T. K. Adhya. 2012. Dynamics of methanogenesis and methanotrophy in tropical paddy soils as influenced by elevated CO<sub>2</sub> and temperature interaction. *Soil Biology and Biochemistry* 47, 36-45.

Davidson, E. A., and J. P. Schimel. 1995. Microbial processes of production and consumption of nitric oxide, nitrous oxide and methane. In: Matson, P.A., Harriss, R.C. Eds., *Biogenic Trace Gases: Measuring Emissions from Soil and Water*. Blackwell Sci, Malden, Mass, pp. 327-357.

Davidson, E.A., M. Keller, H.E. Erickson, L.V. Verchot, and E. Veldkamp. 2000. Testing a conceptual model of soil emissions of nitrous and nitric oxides. *BioScience*, 50: 667-680.

Deardoff, J. W. 1970. Convective velocity and temperature scales for unstable planetary boundary layer and for Rayleigh convection. *J. Atmos. Sci.* 27: 1211-1213.

del Giorgio P. A. and R. H. Peters. 1993. Balance between phytoplankton production and plankton respiration in lakes. *Can J Fish Aquat Sci* 50:282-9.

del Giorgio, P. A., J. J. Cole, N. F. Caraco, and R. H. Peters. 1999. Linking planktonic biomass and metabolism to net gas fluxes in northern temperate lakes, *Ecology*, 80, 1422-1431.

Delmas, R., C. Galy-Lacaux, and S. Richard. 2001. Emissions of greenhouse gases from the tropical hydroelectric reservoir of Petit Saut French Guiana compared with emissions from thermal alternatives. *Global Biogeochem. Cycles*; 15:993-1003.

Delmas, R., S. Richard, F. Guérin, G. Abril, C. Galy-Lacaux, C. Delon, and A. Gregoire. 2004. Long term greenhouse gas emissions from the hydroelectric reservoir of Petit Saut (French Guiana) and potential impacts in

Greenhouse Gas Emissions. In Tremblay, L. Varfalvy, C. Roehm and M. Garneau (Eds), *Fluxes and Processes. Hydroelectric Reservoirs and Natural Environments*. Environmental Science Series, Springer-Verlag, Berlin Heidelberg. pp. 293-312.

Delon, C., D. Serça, C. Boissard, R. Dupont, A. Dutot, P. Laville, P. De Rosnay, and R. Delmas. 2007. Soil NO emissions modelling using artificial neural network. *Tellus B* 59 3: 502-513.

DelSontro, T., D. F., McGinnis, S., Sobek, I., Ostrovsky, and B., Wehrli. 2010. Extreme Methane Emissions from a Swiss Hydropower Reservoir: Contribution from Bubbling Sediments. *Environ. Sci. Technol.* 44:2419-25.

DelSontro, T., M. J. Kunz, T. Kempter, A. Wüest, B. Wehrli, and D. B. Senn. 2011. Spatial heterogeneity of methane ebullition in a large tropical reservoir. - *Environ. Sci. Technol.* 45: 9866-9873.

Demarty, M. and J. Bastien. 2011. GHG emissions from hydroelectric reservoirs in tropical and equatorial regions: Review of 20 years of CH<sub>4</sub> emission measurements, *Energy Policy*, 39.

Demarty, M., J. Bastien, A. Tremblay, R. H. Hesslein, and R. Gill. 2009. Greenhouse gas emissions from boreal reservoirs in Manitoba and Quebec, *Canada, Environ. Sci. Technol.*, 43:23, 8905-8915, doi:10.1021/es8035658.

Demarty, M., J. Bastien, and A. Tremblay. 2011. Annual follow-up of gross diffusive carbon dioxide and methane emissions from a boreal reservoir and two nearby lakes in Québec, Canada, *Biogeosciences*, 8, 41-53, doi:10.5194/bg-8-41-2011.

Descloux, S., V. Chanudet, H. Poilvé, and A. Grégoire. 2011. Co-assessment of biomass and soil organic carbon stocks in a future reservoir area located in Southeast Asia. *Environ. Monit. Assess.* 173, 723-741.

Detto, M., J. Verfaillie, F. Anderson, L. Xu, and D. Baldocchi. 2011. Comparing laser-based open- and closed-path gas analyzers to measure methane fluxes using the eddy covariance method, *Agric. Forest Meteorol.*, 151, 1312-1324, doi:10.1016/j.agrformet.2011.05.014.

Diem, T., S. Koch, S. Schwarzenbach, B. Wehrli, and C. J. Schubert. 2012. Greenhouse gas emissions CO<sub>2</sub>, CH<sub>4</sub> and N<sub>2</sub>O from several perialpine and alpine hydropower reservoirs by diffusion and loss in turbines. *Aquat. Sci. Res.*, Aquatic Sciences - Research Across Boundaries, 2012, Volume 74, Number 3, Pages 619-635.

Dlugokencky, E. J., K. A. Masarie, P. M. Lang, and P. P. Tans. 1998. Continuing decline in the growth rate of the atmospheric methane burden, *Nature*, 393, 447-450.

Dlugokencky, E. J., L. Bruhwiler, J. W. C. White, L. K. Emmons, P. C. Novelli, S. A. Montzka, K. A. Masarie, P. M. Lang, A. M. Crotwell, J. B. Miller, and L. V. Gatti. 2009. Observational constraints on recent increases in the atmospheric CH<sub>4</sub> burden, *Geophys. Res. Lett.*, 36, L18803, doi:10.1029/2009GL039780.

Dlugokencky, E. J., S. Houweling, L. Bruhwiler, K. A. Masarie, P. M. Lang, J. B. Miller, and P. P. Tans. 2003. Atmospheric methane levels off: Temporary pause or a new steady-state?, *Geophys. Res. Lett.*, 19, doi:10.1029/2003GL018126.

Dong, L.F., D.B. Nedwell, I. Colbeck, and J. Finch. 2004. Nitrous oxide emission from some English and Welsh rivers and estuaries. *Water, Air and Soil Pollution: Focus* 4, 127-134.

Dorrestein, R., 1979. On the vertical buoyancy flux below the sea surface as induced by atmospheric factors. *J. Phys. Oceanogr.* 9 (1), 229-231.

Dos Santos M. A., B. Matvienko, L.P. Rosa, E. Sikar, and E.O. Dos Santos. 2005. Gross greenhouse gas emissions from Brazilian hydro reservoirs. In: Tremblay A, Varfalvy L, Roehm C, Garneau M, editors.,



*Greenhouse gas emissions - fluxes and processes. Hydroelectric reservoirs and natural environments.* Berlin: Springer Verlag;. p. 267-91.

Dos Santos, M.A., L.P. Rosa, B. Sikar, E. Sikar, and E.O. Dos Santos. 2006. Gross greenhouse gas fluxes from hydro-power reservoir compared to thermo-power plants. *Energy Policy*, Vol.34. No.4, Mar, pp. 481-488, 0301-4215.

Downing, J. A., Y. T. Prairie, J. J. Cole, C. M. Duarte, L. Tranvik, R. Striegl, W. H. McDowell, P. Kortelainen, N. Caraco, J. M. Melack, and J. Middelburg. 2006. The global abundance and size distribution of lakes, ponds, and impoundments. *Limnol. Oceanogr.* Vol: 51(5). Pages 2388-2397.

Duarte, C.M., and Y.T. Prairie. 2005. Prevalence of heterotrophy and atmospheric CO<sub>2</sub> emissions from aquatic ecosystems. *Ecosystems* 8:862-870.

Duc, N.T., P. Crill, and D. Bastviken. 2010. Implications of temperature and sediment characteristics on methane formation and oxidation in lake sediments. *Biogeochemistry* 100, 185-196.

Duchemin, E., M. Lucotte, and R. Canuel. 1999. Comparison of static chamber and thin boundary layer equation methods for measuring greenhouse gas emissions from large water bodies. *Environ. Sci. Technol.* 33:350-7.

Duchemin, E., M. Lucotte, R. Canuel, A. G. Queiroz, D. C. Almeida, H. C. Pereira, and J. Dezincourt. 2000. Comparison of greenhouse gas emissions from an old tropical reservoir with those of 355 other reservoirs worldwide, *Verh. Int. Ver. für Limnol.*, 27, 1391-1395.

Duchemin, E., M. Lucotte, R. Canuel, and A. Chamberland. 1995. Production of the greenhouse gases CH<sub>4</sub> and CO<sub>2</sub> by hydroelectric reservoirs of the boreal region. *Global Biogeochem. Cycles*, Vol.9. No.4, pp. 529-540.

Duchemin, E.; M. Lucotte, R. Canuel, and N Soumis. 2006. First assessment of methane and carbon dioxide emissions from shallow and deep zones of boreal reservoirs upon ice break-up. *Lakes & Reservoirs: Research & Management*, Vol.11. No.1, pp. 9-19, 1440-1770.

Dumestre, J. F., E. O. Casamayor, R. Massana, and C. Pedros-Alio. 2001. Changes in bacterial and archeal assemblages in an equatorial river induced by the water eutrophication of Petit-Saut Dam reservoir French Guiana. *Aquat. Microb. Ecol.* 26 : 206-221.

Dumestre, J. F., J. Guezennec, C. Galy-Lacaux, R. Delmas, S. Richard, and L. Labroue. 1999. Influence of light intensity on methanotrophic bacterial activity in the Petit Saut reservoir, French Guiana. *Appl. Environ. Microbiol.* 65 : 534-539.

Dunfield, P.F., and R. Conrad. 2000. Starvation alters the apparent half-saturation constant for methane in the type II methanotroph *Methylocystis* strain LR1. *Appl. Environ. Microbiol.* 66: 4136-4138.

Eggleton, H. S., L. Buendia, K. Iwa, T. Ngara and K. Tanabe eds. 2006. Intergovernmental Panel on Climate Change IPCC, National Greenhouse Gas Inventories Guidelines, Vol. 4 - Agriculture, Forestry and Other Land Use. Kanagawa, Japan: IGES. AP2.1-AP2.9.

Ehrlich, H. L., and K.N. Dianne. 2009. *Geomicrobiology*. 5th ed. Boca Raton, FL: CRC Press.

Eugster, W., and P. Plüss. 2010. A fault-tolerant eddy covariance system for measuring CH<sub>4</sub> fluxes. *Agric. Forest Meteorol.* 150: 841-851.

Eugster, W., G. T. Kling, J. P. Jonas, A. McFadden, S. MacIntyre, and F. S. Chapin III. 2003. CO<sub>2</sub> exchange between air and water in an arctic Alaskan and midlatitude Swiss lake: importance of convective mixing. *J. Geophys. Res.* 108:4362-4380. doi:10.1029/2002JD002653.

Eugster, W., T. Delontro, and S. Sobek. 2011. Eddy covariance flux measurements confirm extreme CH<sub>4</sub> emissions from a Swiss hydropower reservoir and resolve their short-term variability. *Biogeosciences*, 8: 2815-2831. doi:10.5194/bg-8-2815-2011.

Fearnside, P. M. 1997. Greenhouse-gas emissions from Amazonian hydroelectric reservoirs: the example of Brazil's Tucuruí Dam as compared to fossil fuel alternatives. *Environ. Conserv.*, Vol.24. No.1, Mar, pp. 64-75, 0376-8929.

Fearnside, P. M. 2002. Greenhouse gas emissions from a hydroelectric reservoir (Brazil's Tucuruí dam) and the energy policy implication. *Water Air Soil Pollut.* 133: 69-96.

Fearnside, P. M. 2004. Greenhouse gas emissions from hydroelectric dams: Controversies provide a springboard for rethinking a supposedly 'clean' energy source - An editorial comment. *Clim. Change*, Vol.66. No.1-2, Sep, pp. 1-8, 0165-0009.

Fearnside, P. M. 2005a. Do hydroelectric dams mitigate global warming? The case of Brazil's Curuá-Una dam. *Mitigation and Adaptation Strategies for Global Change*, Vol.10. No.5, pp. 675-691.

Fearnside, P. M. 2005b. Greenhouse Gas Emissions from Hydroelectric Dams: Reply to Rosa et al., *Clim. Change* 75:1-2.

Fearnside, P. M. 2006. Greenhouse gas emissions from hydroelectric dams: Reply to Rosa et al. *Clim. Change*, Vol.75. No.1-2, Mar, pp. 103-109, 0165-0009.

Fearnside, P.M. 1995. Hydroelectric dams in the Brazilian amazon as sources of greenhouse gases. *Environ. Conserv.*, Vol.22. No.1, Spr, pp. 7-19, 0376-8929.

Fearnside, P.M., 1996. Hydroelectric dams in Brazilian Amazonia: response to Rosa, Schaeffer and dos Santos. *Environ. Conserv.* 23:105-108.

Fey, A., and R. Conrad. 2000. Effect of temperature on carbon and electron flow and on the archaeal community in methanogenic rice field soil. *Appl. Environ. Microbiol.* 66, 4790e4797.

Foken, T., and B. Wichura. 1996. Tools for quality assessment of surface based flux measurements, *Agric. Forest Meteorol.*, 78, 83-105, doi:10.1016/0168-1923(95)02248-1.

Forster, P., V. Ramaswamy, P. Artaxo, T. Berntsen, R. Betts, D.W. Fahey, J. Haywood, J. Lean, D. C. Lowe, G. Myhre, J. Nganga, R. Prinn, G. Raga, M. Schulz, and R. Van Dorland. 2007. Changes in Atmospheric Constituents and in Radiative Forcing. In: *Climate Change 2007: The Physical Science Basis. Contribution of Working Group I to the Fourth Assessment Report of the Intergovernmental Panel on Climate Change* (Solomon, S., D. Qin, M. Manning, Z. Chen, M. Marquis, K.B. Averyt, M.Tignor and H.L. Miller eds.). Cambridge University Press, Cambridge, United Kingdom and New York, NY, USA.

Frankignoulle, M. 1988. Field-measurements of air sea CO<sub>2</sub> exchange. *Limnol. Oceanogr.* 33, 313-322.

Frankignoulle, M., G. Abril, A. Borges, I. Bourge, C. Canon, B. Delille, E. Libert, and J.M.Theate. 1998. Carbon dioxide emission from European estuaries, *Science* 282, 434-436.

Frankignoulle, M., I. Bourge, and R. Wollast, 1996. Atmospheric CO<sub>2</sub> fluxes in a highly polluted estuary (The Scheldt). *Limnol. Oceanogr.* 41, 365-369.

Frenzel, P., B. Thebrath, and R. Conrad. 1990. Oxidation of methane in the oxic surface layer of a deep lake sediment Lake Constance. *FEMS Microbiol. Lett.* 73, 149-158.

Frew, N. M., J. C. Goldman, M. R. Dennett, and A. S. Johnson. 1990. Impact of phytoplankton-generated surfactants on air-sea gas exchange. *J. Geophys. Res.* 95: 3337-3352, doi:10.1029/JC095iC03p03337.

- Froelich, P. N., G. P. Klinkhammer, M. L. Bender, N. A. Luedtke, G. R. Heath, D. Cullen, and P. Dauphin. 1979. Early oxidation of organic matter in pelagic sediments of eastern equatorial Atlantic: suboxic diagenesis. *Geochim. Cosmochim. Acta* 43, 1075-1090.
- Frost, T., and R.C. Upstill-Goddard. 2002. Meteorological controls of gas exchange at a small English lake. *Limnol. Oceanogr.* 47, 1165-1174.
- Galchenko, V.F., A. Lein, and M. Ivanov. 1989. Biological sinks of methane. In: Andrea MO, and Schimel DS (eds) *Exchange of trace gases between terrestrial ecosystems and the atmosphere*. Wiley and Sons, New York, pp 59-71.
- Galy-Lacaux, C., R. Delmas, C. Jambert, J. F. Dumestre, L. Labroue, S. Richard, and P. Gosse. 1997. Gaseous emissions and oxygen consumption in hydroelectric dams: A case study in French Guiana. *Global Biogeochem. Cycles*. 11 : 471-483.
- Galy-Lacaux, C., R. Delmas, G. Kouadio, S. Richard, and P. Gosse. 1999. Long term greenhouse gas emission from a hydroelectric reservoir in tropical forest regions. *Global Biogeochem. Cycles*. 13 :503-517.
- García-Ruiz, R., S. N. Pattinson, and B. A. Whitton. 1999. Nitrous oxide production in the river Swale-Ouse, North-East England. *Water Research* 33, 1231-1237.
- Garnier, J., G. Billen, G. Vilain, A. Martinez, M. Silvestre, E. Mounier, and F. Toche. 2009. Nitrous oxide N<sub>2</sub>O in the Seine River and basin: observations and budgets. *Agric. Ecosyst. Environ.* 133, 223-233.
- Gebert, J., A. Groengroeft, and G. Miehlich. 2003. Kinetics of microbial landfill methane oxidation in biofilters. *Waste Manage.* 23: 609-619.
- Gebert, J., H. Köthe, and A. Gröngröft. 2006. Prognosis of methane formation by river sediments. *J. Soils Sediments* 6, 75-83.
- Glaser, P. H., J. P. Chanton, P. Morin, D. O. Rosenberry, D. I. Siegel, O. Ruud, L. I. Chasar, and A. S. Reeve. 2004. Surface deformations as indicators of deep ebullition fluxes in a large northern peatland. *Global Biogeochem. Cycles* 18, GB1003.
- Groffman P. M., A.J. Gold and R.C. Simmons. 1992. Nitrate dynamics in riparian forests. *J. Environ. Qual.* 21:666-71.
- Groffman, P.M., A.J. Gold, and K. Addy. 2000. Nitrous oxide production in riparian zones and its importance to national emission inventories. *Chemosphere-Global Change Science* 2, 291-299.
- Guérin F., G. Abril A. Tremblay and R. Delmas. 2008b. Nitrous oxide emissions from tropical hydroelectric reservoirs. *Geophys. Res. Lett.*, 35, doi:10.1029/2007GL033057.
- Guerin, F., and G. Abril. 2007. Significance of pelagic aerobic methane oxidation in the methane and carbon budget of a tropical reservoir. *J. Geophys. Res. Biogeosci.* 112:G03006.
- Guérin, F., G. Abril, A. de Junet, and M. P. Bonnet. 2008a. Anaerobic decomposition of tropical soils and plant material: implication for the CO<sub>2</sub> and CH<sub>4</sub> budget of the Petit Saut Reservoir. *Appl. Geochem.*; 23:2272-83.
- Guérin, F., G. Abril, D. Serça, C. Delon, S. Richard, R. Delmas, A. Tremblay, and L. Varfalvy. 2007. Gas transfer velocities of CO<sub>2</sub> and CH<sub>4</sub> in a tropical reservoir and its river downstream, *J. Mar. Syst.*, 66, 161- 172.
- Guérin, F., G. Abril, S. Richard, B. Burban, C. Reynouard, P. Seyler, and R. Delmas. 2006. Methane and carbon dioxide emissions from tropical reservoirs: Significance of downstream rivers, *Geophys. Res. Lett.*, 33, L21407, doi:10.1029/2006GL027929.

- Hahn, M., K. Gartner, and S. Zechmeister-Boltenstern. 2000. Greenhouse gas emission (N<sub>2</sub>O, CO<sub>2</sub>, CH<sub>4</sub>) from three different soils near Vienna (Austria) with different water and nitrogen regimes. *Die Bodenkultur* 51(2):115-125.
- Hamilton, J.D., C.A. Kelly, J.W.M. Rudd, R.H. Hesslein, and N.T. Roulet. 1994. Flux to the atmosphere of CH<sub>4</sub> and CO<sub>2</sub> from wetland ponds on the Hudson Bay lowlands (HBLs). *J. Geophys. Res.* 99 (D1):1495-1510.
- Hamilton, S.K., S. J. Sippel, and J. M. Melack. 1995. Oxygen depletion and carbon dioxide and methane production in waters of the Pantanal wetland of Brazil. *Biogeochemistry* 30:115-141.
- Hansen, J., M. Sato, R. Ruedy, K. Lo, D. W. Lea, and M. Medina-Elizade. 2006. Global temperature change, *Proc. Natl. Acad. Sci. U. S. A.*, 103, 14,288-14,293.
- Hanson, R., and T. E. Hanson. 1996. Methanotrophic bacteria, *Microbiol. Rev.*, 60, 439-471.
- Haslwanter, A., Hammerle, A., Wohlfahrt, G., 2009. Open- vs. closed-path eddy covariance measurements of the net ecosystem carbon dioxide and water vapour exchange: a long-term perspective. *Agric. Forest Meteorol.* 149, 291-302.
- Hendriks, D. M. D., J. van Huissteden, and A. J., Dolman. 2009. Multi-technique assessment of spatial and temporal variability of methane fluxes in a peat meadow, *Agric. Forest Meteorol.*, 150, 757-774.
- Hendriks, D.M.D., A.J., Dolman, M.K., van der Molen, and J. van Huissteden. 2008. A compact and stable eddy covariance set-up for methane measurements using off-axis integrated cavity output spectroscopy. *Atmospheric Chemistry and Physics*. 8 2, 431-443.
- Hendzel, L., C. Matthews, J. Venkiteswaran, V. St Louis, D. Burton, E. Joyce, and R. Bodaly. 2005. Nitrous oxide fluxes in three experimental boreal forest reservoirs. *Environ. Sci. Technol.* 39, 4353e4360.
- Herbst, M., T. Friberg, R. Ringgaard, and H. Soegaard. 2011. Interpreting the variations in atmospheric methane fluxes observed above a restored wetland, *Agric. Forest Meteorol.*, 151, 841-853.
- Hernandez, M. E., and W. J. Mitsch. 2006. Influence of hydrologic pulses, flooding frequency, and vegetation on nitrous oxide emissions from created riparian marshes. *Wetlands* 26, 862-877.
- Hill A. R., K. J. Devito, S. Campagnolo and K. Sanmugas. 2000. Subsurface denitrification in a forest riparian zone. *Biogeochemistry* 51:193-223.
- Hinrichs, K. U., and A. B. Boetius. 2002. The anaerobic oxidation of methane: new insights in microbial ecology and biogeochemistry. In *Ocean Margin Systems*. Wefer, G., Billett, D., Hebbeln, D., Jørgensen, B.B., Schlüter, M., and van Weering, T. eds, Heidelberg: Springer-Verlag, p. 457-477.
- Hirano, T., H. Segah, T. Harada, S. Limin, T. June, R. Hirata, and M. Osaki. 2007. Carbon dioxide balance of a tropical peat swamp forest in Kalimantan, Indonesia, *Glob. Change Biol.*, 13(2), 412-425.
- Ho, D. T., F. Veron, E. Harrison, L. F. Bliven, N. Scott, and W. R. Mcgillis. 2007. The combined effect of rain and wind on air-water gas exchange: A feasibility study. *J. Mar. Syst.* 66: 150-160, doi:10.1016/j.jmarsys.2006.02.012.
- Ho, D. T., L. F. Bliven, R. Wanninkhof, and P. Schlosser. 1997. The effect of rain on air-water gas exchange. *Tellus* 49B, 149-158.
- Hoffert, M. I., K. Caldeira, A. K. Jain, E. F. Haites, L. D. D. Harvey, S. D. Potter, M. E. Schlesinger, S. H. Schneider, R.G. Watts, T. M. L Wigley, and D. J. Wuebbles. 1998. Energy implications of future stabilization of atmospheric CO<sub>2</sub> content. *Nature* 395, 881-884.

- Holmes, R.M., J. Jeremy, B. Jones, S. G. Fisher, N. B. Grimm. 1996. Denitrification in a nitrogen-limited stream ecosystem. *Biogeochemistry* 33:125-46.
- Hou, A., H. Akiyama, Y. Nakajima, S. Sudo, and H. Tsuruta. 2000. Effects of urea form and soil moisture on N<sub>2</sub>O and NO emissions from Japanese Andosols. *Chemosphere* 2: 321-327.
- Houghton, J. T., Y. Ding, D. J. Griggs, M. Noguer, P. J. van der Linden, X. Dai, K. Maskell, and C. A. Johnson. 2001. Eds. Climate change 2001. The scientific basis. Contribution of Working Group I to the Third Assessment Report of the Intergovernmental Panel on Climate Change, Cambridge University Press, Cambridge and New York.
- Hulthe, G., S. Hulth and P. O. J. Hall. 1998. Effect of oxygen on degradation rate of refractory and labile organic matter in continental margin sediments. *Geochim. Cosmochim. Acta.* 62:1319-1328.
- Huotari, J., A. Ojala, E. Peltomaa, A. Nordbo, S. Launiainen, J. Pumpanen, T. Rasilo, P. Hari, and T. Vesala. 2011. Long-term direct CO<sub>2</sub> flux measurements over a boreal lake: Five years of eddy covariance data. *Geophys. Res. Lett.* 38. doi:10.1029/2011GL048753.
- Huttunen, J. T., T. S. Vaisanen, S. K. Hellsten, and P. J. Martikainen. 2006. Methane fluxes at the sediment-water interface in some boreal lakes and reservoirs. *Boreal Environ. Res.* 11: 27-34.
- Huttunen, J.T., J., Alm, A., Liikanen, S., Juutinen, T., Larmola, T., Hammar, J., Silvola, and P.J., Martikainen. 2003a. Fluxes of methane, carbon dioxide and nitrous oxide in boreal lakes and potential anthropogenic effects on the aquatic greenhouse gas emissions. *Chemosphere* 52, 609-621.
- Huttunen, J.T., S., Juutinen, J., Alm, T., Larmola, T., Hammar, J., Silvola, and P.J., Martikainen. 2003b. Nitrous oxide flux to the atmosphere from the littoral zone of a boreal lake. *J. Geophys. Res.* 108 D14, 4421-4430.
- Huttunen, J.T., T.S. Väisänen, S.K. Hellsten, M. Heikkikinen, H. Nykänen, H. Jungner, A. Niskanen, M.O. Virtanen, O.V. Lindqvist, O. Nenonen, and P.J. Martikainen. 2002. Fluxes of CH<sub>4</sub>, CO<sub>2</sub>, and N<sub>2</sub>O in hydroelectric reservoirs Lokka and Porttipahta in the northern boreal zone in Finland. *Global Biogeochem. Cycles* 16, 1-17.
- Idso, S.B., and R.G. Gilbert. 1974. On the universality of the Poole and Atkins secchi disk-light extinction equation. *J. Appl. Ecol.* 11, 399-401.
- IEA (2008). International Energy Agency. Electricity/Heat in World in 2008. available via <http://go.nature.com/6mAAWK>.
- IJHD (2010). *World Atlas & Industry Guide*. International Journal of Hydropower and Dams, Wallington, Surrey, UK, 405 pp.
- Intergovernmental Panel on Climate Change IPCC. 2007. In: Solomon, S., et al. Eds., Climate Change 2007: The Physical Science Basis: Working Group I Contribution to the Fourth Assessment Report of the IPCC. Cambridge Univ. Press, New York.
- Intergovernmental Panel on Climate Change IPCC. 2011. Special Report on Renewable Energy Sources and Climate Change Mitigation (O. Edenhofer, R. Pichs-Madruga, Y. Sokona, K. Seyboth, P. Matschoss, S. Kadner, T. Zwickel, P. Eickemeier, G. Hansen, S. Schlomer, C. von Stechow eds), Cambridge University Press, Cambridge, United Kingdom and New York, NY, USA.
- Jähne, B., K. O. Munnich, R. Bosinger, A. Dutzi, W. Huber, and P. Libner. 1987. On parameters influencing air-water exchange. *J. Geophys. Res.* 92, 1937-1949.

- Jauhiainen, J., H. Takahashi, J. E. P. Heikkinen, P. J. Martikainen, H. Vasander. 2005. Carbon fluxes from a tropical peat swamp forest floor. *Glob. Change Biol.* 11, 1788-1797.
- Johnston, C. A., S.D. Bridgman, and J.P. Schubauer-Berigan. 2001. Nutrient dynamics in relation to geomorphology of riverine wetlands. *Soil Sci. Soc. Am. J.* 65:557-77.
- Jonsson, A., J. Aberg, A. Lindroth, and M. Jansson. 2008. Gas transfer rate and CO<sub>2</sub> flux between an unproductive lake and the atmosphere in northern Sweden. *J. Geophys. Res.* 113:G04006. doi:10.1029/2008JG000688.
- Joyce, J., and P. W. Jewell. 2003. Physical controls on methane ebullition from reservoirs and lakes. *Environ. Eng. Geosci.* IX: 167-178.
- Keller, M. and R. F. Stallard. 1994. Methane emission by bubbling from Gatun Lake, Panama. *J Geophys Res* 99:8307-8319.
- Keller, M., W. A. Kaplan, and S. C. Wofsy. 1986. Emissions of N<sub>2</sub>O, CH<sub>4</sub> and CO<sub>2</sub> from tropical forest soils, *J. Geophys. Res.*, 91, 11,791- 11, 802.
- Kelly, C. A., and D. P. Chynoweth. 1981. The contribution of temperature and the input of organic matter in controlling rates of sediment methanogenesis. *Limnol. Oceanogr.* 26, 891-897.
- Kelly, C., J. W. M. Rudd, V. L. St. Louis, and T. Moore. 1994. Turning attention to reservoir surfaces, a neglected area in greenhouse studies. *Eos. Trans. AGU*, Vol.75. No.29, pp. 332.
- Kelly, V. J. (2001). Influence of reservoirs on solute transport: a regional-scale approach. *Hydrol. Processes*, Vol.15. No.7, May, pp. 1227-1249, 0885-6087.
- Kemenes, A., B. R. Forsberg, and J. M. Melack. 2007. Methane release below a tropical hydroelectric dam. *Geophys. Res. Lett.*, 34:L12809. doi:10.1029/2007GL029479.
- Kemenes, A., B. R. Forsberg, and J. M., Melack. 2011. CO<sub>2</sub> emissions from a tropical hydroelectric reservoir Balbina, Brazil. *J. Geophys. Res.*, 106:G03004. doi:10.1029/2011JG001465.
- Kiehl, J., and K. Trenberth, 1997: Earth's annual global mean energy budget. *Bull. Am. Meteorol. Soc.*, 78, 197-206.
- Kiene, R. P. 1991. Production and consumption of methane in aquatic systems, in: *Microbial production and consumption of greenhouse gases: methane, nitrogen oxides, and halomethanes*, edited by: Rogers, J. E. and Whitman, W. E., American Society for Microbiology Press, Washington, DC, 111-146.
- Kiese, R., and K. Butterbach-Bahl. 2002. N<sub>2</sub>O and CO<sub>2</sub> emissions from three different tropical forest sites in the wet tropics of Queensland, Australia. *Soil Biol. Biochem.*, 34: 975-987.
- Kljun, N., P. Calanca, M. W. Rotach, and H. P. Schmid. 2004. A simple parameterization for flux footprint predictions. *Boundary-Layer Meteorol.* 112: 503-523.
- Knowles R. 1981. Denitrification. In: Paul EA, Ladd J. N., editors. *Soil biochemistry* vol 5. New York: Marcel Dekker.
- Knowles, R., D. R. S. Lean, and Y. K. Chan. 1981. Nitrous oxide concentrations in lakes: Variations with depth and time. *Limnol. Oceanogr.*, 26:855-866.
- Kosolapov, D. B. 2002. Methane formation and consumption processes in the littoral zone of the Rybinsk reservoir. *Water Resources*, 29 2, pp. 174-180.

- Kroeze, C., E. Dumont, and S. Seitzinger. Future trends in emissions of N<sub>2</sub>O from rivers and estuaries, *J. Integr. Environ. Sci.*, 7, 71-78.
- Kroon, P. S., A. Hensen, H. J. J. Jonker, H. G. Ouwersloot, A. T. Vermeulen, and F. C. Bosveld. 2009. Uncertainties in eddy covariance flux measurements assessed from CH<sub>4</sub> and N<sub>2</sub>O observations, *Agric. Forest Meteorol.*, 150, 806-816.
- Kroon, P. S., T. Vesala, and J. Grace. 2010. Flux measurements of CH<sub>4</sub> and N<sub>2</sub>O exchanges. *Agric. Forest Meteorol.*, 150, 6, 745-747.
- Kumar, A., T. Schei, A. Ahenkorah, R. Caceres Rodriguez, J. M. Devernay, M. Freitas, D. Hall, A. Killingtveit, and Z. Liu. 2012. Hydropower. In *IPCC Special Report on Renewable Energy Sources and Climate Change Mitigation* (O. Edenhofer, R. Pichs) Madruga, Y. Sokona, K. Seyboth, P. Matschoss, S. Kadner, T. Zwickel, P. Eickemeier, G. Hansen, S. Schlomer, C. von Stechow eds), Cambridge University Press, Cambridge, United Kingdom and New York, NY, USA.
- Law, C. S., A. P. Rees, and N. J. P. Owens. 1993. Nitrous oxide production by estuarine epiphyton. *Limnol. Oceanogr.* 38, 435-441.
- Le Mer, J., and P. Roger. 2001. Production, oxidation, emissions and consumption of methane in soils: a review. *Eur. J. Soil Biol.* 37, 25-50.
- Lehner, B., C.R. Liermann, C. Revenga, C. Vörösmarty, B. Fekete, P. Crouzet, P. Döll, M. Endejan, K. Frenken, J. Magome, C. Nilsson, J.C. Robertson, R. Rödel, N. Sindorf, and D. Wisser. 2011. High-resolution mapping of the world's reservoirs and dams for sustainable river-flow management. *Frontiers in Ecology and the Environment* 9, 494-502.
- Lehours, A.C., C. Bardot, A. Thenot, D. Debroas, and G. Fonty. 2005. Anaerobic microbial communities in Lake Pavin, a unique meromictic lake in France. *Appl. Environ. Microbiol.* 71, 7389.
- Lidstrom, M. E., and L. Somers. 1984. Seasonal study of methane oxidation in Lake Washington. *Appl. Environ. Microbiol.* 47 : 1255-1260.
- Lienggaard, L., L. P. Nielsen, N. P. Revsbech, A. Prieme, B. Elberling, A. Enrich-Prast, and M. Kuhl. 2013. Extreme emission of N<sub>2</sub>O from tropical wetland soil (Pantanal, South America). *Front. Microbiol.* 3, 4.
- Liikanen, A., J. T. Huttunen, K. Valli, and P. J. Martikainen. 2002. Methane cycling in the sediment and water column of mid-boreal hyper-eutrophic Lake Kevaton. Finland. *Arch. Hydrobiol.* 154, 585-603.
- Liikanen, A., and P. J. Martikainen. 2003. Effect of ammonium and oxygen on methane and nitrous oxide fluxes across sediment-water interface in a eutrophic lake. *Chemosphere* 52, 1287-1293.
- Lima, I. B. T. 2005. Biogeochemical distinction of methane releases from two Amazon hydroreservoirs. *Chemosphere* 59:1697-702.
- Lima, I. B. T., and E. M. L. M. Novo. 1999. Carbon Flows in the Tucuruí Reservoir, in L. P. Rosa and M. A. dos Santos (eds.), *Dams and Climate Change*, Coordenação dos Programas de Pós-Graduação de Engenharia (COPPE), Universidade Federal de Rio de Janeiro (UFRJ), Rio de Janeiro, Brazil, pp. 78-84.
- Lima, I. B. T., F. M. Ramos, L. A. W. Bambace, and R. R. Rosa. 2007. Methane Emissions from Large Dams as Renewable Energy Resources: A Developing Nation Perspective," *Mitigation and Adaptation Strategies for Global Change*, published online March 2007.
- Lima, I. B. T., R. L. Victoria, E. M. L. M. Novo, B. J. Feigl, M. V. R. Ballester, and J. P. Ometto. 2002. Methane, carbon dioxide and nitrous oxide emissions from two Amazonian reservoirs during high water table, *Verh. Int. Ver. Limnol.*, 28, 438-442.

Liss, P. and L. Merlivat. 1986. Air-sea exchange rates: introduction and synthesis. In: The role of air-sea exchanges in geochemical cycling, (eds. P. Buat-Menard), Reidel, Dordrecht, 113-127.

Liss, P. S. P. W. Balls, F. N. Martinelli, and M. Coantic. 1981. The effect of evaporation and condensation on gas transfer across an air- water interface. *Oceanol. Acta* 4, 129-138.

Liu, X., C. Liu, S. Li, F. Wang, B. Wang, and Z. Wang. 2011. Spatiotemporal variations of nitrous oxide (N<sub>2</sub>O) emissions from two reservoirs in SW China, *Atmospheric Environ.*, 4531, 5458, doi:10.1016/j.atmosenv.2011.06.074.

Liu, Y., R. Zhu, D. Ma, H. Xu, Y. Luo, T. Huang, and L. Sun. 2011. Temporal and spatial variations of nitrous oxide fluxes from the littoral zones of three alga-rich lakes in coastal Antarctica. *Atmospheric Environ.* 45, 1464-1475.

Long, K. D., L. B. Flanagan, and T. Cai. 2010. Diurnal and seasonal variation in methane emissions in a northern Canadian peatland measured by eddy covariance, *Glob. Change Biol.*, 16, 2420- 2435.

Louis, B.J., R. Roy, M. C. Pacheco-Oliver, C. B. Miguez, and C.W. Greer. 2005. Production and Consumption of Methane in Soil, Peat, and Sediments from a Hydro-Electric Reservoir (Robert-Bourassa) and Lakes in the Canadian Taiga In: Tremblay A, Varfalvy L, Rhoem C et al (eds) *Greenhouse gases emissions from natural environments and hydroelectric reservoirs: fluxes and processes*. Springer-Verlag, Berlin Heidelberg.

Lovely, D. R., J. D. Coates, E. L. Blunt-Harris, E.J.P. Phillips, and J.C. Woodward. 1996. Humic acids as electron acceptors for microbial respiration. *Nature* 382, 445-448.

Lovley, D. R., and E. J. P. Phillips. 1987. Competitive Mechanisms for inhibition of sulfate reduction and methane production in the zone of ferric iron reduction in sediments. *Appl. Environ. Microbiol.* 53, 2636-2641.

Luyssaert, S., Inghima, I., Jung, M., Richardson, A.D., Reichstein, M., Papale, D., Piao, S.L., Schulze, E.D., Wingate, L., Matteucci, G., Aragao, L., Aubinet, M., Beer, C., Bernhofer, C., Black, K.G., Bonal, D., Bonnefond, J.M., Chambers, J., Ciais, P., Cook, B., Davis, K.J., Dolman, A.J., Gielen, B., Goulden, M., Grace, J., Granier, A., Grelle, A., Griffis, T., GrÜNwald, T., Guidolotti, G., Hanson, P.J., Harding, R., Hollinger, D.Y., Hutya, L.R., Kolari, P., Kruijt, B., Kutsch, W., Lagergren, F., Laurila, T., Law, B.E., Le Maire, G., Lindroth, A., Loustau, D., Malhi, Y., Mateus, J., Migliavacca, M., Misson, L., Montagnani, L., Moncrieff, J., Moors, E., Munger, J.W., Nikinmaa, E., Ollinger, S.V., Pita, G., Rebmann, C., Rouspard, O., Saigusa, N., Sanz, M.J., Seufert, G., Sierra, C., Smith, M.L., Tang, J., Valentini, R., Vesala, T., Janssens, I.A. 2007. CO<sub>2</sub> balance of boreal, temperate, and tropical forests derived from a global database. *Global Change Biology* 13, 2509-2537.

Maag, M., and F. P. Vinther. 1996. Nitrous oxide emissions by nitrification and denitrification in different soil types and at different soil moisture contents and temperatures. *Appl. Soil Ecol.*, 4: 5-14.

MacIntyre, S., A., Jonsson, M., Jansson, J., Aberg, D. E., Turney, and S. D., Miller. 2010. Buoyancy flux, turbulence, and the gas transfer coefficient in a stratified lake. *Geophys. Res. Lett.*, 37 24, L24604.

MacIntyre, S., and J. M. Melack. 2009. Mixing dynamics in lakes across climatic zones, in *Encyclopedia of Inland Waters*, edited by G. Likens, pp. 603-612, Elsevier, Oxford, U. K.

MacIntyre, S., J. R. Romero, and G. W. Kling. 2002. Spatial-temporal variability in mixed layer deepening and lateral advection in an embayment of Lake Victoria, East Africa, *Limnol. Oceanogr.*, 47, 656-671, doi:10.4319/lo.2002.47.3.0656.

MacIntyre, S., R. Wanninkhof, and J. Chanton. 1995. Trace gas exchange across the air-water interface in freshwater and coastal marine environments, in *Biogenic Trace Gases: Measuring Emissions From Soil and Water*, edited by P. Matson and R. Harriss, pp. 52-97, Blackwell, New York.



- MacIntyre, S., W. Eugster, and G. W. Kling. 2001. The critical importance of buoyancy flux for gas flux across the air-water interface, in *Gas Transfer at Water Surfaces*, edited by M. A. Donelan et al., pp. 135-139, AGU, Washington, D. C.
- Macintyre, S.; J.R. Romero, and G.W. Kling. 2002. Spatial-temporal variability in surface layer deepening and lateral advection in an embayment of Lake Victoria, East Africa. *Limnol. Oceanogr.*, Vol.47. No.3, May, pp. 656-671, 0024-3590.
- Magnusson, T. 1993. Carbon dioxide and methane formation in forest mineral and peat soils during aerobic and anaerobic incubations. *Soil Biol. Biochem.* 25, 877-883.
- Mahrt, L., J. Sun, W. Blumen, T. Delany, and S. Oncley. 1998. Nocturnal boundary-layer regimes, *Boundary Layer Meteorol.*, 88, 255-278, doi:10.1023/A:1001171313493.
- Marino, R., and R. W. Howarth. 1993. Atmospheric oxygen-exchange in the Hudson River-dome measurements and comparison with other natural waters. *Estuaries* 16, 433-445.
- Markfoged, R., L. P. Nielsen, T. Nyord, L. D. M. Ottosen, and N. P. Revsbech . 2011. Transient N<sub>2</sub>O accumulation and emission caused by O<sub>2</sub> depletion in soil after liquid manure injection. *Eur. J. Soil Sci.* 62, 497-655.
- Martens, C. S., and J. V. Klump. 1984. Biogeochemical cycling in an organic-rich coastal marine basin. 4. An organic carbon budget for sediments dominated by sulfate reduction and methanogenesis: *Geochim. Cosmochim. Acta*, Vol. 48, pp. 1987-2004.
- Martens, C. S., and J. Val Klump. 1980. Biogeochemical cycling in an organic-rich coastal marine basin-I. Methane sediment-water exchange processes. *Geochim. Cosmochim. Acta* 44: 471-490.
- Martens, C. S., and R. A. Berner. 1974. Methane production in the interstitial waters of sulfate depleted marine sediments. *Science* 185: 1167-1169.
- Matthews, C. J. D., V. L. St-Louis, and R. H., Hesslein. 2003. Comparison of three techniques used to measure diffusive gas exchange from sheltered aquatic surfaces. *Environ. Sci. Technol.* 37, 772-780.
- Mattson, M. D., and G. E. Likens. 1990. Air pressure and methane fluxes. *Nature* 347: 718-719.
- McClain M. E., E. W. Boyer, C. L. Dent, S. E. Gergel, N. B. Grimm, P. M. Groffman, S. C. Hart, J. W. Harvey, C. A. Johnston, E. Mayorga, W. H. McDowell, and G. Pinay. 2003. Biogeochemical hot spots and hot moments at the interface of terrestrial and aquatic ecosystems. *Ecosystems* 6, 301-312.
- McCrackin, M. L. and J. J. Elser. 2011. Greenhouse gas dynamics in lakes receiving atmospheric nitrogen deposition. *Global Biogeochem. Cycles* 25:GB4005, DOI:10.1029/2010GB003897.
- McGillis, W. R., J. B. Edson, J. D. Ware, J. W.H. Dacey, J. H. Hare, C. W. Fairall, and R. Wanninkhof. 2001. Carbon dioxide flux techniques performed during GasEx-98. *Mar. Chem.* 75, 267-280.
- McGinnis, D. F., J. Greinert, Y. Artemov, S. E. Beaubien, and A. Wüest. 2006. The fate of rising methane bubbles in stratified waters: How much methane reaches the atmosphere? *J. Geophys. Res.* 111: C09007.
- Mckenna, S. P., and W. R. McGillis. 2004. The role of free-surface turbulence and surfactants in air-water gas transfer. *Int. J. Heat Mass Transfer* 47: 539-553, doi:10.1016/j.ijheatmasstransfer. 2003.06.001.
- McMahon, P., and K. Dennehy. 1999. N<sub>2</sub>O emissions from a nitrogen-enriched river. *Environ. Sci. Technol.* 33, 21-25.

McSwiney C., W. H. McDowell, and M. Keller. 2001. Distribution of nitrous oxide and regulators of its production across a tropical rainforest catena in the Luquillo Experimental Forest, Puerto Rico, *Biogeochemistry* 56: 265-286.

Mendonça, R., N. Barros, L. O. Vidal, F. Pacheco, S. Kosten, and F. Roland. 2012. Greenhouse Gas Emissions from Hydroelectric Reservoirs: What Knowledge Do We Have and What is Lacking?, in *Greenhouse Gases - Emission, Measurement and Management*, Guoxiang Liu Ed., ISBN: 978-953-51-0323-3.

Mengis, M., R. Gachter, and B. Wehrli. 1996. Nitrous oxide emissions to the atmosphere from an artificially oxygenated lake. *Limnol. Oceanogr.* 41, 548-553.

Mengis, M., R. Gachter, and B. Wehrli. 1997. Sources and sinks of nitrous oxide N<sub>2</sub>O in deep lakes. *Biogeochemistry* 38, 281-301.

Montzka, S. A., E. J. Dlugokencky, and J. H. Butler. 2011. Non-CO<sub>2</sub> greenhouse gases and climate change, *Nature*, 476, 43-50.

Moore, T.R., and M. Dalva. 1993. The influence of temperature and water table position on carbon dioxide and methane emissions from laboratory columns of peatland soils. *J. Soil Sci.* 44, 651-664.

Morison, J.I.L., M.T.F. Piedade, E. Muller, S. P. Long W. J. Junk, and M. B. Jones. 2000. Very high productivity of the C<sub>4</sub> aquatic grass *Echinochloa polystachya* in the Amazon floodplain confirmed by net ecosystem CO<sub>2</sub> flux measurements. *Oecologia* 125:400-411.

Murase, J., and A. Sugimoto. 2005. Inhibitory effect of light on methane oxidation in the pelagic water of a mesotrophic lake Lake Biwa, Japan, *Limnol. Oceanogr.*, 50, 1339-1343.

Nozhevnikova A. N., V. Nekrasova, A. Ammann, A. J. B. Zehnder, B. Wehrli, and C. Holliger. 2007. Influence of temperature and high acetate concentrations on methanogenesis in lake sediment slurries. *FEMS Microbiol. Ecol.* 62:336-344.

NTPC Nam Theun 2 Power Company. 2005. Environmental Assessment and Management Plan - Nam Theun 2 Hydroelectric Project. Nam Theun 2 Power Company, Vientiane. Internal report, 212 pp.

Ometto, J. P. F. S. Pacheco, A. C. P. Cimblaris, J. L. Stech, J. A. Lorenzetti, A. Assireu, M. A. Santos, B. Matvienko, L. P. Rosa, C. S. Galli, D. S. Abe, J. G. Tundisi, N. Barros, R. F. Mendonça, and F. Roland. 2011. Carbon dynamic and emissions in Brazilian hydropower reservoirs. In: *Energy Resources: Development, Distribution, and Exploitation*, Alcântara, E., Nova Science Publishers, New York.

Oremland, R. S., L. M. Marsh, and S. Polcin. 1982. Methane production and simultaneous sulphate reduction in anoxic, salt marsh sediments. *Nature* 296, 143-145.

Ostrovsky, I., 2003. Methane bubbles in Lake Kinneret: quantification and temporal and spatial heterogeneity. *Limnol. Oceanogr.*, vol. 48, N.3.

Ostrovsky, I., D. F. McGinnis, L. Lapidus, and W. Eckert. 2008. Quantifying gas ebullition with echosounder: the role of methane transport by bubbles in a medium-sized lake, *Limnol. Oceanogr. Meth.*, 6, 105-118.

Parkin T. B. 1987. Soil microsites as a source of denitrification variability. *Soil Sci. Soci. Am. J.* 51:1194-9.

Pasche, N., M. Schmid, F. Vazquez, C. J. Schubert, A. Wüest, J. D. Kessler, M. A. Pack, W. S. Reeburgh, and H. Bürgmann. 2011. Methane sources and sinks in Lake Kivu, *J. Geophys. Res.*, 116, G03006, doi:10.1029/2011JG001690 Reeburgh, W. S. 2007. Oceanic methane biogeochemistry. *Chemical Reviews* 107: 486-513.

- Paterson, M. J., D. Findlay, K. Beaty, E.U. Schindler, M. Stainton, and G. McCullough. 1997. Changes in the planktonic food web of a new experimental reservoir. *Can. J. Fish Aquat. Sci.* 54:1088-1102.
- Patt, T.E., G.C. Cole, J. Bland, and R.S. Hanson. 1974. Isolation and characterization of bacteria that grow on methane and organic compounds as sole sources of carbon and energy. *J. Bacteriol.* 120, 955-964.
- Pavlostathis, S.G., and E. Giraldo-Gomez. 1991. Kinetics of anaerobic treatment. *Water Sci. Technol.* 24 8, 35-59.
- Piker, L., R., Schmaljohann, and J. F. Imhoff. 1998. Dissimilatory sulfate reduction and methane production in Gotland Deep sediments Baltic Sea during a transition period from oxic to anoxic bottom water 1993-1996, *Aquat. Microb. Ecol.*, 14, 183-193.
- Pinay, G., L. Roques, and A. Fabre. 1993. Spatial and temporal patterns of denitrification in riparian forest. *J. Appl. Ecol.* 30:581-91.
- Powlson D. S. 1980. The effects of grinding on microbial and non-microbial organic matter In *Soil Journal of Soil Science* Volume 31, Issue 1. pages 77-85, March.
- Ramakrishnan, B., T., Lueders, R. Conrad, and M. Friedrich. 2000. Effect of soil aggregate size on methanogenesis and archaeal community structure in anoxic rice field soil. *FEMS Microbiol. Ecol.* 32,261-270.
- Ravishankara, A., J. S. Daniel, and R.W. Portmann. 2009. Nitrous oxide N<sub>2</sub>O: the dominant ozone-depleting substance emitted in the 21st century. *Science* 326, 123.
- Raymond, P.A., and J. J. Cole. 2001. Gas exchange in rivers and estuaries: choosing a gas transfer velocity. *Estuaries* 24, 312-317.
- Reeburgh W. S., S. C. Whalen and M. J. Alperin. 1993. The role of methylotrophy in the global methane budget. In *Microbial Growth on C-1 Compounds* (ed. J. C. Murrell and D. P. Kelly), pp. 1-14. Intercept, Ltd, Andover.
- Richard, S., P. Gosse, A. Gregoire, R. Delmas, and C. Galy-Lacaux. 2004. Impact of methane oxidation in on tropical reservoir on greenhouse gases fluxes and water quality. Chap.22. In : *Greenhouse gases emissions from natural environments and hydroelectric reservoirs : fluxes and processes*, A. Tremblay, L. Varfalvy, C. Roehm and M. Garneau Eds Springer-Verlag.
- Rinne, J., T. Riutta, M. Pihlatie, M. Aurela, S. Haapanala, J. P. Tuovinen, E. S. Tuittila, and T. Vesala. 2007. Annual cycle of methane emission from a boreal fen measured by the eddy covariance technique, *Tellus B*, 59, 449-457.
- Roehm, C., and A. Tremblay. 2006, Role of turbines in the carbon dioxide emissions from two boreal reservoirs, Quebec, Canada, *J. Geophys. Res.*, 111 , D24101, doi:10.1029/2006JD007292.
- Roland, F. A. C. P. Cimleris, L.M. Lobão, and L.O. Vidal. 2011. Bacterioplankton Metabolism in Hydroelectric Reservoirs. *Oecologia Australis*, Vol.15. pp. 605-617.
- Roland, F. L. O. Vidal, F. S. Pacheco, N. O. Barros, A. Assireu, J. Ometto, A. C. P. Cimleris, and J. J. Cole. 2010. Variability of carbon dioxide flux from tropical (Cerrado) hydroelectric reservoirs. *Aquatic Sciences*, Vol.72. No.3, Jun, pp. 283-293, 1015-1621.
- Roland, F., L. O. Vidal, F. S. Pachero, N. O. Barros, A. Assireu, and J. P. H. B. Ometto. 2010. Variability of carbon dioxide flux from tropical Cerrado hydroelectric reservoirs. *Aquat. Sci.* 72:283-93.
- Rosa, L. P. and R. Schaeffer. 1994. Greenhouse-Gas Emissions from Hydroelectric Reservoirs. *Ambio*, Vol.23. No.2, Mar, pp. 164-165, 0044-7447 .

- Rosenberg, D. M., F. Berkes, R. A. Bodaly, R. E. Hecky, C. A. Kelly, and J. W. M. Rudd. 1997. Large-scale impacts of hydroelectric development, *Environ. Rev.*, 51, 27-54, doi:10.1139/a97-001.
- Rothfuss, F., M. Bender, and R. Conrad. 1997. Survival and activity of bacteria in a deep, aged lake sediment Lake Constance. *Microbial. Ecology* 33: 69-77.
- Roy, R., and R. Knowles. 1994. Effects of methane metabolism on nitrification and nitrous oxide production in polluted freshwater sediment, *Appl. Environ. Microbiol.*, 60, 3307-3314.
- Rudd, J. W., and R. D. Hamilton. 1975. Factors controlling rates of methane oxidation and the distribution of the methane oxidizers in a small stratified lake. *Arch. Hydrobiol.* 75 : 522-538.
- Rudd, J.W.M., and C.D. Taylor. 1980. *Methane cycling in aquatic environments*. 2: 77-150.
- Rudd, J.W.M., R. Harris, C.A. Kelly, and R.E. Hecky. (1993). Are hydroelectric reservoirs significant sources of greenhouse gases. *Ambio.*, Vol.22. No.4, Jun, pp. 246-248, 0044- 7447.
- Satoh, T.H., S.S.M. Hom, and K.T. Shanmugam. 1981. Production of nitrous oxide as a product of nitrite metabolism by enteric bacteria. In: *Genetic Engineering of Symbiotic Nitrogen Fixation and Conservation of Fixed Nitrogen* eds.: Lyons, J.M., Valentine, R.C., Phillips, D.A., Rains, D.W., Huffaker, R.C. 481-497. Plenum Press, New York.
- Satpathy, S. N., A. K. Rath, B. Ramakrishnan, V. R., Rao, T. K. Adhya, and N. Sethunathan. 1997. Diurnal variation in methane efflux at different growth stages of tropical rice, *Plant Soil*, 195, 267-271.
- Schetagne, R., 1994. Water quality modifications after impoundment of some large northern reservoirs. *Archiv. Hydrobiol. Adv. Limnol.* 40:223-229
- Schindlbacher, A., S. Zechmeister-Bolternstern, and K. Butterbach-Bahl. 2004. Effects of soil moisture and temperature on NO, NO<sub>2</sub>, and N<sub>2</sub>O emissions from European forest ecosystems. *J. Geophys. Res.*, 109: 1-12.
- Schladow, S. G., M. Lee, B. E. HuRzeler, and P. B. Kelly. 2002. Oxygen transfer across the air-water interface by natural convection in lakes. *Limnol. Oceanogr.*, 47: 1394-1404.
- Schlesinger, W. H. and J. M. Melack. 1981. Transport of organic-carbon in the worlds rivers. *Tellus*, Vol.33. No.2, pp. 172-187, 0040-2826.
- Schlesinger, W.H., 1997. *Biogeochemistry: an analysis of global change*. 2nd ed Academic Press, San Diego, California.
- Schonheit, P., H. Keweloh, and R. K. Thauer. 1981. Factor F<sub>420</sub> degradation in Methanobacterium thermoautotrophicum during exposure to oxygen. *FEMS Microbiol. Lett.* 12, 347-349.
- Schoun, H., D. Kim, H. Uchiyama, and J. Sugiyama. 1992. Denitrification by fungi. *FEMS Microbiol. Lett.*, 94: 277-282.
- Schrier-Uijl, A. P., P. S. Kroon, A. Hensen, P. A. Leffelaar, F. Berendse, and E. M. Veenendaal. 2010. Comparison of chamber and eddy covariance-based CO<sub>2</sub> and CH<sub>4</sub> emission estimates in a heterogeneous grass ecosystem on peat, *Agric. Forest Meteorol.*, 150, 825-831.
- Schubert, C. J., T. Diem, and W. Eugster. 2012. Methane emissions from a small wind shielded lake determined by eddy covariance, flux chambers, anchored funnels, and boundary model calculations: a comparison. *Environ. Sci. Technol.*, 46 (8), 4515-4522.
- Schubert, C.J., F.S. Lucas, E. Durisch-Kaiser, R. Stierli, T. Diem, O. Scheidegger, F. Vazquez, and B. Müller. 2010. Oxidation and emission of methane in a monomictic lake (Rotsee, Switzerland). *Aquat. Sci.* 72, 455-466.

Schulz, S. and R. Conrad. 1996. Influence of temperature on pathways to methane production in the permanently cold profundal sediment of Lake Constance. *FEMS Microbiol. Ecol.* 20, 1-14.

Scranton, M.I., P. Crill, M.A. de Angelis, P.L. Donaghay, and J.M. Sieburth. 1993. The importance of episodic events in controlling the flux of methane from an anoxic basin. *Global Biogeochem. Cycles* 7: doi: 10.1029/93GB00869. issn: 0886-6236.

Sebacher, D.I., R.C. Harriss, and K.B. Barlett. 1985. Methane emissions to the atmosphere through aquatic plants., *J. Env. Qual.* 14:40-46.

Segers, R. 1998. Methane production and methane consumption: a review of processes underlying wetland methane fluxes. *Biogeochemistry* 41, 23-51.

Seitzinger, S.P., and C. Kroeze. 1998. Global distribution of nitrous oxide production and N inputs in freshwater and coastal marine ecosystems. *Global Biogeochem. Cycles* 12, 93-113.

Seitzinger, S.P., C. Kroeze, and R.V. Styles. 2000. Global distribution of N<sub>2</sub>O emissions from aquatic systems: natural emissions and anthropogenic effects. *Chemosphere- Global Change Science* 2, 267-279.

Serça, D., R. Delmas, C. Jambert, and L. Labroue. 1994. Emission of nitrogen oxides from equatorial rainforest in central Africa, *Tellus, Ser. B*, 46, 243-254.

Sikar, E., M.A. Santos, B. Matvienko, M.B. Silva, C.H.E.D. Rocha, E. Santos, and A.P.B. Junior. 2005. Greenhouse gases and initial findings on the carbon circulation in two reservoirs and their watersheds, *Verh. Int. Ver. Limnol.*, 29, 573- 576.

Simpson, I. J., G. W. Thurtell, G. E. Kidd, M. Lin, T. H. Demetriades-Shah, I. D. Flitcroft, E. T. Kanemasu, D. Nie, K. F. Bronson, and H. U. Neue. 1995. Tunable diode laser measurements of methane fluxes from an irrigated rice paddy field in the Philippines, *J. Geophys. Res.*, 100, 7283-7290.

Sitaula, B. K., and L. R. Bakken. 1993. N<sub>2</sub>O release from spruce forest soil, relation with nitrification, CH<sub>4</sub> uptake, temperature, moisture and fertilization. *Soil Biol. Biochem.* 25:1415-1421.

Smith, K. A., P. E. Thomson, H. Clayton, I. P. McTaggart, and F. Conen. 1998. Effects of temperature, water content and nitrogen fertilisation on emissions of nitrous oxide by soils. *Atmospheric Environ.* 32 19, 3301-3309.

Smith, L. K., W. M. Lewis, J. P. Chanton, G. Cronin, and S. K. Hamilton. 2000. Methane emissions from the Orinoco River floodplain, Venezuela. *Biogeochemistry* 51, 113-140.

Smith, M. S. 1982. Dissimilatory reduction of NO<sub>2</sub><sup>-</sup> to NH<sub>4</sub><sup>+</sup> and N<sub>2</sub>O by a soil *Citrobacter* sp. *Appl. Environ. Microbiol.* 43: 854-860.

Sobek, S., Tranvik, L. J. and Cole, J. J. 2005. Temperature independence of carbon dioxide supersaturation in global lakes. *Global Biogeochem. Cycles*, Vol.19. No.2, Apr 5, pp. -, 0886-6236.

Sobek, S., T. DelSontro, N. Wongfun, and B. Wehrli. 2012. Extreme organic carbon burial fuels intense methane bubbling in a temperate reservoir, *Geophys. Res. Lett.*, 39, L01401, doi:10.1029/2011GL050144.

Sorrell, B.K., and P.I. Boon. 1992. Biogeochemistry of billabong sediments: II. Seasonal variations in methane production. *Freshwater Biol.* 27:435-445.

Soumis N., É. Duchemin, R. Canuel and M. Lucotte. 2004. Greenhouse gas emissions from reservoirs of the western United States. *Global Biogeochem. Cycles* 18.

Soumis, N., M. Lucotte, C. Larose, F. Veillette, and R. Canuel. 2007. Photomineralization in a boreal hydroelectric reservoir: a comparison with natural aquatic ecosystems. *Biogeochemistry*, Vol.86. pp. 123-135, s10533-007.

Soumis, N., R. Canuel, and M. Lucotte. 2008. Evaluation of two current approaches for the measurements of carbon dioxide diffusive flux from lentic ecosystems. *Environ. Sci. Technol.* 42:2964-9.

Sovacool, B. K. 2008. Valuing the greenhouse gas emissions from nuclear power: A critical survey, *Energy Policy* 36: 2950-2963.

St Louis, V. L., C.A., Kelly, E., Duchemin, J.W.M., Rudd, and D.M. Rosenberg. 2000. Reservoir surfaces as sources of greenhouse gases to the atmosphere: a global estimate. *BioScience*, Vol.50. No.9, Sep, pp. 766-775, 0006-3568.

Stadmark, J., A.G. Seifert, and L. Leonardson. 2008. Transforming meadows into free surface water wetlands: Impact of increased nitrate and carbon loading on greenhouse gas production, *Atmospheric Environment* doi: 10.1016/j.atmosenv.2008.09.036.

Stange, F., K. Butterbach-Bahl, H. Papen, S. Zechmeister-Boltenstern, C. Li, and J. Aber. 2000. A process-oriented model of N<sub>2</sub>O and NO emissions from forest soils, 2. Sensitivity analysis and validation. *J. Geophys. Res.* 105(D4):4385-4398.

Stets, E. G., R. G. Striegl, G. R. Aiken, D. O. Rosenberry, and T. C. Winter. 2009. Hydrologic support of carbon dioxide flux revealed by whole lake carbon budgets. *J. Geophys. Res. Biogeosci.* 114:G01008. doi: 10.1029/2008JG000783.

Stevens, C. and Imberger, J. 1996. The initial response of a stratified lake to a surface shear stress. *J. Fluid Mech.*, Vol.312. Apr 10, pp. 39-66, 0022-1120.

Stow, C. A., J. T. Walker, L. Cardoch, P. Spence, and C. Geron. 2005. N<sub>2</sub>O emissions from streams in the Neuse River watershed, North Carolina. *Environ. Sci. Technol.* 39, 6999-7004.

Sundh, I., D. Bastviken, and L. J. Tranvik. 2005. Abundance, activity, and community structure of pelagic methane-oxidizing bacteria in temperate lakes. *Appl. Environ. Microbiol.* 71, 6746e6752.

Suyker, A. E., S. B. Verma, R. J. Clement, and D. P. Billesbach. 1996. Methane flux in a boreal fen: Season-long measurement by eddy correlation, *J. Geophys. Res.-Atmos.* 101, 28637-28647.

Sweerts, J. P. R. A., M. J. Bar-Gilissen, A. A. Cornelese, and T. E. Capapenberg. 1991. Oxygen consuming processes at the profundal and littoral sediment-water interface of a small meso-eutrophic lake Lake Vechten, The Netherlands. *Limnol Oceanogr.*, 36 6, 1124-1133.

Teodoru CR, J, Bastien M-C, Bonneville PA, del Giorgio M, Demarty M, Garneau J-F, Hélie L, Pelletier YT, Prairie N, Roulet I, Strachan and A Tremblay. 2012. The net carbon footprint of a newly-created boreal hydroelectric reservoir. *Glob Biogeochem. Cycles* 26, GB2016. doi:10.1029/2011 GB004187.

Teodoru, C. R., Y. T. Prairie, and P. A. del Giorgio. 2010. Spatial heterogeneity of surface CO<sub>2</sub> fluxes in a newly created Eastmain-1 Reservoir in Northern Quebec, Canada. *Ecosystems* 14:28-46.

Tranvik, L. J., J. A. Downing, J. B. Cotner, S. A. Loiselle, R. G. Striegl, T. J. Ballatore, P. Dillon, K. Finlay, K. Fortino, L. B. Knoll, P. L. Kortelainen, T. Kutser, S. Larsen, I. Laurion, D. M. Leech, S. L. McCallister, D. M. McKnight, J. M. Melack, E. Overholt, J.A. Porter, Y.T. Prairie, W.H. Renwick, F. Roland, B. S. Sherman, D. W. Schindler, S. Sobek, A. Tremblay, M. J. Vanni, A. M. Verschoor, E. von Wachenfeldt, and G. A. Weyhenmeyer. 2009. Lakes and reservoirs as regulators of carbon cycling and climate. *Limnol. Oceanogr.*, 54:2298-2314.

Tremblay, A., J. Bastien, M. C. Bonneville, P. A. del Giorgio, M. Demarty, M. Garneau, J. F. Helie, L. Pelletier, Y. T. Prairie, N. Roulet, I. Strachan, and C.R. Teodoru. 2010. Net Greenhouse Gas Emissions at Eastmain 1 Reservoir, Quebec, Canada World Energy Congress, Montréal, September 12 to 16.

Tremblay, A., L. Varfalvy, C. Roehm, and M. Garneau. Eds. 2005. *Greenhouse Gas Emissions: Fluxes and Processes. Hydroelectric Reservoirs and Natural Environments, Environmental Science Series*, 732 pp. Springer-Verlag, Berlin, Heidelberg, New York.

Triska, F. J., V. C. Kennedy, R. J. Avanzino, G. W. Zellweger, and K.E. Bencala. 1989. Retention and transport of nutrients in a third-order stream in northwest California. *Ecology* 70:1894-905.

Tseng, K. H., J. L. Tsai, A. Alagesan, B. J. Tsuang, M. H. Yao, and P. H. Kuo. 2010. Determination of methane and carbon dioxide fluxes during the rice maturity period in Taiwan by combining profile and eddy covariance measurements, *Agric. Forest Meteorol.*, 150, 852-859.

Twining, B. S., S. E. Mylon, and G. Benoit. 2007. Potential role of copper availability in nitrous oxide accumulation in a temperate lake, *Limnol. Oceanogr.*, 524, 1354-1366, doi:10.4319/lo.2007.52.4.1354.

UNESCO-IHA. 2009. The UNESCO-IHA measurement specification guidance for evaluating the GHG status of man-made freshwater reservoirs. Published: IHA, London.

Upstill-Goddard, R. C., A. J. Watson, P. S. Liss, and M. I. Liddicoat. 1990. Gas transfer velocities in lakes measured with SF<sub>6</sub>. *Tellus* 42: 364-377, doi:10.1034/j.1600-0889.1990.t01-3-00006.x

Utsumi, M., Y. Nojiri, T. Nakamura, T. Nozawa, A. Otsuki, and H. Seki. 1998a. Oxidation of dissolved methane in a eutrophic, shallow lake: lake Kasumigaura, Japan. *Limnol. Oceanogr.* 43, 471-480.

Utsumi, M., Y. Nojiri, T. Nakamura, T. Nozawa, A. Otsuki, N. Takamura, M., Watanabe, and H., Seki. 1998b. Dynamics of dissolved methane and methane oxidation in dimictic Lake Nojiri during winter. *Limnol. Oceanogr.* 43, 10-17.

Vachon, D., Y. T. Prairie, and J. J. Cole. 2010. The relationship between near-surface turbulence and gas transfer velocity in freshwater systems and its implications for floating chamber measurements of gas exchange, *Limnol. Oceanogr.*, 55, 1723-1732, doi:10.4319/lo.2010.55.4.1723.

Vapnik, V. N. 1995. *The nature of statistical learning theory*. Springer.

Varis, O., M. Kummu, S. Härkönen, and J. Huttunen. 2012. Greenhouse gas emissions from reservoirs. In: Tortajada, C. Altinbilek, D. Biswas, A.K. (Eds.), *Impacts of large dams: A Global Assessment*, pp. 69-94. Springer, Berlin. doi:10.1007/978-3-642-23571-94

Venkiteswaran, J. J., and S. L. Schiff. 2005. Methane oxidation: isotopic enrichment factors in freshwater boreal reservoirs. *Appl. Geochem.* 20: 683-690.

Vesala, T., J. Huotari, Ü. Rannik, T. Suni, S. Smolander, A. Sogachev, S. Launiainen, and A. Ojala. 2006. Eddy covariance measurements of carbon exchange and latent and sensible heat fluxes over a boreal lake for a full open-water period, *J. Geophys. Res.*, 111, D11101, doi:10.1029/2005JD006365.

Vickers, D., and L. Mahrt. 1997. Quality control and flux sampling problems for tower and aircraft data, *J. Atmos. Oceanic Technol.*, 14, 512-526, doi:10.1175/1520-0426(1997)014<0512:QCAFSP>2.0.CO;2.

Victor, D. G. 1998. Strategies for cutting carbon, *Nature*, 395, 837-838, doi:10.1038/27532.

Vogels, G. D., J. T. Keltjens, and C. van der drift. 1988. Biochemistry of methane production. In ed. A.J.B. Zehnder, *Biology of anaerobic Microorganisms*, pp. 707-770. New York: Wiley.

- Wang, F., B. Wang, C.Q. Liu, Y. Wang, J. Guan, X. Liu, and Y. Yu. 2011. Carbon dioxide emission from surface water in cascade reservoirs-river system on the Maotiao River, southwest of China. *Atmospheric Environ.*, Vol.45. No.23, Jul, pp. 3827- 3834, 1352-2310.
- Wang, S. L., C. Q., Liu, K.M., Yeager, G. J., Wan, J., Li, F. X., Tao, Y.C., Lue, F., Liu, and C. X., Fan. 2009. The spatial distribution and emission of nitrous oxide N<sub>2</sub>O in a large eutrophic lake in eastern China: anthropogenic effects. *Sci. Total Environ.* 407, 3330-3337.
- Wanninkhof, R and W. R. McGillis. 1999. A cubic relationship between air-sea CO<sub>2</sub> exchange and wind speed. *Geophys. Res. Lett.* 26: 1889-1892, doi:10.1029/1999GL900363.
- Wanninkhof, R. 1992. Relationship between gas exchange and wind speed over the ocean. *J. Geophys. Res.* 97, 7373-7382.
- Wanninkhof, R., J. R. Ledwell, and W. S. Broecker. 1985. Gas exchange wind speed relationship measured with sulfur hexafluoride on a lake. *Science* 227, 1224-1226.
- Ward B. B. and K. A. Kilpatrick. 1990. Relationship between substrate concentration and oxidation of ammonium and methane in a stratified water column. *Continental Shelf Research*, 10, 1193-1208.
- Ward, B., R. Wanninkhof, W. R. McGillis, A. T. Jessup, M. D. DeGrandpre, J. E. Hare, and J. B. Edson. 2004. Biases in the air-sea flux of CO<sub>2</sub> resulting from ocean surface temperature gradient. *J. Geophys. Res.* 109. doi:10.1029/2003JC001800.
- Wassmann, R., H. U. Neue, C., Bueno, R. S. Lantin, M. C. R. Alberto, L.V. Buendia, K. Bronson, H. Papan, and H. Rennenberg. 1998. Methane production capacities of different rice soils derived from inherent and exogenous substrates. *Plant Soil* 203, 227-237.
- WCD, World Commission on Dams. 2000. Dam reservoirs and greenhouse gases. Report on the workshop held on February 24-25, 2000, Hydro-Quebec, Montreal, World Commission on Dams Secretariat.
- Weathers, P. 1984. N<sub>2</sub>O evolution by green algae. *Appl. Environ. Microbiol.* 48, 1251-1253.
- Webb, E. K., G. I. Pearman, and R. Leuning (1980), Correction of flux measurements for density effects due to heat and water vapour transfer, *Q. J. R. Meteorol. Soc.*, 106, 85-100.
- Webster, E. A., and D. W. Hopkins. 1996. Contributions from different microbial processes to N<sub>2</sub>O emission from soil under different moisture regimes. *Biol. Fertil. Soils*, 22: 331-335.
- Weiss, R. F., and B. A. Price, Nitrous oxide solubility in water and seawater, *Mar Chem* 8, 347-359, 1980.
- Weiss, RF. 1974. Carbon dioxide in water and seawater: the solubility of a non-ideal gas. *Mar Chem* 2:203-15.
- Weissenberger, S., É. Duchemin, S. Houel, R. Canuel, and M. Lucotte. 1999. Greenhouse gas emissions and carbon cycle in boreal reservoirs. In: Proceedings of the International Conference on Greenhouse Gas Emissions from Dams and Lakes, December 1998, Rio de Janeiro.
- Werle, P. and R. Kormann. 2001. Fast chemical sensor for eddy correlation measurements of methane emissions from rice paddy fields, *Appl. Opt.*, 40, 846-858.
- Whitfield, C. J., J. Aherne, and H. M. Baulch. 2011. Controls on greenhouse gas concentrations in polymictic headwater lakes in Ireland. *Sci. Total Environ.* 1;410-4110:217-25.
- Williams, R. J., and R. L. Crawford. 1984. Methane production in Minnesota peatlands. *Appl. Environ. Microbiol.* 47, 1266-1271.



- Winfrey, M.R., and J.G. Zeikus. 1977. Effect of sulfate on carbon and electron flow during microbial methanogenesis in freshwater sediments. *Appl. Environ. Microbiol.* 33, 275-281.
- Winfrey, M.R., and J.G. Zeikus. 1979. Microbial methanogenesis and acetate metabolism in a meromictic lake. *Appl. Environ. Microbiol.* 37, 213.
- WMO, 2008. Guide to Meteorological Instruments and Methods of Observation WMO-No. 8 page I.5-12.
- Wuebbles, D. J., and K. Hayhoe. 2002. Atmospheric methane and global change. *Earth-Sci. Reviews.* 57 : 177-210.
- Wuebbles, D.J. 2009. Nitrous oxide: no laughing matter. *Science* 326, 56-57.
- Yamamoto, S., J. B. Alcauskas, and T. E. Crozier. 1976. Solubility of methane in distilled water and seawater. *J. Chem. Eng. Data* 21, 78-80.
- Yang, L., F. Lu, X. Wang, X. Duan, W. Song, B. Sun, S. Chen, Q. Zhang, P. Hou, F. Zheng, Y. Zhang, X. Zhou, Y. Zhou, and Z. Ouyang. 2012. Surface methane emissions from different land use types during various water levels in three major drawdown areas of the Three Gorges Reservoir. *J. Geophys. Res.* 117
- Yao, H., R. Conrad, R. Wassmann, and H. U. Neue. 1999. Effect of soil characteristics on sequential reduction and methane production in sixteen rice paddy soils from China, the Philippines, and Italy. *Biogeochemistry* 47, 269-295.
- Yoshinari, T. 1985. Nitrite and nitrous oxide production by *Methylosinus trichosporium*. *Can. J. Microbiol.* 31: 139-144.
- Zappa, C. J., W. E. Asher, A. T. Jessup, J. Klinke, and S. R. Long. 2004. Microbreaking and the enhancement of air-water transfer velocity. *J. Geophys. Res.* 109: C08S16, doi:10.1029/2003JC001897
- Zappa, C. J., W. R. McGillis, P. A. Raymond, J. B. Edson, E. J. Hints, H. J. Zemmeling, J. W. H. Dacey, and D. T. Ho. 2007. Environmental turbulent mixing controls on air-water gas exchange in marine and aquatic systems, *Geophys. Res. Lett.*, 34, L10601, doi:10.1029/2006GL028790.
- Zappa, C., P. A. Raymond, E. A. Terray, and W. R. McGillis. 2003. Variation in surface turbulence and the gas transfer velocity over a tidal cycle in a macro-tidal estuary. *Estuaries* 26, 1401-1415.
- Zehnder, A. J. B. 1978. Ecology of methane formation. In: *Water Pollution Microbiology*, ed. R. Mitchell, vol.2, pp. 349-376, New York: Wiley.
- Zeikus, J. G. and M. R. Winfrey. 1976. Temperature limitation of methanogenesis in aquatic sediments. *Appl. Environ. Microbiol.* 31, 99-107.
- Zheng, H., X.J. Zhao, T.Q. Zhao, F.L. Chen, W.H. Xu, X.N. Duan, X.K. Wang, and Z.Y. Ouyang. 2011. Spatial-temporal variations of methane emissions from the Ertan hydroelectric reservoir in southwest China. *Hydrol. Processes*, Vol.25. No.9, Apr, pp. 1391-1396, 0885-6087.
- Zheng, X. H., S. H. Han, Y. Huang, Y.S. Wang, and M.X. Wang. 2004. Re-quantifying the emission factors based on field measurements and estimating the direct N<sub>2</sub>O emission from Chinese croplands. *Global Biogeochem. Cycles* 18, GB2018. doi:10.1029/2003GB002167.
- Zheng, X., M. Wang, Y. Wang, R. Shen, J. Gou, J. Li, J. Jin, and L. Li. 2000. Impacts of soil moisture on nitrous oxide emission from croplands: a case study on the rice-based agroecosystem in Southeast China. *Chemosphere*, 2: 207-224.
- Zinder, S. H. 1993. Physiological ecology of methanogens, In J. G. Ferry ed., *Methanogenesis: ecology, physiology, biochemistry and genetics*. Chapman & Hall, New York. p. 128-206.

**Résumé:** L'augmentation de l'intérêt concernant la part des réservoirs hydroélectrique dans l'augmentation de la concentration atmosphérique des Gaz à Effet de Serre (GES) a amené à mesurer les émissions nettes d'un réservoir hydroélectrique, Nam Theun 2 (NT2) dans la région subtropicale de la République Démocratique Populaire du Laos, Asie. Ce travail est la première évaluation de l'empreinte carbone des GES (c'est à dire : les émissions après ennoisement moins les émissions avant ennoisement) en relation avec la création d'un réservoir hydroélectrique. C'est le résultat d'une étude à grande échelle qui s'est déroulée pendant cinq ans (2008-2012). Nous avons tout d'abord quantifié les sources et les puits majeurs des GES des composants terrestres et aquatiques du paysage avant ennoisement (Mai 2008). Ensuite, à partir d'Avril 2009, cette étude similaire a été réalisée au niveau du réservoir, sa zone de marnage et son aval. C'est en Octobre 2009 que le réservoir hydroélectrique NT2 a, pour la première fois, atteint son niveau maximal et c'est huit mois plus tard, en Mars 2010, que les turbines ont fonctionnées pour la première fois. En se basant sur un suivi bimensuel et sur cinq missions de terrain couvrant toutes les saisons, les émissions des principaux GES (c'est à dire l'oxyde nitreux (N<sub>2</sub>O), le méthane (CH<sub>4</sub>) et le dioxyde de carbone (CO<sub>2</sub>)) ont été mesurées d'Avril 2009 à Décembre 2011. Les émissions ont été déterminées à la surface du réservoir (flux diffusifs et ébullitifs) ainsi que dans les sols de la zone de marnage, qui peut atteindre 370 km<sup>2</sup> pour une surface totale de réservoir de 450 km<sup>2</sup>.

**Summary:** The identification and accurate quantification of sinks or sources of GHG has become a key challenge for scientists and policy makers groups working on climate change or global warming. The creation of a hydro-reservoir while damming a river for power generation converts the terrestrial ecosystems into aquatic ecosystem and subsequently decomposition of flooded terrestrial soil organic matter stimulates GHG productions and thereby emissions to atmosphere. Tropical or subtropical hydroelectric reservoirs are more significant sources of GHG than boreal or temperate one. The number of hydroelectric reservoirs continues to increase at fast pace specially in the tropical or sub-tropical regions which still hold significant amount of hydropower resources to be exploited. In this context, we study the subtropical hydroelectric Nam Theun 2 (NT2) Reservoir, a complex-structural-designed, created on the Nam Theun River in Laos PDR. The main aims of our study are to: (1) Study the GHG dynamics (CH<sub>4</sub>, N<sub>2</sub>O and CO<sub>2</sub>) in the reservoir and in the whole area of influence (downstream and drawdown areas), (2) explore the effectiveness of different methodology (eddy covariance, floating chamber, submerged funnel and thin boundary layer) to assess of GHG emission from a hydroelectric reservoir, (3) determine the environmental controls on the different emission terms; (4) attempt to determine the first net GHG budget of a subtropical hydroelectric reservoir.